UNCLASSIFIED

SECURITY CLASSIFICATION OF THIS PAGE (When Data Entered)

REPORT DOCUMENTATION PAGE

READ INSTRUCTIONS BEFORE COMPLETING FORM

REPORT NUMBER: AFIT/CI/NR 88- 112

2. GOVT ACCESSION NO.

3. RECIPIENT'S CATALOG NUMBER

TITLE (and Subtitle): SAMPLE INTRODUCTION USING THE HILDEBRAND GRID NEBULIZER FOR PLASMA SPECTROMETRY

5. TYPE OF REPORT & PERIOD COVERED: MS THESIS

6. PERFORMING ORG. REPORT NUMBER

AUTHOR(s): TIMOTHY J. BROTHERTON

8. CONTRACT OR GRANT NUMBER(s)

PERFORMING ORGANIZATION NAME AND ADDRESS: AFIT STUDENT AT: UNIVERSITY OF CINCINNATI

10. PROGRAM ELEMENT, PROJECT, TASK AREA & WORK UNIT NUMBERS

CONTROLLING OFFICE NAME AND ADDRESS

12. REPORT DATE: 1988

13. NUMBER OF PAGES: 133

14. MONITORING AGENCY NAME & ADDRESS (if different from Controlling Office): AFIT/NR, Wright-Patterson AFB OH 45433-6583

15. SECURITY CLASS. (of this report): UNCLASSIFIED

15a. DECLASSIFICATION/DOWNGRADING SCHEDULE

16. DISTRIBUTION STATEMENT (of this Report): DISTRIBUTED UNLIMITED: APPROVED FOR PUBLIC RELEASE

17. DISTRIBUTION STATEMENT (of the abstract entered in Block 20, if different from Report): SAME AS REPORT

18. SUPPLEMENTARY NOTES: Approved for Public Release: IAW AFR 190-1
LYNN E. WOLAVER 20 July 88
Dean for Research and Professional Development
Air Force Institute of Technology
Wright-Patterson AFB OH 45433-6583

19. KEY WORDS (Continue on reverse side if necessary and identify by block number)

20. ABSTRACT (Continue on reverse side if necessary and identify by block number): ATTACHED

DD FORM 1 JAN 73 1473 EDITION OF 1 NOV 65 IS OBSOLETE

UNCLASSIFIED

SECURITY CLASSIFICATION OF THIS PAGE (When Data Entered)

ABSTRACT

The Hildebrand grid nebulizer is evaluated for use with Inductively Coupled Plasma-Optical Emission Spectrometry (ICP-OES) and Mass Spectrometry (ICP/MS) detection.

Limiting aspiration rates for various organic solvents were determined for the grid nebulizer with a mini-pyrex spray chamber, a cooled spray chamber and a conical spray chamber. Detection limits and linear dynamic ranges were determined for various species. Indirect solvent transport efficiencies were determined as a function of spray chamber, flow rate, temperature and solvent. A comparison was made between the grid, cross-flow, concentric and glass frit.

Three interfaces for volatile organic solvents used to couple Flow Injection Analysis (FIA) with ICP-OES detection were evaluated. Detection limits, linear dynamic ranges, precision, and peak width were determined for elements in methanol and acetonitrile solutions.

The grid nebulizer was evaluated for ICP-OES use with high dissolved salt solutions. Analytical figures of merit determined were stability, precision, detection limits, clogging, memory effects, use with acid digested samples and linear dynamic ranges.

Aqueous, high dissolved salt, urine and volatile organic solvents were introduced with the grid nebulizer for ICP/MS detection. Optimization studies of ICP power, plasma sampling position and nebulizer flow were performed. Detection limits of elements in various matrices were determined. Ionization suppression effects as a function of concomitant elements were studied.

UNIVERSITY OF CINCINNATI

May 18 19 87

I hereby recommend that the thesis prepared under my supervision by Timothy J. Brotherton

entitled SAMPLE INTRODUCTION USING THE HILDEBRAND GRID NEBULIZER FOR PLASMA SPECTROMETRY

be accepted as fulfilling this part of the requirements for the degree of Doctor of Philosophy

Approved by:

Joseph A. Caruso

William R. Heineman

R. Marshall Wilson

SAMPLE INTRODUCTION

USING THE

HILDEBRAND GRID NEBULIZER

FOR

PLASMA SPECTROMETRY

A dissertation submitted to the Division of Graduate Studies and Research of the University of Cincinnati in partial fulfillment of the requirements for the degree of

DOCTOR OF PHILOSOPHY

in the Department of Chemistry of the College of Arts and Sciences

1987

by

Timothy J. Brotherton

B.S. University of Cincinnati, 1978

M.S. Northeastern University, 1982

ABSTRACT

The Hildebrand grid nebulizer is evaluated for use with Inductively Coupled Plasma-Optical Emission Spectrometry (ICP-OES) and Mass Spectrometry (ICP/MS) detection.

Limiting aspiration rates for various organic solvents were determined for the grid nebulizer with a mini-pyrex spray chamber, a cooled spray chamber and a conical spray chamber. Detection limits and linear dynamic ranges were determined for various species. Indirect solvent transport efficiencies were determined as a function of spray chamber, flow rate, temperature and solvent. A comparison was made between the grid, cross-flow, concentric and glass frit.

Three interfaces for volatile organic solvents used to couple Flow Injection Analysis (FIA) with ICP-OES detection were evaluated. Detection limits, linear dynamic ranges, precision, and peak width were determined for elements in methanol and acetonitrile solutions.

The grid nebulizer was evaluated for ICP-OES use with high dissolved salt solutions. Analytical figures of merit determined were stability, precision, detection limits, clogging, memory effects, use with acid digested samples and linear dynamic ranges.

Aqueous, high dissolved salt, urine and volatile organic solvents were introduced with the grid nebulizer for ICP/MS detection. Optimization studies of ICP power, plasma sampling position and nebulizer flow were performed. Detection limits of elements in various matrices were determined. Ionization suppression effects as a function of concomitant elements were studied.

DEDICATION

To Mary, T.J., Sean and Traci.

ACKNOWLEDGEMENTS

I thank Dr. Joe Caruso for his expert guidance, his motivational yet unassuming management style, and his support and encouragement to my research activities. I also thank Dr. William R. Heineman and Dr. R. Marshall Wilson for their support and review of my dissertation, and I thank Dr. Sotiris Pratsinis (Dept. Chem. Engr.) for his consultation support. I thank the U.S. Air Force Institute of Technology which provided me this unique educational opportunity.

I thank all members of my research group including Pete Pfannerstill, H. J. Mohamad, Jack Creed, Doug Heitkemper, Barbara Barnes, Nohora Vela, Wei-Lun Shen, Tim Davidson, Pete Brown, Jack Pretty, Hamzaar Suyani, John Workman, Guli Ataman, Mrs. Zhang and Mark Bruce for their cooperation, friendship and support.

I thank my parents for providing me a good education, instilling strong values and teaching me the perseverance to better myself.

Finally, I thank my wife, Mary, for her patience, love and understanding during these years.

TABLE OF CONTENTS

TABLE OF CONTENTS

List of Figures

TABLE OF CONTENTS

List of Tables

CHAPTER 1

OVERVIEW OF SAMPLE INTRODUCTION FOR INDUCTIVELY COUPLED PLASMA SPECTROMETRY

1.1 INTRODUCTION

The famous analytical chemist, G.E.F. Lundell, in his 1933 paper entitled "The Chemical Analysis of Things as They Are" stated, "The determinator's salvation lies in the development of selective methods of analysis, and his final resting place will be a heaven in which he has a shelf containing 92 reagents, one for each element where No. 13 is the infallible specific for Al, No. 26 the sure shot for Fe, No. 39 the unfailing relief for Y, and so on to U...".[1,2] Over 50 years later today's analytical chemists are still pursuing element selective detection at lower and lower detection levels. This is because there is a great need for major, minor, trace and ultratrace elemental analysis of complex environment, clinical, toxicological and biological samples. Therefore, current research is directed at development of techniques that are sensitive yet accurate and precise, quick yet inexpensive and have a multielement capability.[3]

The modern analytical chemist has many elemental analysis techniques from which to choose. Atomic Absorption Spectrometry (AAS) and furnace AAS, which have been the traditional techniques for elemental analysis, provide sensitive single element detectors. Multielement emission detection techniques include X-ray fluorescence (XRF), arc spark direct current (DC) emission, DC plasma, microwave induced plasma (MIP)

and conductively coupled plasma (ICP). The merits and disadvantages are discussed in recent reviews.[3,4,5] Use of the MIP has been restricted primarily to research laboratories, whereas the ICP is quickly becoming the standard for quick, sensitive multielement detection. Skidmore et al. suggest, "For the large laboratory, the best combination of techniques would be an ICP and electrothermal AAS, whereas for the smaller lab flame and electrothermal AAS would suffice."[5]

The subject of this thesis considers sample introduction using the Hildebrand grid nebulizer into the Inductively Coupled Plasma (ICP) with detection from optical emission spectrometry (OES) and mass spectrometry (MS). The remainder of this chapter briefly describes ICP-OES, ICP/MS and various sample introduction techniques. Chapter 2 evaluates the use of the grid nebulizer and various spray chambers for use with organic solvents and compares the grid to the glass frit, concentric and cross-flow nebulizers. Chapter 3 considers three interfaces used for HPLC/FIA with ICP-OES detection. The grid nebulizer is evaluated in Chapter 4 for use with high dissolved salt/solid solutions using ICP-OES. Chapter 5 considers ICP/MS detection using of the grid nebulizer for a variety of sample introduction situations including organic solvents, high dissolved solids and biological fluids.

1.2 ICP-OES

Inductively coupled plasma optical emission spectrometry has become a very popular elemental technique in recent years. The plasma is formed by passing rf current (27.1 MHz) through a water cooled induction coil (Figure 1). The high frequency currents flowing in the coil generate oscillating magnetic fields axially oriented inside the quartz torch. These fields induce the electrons and ions to flow in closed annular

paths, which resistively heats other species resulting in additional ionization. By matching the output impedance of the generator to the impedance of the plasma, the efficiently coupled rf energy forms a stable plasma discharge. The plasma is stabilized by a pattern of three argon flows. The ICP is formed by a coolant argon flow (12-20 L/min). Auxiliary argon flow (0.5-2 L/min) is used to stabilize and/or move the plasma vertically within the ICP torch. Sample is introduced through the injector, typically in aerosol form.[6,7,8]

ICP as an excitation source offers many advantages over other spectroscopic techniques. High plasma temperatures (6,000-10,000^{o}K) result in complete atomization of solute molecules and thus eliminates most matrix and interference problems often associated with AAS and DC emission techniques. ICP also provides the energy to excite many elements simultaneously. Detection limits commonly achieved for metals are in the low to sub ng/mL range. Multielement analysis of biological fluids such as blood or urine can be accomplished on microgram samples. In addition, ICP can provide five to six orders of magnitude linear dynamic range.[9-13]

Typically, the ICP is used for elemental analysis of aqueous samples. Many researchers have used the ICP as a detector for liquid chromatography (LC). Ebdon, Hill and Ward recently published a review on liquid chromatography using atomic spectrometric detection techniques.[14] **Table 1-1** lists various chromatographic separations using ICP-OES detection.

The ICP also has been used for a wide variety of materials including animal feeds, biological materials, brasses, calcined bauxites, chemical streams, coal fly ash, cosmetic products, EDTA, Egyptian sugar cane,

Table 1-1

ICP Detection for Liquid Chromatography

Column	Mobile Phase	Sample	Reference
250 x 4.6 mm Zorbax C-8 column	50-80% EtOH	Iron and molybdenum carbonyl complexes	15
Hypersil 100 x 4.6 mm	30% MeOH	DMA, MAA, p-APP, As^{V}, phenylarsonic acid	15
100-Å Styragel Waters column	Pyridine	Ferrocene, copper & cobalt complexes in coal	16
250 x 1.6 mm anion exchange resin	Ammonium sulfate	NTA and EDTA chelates of Cu, Zn, Ca, Ng	17
600 x 7.5 mm TSIC 3000 SW Size exclusion	Water	Cu, Ca, Mg, Zn filtrates	18
Cation exchange Resin (UlPX-210SC)	Sodium phosphate	Amino Acids	19
Hamilton PRP-1 resin-based, reversed-phase column	Water	Arsenic, selenium and phosphorus compounds	20

Table 1-1 (continued)

ICP Detection for Liquid Chromatography

Column	Mobile Phase	Sample	Reference
Micro-HPLC (0.5x120 mm) Jasco SC-01 silica packing	MeOH/Water	Cu, Zn, Fe, Co organometallic compounds	21
600 x 2 mm, TSK GEL 3000 SW	0.9% NaCl Solution	Separation of Vitamin B_{12}, various proteins, etc.	22
Nagel-Nucleosil 10-SP cation exchange resin	Sodium phosphate	Arsenobetaine in shark muscle	23
Strong cation Exchange resin (1EX-2 10SC)	Ammonium lactate	Rare earth elements	24
Microbore 1 x 500 nm C_{18} coluumn	Tetrabutyl ammonium sulfate in MeOH and water	Inorganic and organometallic compounds	25
Microcolumn gel permeation chromatography	Water	Saccharides	26
Anion exchange resin 1EX-260-SA-SIL	Ammonium carbonate	Ribonucleotides	27

food, geological materials grapefruit and many more.[28] Listings of individual papers on the above are specified in reference 28.

One limitation of ICP-OES is the large number of spectral lines produced from concomitants within the high energy plasma. Thus, line rich spectra can interfere with elemental lines of interest. To overcome this, high resolution spectrometers are required to resolve those interferences. One alternative to ICP optical emission detection is to couple the ICP with a quadrupole mass spectrometer. This technique, known as Inductively Coupled Plasma Mass Spectrometry (ICP/MS), can provide many advantages over ICP optical emission.

1.3 ICP/MS

Inductively Coupled Plasma/Mass Spectrometry (ICP/MS) is quickly becoming the method of choice for ultratrace elemental analysis. As with ICP-OES, ICP/MS is a very sensitive technique that is amenable to precise, rapid sample throughput. In addition, ICP/MS offers many advantages over ICP-OES. Detection limits of 0.01-0.1 ng/mL can be achieved across most of the elements in the periodic table. This is an improvement of 1-2 orders of magnitude over ICP/OES. Major, minor and trace constituents can be identified in an unknown in as little as one minute. ICP/MS provides a direct method for isotope ratio determintion with precision of 1% or better. ICP/MS spectra are simpler than ICP/OES line rich spectra because they consist of only integer mass/charge ratios of 1 to 240.[29-31]

There are some disadvantages of ICP/MS. Isobaric interferences, which result from the ionization of the plasma gas and solution that is being analyzed, inhibit analysis of elements such as Si, S and Ca.[32] Because this technique is so sensitive, overload of the electron multi-

plier can occur at concentrations >10 ng/mL. Thus, the concentration may not be linear with intensity for concentrations much above 10 ng/mL.

1.4 SAMPLE INTRODUCTION

One inherent limitation of both ICP/MS and ICP/OES is sample introduction into the plasma. Sample introduction is often described as the "Achilles heel" of atomic spectrometry because the utility of a particular spectroscopic technique is usually only as good as how one introduces the sample.[33,34] The typical method of sample introduction into the ICP is solution nebulization. Other exotic methods such as hydride generation, powder injection, electrothermal vaporization, etc. are also used.

The requirements for sample introduction into the ICP are relatively straightforward. Browner et al. defines them as "...reproducible transfer of a representative portion of sample material with high efficiency and no adverse interelement effects".[33] In addition to these general requirements, the method should be quick and simple, require minimal amount of sample, tolerant to many kinds of solutions (i.e. high salt/solid and organic solvents), and inexpensive. Satisfying all of these requirements at once, can be mutually exclusive. Thus, one may opt for a system that is a compromise of all the above requirements. A brief description of some typical sample introduction techniques are listed below.

1.4.1 Solution Nebulization

Solution nebulization is the most common form of sample introduction into the ICP. Solution nebulization converts a liquid into an aerosol (which consists of many small droplets (0.1 μm-10 μm) along with solvent vapor). The aerosol is carried to the plasma by a carrier gas

(usually argon). The aerosol is passed through a spray chamber that allows only droplets smaller than or equal to about 1 μm reach the plasma. The spray chamber can also be cooled to remove unwanted solvent vapor that can destabilize and extinguish the plasma.

The transport of analyte via solution nebulization has been studied both theoretically and empirically. Determination of nebulizer efficiencies (measure of how much sample is transported to the plasma) via direct methods[35-38] and indirect methods[39] have been studied and compared.[40] Various nebulizer spray chamber combinations have been evaluated in terms of particle size distributions,[41-44] solution uptake rates,[45-47] matrix effects,[48,49] precision,[50] memory effects,[51,52] ability to tolerate organic solvents[53,54,55] and high dissolved salt solutions[56,57] and long term stability.[58,59]

1.4.1.1 Pneumatic Nebulizers

Aerosols that are formed by flowing gas are defined as pneumatic nebulizers. However, by convention only the cross flow and concentric are referred to as pneumatic nebulizers. Both the crossflow and concentric operate by flowing a high velocity gas stream by a liquid which results in the shearing off of liquid droplets. Efficiencies for the crossflow and concentric nebulizers are comparable and are approximately 1-3%.[33] High precision and minimization of long term drift can be achieved by careful control of the nebulizer gas flow and pressure. Fluctuations in either (gas flow or nebulizer pressure) result in poor stability. The crossflow nebulizer can tolerate nebulization of solutions containing as much as 2.5% dissolved salt solutions.[57] Use of the concentric nebulizer for salt solutions can result in clogging of the capillary tip. Use of the crossflow and concentric nebulizers for intro-

duction of volatile organic solvents such as acetonitrile and methanol is possible, but a cooled spray chamber should be used.[55] Some commonly used nebulizers are compared in terms of qualitative evaluation factors in **Table 1-2.**

1.4.1.2 Babington Nebulizer

The Babington nebulizer was designed for the introduction of high dissolved salt/solid solutions. The aerosol is formed by passing a high velocity gas through an orifice over which a stream of liquid is flowing.[60] The liquid does not pass through a small capillary tube as it does in the concentric and crossflow nebulizers, and thus does not become clogged. Suddendorf and Boyer in 1978 reported using a "V" type Babington nebulizer for high dissolved solids yielding detection limits comparable to a conventional pneumatic nebulizer.[61] Garbarino and Taylor in 1980 reported on the use of a sphere type Babington nebulizer that was insensitive to suspended particulate matter and yielded detection limits equivalent to or better than pneumatic nebulizers.[56] Thelin reported another variation of a "V" nebulizer that was used for high salt (10%) content steel samples.[62] Variations of the Babington nebulizer that could utilize solutions containing as high as 20% w/v of dissolved solids or slurries have been reported by Ebdon and Cave[63] and Wichman, Mohamed and Fry[64,65] Baginski and Meinhard have reported use of a Meinhard Type C nebulizer with a recessed capillary tip nozzle that is used for high dissolved solids.[66] Walton and Goulter described a new slotted maximum dissolved solid nebulizer (MDSN) and compare against the Meinhard nebulizer in terms of sensitivity, precision, clean out and drift.[59]

1.4.1.3 Glass Frit Nebulizer

The original glass frit nebulizer was introduced by Apel et

Table 1-2

Comparison of Various Nebulizers

	Concentric		Fixed Crossflow	Babington	Glass Frit	Hildebrand Grid	Ultra-sonic	DIN
	Meinhard A	Meinhard C (Recessed Tip)						
Efficiency	1-3	1-3	1-3	10	10	2-5	9-12	100%
Precision	Gas flow, Temp Dep	Gas flow, Temp Dep	Gas flow, Temp Dep	Gas flow, Temp Dep	Low	Gas flow, Temp Dep	Gas flow, Temp, RF Dep	Gas flow, Temp, Uptake Dep
Drift	Gas flow Temp Dep	Gas flow Temp Dep	Gas flow Temp Dep	Gas flow Temp Dep	High	Gas flow Temp Dep	Gas flow, Temp, RF	Gas flow, Temp, Uptake Dep
Memory Effects	Minimal	Minimal	Minimal	Minimal	High	Minimal	Minimal to Low	None
Amount of Sample	Avg	Avg	Avg	High	Low-Avg	Avg	Low-Avg	Very Low
Use with Salt Solutions (2.5%)	No	Yes	Yes	Yes	No	Yes	No	No
Use with Volatile Organics	No	No	No	No	Yes	Yes	Yes	Yes
Cost ($)	230	350	600	800	300	500	13,000	800
Typical Solution Uptake (mL/min)	1-4	0.5-1.5	4-6	0.5-1.5	0.5-1.5	0.5-1.5	0.5-1.5	0.1-0.2

al.[67,68] in 1977. In 1982, Layman and Lichte documented the performance of the glass frit nebulizer with laser scattering, ICP-OES and flame AA measurements.[42] The glass frit nebulizer has been used for volatile organic solvent introduction and as an interface for HPLC/FIA.[69,70,71]

Aerosol is formed by passing gas over a sintered glass frit (typical pore size 4-5 μm). The sample solution is pumped to the surface of the frit with a peristaltic pump. The glass frit nebulizer provides an efficient method of introducing sample (especially organic solvents) to the plasma. However, it suffers from poor reproducibility, long-term drift and memory effects. The glass frit nebulizer cannot nebulize high salt solutions.

1.4.1.4 Ultrasonic Nebulizer

In 1965, one of the first samole introduction techniques for ICP-OES was ultrasonic nebulization.[72] There are many reports which describe the advantages of continuous flow ultrasonic nebulization with aerosol desolvation.[73-76] However, there are other reports which describe problems such as long and short term stability, reliability, matrix effects, memory effects, clean out time and drift in aerosol generation efficiency.[34,77-79] Some proponents of ultrasonic sample introduction feel that the reasons for the many negative reports on the technique are due to design and operating deficiencies of laboratory built ultrasonic systems.[80] Commercial ultrasonic/desolvation systems may offer the reliability lacking in laboratory built systems, but they are very expensive. (A Baird UDX ultrasonic nebulization system costs approximately $13,000.)

Ultrasonic nebulization produces an aerosol by subjecting the sample solution to high frequency (1.3 MHz) agitation via a piezo electric

transducer in contact with the solution. Usually solution is flowed over the system. Advantages of this technique are high nebulizer efficiencies (11%) and uniform droplet size (dependent on frequency).[74] Aerosol production is not a function of the argon carrier gas (as is the case with pneumatic nebulizers). Thus, higher aerosol concentrations can be obtained by lower argon flow rates. Detection limits with ultrasonic nebulizers are improved (1.1-12 times) over conventional pneumatic nebulizers. Loss of analyte can occur in the desolvation system when nebulizing 0.1% dissolved solid solutions.[77]

1.4.1.5 Jet Impactor Nebulizer

Hieftje and Doherty described formation of an aerosol by pumping a solution through a small orifice (25-60 μm).[81] The high velocity stream impacts directly onto a solid surface thereby generating a fine aerosol. For use with ICP-OES, this nebulizer compared favorably with conventional nebulizers in terms of precision, linearity, detection limits and efficiency. As with the ultrasonic nebulizer, aerosol is independent of aerosol gas. Because of the small orifice, this nebulizer is prone to clogging. Applications for this nebulizer could be a low flow ICP torch or LC/ICP interface.

1.4.1.6 Direct Injection Nebulizer

In 1984, Fassel et al. described the use of microconcentric nebulizer as an interface for HPLC/FIA.[82] Figure 1-1 depicts the schematic of this nebulizer. Solution is pumped through a 0.05 mm ID inner capillary. Nebulizer argon is passed in an annular flow through a 0.7 mm OD by 0.5 mm ID capillary resulting in the formation of an aerosol. Advantages of this system is that it is 100% efficient and there is no dead volume for transient HPLC/FIA data. Solution uptake rates are 0.1-0.2

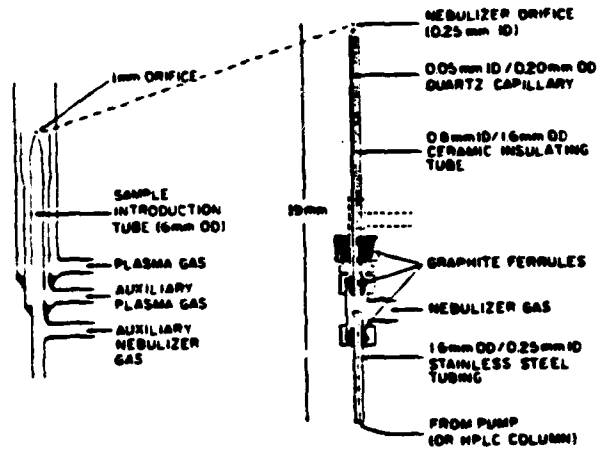

Schematic diagram of microconcentric nebulizer and torch assembly.

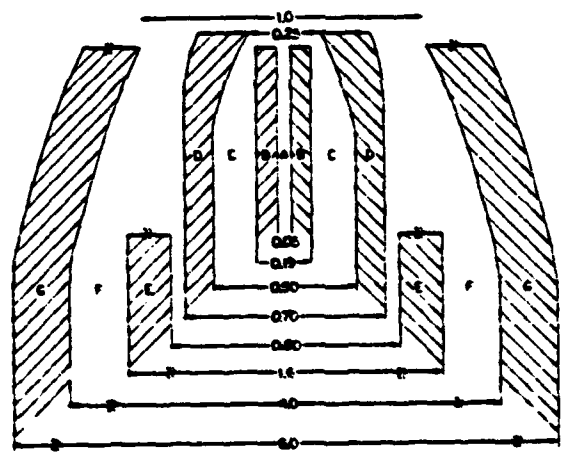

A magnified view of the microconcentric nebulizer tip: [A] liquid sample; [B] fused-silica, inner capillary tube; [C] nebulizer argon gas flow; [D] fused-silica, outer capillary tube; [E] ceramic insulating tube; [F] auxiliary nebulizer argon gas; [G] normal sample introduction tube. All dimensions are in mm.

82

Figure 1-1. Direct Injection Nebulizer

mL/min. Because the velocity of the aerosol entering the plasma is so high, detection limits are slightly degraded (1.1-4.6 times). The microconcentric nebulizer, now referred to as the direct injection nebulizer (DIN), has been compared to conventional pneumatic and ultrasonic nebulizers.[83]

1.4.1.7 Hildebrand Grid Nebulizer

The Hildebrand grid nebulizer was introduced commercially in January 1986 by Leeman Labs (Lowell, MA). Figure 1-2 depicts the schematic of grid nebulizer. Solution is pumped through a large cross section tube to the top of a 100 mesh, inert platinum screen. The solution wets the surface of the grid and high velocity gas coming from a 0.2 mm ID sapphire rod shears the liquid off the screen. A second platinum grid which is positioned approximately 0.2 mm in front of the first grid, dampens pulsations typical with peristaltic pumps. Advantages of the grid nebulizer are tolerance to high salt solutions and slightly better efficiency (measured indirectly) than conventional pneumatic nebulizers.[55,57]

1.4.2 Other Sample Introduction Techniques

In solution nebulization, liquid aerosol is transported to the plasma where it is desolvated, vaporized, atomized and excited (or ionized) for either optical emission or mass spectrometry. Many researchers have separated the steps of desolvation and vaporization from atomization and excitation.[84] This can allow the analyst to optimize the desolvation and vaporization steps independent of the atomization and excitation steps. In solution nebulization, since all steps are accomplished sequentially within the plasma, compromise conditions may exist. In addition, by separating desolvation and vaporization from atomization

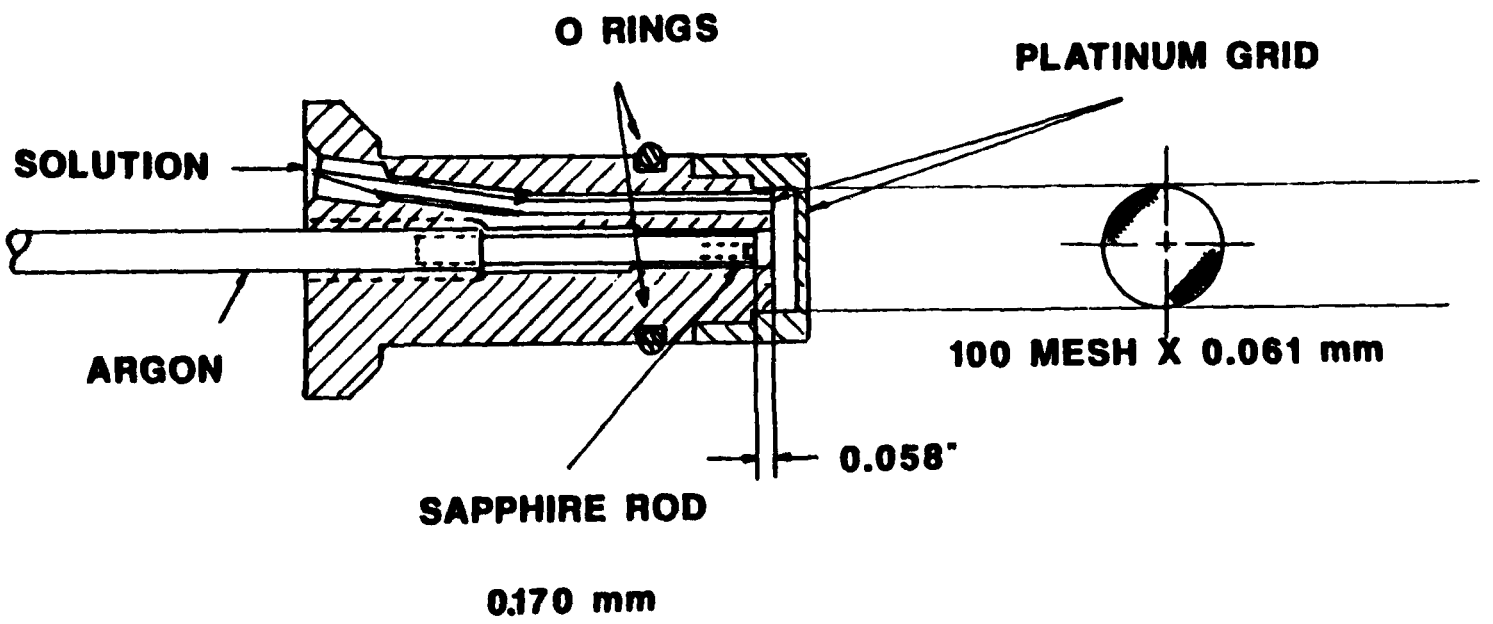

Figure 1-2. Hildebrand Grid Nebulizer

and excitation, the plasma can devote all of its energy to the excitation of analyte. Disadvantages of this technique can include dilution of the analyte with the carrier gas and analyte loss by absorption to the tube walls.

1.4.2.1 Electrothermal Vaporization

Liquid sample (10-200 μL) is deposited into a graphite cup or rod. The cup is heated slowly to evaporate solvent and ash the sample after which the sample is vaporized and carried to the plasma via a carrier gas. This technique can provide lower limits of detection and prevent interference problems. Sugimae and Barnes recently used ETV with ICP-OES to determine trace elements in suspended particulate matter.[85] Ng and Caruso have reviewed use of ETV for optical emission spectroscopy.[86]

1.4.2.2 Hydride Generation

Hydride generation enhances sensitivity of elements capable of forming hydrides (i.e. As, Bi, Se, Te, Ge, Sn, Sb). Hydrides are formed by reacting acidic sample solutions with an alkaline sodium tetrahydroborate(III) solution. They can be introduced into the plasma on a continuous flow[87,88] or batch basis.[89,90] Hydride generation techniques enhance detection capability for elements which form hydrides, and matrix effects minimized.

1.4.2.3 Powder Injection

Solid samples are finely ground (particle size 10 m) and introduced into a carrier gas stream by agitation,[91] pulsation,[92] or by vibrational energy of a spark.[93,94] Advantages of solid powder introduction is that it eliminates timely sample preparation steps (i.e. acid digestions), detection levels can be enhanced, and matrix effects are minimized. Disadvantages are that precision grinding equipment may be re

quired and reproducible particle sizes (and hence overall precision) may be difficult to replicate from one sample to the next.

Other unique sample introduction methods include Nieftje's et al. microarc atomizer[95] and rf arc sampler,[96] tandem ICPs (one for sample introduction, the other for excitation)[97] laser ablation[98-100] that pulses a small mount of vaporized matter into the plasma, and Salin et al. Direct Sample Insertion Device (DSID) that mechanically inserts a weighed amount of sample into the plasma.[101,102,103]

References

1. G.E.F. Lundell, **Ind. Eng. Chem. Anal. Ed.**, 5, 221 (1933).
2. V. A. Fassel, **Anal. Chem.**, 51, 1290A (1979).
3. G. Morrison, **CRC Crit. Rev. Anal. Chem.**, 287 (1979).
4. W. Slavin, **Anal. Chem.**, 58, 589A (1986).
5. P. R. Skidmore, S. S. Greetham, **Analyst**, 108, 171 (1983).
6. V. A. Fassel, **Anal. Chem.**, 46, 13, 1155A (1974).
7. D. A. Skoog, D. M. West, **Principles of Instrumental Analysis Ed. 2**, 340.
8. D. J. Kalnicky, R. N. Kniseley, V. A. Fassel, **Spectrochim. Acta**, 30B, 511 (1977).
9. R. H. Wednt, V. A. Fassel, **Anal. Chem.**, 37, 920 (1965).
10. S. Greenfield, I.L.L. Jones, C. T. Berry, **Analyst**, 89, 713 (1964).
11. V. A. Fassel, R. N. Kniseley, **Anal. Chem.**, 46, 13, 1110A (1974).
12. P. W. Bowman, J.J.A.M. Vrakking, **Spectrochim. Acta 40B**, 108 (1985).
13. C. B. Sobel, **Appl. Spec.**, 38, 3, 444 (1984).
14. L. Ebdon, S. Hill, R. W. Ward, **Analyst**, 112, 1 (1987).
15. C. H. Gast, J. C. Kraak, H. Poppe, F.J.M.J. Maessen, **J. Chromatog.**, 185, 549 (1979).
16. D. W. Hausler, L. T. Taylor, **Anal. Chem.**, 53, 1227 (1981).
17. D. M. Fraley, D. Yates, S. E. Manahan, D. Stalling, J. Petty, **Appl. Spectrosc.**, 35, 525 (1981).
18. W. S. Gardner, P. F. Landrum, D. A. Yates, **Anal. Chem.**, 54, 1198 (1982).
19. K. Yoshida, T. Hasegawa, H. Haraguchi, **Anal. Chem.**, 55, 2106 (1983).
20. K. J. Irgolic, R. A. Stockton, D. Chakraborti, W. Beyer, **Spectrochim. Acta 38B**, 437 (1983).
21. E. D. Katz, R. P. Scott, **Analyst**, 110, 253 (1985).
22. M. Morita, T. Vehiro, K. Fuwa, **Anal. Chem.**, 52, 349 (1980).
23. D. W. Hausler, L. T. Taylor, **Anal. Chem.**, 53, 1223 (1981).

24. K. Yoshida, H. Haraguchi, **Anal. Chem.**, **56**, 2580 (1984).

25. K. E. Lawrence, G. W. Rice, V. A. Fassel, **Anal. Chem.**, **54**, 292 (1984).

26. K. Jinno, S. Nakanishi, C. Fugimoto, **Anal. Chem.**, **56**, 1977 (1985).

27. K. Yoshida, H. Haraguchi, K. Fuwa, **Anal. Chem.**, **55**, 1009 (1983).

28. P. N. Keliher, W. J. Boyko, R. H. Clifford, J. L. Snyder, S. F. Zhu, **Anal. Chem.**, **58**, 348R (1986).

29. D. J. Douglas, E.S.K. Quan, R. G. Smith, **Spectrochim. Acta**, **38B**, 39 (1983).

30. A. R. Date, A. L. Gray, **Spectrochim. Acta**, **38B**, 29 (1983).

31. A. L. Gray, A. R. Date, **Analyst**, **108**, 1033 (1983).

32. A. L. Gray, **Spectrochim. Acta**, **41B**, 151 (1985).

33. R. F. Browner, A. W. Boorn, **Anal. Chem.**, **56**, 786A (1984).

34. R. F. Browner, A. W. Boorn, **Anal. Chem.**, **56**, 875A (1984).

35. P.A.M. Ripson, L. De Galan, **Spectrochim. Acta**, **36B**, 71 (1981).

36. D. D. Smith, R. F. Browner, **Anal. Chem.**, **54**, 533 (1982).

37. P.A.M. Ripson, L. De Galan, **Anal. Chem.**, **55**, 372 (1983).

38. R. F. Browner, D. D. Smith, **Anal. Chem.**, **55**, 373 (1983).

39. A. Gustavsson, **Spectrochim. Acta**, **39B**, 743 (1984).

40. A. Gustavsson, **Spectrochim. Acta**, **41B**, 291 (1986).

41. M. S. Cresser, R. F. Browner, **Spectrochim. Acta**, **35B**, 73 (1980).

42. L. R. Layman, F. E. Lichte, **Anal. Chem.**, **54**, 638 (1982).

43. S. D. Olsen, A. Strashein, **Spectrochim. Acta**, **38B**, 973 (1983).

44. R. K. Skogerboe, S. J. Freeland, **Appl. Spec.**, **39**, 920 (1985).

45. H. Z. Zhuang, R. M. Barnes, **Spectrochim. Acta**, **40B**, 11 (1985).

46. R. K. Skogerboe, S. J. Freeland, **Appl. Spec.**, **39**, 6, 916 (1985).

47. M. W. Routh, J. E. Goulter, D. B. Tasker, S. D. Arellano, **American Laboratory**, 98, February (1987).

48. J. A. Borowiec, A. W. Boorn, J. H. Dillard, M. S. Cresser, R. F. Browner, **Anal. Chem.**, **52**, 1054 (1980).

49. R. K. Skogerboe, S. J. Freeland, **Appl. Spec.**, **39**, 6, 925 (1985).

50. S. W. McGeorge, E. D. Salin, **Appl. Spec.**, **39**, 6, 989 (1985).

51. D. E. Dobb; D. R. Jenke, **Appl. Spec.**, **37**, 378 (1983).

52. M. H. Ramsey, M. Thompson, B. J. Coles, **Anal. Chem.**, **55**, 1626 (1983).

53. A. W. Boorn, R. F. Browner, **Anal. Chem.**, **54**, 1402 (1982).

54. D. D. Nygaard, R. G. Schleicher, J. J. Sotera, **Appl. Spec.**, **40**, 7, 1074 (1986).

55. T. J. Brotherton, B. S. Barnes, N. Vela, J. A. Caruso, **Journal of Atomic Analytical Spectrometry**, submitted October 1986.

56. J. R. Garbarino, H. E. Taylor, **Appl. Spec.**, **34**, 5584 (1980).

57. T. J. Brotherton, J. A. Caruso, **Journal of Atomic Analytical Spectrometry**, submitted December 1986.

58. D. H. Tracy, S. A. Myers, B. G. Balista, **Spectrochim. Acta**, **37B**, 739 (1982).

59. S. J. Walton, J. E. Goulter, **Analyst**, **110**, 531 (1985).

60. R. S. Babington, U.S. Patent #3,421,692 (1969).

61. R. F. Suddendorf, K. W. Boyer, **Anal. Chem.**, **50**, 1769 (1978).

62. B. Thelin, **Analyst**, **106**, 54 (1981).

63. Ebdon, M. R. Cave, **Analyst**, **107**, 172 (1982).

64. N. Mohamed, R. C. Fry, **Anal. Chem.**, **53**, 450 (1981).

65. M. D. Wichman, R. C. Fry, N. Mohammed, **Appl. Spec.**, **37**, 254 (1983).

66. B. R. Baginski, J. E. Meinhard, **Appl. Spec.**, **38**, 568 (1984).

67. C. T. Apel, T. M. Bieniewski, L. E. Cox, D. W. Steinlaos, **ICP Inf. Newsl.**, **3**, 1 (1977).

68. C. T. Apel, D. V. Duchane, Pittsburgh Conference on Analytical Chemistry and Applied Spectroscopy, paper 411, 1979.

69. I. M. Ibrahim, W. Nisamaneepong, D. L. Haas, J. A. Caruso, **Spectrochim. Acta**, **40B**, 385 (1985).

70. M. Ibrahim, T. Gilbert, J. A. Caruso, **J. of Chrom. Science**, **22**, 111 (1984).

71. W. Nisamaneepong, D. L. Haas, J. A. Caruso, **Spectrochim. Acta, 40B,** 3 (1985).

72. R. H. Wendt, V. A. Fassel, **Anal. Chem., 37,** 920 (1965).

73. P.W.J.M. Boumans, F. J. de Boer, **Spectrochim. Acta, 30B,** 309 (1975).

74. K. W. Olson, W. J. Haas, Jr., V. A. Fassel, **Anal. Chem., 49,** 632 (1977).

75. C. E. Taylor and T. L. Floyd, **Appl. Spec., 35,** 408 (1981).

76. P. D. Goulden, D.H.J. Anthony, **Anal. Chem., 56,** 2327 (1984).

77. P.W.J.M. Boumans, F. J. de Boer, **Spectrochim. Acta, 31B,** 355 (1976).

78. P. Schramel, **Spectrochim. Acta, 38B,** 199 (1983).

79. M. P. Doherty and G. M. Hieftje, **Appl. Spec., 38,** 405 (1984).

80. V. A. Fassel, B. R. Bear, **Spectrochim. Acta, 41B,** 1089 (1986).

81. M. P. Doherty, G. M. Hieftje, **Appl. Spec., 38,** 3, 405 (1984).

82. K. E. Lawrence, G. W. Rice, V. A. Fassel, **Anal. Chem.,** 289 (1984).

83. K. E. La Freniere, G. W. Rice, V. A. Fassel, **Spectrochim. Acta, 40B,** 1495 (1985).

84. T. Kantor, **Spectrochim. Acta, 38B,** 1483 (1983).

85. A. Sugimae, R. M. Barnes, **Anal. Chem., 58,** 785 (1986).

86. K. C. Ng, J. A. Caruso, **Appl. Spec., 39,** 719 (1985).

87. B. Pahlavanpour, M. Thompson, L. Thorne, **Analyst, 106,** 467 (1981).

88. T. Nakahara, **Appl. Spec., 37,** 539 (1983).

89. M. A. Eckhoff, J. P. McCarthy, J. A. Caruso, **Anal. Chem., 54,** 165 (1982).

90. M. H. Hahn, K. A. Wolnik, F. L. Fricke, J. A. Caruso, **Anal. Chem., 54,** 1048 (1982).

91. R. M. Dagnall, D. J. Smith, T. S. West, S. Greenfield, **Anal. Chim. Acta, 54,** 397 (1971).

92. K. C. Ng, M. Zerezghi, J. A. Caruso, **Anal. Chem., 56,** 417 (1984).

93. H. Benli, **Spectrochim. Acta, 38B,** 81 (1983).

94. P. W. Beckwith, R. L. Mullins, D. M. Coleman, **Anal. Chem., 59,** 163 (1987).

95. R. D. Deutsch, G. M. Hieftje, **Appl. Spec.**, **37**, 101 (1983).

96. P. B. Farnsworth, G. M. Hieftje, **Anal. Chem.**, **55**, 1417 (1983).

97. G. M. Allen, D. M. Coleman, **Appl. Spec.**, **41**, 381 (1987).

98. J. W. Carr, G. Horlick, **Spectrochim. Acta**, **37B**, 1 (1982).

99. M. Thompson, J. E. Goulter, F. Sieper, **Analyst**, **106**, 32 (1981).

100. T. Ishizuka, Y. Uwamino, **Spectrochim. Acta**, **38B**, 519 (1983).

101. C. V. Monasterios, A. M. Jones, E. D. Salin, **Anal. Chem.**, **58**, 780 (1986).

102. D. W. Boomer, M. Powell, R.L.A. Sing, E. D. Salin, **Anal. Chem.**, **58**, 975 (1986).

103. R.L.A. Sing, Ph.D. Dissertation, McGill University, Montreal, Quebec, Canada (1987).

CHAPTER 2

USE OF THE GRID NEBULIZER FOR ORGANIC SOLVENT INTRODUCTION INTO THE ICP

2.1 INTRODUCTION

One of the active areas of analytical research is the quantitative determination of metal species in a variety of samples. The increased commercial availability of reasonably priced systems for inductively-coupled plasma (ICP) spectrometry in the past several years has heightened interest in exploring their usefulness for difficult and complex sample analyses. The ICP is sensitive for metal detection, and a large number of elements can be simultaneously excited under one set of conditions.[1-3] The selectivity of spectrometric techniques for metal species and the potential for obtaining speciation information (i.e. chromatographic separation with ICP detection) make the ICP particularly attractive. Matrix effects and interferences, which can pose serious problems with atomic absorption (AA) and DC emission, are reduced or eliminated. In addition, the ICP offers linear dynamic ranges up to five orders of magnitude.

There are several methods of sample introduction into an ICP, the most common being pneumatic nebulization of liquid samples. These pneumatic nebulizers can be a limiting factor in ICP emission spectrometry. Both cross flow and concentric nebulizers exhibit short-term noise, long-term drift and are inefficient in sample transport.[4] Since these nebulizers produce a wide range of droplet sizes, large droplets are lost

during aerosol transport, resulting in inefficient sample delivery.[5]

The glass frit nebulizer operates by passing gas through a sintered frit. The sample liquid passes over the frit and the carrier gas shears the liquid into a fine aerosol. The glass frit nebulizer is highly efficient and has been used for organic solvent sample introduction.[6] The glass frit nebulizer, however, exhibits memory effects and can also become clogged when aspirating solutions with high dissolved solids.

The Hildebrand grid nebulizer design features a fine mesh grid of inert material positioned in front of a high velocity argon stream. Sample is introduced to the grid through a large cross section tube, and the liquid flows over the grid past the stream of high velocity gas. Nebulization takes place as a result of shearing from the wetted surface.

When the nebulizer becomes the interface in a liquid chromatography ICP system, certain factors must be considered. Aerosol droplet size must be optimized and solvent loading minimized and carefully controlled to maximize reproducibility and accuracy. In addition, since only a small percentage (<5% usually) of the analyte species is actually utilized, the sample introduction system's design and separating conditions must be carefully chosen so that peak broadening and tailing are not a problem, memory effects are minimized, and spray chamber washout is rapid and quantitative with rapid drainage of waste from the spray chamber.

The tolerance of the ICP for the mobile phase must be taken into account. Many of the commonly used mobile phases for normal and reversed-phase HPLC, such as methanol, acetonitrile, and hexane, are not readily accepted by the ICP. Boorn and Browner have made a quantitative study of the effects of organic solvents on the ICP.[7] They related

the "limiting aspiration rate" (LAR) of a solvent to the evaporation factor (rate of solvent evaporation) for the solvent. They reported that with some exceptions, as the evaporation factor increases, the limiting aspiration rate decreases. Boorn and Browner also determined from signal enhancement studies that organic solvent vapor causes increases in the ratio of atom line to ion line intensities, indicating a decrease in plasma excitation temperatures. Blades and Caughlin found that an ICP with organic aerosol has excitation temperatures similar to an ICP with aqueous aerosol operating at 0.5 kilowatts lower rf input power.[8] The use of higher forward power (to ca. 1.75 kW) to aid in the decomposition of solvent vapor increases the tolerance of the ICP to most organic solvents. The limiting aspiration rates for some organic solvents as determined by Boorn and Browner are listed in Table 2-1.

Furthermore, in order to optimize analytical performance, other plasma parameters must be carefully chosen. While higher incident power helps in degradation of the organic matrix, background emission also increases because of the presence of band and line emission from the solvent. Net analyte emission may or may not be improved with increased power, depending upon the excitation potentials of the analyte species. Analyte emission intensity is also affected by the diameter of the injector and by nebulizer gas flow rate, which may cool the plasma due to solvent vapor loading and decreased residence time at high flow rates.[9]

There is an increasing amount of work appearing which describes utilizing the ICP-OES for liquid chromatographic detection. The bulk of this work describes ion exchange chromatography using aqueous solutions as mobile phases and gel permeation or size exclusion chromatography

Table 2-1

Limiting Aspiration Rates (LAR) for Organic Solvents*
(from reference 7)

Solvent	LAR (mL/min)
Methanol	0.1
Ethanol	2.5
Propanol	3.0
Butanol	5.0
Hexane	0.1
Toluene	1.0
Xylene	4.0
4-Methylpentan-2-one	3.0
Pyridine	1.0
Acetonitrile	0.2

*ICP operating conditions: 1.75 KW rf power, 12 L/min Ar coolant flow, 2.0 L/min Ar auxiliary flow; cross flow nebulizer at 1.0 L/min.

with aqueous solutions, toluene or xylenes as mobile phases.[10-15] The limiting aspiration rates determined by Boorn and Browner for these organic solvents (toluene, xylene, MIBK) are at least 1 mL/min and their introduction into the ICP poses few problems. Little has been reported using methanol, acetonitrile, or hexane, which all have limiting aspiration rates of 0.2 mL/min or less. Ibrahim et al. performed reversed-phase separations of alkyllead compounds using 90% methanol, 85% methanol, and 100% acetonitrile with a glass frit nebulizer.[16] Tetraalkyllead compounds were also analyzed by reversed-phase HPLC using ethanol-water, butanol-ethanol-water, and ethanol-propanol-water mixtures.[17]

The objective of this study is to determine the suitability of the Hildebrand nebulizer for high evaporation rate organic solvents. The organic solvents used were 70% methanol, 100% methanol, and 70% acetonitrile. The parameters of power and spray chamber design were varied to determine:

1. Limiting aspiration rate
2. Detection limits of a variety of metals
3. Solvent transport efficiency
4. Linear dynamic range of emission intensity with concentration

2.2 EXPERIMENTAL

2.2.1 Instrumentation

The experiments were carried out using a Leeman Labs Plasma Spec ICP 2.5 (Leeman Labs, Lowell, MA). The Plasma Spec is an echelle grating spectrometer and uses a free running tuned cavity oscillator as the rf power supply.

One feature of the Leeman Labs ICP instrument which distinguishes it from most other instruments commercially available in the United

States is the rf power supply used. The majority of instruments manufactured use crystal-controlled, constant frequency generators which operate with a constant output impedance. The Leeman Labs ICP power supply is a free running tuned cavity oscillator. Constant foward rf power is maintained by slightly changing the rf frequency to account for changes in plasma impedance and plasma coupling[18,19] that are most notable when organic solvents are introduced into the plasma. The operation and technical requirements for these generators have been discussed by Linn.[20] The merits of the different types of power sources have been presented by Greenfield et al.[21]

Some minor modifications were made to the Leeman Labs instrument for this work. Solution uptake was with a Gilson Minipuls-2 peristaltic pump (Rainin Instruments Co., Woburn, MA) using PVC manifold pump tubing, which was calibrated prior to use.

The Hildebrand nebulizer used was supplied and developed by Leeman Labs. Figure 2-1 depicts this nebulizer as well as others used in the study.

Initial experiments with a Scott spray chamber indicated that it was not well suited for organic solvents due to long wash out periods. Three pyrex conical spray chambers locally made by Thomas Scientific Inc. were used instead. These spray chambers are shown in Figure 2-2. A Neslab recirculation cooler (Model RTE-8) was used for the temperature study.

Reagent grade methanol and HPLC grade acetonitrile were obtained from Fisher Scientific. Mixed organic solvents (70% methanol and 70% acetonitrile were prepared by mixing 7 parts organic solvent measured with a graduated cylinder with 3 parts distilled deionized water.

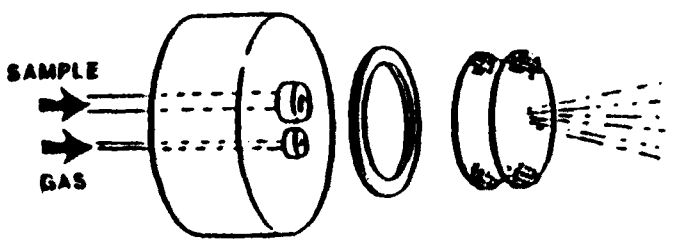

HILDEBRAND

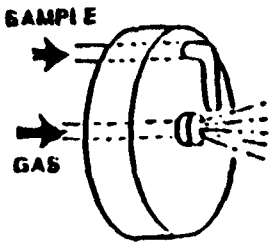

CROSS FLOW

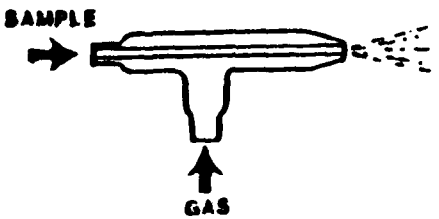

CONCENTRIC

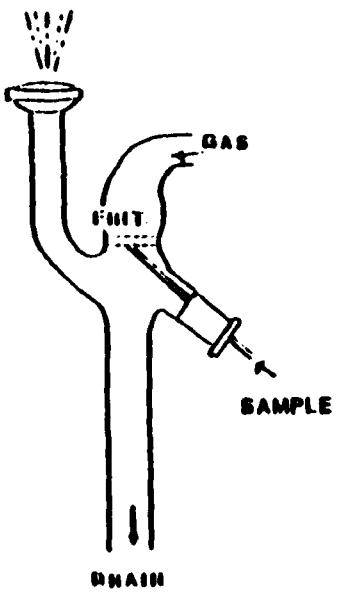

GLASS FRIT

Figure 2-1. Several Types of Nebulizers

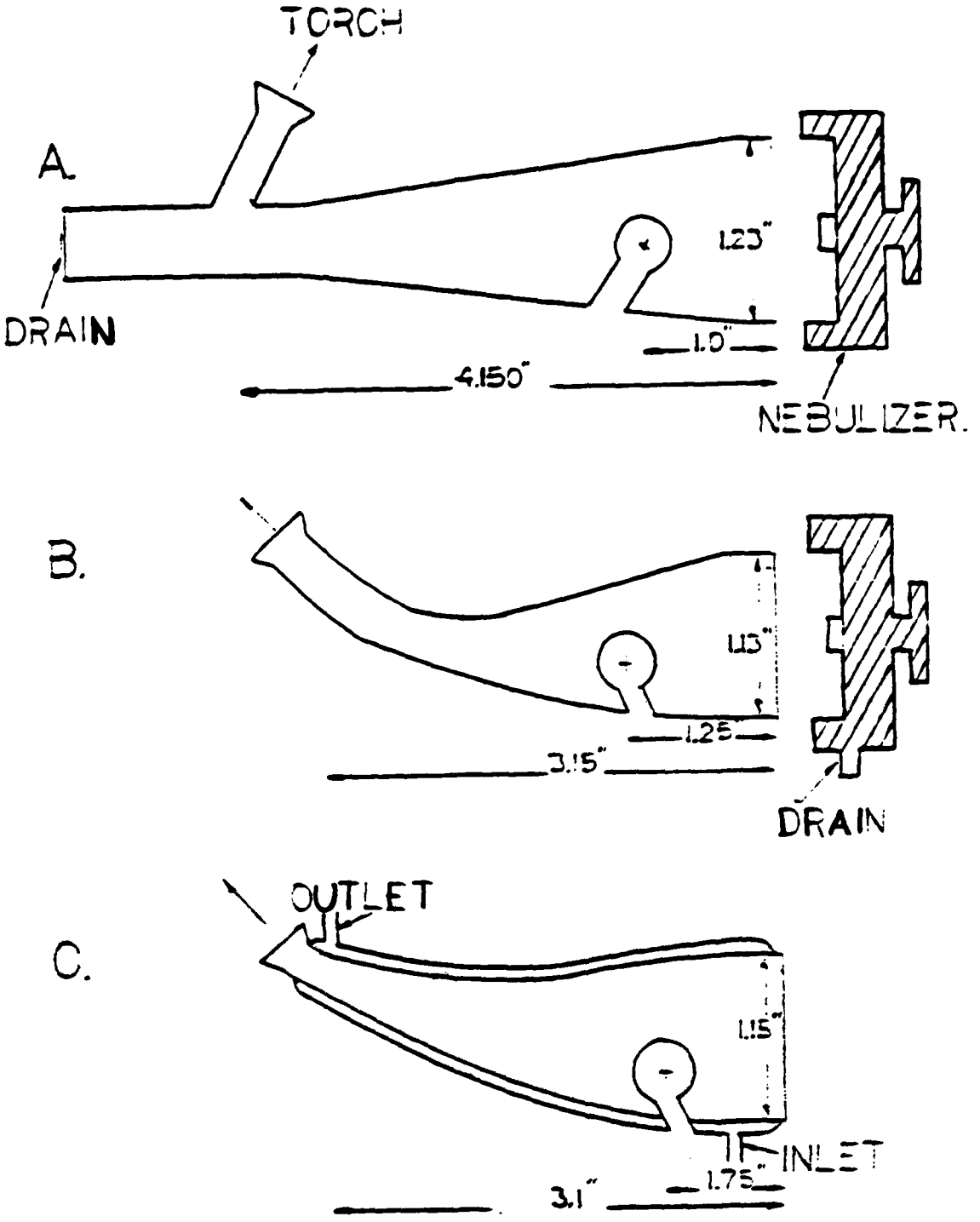

Figure 2-2. A. Conical Pyrex Spray Chamber; B. Mini-Pyrex; C. Cooled Mini-Pyrex

Metal solutions were prepared and stored in glassware that had been rinsed in nitric acid and the organic solvent prior to use. Standard solutions were prepared by serial dilutions of certified atomic absorption standards (Fisher Scientific).

2.2.2 Optimizing ICP Viewing Conditions

In performing sequential multielement detection, compromise viewing conditions must be used, since optimum viewing height is not the same for all elements. The Leeman Labs Spectrometer automatically maximizes the signal intensity of one particular element in both the horizontal and vertical directions by initializing the auto peaking function of the instrument. In this study Cu was the element that was optimized when using the sequential multielement mode.

2.3 RESULTS AND DISCUSSION

2.3.1 Limiting Aspiration Rate (LAR)

Boorn and Browner described limiting aspiration rate as that rate which results in "stable plasma operation with no appreciable carbon deposition on the inner torch...".[7] The objectives of this work were to determine the effect of power and spray chamber design on the limiting aspiration rates of 70% methanol, 100% methanol, 70% acetonitrile (ACN) for a given set of plasma operating conditions. These operating conditions are given in Table 2-2. All elements were detected in the Sequential Multielement Mode using compromise plasma viewing conditions.

2.3.2 Procedure

To determine the limiting aspiration rate for an organic solvent, the procedure used was as follows. After plasma ignition and during warm-up, water was nebulized into the plasma. Organic solvent was then nebulized into the plasma. The limiting aspiration rate was taken to be

Table 2-2

Standard ICP Operating Conditions

Plasma Power	1.0-1.5 Kilowatts
Coolant Flow	17.5 L/min
Auxiliary Flow	1.5 L/min (with acetonitrile only)
Nebulizer Flow	0.5 L/min
Wavelength Monitored	nm
Mn II	257.61
Cu I	324.75
Zn I	213.86
Cd II	214.44
Ni II	221.65

that which gave a stable plasma with no carbon deposited on either the torch or the injector tube after thirty minutes operation. In all experiments, it was observed that the limiting aspiration rates, measured as solution uptake rates, produced stable plasmas during several hours' operation.

2.3.3 Plasma Conditions

Plasma conditions also greatly affect how much organic solvent can be aspirated. **Tables 2-3, 2-4,** and **2-5** show that for 70% methanol, LAR increases significantly with increase in power. For 100% methanol and 70% ACN, LAR is not greatly affected by increase in rf power. Increased argon coolant flow results in a much more stable plasma, which in turn increases the LAR. Increasing the argon coolant flow rate from 17.5 L/min to 30 L/min resulted in an increase in LAR from 0.1 to 0.2 mL/min of 100% methanol with the cooled spray chamber. Increasing the nebulizer gas flow will result in a higher LAR, but this has the concomitant effect of decreasing residence time of the analyte in the plasma and thus reducing the overall emission intensity.

2.3.4 Spray Chamber

The Hildebrand nebulizer was used with a mini-pyrex, a large pyrex and a cooled mini-pyrex spray chamber. Tap water was used for the cooled spray chamber and the temperature was approximately 25^{o}C. **Figures 2-2a-c** depict these spray chambers.

Tables 2-3, 2-4, and **2-5** show the limiting aspiration rates (LAR) for 70% methanol, 100% methanol and 70% ACN at powers of 1.0, 1.25, 1.5 kW for the three spray chambers tested. These data indicate that for 100% methanol and 70% ACN, LAR is not greatly affected by different spray chamber design. The LAR is approximately 0.1 mL/min for all the spray

Table 2-3

Limiting Aspiration Rates (mL/min) for 70% MeOH
(Hildebrand Nebulizer)

Spray Chamber	Power (KW)		
	1.0	1.25	1.50
Mini-Pyrex	< 0.1	< 0.1	0.1
Large Pyrex	< 0.1	0.2	0.3
Cooled Mini-Pyrex(25°C)	0.1	0.3	0.5

Table 2-4

Limiting Aspiration Rates (mL/min) for 100% MeOH
(Hildebrand Nebulizer)

Spray Chamber	Power (KW)		
	1.0	1.25	1.50
Mini-Pyrex	< 0.1	< 0.1	0.1
Large Pyrex	< 0.1	0.1	0.1
Cooled Mini-Pyrex(25°C)	< 0.1	0.1	0.1

Table 2-5

Limiting Aspiration Rates (mL/min) for 70% Acetonitrile
(Hildebrand Nebulizer)

Spray Chamber	Power (KW)		
	1.0	1.25	1.50
Mini-Pyrex	< 0.1	< 0.1	0.1
Large Pyrex	< 0.1	0.1	0.1
Cooled Mini-Pyrex(25°C)	0.1	0.1	0.1

chambers. For 70% methanol, higher LAR's are achieved with a larger spray chamber or with a cooled spray chamber.

2.3.5 Solvent

With some exceptions, as the evaporation factor of a particular solvent increases, the limiting aspiration rate decreases.[7] As will be described later, as the evaporation factor of a solvent increases, the solvent transport efficiency (STE) increases. Unfortunately, this increase in efficiency results in an increased solvent vapor loading to the plasma, which is the major factor influencing plasma stability. The instability with methanol and ethanol results from the gradual quenching of the plasma core from beneath the coil. Plasma stability is greatly enhanced by use of a cooled spray chamber.[22] Though the LAR for 100% methanol and 70% ACN, when aspirated through the water cooled mini-pyrex spray chamber, is not much different from the non-cooled mini-pyrex spray chamber, the plasma was much more stable.

For 70% ACN the LAR was not so much a function of plasma stability as carbon deposition on the torch. Higher flow rate of 70% ACN could be achieved without extinguishing the plasma, but as flow was increased, carbon quickly deposited on the inner torch and injector. An auxiliary flow of 1.5 L/min was used to minimize carbon deposition.

Figure 2-3 shows the effect of spray chamber cooling temperature on the LAR. In the temperature range 20°C to -8°C, the LAR of methanol increased from approximately 0.1 mL/min to almost 0.5 mL/min; the LAR of 70% ACN increased from approximately 0.1 at 20°C to 0.3 mL/min at -10°C. The LAR of 70% methanol also increased significantly. By cooling the spray chamber to about -10°C, the solvent vapor is efficiently condensed, therefore, increasing the ratio of aerosol transport to solvent

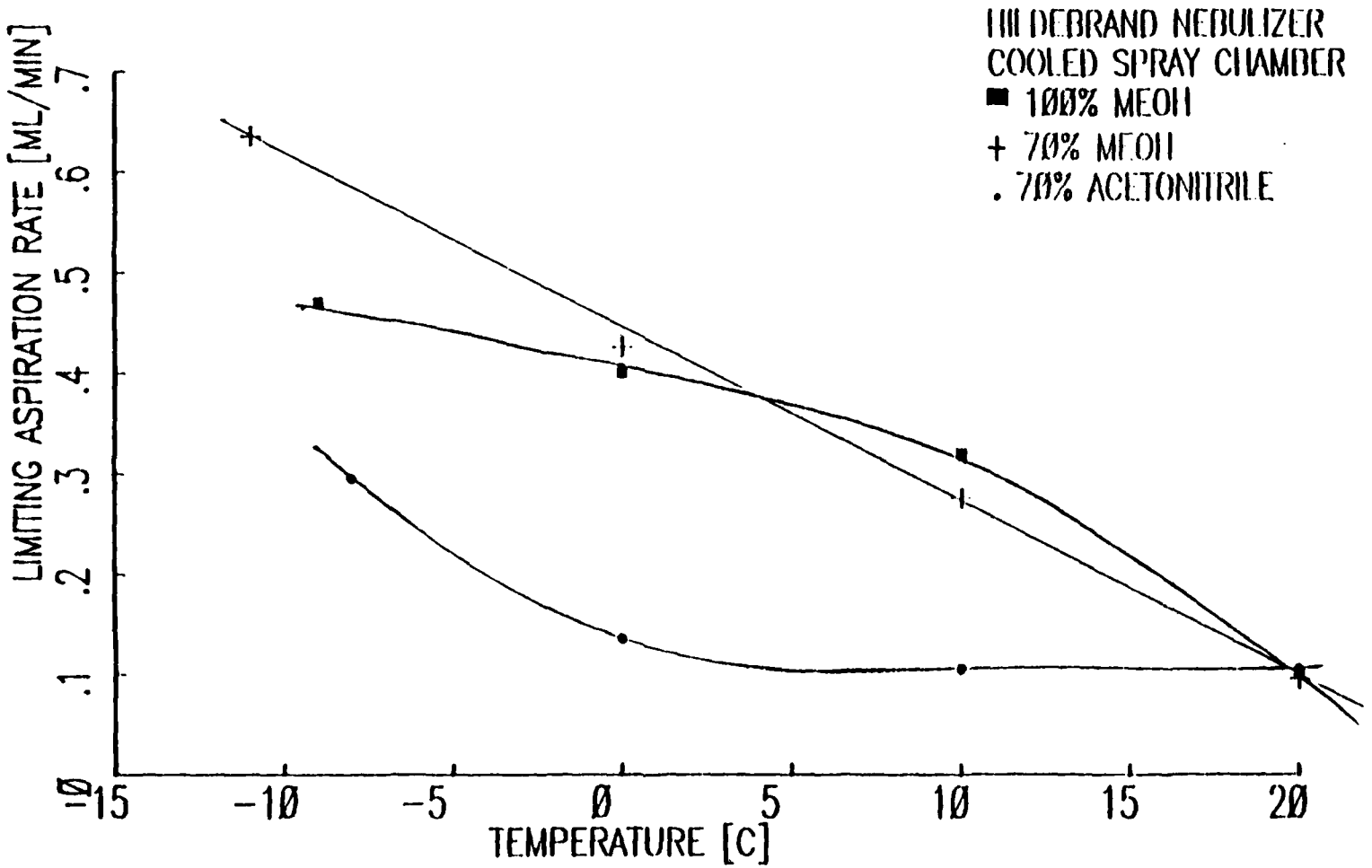

Figure 2-3. Temperature vs. Limiting Aspiration Rate

vapor transport.

2.4 Nebulizer Comparison

A comparison of the various types of nebulizers is presented in **Table 2-6.** The data indicate that LAR is not greatly affected by increasing rf power. The highest LAR's are achieved with the Hildebrand and glass frit nebulizers. The particular Meinhard concentric nebulizer (C2, without spray chamber cooling) that we used was judged unsatisfactory for volatile solvent introduction because the LAR's for all solvents with this nebulizer were much less than 0.1 mL/min. The cross-flow nebulizer could be used with volatile organic solvents, but the LAR's for the cross flow for all solvents were ca. 0.1 mL/min or less.

2.5 Detection Limits

The 3σ detection limits were calculated from a total of 25 data points. Since the data were acquired in the sequential multielement mode, compromise viewing conditions were used. Improved detection limits could be obtained by using viewing conditions optimized for each element.

For each solvent, the Hildebrand nebulizer was used with three different spray chambers and for each spray chamber three powers were studied (except for ACN). **Tables 2-7, 2-8** and **2-9** show the various detection limits. The primary reason detection limits are improved (as shown in **Tables 2-7, 2-8,** and **2-9**), when using the water cooled spray chamber ($25^{o}C$), is because the plasma is much more stable. Plasma flicker is minimized and the background is relatively constant. The real improvement in detection is achieved when the temperature of the spray chamber is reduced to the point where a maximal amount of the solvent vapor is condensed. This results in increasing the solution uptake rate

Table 2-6

Comparison of Limiting Aspiration Rates (mL/min)

Spray Chamber	Nebulizer	Power (KW) 1.0	1.25	1.5
70% MeOH				
Pyrex	Hildebrand	< 0.1	0.2	0.3
	Cross Flow	< 0.1	< 0.1	< 0.1
	Concentric	< 0.1	< 0.1	< 0.1
Water Cooled Chamber (25°C)	Hildebrand	0.1	0.3	0.5
	Cross Flow	< 0.1	0.1	0.1
	Concentric	< 0.1	< 0.1	< 0.1
---	Glass Frit	0.1	0.3	0.3
100% MeOH				
Pyrex	Hildebrand	< 0.1	0.1	0.1
	Cross Flow	< 0.1	< 0.1	< 0.1
	Concentric	< 0.1	< 0.1	< 0.1
Water Cooled Chamber (25°C)	Hildebrand	< 0.1	0.1	0.1
	Cross Flow	< 0.1	< 0.1	< 0.1
	Concentric	< 0.1	< 0.1	< 0.1
---	Glass Frit	0.1	0.1	0.2
70% ACN				
Pyrex	Hildebrand	< 0.1	0.1	0.1
	Cross Flow	< 0.1	< 0.1	< 0.1
	Concentric	< 0.1	< 0.1	< 0.1
---	Glass Frit	< 0.1	< 0.1	< 0.1
Water Cooled Chamber (25°C)	Hildebrand	0.1	0.1	0.1
	Cross Flow	--	--	--
	Concentric	< 0.1	< 0.1	< 0.1

Table 2-7

Detection Limits 70% MeOH (ppb)*

Element	Spray Chamber	Power (KW)		
		1.0	1.25	1.50
Mn	Large	57.0	67.0	37.0
	Mini	132	59.6	48.0
	Cooled	10.7	4.6	4.2
Cu	Large	523	299	301
	Mini	410	174	280
	Cooled	86.5	8.9	63.7
Zn	Large	149	79.6	49.0
	Mini	123	96.3	119
	Cooled	29.3	10.3	3.3
Cd	Large	72.0	73.0	48.0
	Mini	106	66.7	67.8
	Cooled	16.8	3.0	3.3
Ni	Large	ND	210	154
	Mini	281	167	118
	Cooled	111	12.2	30.0

*The cooled spray chamber was cooled with tap water at approximately 25°C.

Table 2-8

Detection Limits 100% MeOH (ppb)*

Element	Spray Chamber	Power (KW)		
		1.0	1.25	1.50
Mn	Large	87.1	18.5	13.1
	Mini	227	8.3	17.3
	Cooled	3.3	7.2	6.8
Cu	Large	1000	541	194
	Mini	ND	36.5	213
	Cooled	34.2	57.3	119
Zn	Large	95.0	34.3	23.1
	Mini	ND	34.4	72.0
	Cooled	20.3	44.1	34.0
Cd	Large	77.9	24.9	15.7
	Mini	346	13.8	25.1
	Cooled	24.9	9.6	7.7
Ni	Large	443	146	71.5
	Mini	591	50.1	104
	Cooled	22.6	59.8	80.5

*The cooled spray chamber was cooled with tap water at approximately 25°C.

Table 2-9

Detection Limits 70% Acetonitrile (ppb)*

Element	Spray Chamber	Power (KW)		
		1.0	1.25	1.50
Mn	Large	16.4	20.4	11.6
	Mini	8.6	13.0	18.3
	Cooled	2.3	NA	NA
Cu	Large	135	288	123
	Mini	121	187	175
	Cooled	13.6	NA	NA
Zn	Large	51.8	34.8	35.1
	Mini	80.7	137	36.7
	Cooled	13.2	NA	NA
Cd	Large	23.1	23.2	11.6
	Mini	39.9	21.1	19.7
	Cooled	4.5	NA	NA
Ni	Large	163	63.8	9.1
	Mini	147	116	118
	Cooled	25.7	NA	NA

*The cooled spray chamber was cooled with tap water at approximately 25°C.

and thus having more analyte containing aerosol reach the plasma.

Detection limits are most dependent upon analyte mass transported to the plasma. The best detection limits are achieved by using a cooled spray chamber with a refrigerated recirculating bath. This improves detection limits by removing some of the solvent vapor, for the reasons mentioned above, and allows a higher solution uptake. Table 2-10 shows the detection limits of a variety of metals at different spray chamber temperatures. The sequential multielement viewing conditions were used. The data indicate that as spray chamber temperature decreases, detection levels improve. Table 2-11 shows a list of detection levels obtained by optimizing viewing conditions and using a cooled spray chamber. The enhanced detection limits result from optimizing plasma viewing locations for each particular element using the sequential single mode of the Plasma Spec 2.5 ICP.

2.6 Transport Studies

There are both direct and indirect methods to determine nebulizer efficiency. Direct methods include filter collection such as used by Olson et al.[23] and Smith and Browner, cascade impactor measurements,[24] and a silica gel collection system used by Ripson and De Galan.[25] Indirect methods involve mass or volume measurements of the inlet and outlet of the nebulizer.

Comparing the results of an indirect method with a direct method can result in positive bias error of as much as 300% according to Browner and Smith.[26,27] Gustavsson reports a positive bias error ranging from 50 to 130%.[28]

IUPAC defines nebulization efficiency (ε_n) as (analyte entering the flame)/(analyte aspirated). If solvent vapor transport to the plasma is

Table 2-10

Detection Limits at Various Spray Chamber Temperatures (ppb)*
100% MeOH

Element	Temperature (°C)			
	-8	0	10	20
Mn	4.5	4.1	8.0	25.0
Cu	46.1	72.7	126	550
Zn	16.6	15.1	28.8	71.5
Cd	6.8	7.2	20.6	30.2
Ni	24.3	35.1	86.1	126

*ICP operating conditions: 1.0 kW rf, 15 L/min Ar coolant flow, in 0.5 L/min nebulizer flow; Hildebrand nebulizer.

Table 2-11

Detection Limits Optimum Conditions (ppb)*

Spray Chamber	Element	Solvent		
		70% MeOH	100% MeOH	70% ACN
Cooled Mini-Pyrex	Mn	0.45	1.2	1.5
	Cu	9.4	6.1	8.4
	Zn	4.3	5.7	6.1
	Cd	1.3	1.7	6.2
	Ni	8.1	24.8	8.9

*ICP Operating Conditions: 1.25 KW rf, 30 L/min Ar coolant flow, 1.5 L/min Ar auxiliary flow (ACN only), 0.5 L/min Ar nebulizer flow; Hildebrand nebulizer, cooled spray chamber (0°C for 70% MeOH and 70% ACN, -8°C for 100% MeOH).

minimal, one can approximately equate nebulization efficiency to aerosol transport efficiency. However, in our studies since efficiencies were determined for a variety of volatile organic solvents, one cannot assume that solvent vapor transport is minimal. In fact, without cooling the spray chamber, solvent vapor transport can exceed aerosol transport to the plasma for volatile solvents such as methanol and acetonitrile. Thus, we defined solvent transport efficiency (STE) as the percentage of solvent pumped through the nebulizer that reaches the plasma. STE is determined indirectly by the following calculation:

$$STE = 1 - \frac{\text{(weight solution in drain)}}{\text{(weight feed solution pumped)}}$$

2.6.1 Procedure

The following indirect method represents a procedure by which an empirical measure of solvent transport efficiency can be used to compare the effect of spray chamber temperature, spray chamber design, organic solvent and flow rate.

The procedure used to calculate solvent transport efficiency studies is as follows. Solutions of 1 ppm Cd, Mn, Zn, Ni and Cu were made up with 70% methanol, 100% methanol and 70% ACN. The solutions were pumped into the ICP for approximately 20 minutes, while at the same time, the spray chamber was pumped out. Meanwhile, a closed container containing the same solution (feed) was weighed. Likewise, an empty closed container (drain) was weighed. It was assumed that after ca. 20 minutes steady state was achieved within the spray chamber and there was neither accumulation nor depletion of solution. At this point, both the feed pump and drain pumps were turned off momentarily, and the inlet manifold tubing was connected to the feed bottle and the outlet manifold tubing was connected to the drain. Both pumps were switched on and after 60 min

utes, both the feed and drain container were weighed. **Figure 2-4** depicts the experimental arrangement.

The drain was analyzed for Mn, Cd, Zn, Ni and Cu. An analyte transport efficiency (ATE) was calculated to show the efficiency of analyte transport relative to the total solvent transport efficiency. The analyte transport efficiency was calculated.

$$ATE = STE \times \frac{(\text{Feed Concentration})}{(\text{Drain Concentration})}$$

2.6.2 Parameters Affecting Efficiency

The efficiency of a nebulizer is a function of spray chamber design, temperature, solvent being aspirated and the liquid and gas flow rates. **Figure 2-5** shows the effect of solution uptake rate versus solvent transport efficiency for 2% nitric acid. As flow rate is increased, nebulization efficiency decreases. However, the total amount of aerosol and solvent vapor reaching the plasma reaches a maximum at approximately 1.6 mL/min. As can be seen by **Figure 2-6**, higher solution uptake rate does not necessarily mean higher mass (aerosol and solvent vapor) transport to the plasma.

Figure 2-7 shows solvent transport efficiency with a pyrex conical spray chamber at various flow rates. The Hildebrand nebulizer is 100% efficient for 100% methanol and 70% efficient for acetonitrile with a pyrex spray chamber. Unfortunately, a large amount of solvent vapor reaches the plasma and results in much poorer detection limits.

Figure 2-8 shows the effect of spray chamber temperature for a constant flow rate on efficiency of the nebulizer for 70% methanol, 100% methanol and 70% ACN. As temperature increases, nebulizer efficiency increases. For volatile organic solvents, increase in efficiency means more solvent vapor reaching the plasma. Ideally, one would like to

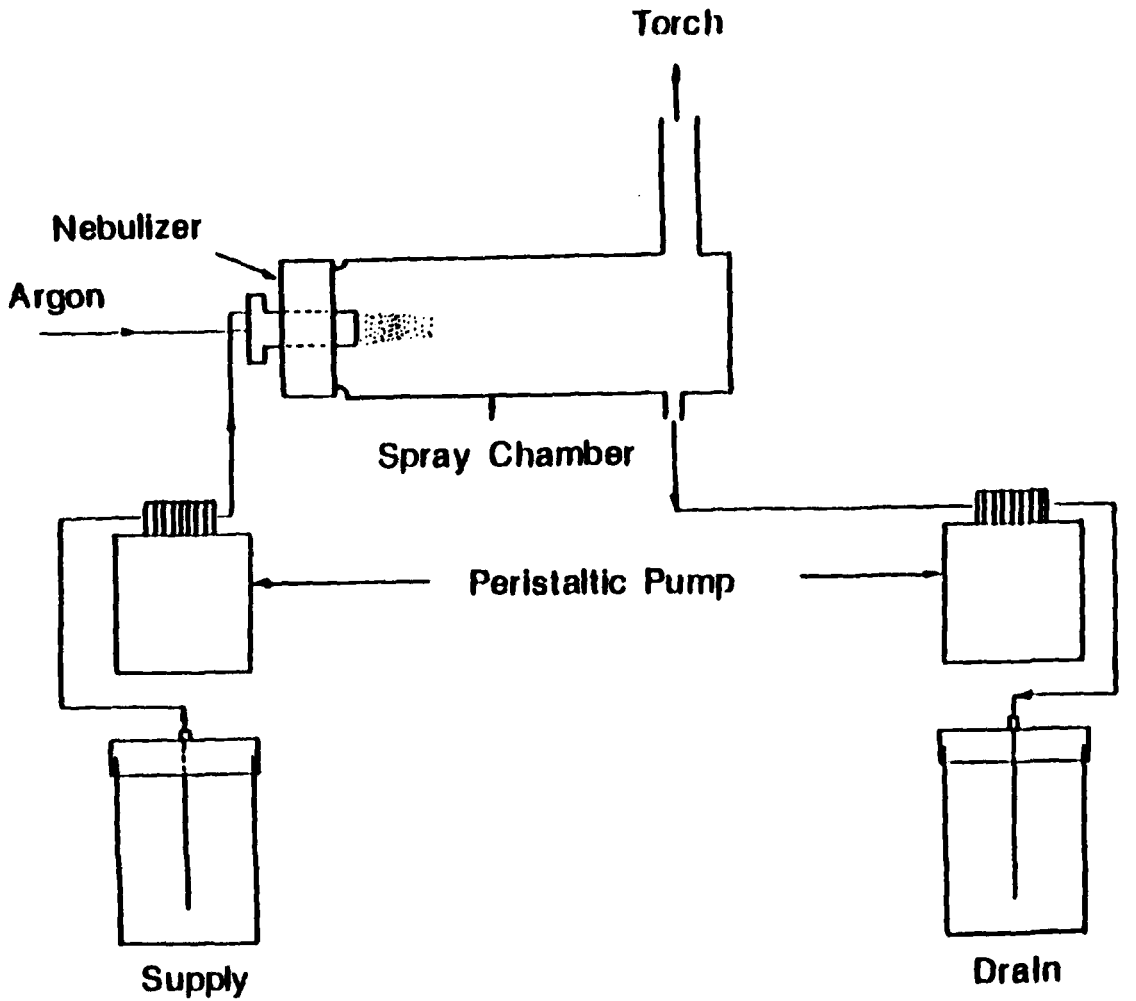

Figure 2-4. Block Diagram for Efficiency Study

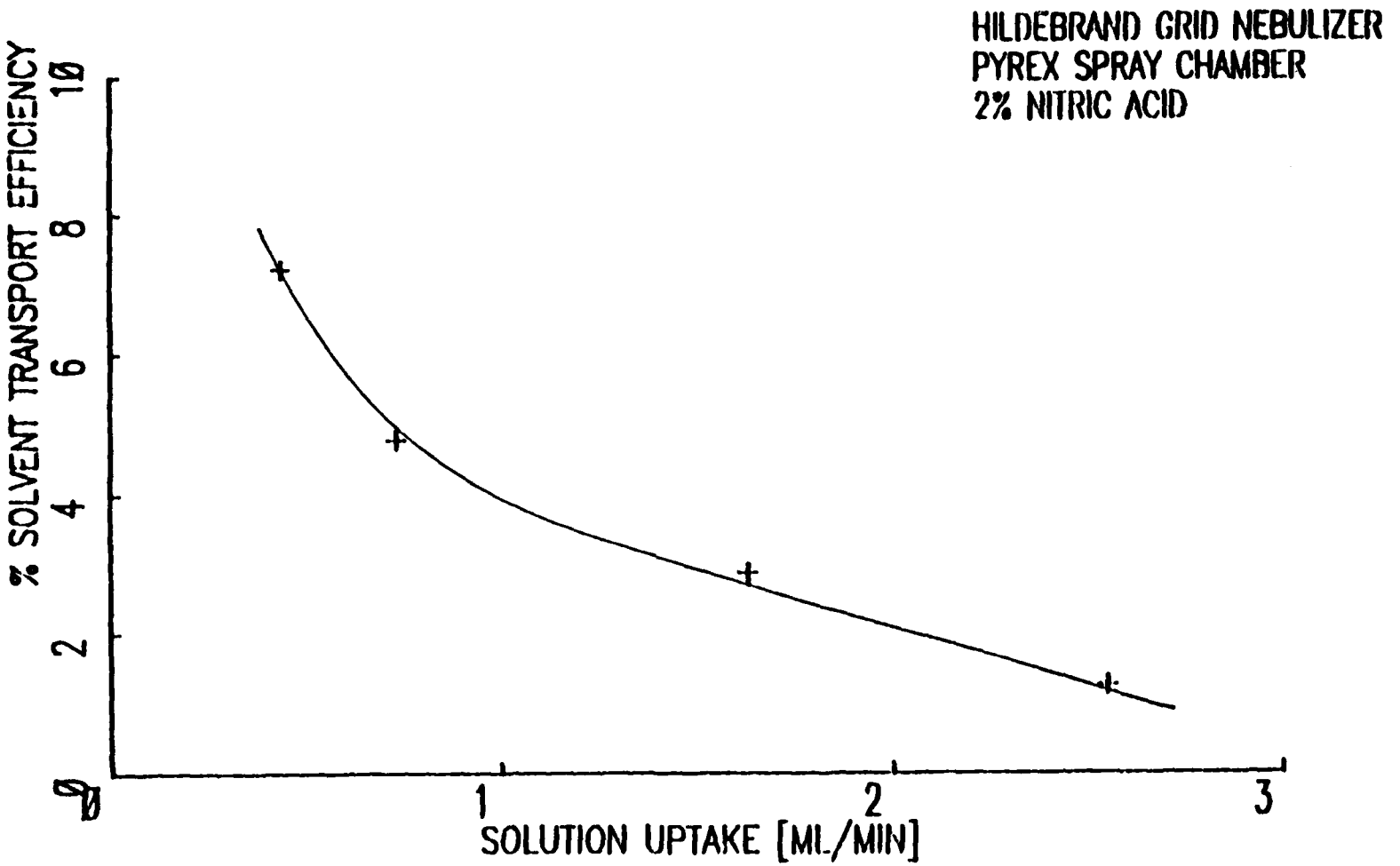

Figure 2-5. Solution Uptake vs. Solvent Transport Efficiency

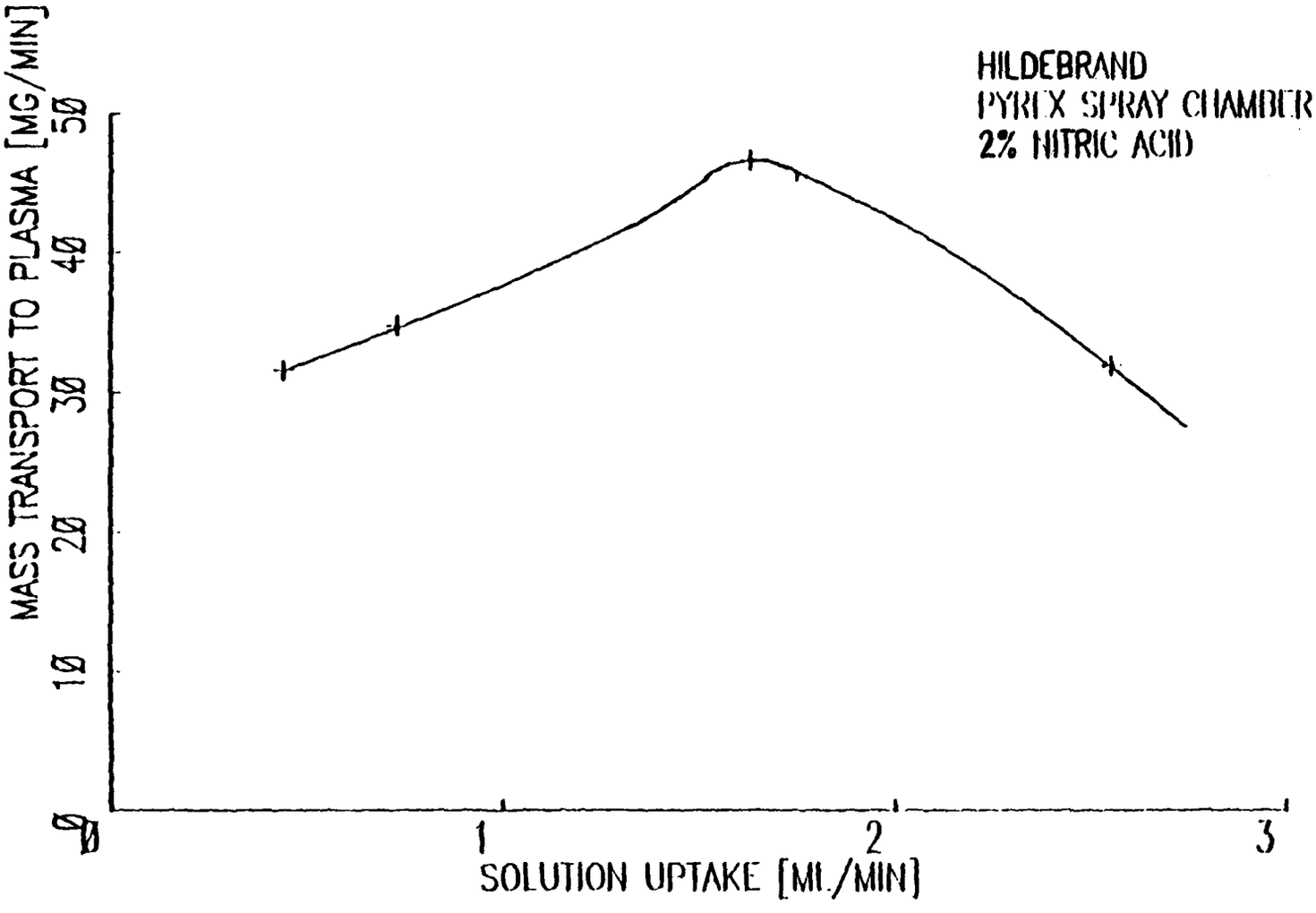

Figure 2-6. Solution Uptake vs. Mass to Plasma

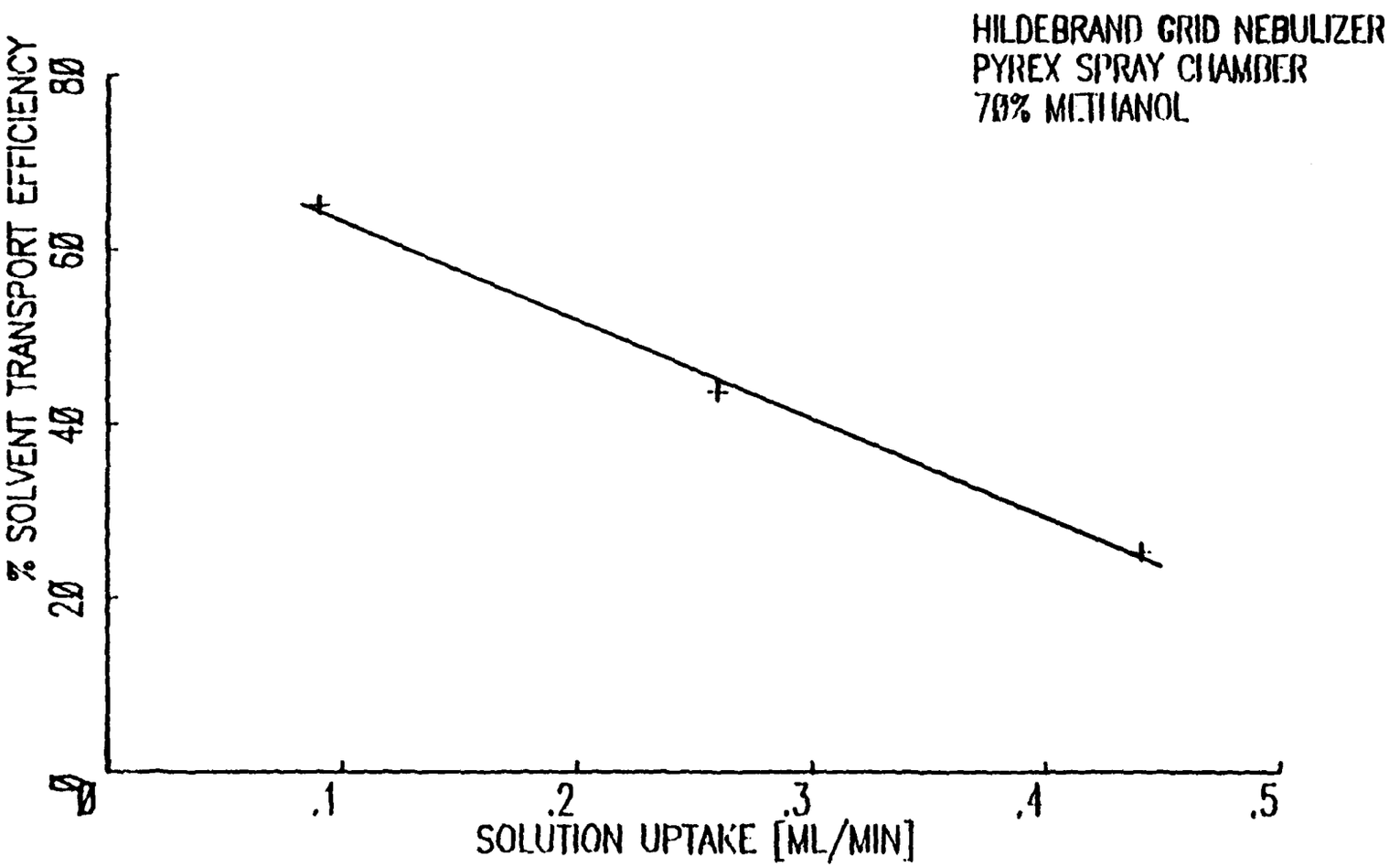

Figure 2-7. Solution Uptake vs. Solvent Transport Efficiency

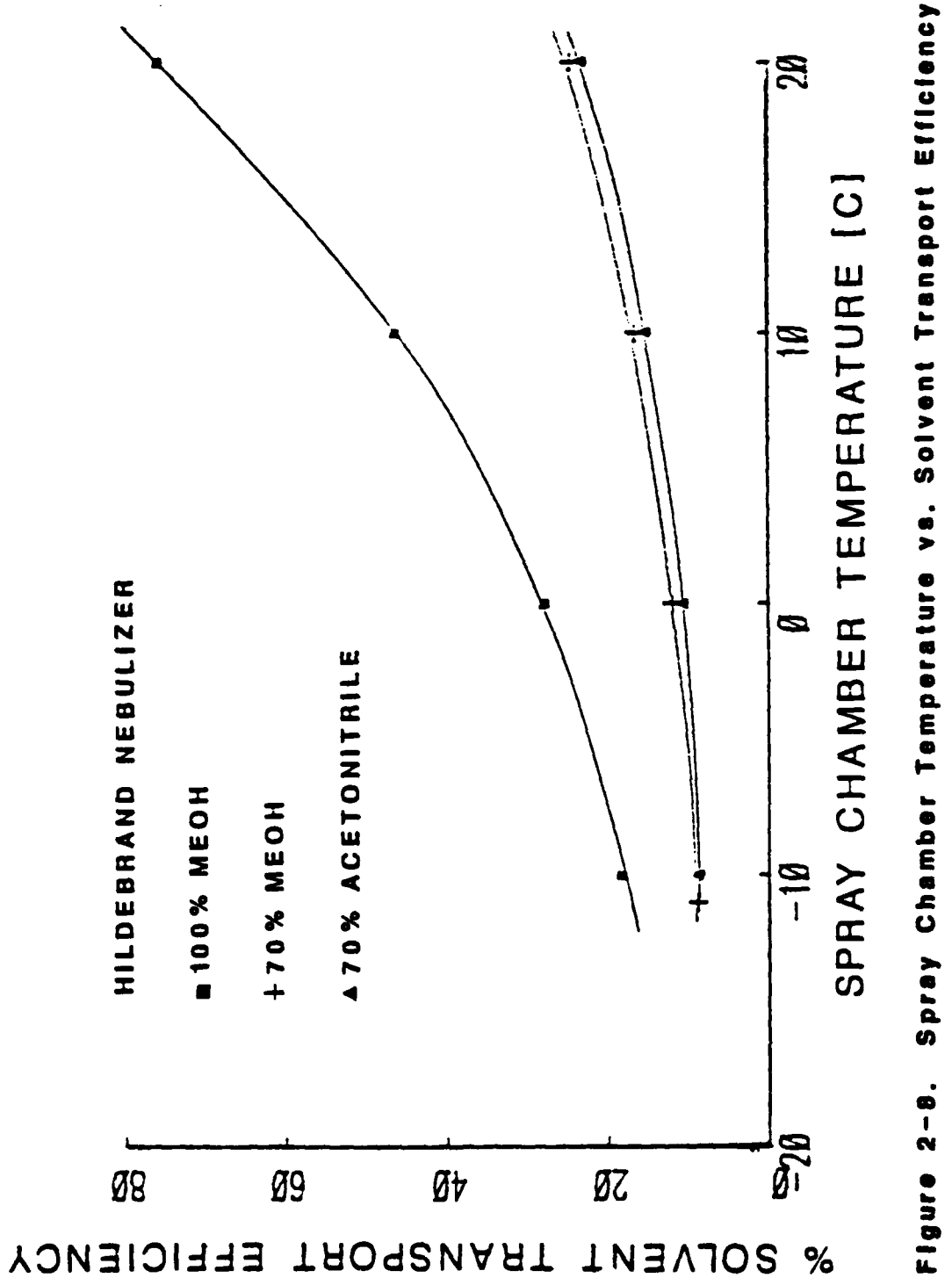

Figure 2-8. Spray Chamber Temperature vs. Solvent Transport Efficiency

maximize aerosol transport and eliminate the solvent vapor transport.

2.6.3 Transport Considerations

The efficient transport of analyte to the plasma is of most concern in the ICP experiment. The process of maximizing analyte transport is not readily predicted by theory. In practice, the way to maximize the transport of analyte contained in a volatile organic solvent is by minimizing the unwanted solvent vapor. **Table 2-12** shows the calculated total amount of methanol vapor present in argon at various temperatures and saturation levels. Assuming that the argon is 75% saturated in methanol at 20°C, there would be 126 mg of methanol per liter of argon. By knowing the temperature of the spray chamber and the % methanol saturation in argon, the vapor transported to the plasma can be estimated through the ideal gas law.

The LAR of 100% methanol at 20°C (spray chamber temperature) is 0.1 mL/min. Since the efficiency of the nebulizer is 100%, that means that 79.1 mg/min of methanol vapor and aerosol is transported to the plasma. As can be seen in **Table 2-13**, the ratio of aerosol to solvent vapor transport is maximized by decreasing the spray chamber temperature and thus decreasing the methanol vapor reaching the plasma. To show what an effect spray chamber temperature has on the ratio of aerosol to solvent vapor transport, consider argon that is 50% saturated with methanol vapor. At -10°C, the LAR is 0.3 mL/min and the solvent transport efficiency is only 18.3%. Only 43.4 mg of aerosol plus methanol vapor are transported to the plasma, but of that an estimated 35.6 mg/min is aerosol (containing analyte) and 7.8 mg/min is solvent vapor (not containing analyte). At 20°C, the LAR is 0.1 mL/min and the solvent transport efficiency is 100%. In this case, 79.1 mg/min of solvent vapor and

Table 2-12

Mass of Methanol in Argon (mg/L)

Temperature	% MeOH Saturation of Argon		
(C)	75	50	25
20	126	84.0	42.0
10	73.8	49.0	24.6
0	36.6	24.6	12.2
-10	23.4	15.6	7.8

Table 2-13

Ratio of Aerosol to Solvent Transport
(Standard Plasma Conditions, 1.25 kW rf)

Temperature (C)	LAR mL/min	Solvent Transport Efficiency	Portion to Plasma (mg/min)	Aerosol/Solvent at % MeOH sat. 75	50	25
20	0.1	100	79.1	0.25	0.88	2.7
10	0.19	66.9	71.2	0.93	1.90	4.7
0	0.24	33.9	64.3	2.51	4.22	9.5
-10	0.30	18.3	43.4	2.71	4.56	10.1

aerosol are transported to the plasma, but 42.0 mg/min is solvent vapor and 35.1 mg/min is aerosol. In the first instance, the analyte to solvent vapor ratio is 4.56 and the second case, the ratio is 0.88. The higher the ratio, the better the detection limits, plus detection limits are further improved because of increased plasma stability that results from minimizing solvent vapor loading. Table 2-14 shows the solvent transport efficiency at various spray chamber temperatures. Analyte transport efficiency decreases at higher spray chamber temperatures. This is because as the solution is nebulized, the solvent begins to evaporate from the aerosol droplets. The solvent vapor is transported to the plasma, but some of the larger droplets which are not transported to the plasma collect in the drain. Those droplets which collect in the drain are now more concentrated than the original solution due to the evaporation which occurred in the spray chamber. Thus, to get more efficient transport of analyte to the plasma requires a cooled spray chamber that by condensation, minimizes solvent vapor transport to the plasma.

Solvent transport efficiency in itself is not an important parameter for optical emission spectroscopy. However, solvent transport efficiency for a particular solution uptake rate will have a direct relationship on emission signal because it will determine how much analyte and solvent are transported to the plasma. In addition, since many chromatographic separations involving organic solvents are optimal for a fixed flow rate, a priori knowledge of solvent transport efficiency would give an indication whether or not ICP could be used as an element selective detector. Table 2-15 shows the comparable efficiencies of the Hildebrand grid, cross flow, concentric and glass frit nebulizers. It

Table 2-14

Solvent Transport Efficiencies

(Standard Plasma Conditions, 1.25 kW rf))

100% Methanol

Temperature (C)	Uptake Rate mL/min	Solvent Transport Efficiency	Analyte Transport Efficiency
20	0.3	76.0	45.0
10	0.3	46.5	37.5
0	0.3	28.8	27.2
-10	0.3	18.3	18.4
20	0.1	100	--
10	0.19	66.9	39.7
0	0.24	33.9	32.3

Table 2-15

Solvent Transport Efficiencies*

Nebulizer Spray Chamber	Solvent	Uptake Rate mL/min	Solvent Transport Efficiency	Analyte Transport Efficiency
Hildebrand w/ Pyrex	70% MeOH	0.44	25.4	16.5
	100% MeOH	0.20	100	--
	70% ACN	0.10	100	--
	2% Nitric	1.60	2.9	2.7
Cross Flow w/ Pyrex	70% MeOH	0.10	89.7	46.2
	100% MeOH	0.10	100	--
Concentric w/ Pyrex	70% MeOH	0.30	22.4	21.1
	100% MeOH	0.11	73.4	48.3
Glass Frit (no spray chamber)	70% MeOH	0.30	24	24
	100% MeOH	0.16	96	96

*ICP operating conditions: 1.25 kW rf, 30 L/min Ar coolant (organics), 1.5 L/min Ar auxiliary flow (ACN only), 0.5 L/min Ar nebulizer flow.

should be noted that these very high solvent transport efficiencies are directly attributable to relatively low solution uptake rates of volatile organic solvents in an uncooled spray chamber.

2.7 Linear Dynamic Range

The Hildebrand nebulizer provided linear dynamic ranges of 3-4 orders of magnitude for all elements. Figures 2-9, 2-10, 2-11 and 2-12 show the LDR for 5 elements from 100 ppm to 25 ppb. As can be seen from the figures, use of a cooled spray chamber provided the most sensitive detection and widest linear dynamic range. Table 2-16 shows some statistics for these plots. With the uncooled conical pyrex spray chamber, the slope of the log concentration versus log intensity ranged from 0.90 to 1.00. By cooling the spray chamber, linearity of the plots improved as the slope of the log concentration versus log intensity graph for most elements approached unity.

2.8 CONCLUSION

The Hildebrand nebulizer is suitable for volatile solvent introduction in terms of limiting aspiration rates, detection limits, efficiency and linear dynamic ranges. It also provides an efficient method of introducing solution into an ICP. The limiting aspiration rates for the Hildebrand nebulizer are comparable to the glass frit nebulizer for volatile organic solvents into the ICP. The LAR's for the Hildebrand grid are slightly higher than the cross flow, and much higher than the concentric nebulizer for volatile solvent sample introduction. Although the glass frit provides similar LAR's as the Hildebrand nebulizer, memory effects, poorer reproducibility and more difficult operation make it less desirable.[29] Good detection limits and a wide linear dynamic range can be achieved with the grid nebulizer.

Cooling the spray chamber allows for a higher LAR, condenses unwanted solvent vapor, produces a much more stable plasma and improves detection limits. This will greatly aid in the use of ICP-OES for HPLC-OES detection.

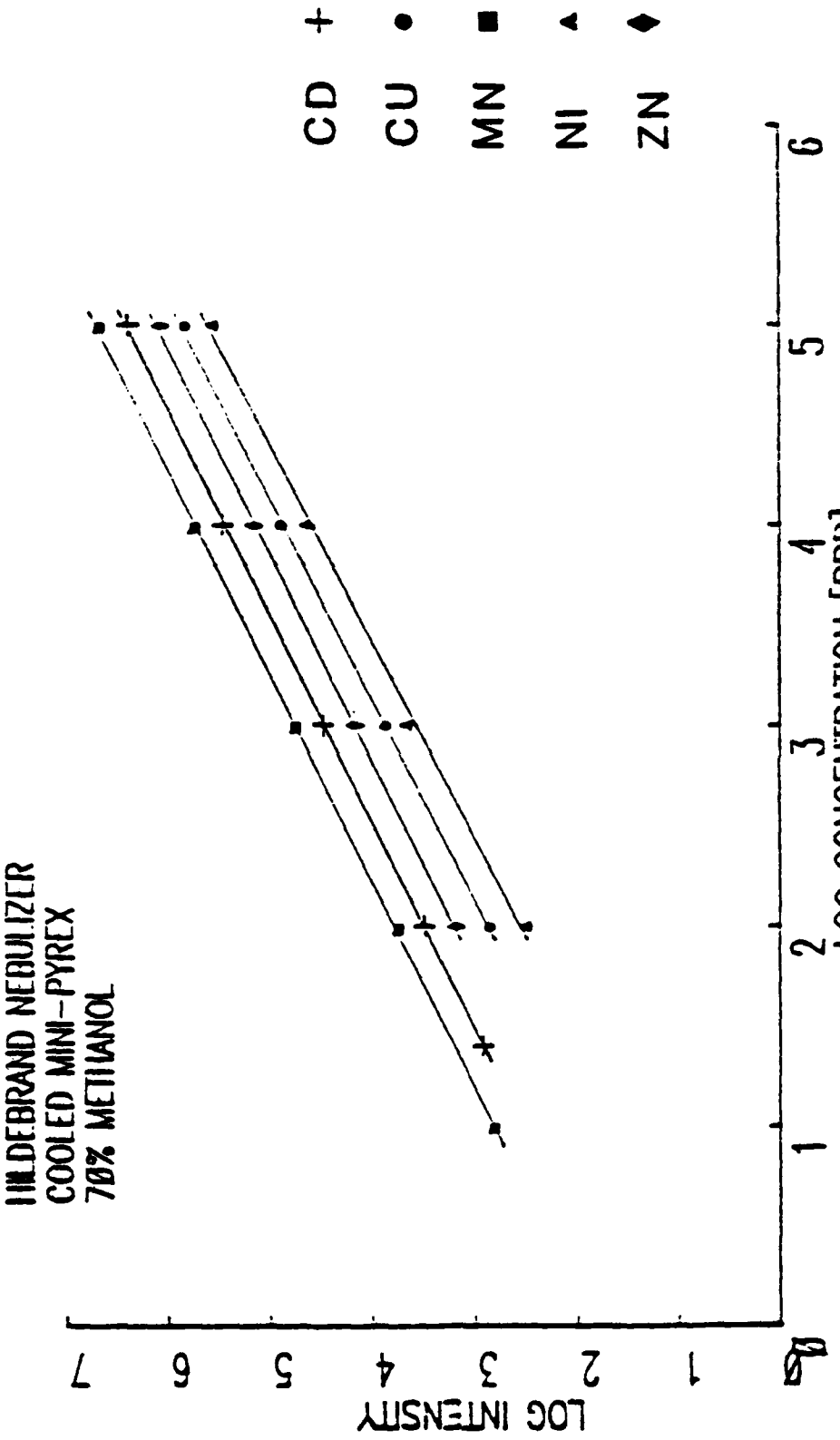

Figure 2-9. Linear Dynamic Range

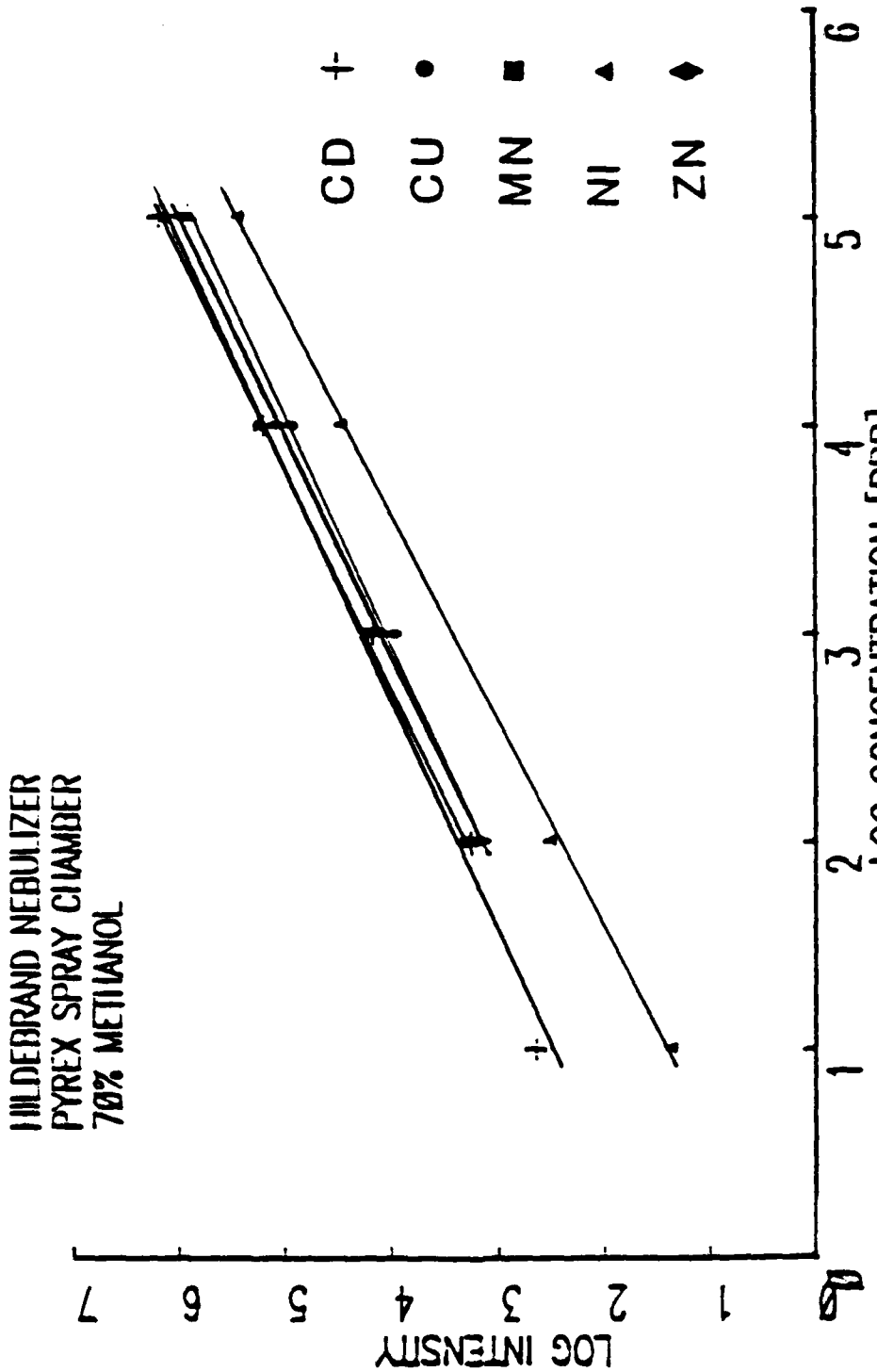

Figure 2-10. Linear Dynamic Range

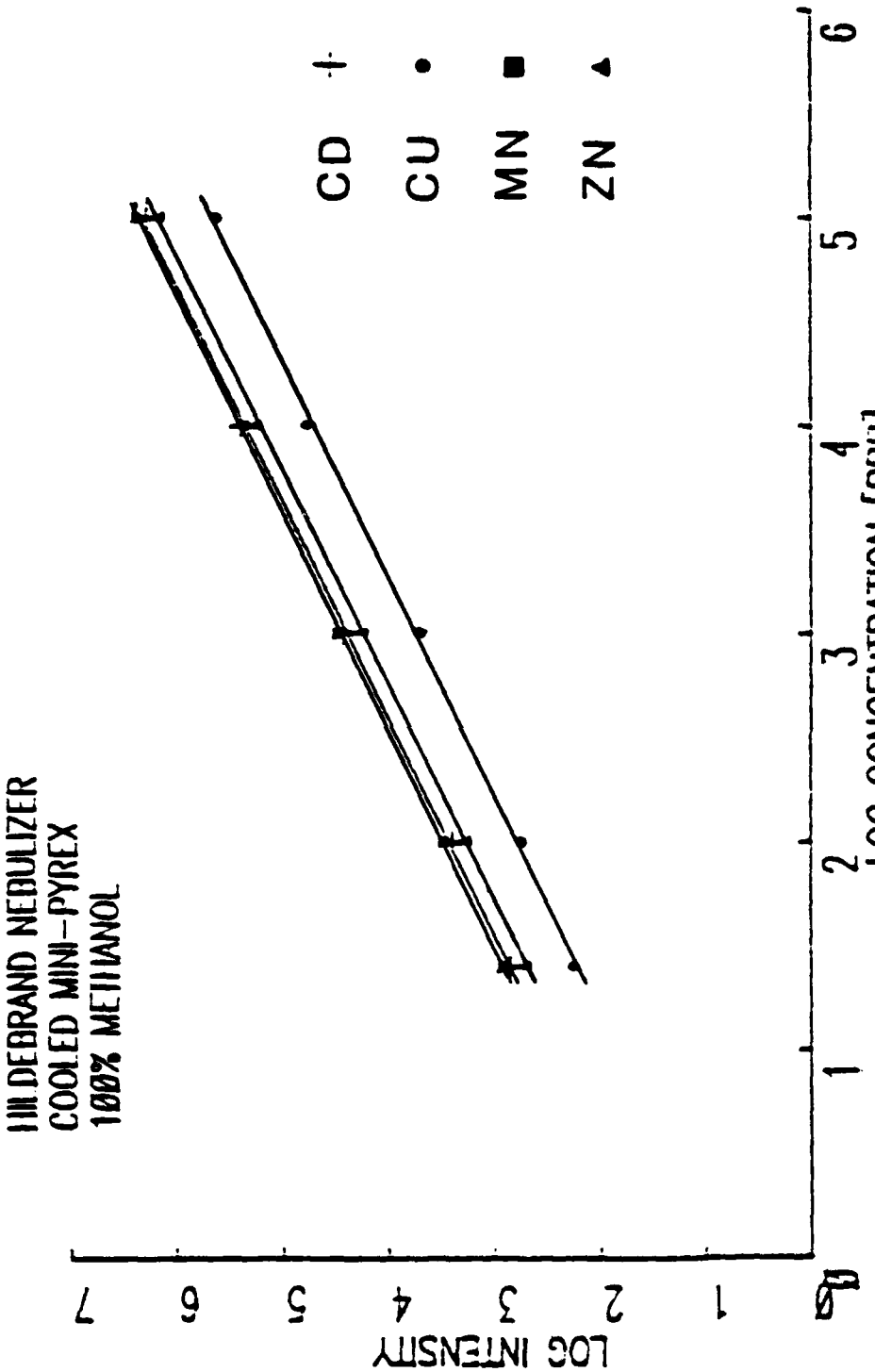

Figure 2-11. Linear Dynamic Range

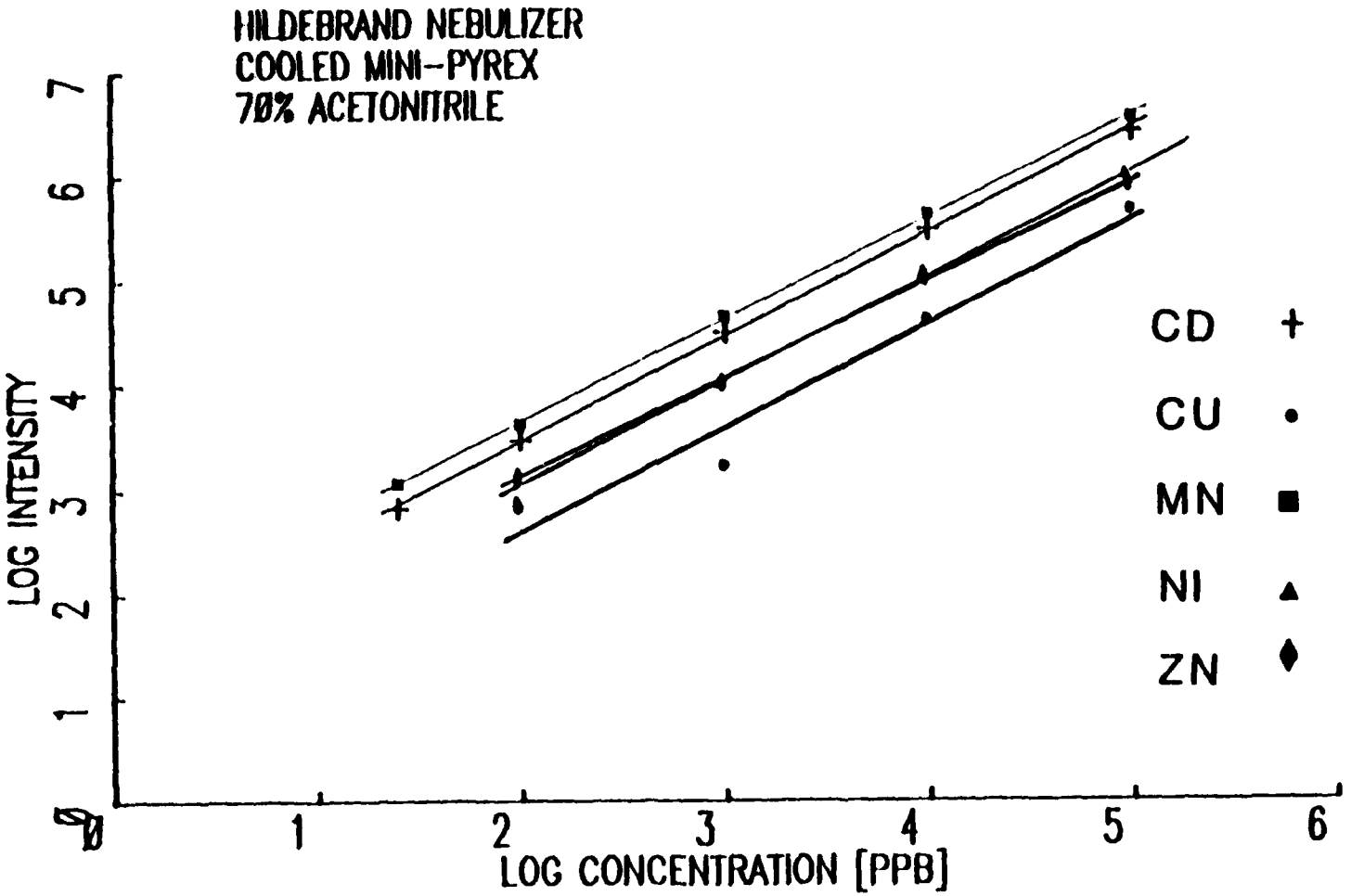

Figure 2-12. Linear Dynamic Range

Table 2-16

Statistics for Calibration Curves
Solvent: 70% MeOH
Hildebrand Nebulizer
Pyrex Spray Chamber

Element	Slope	Intercept	Correlation Coefficient
Cd	0.904	1.583	0.9959
Cu	0.906	1.279	0.9983
Mn	0.950	1.412	0.9998
Ni	0.945	1.284	0.9998
Zn	1.00	0.6390	0.9992

Solvent: 70% MeOH
Hildebrand Nebulizer
Cooled Spray Chamber, 0°C

Cd	0.965	1.578	0.9999
Cu	0.993	0.948	0.9997
Mn	0.967	1.898	0.9999
Ni	1.01	0.594	0.9984
Zn	0.963	1.29	0.9998

Solvent: 70% ACN
Hildebrand Nebulizer
Cooled Spray Chamber, 0°C

Cd	0.995	1.472	0.9997
Cu	0.990	0.627	0.980
Mn	0.973	1.817	0.9998
Ni	1.01	0.6398	0.9997
Zn	1.00	0.6390	0.9992

Solvent: 100% MeOH
Hildebrand Nebulizer
Cooled Spray Chamber, -10°C

Cd	0.960	1.51	0.9997
Cu	0.950	0.89	0.9992
Mn	0.951	1.58	0.9998
Zn	0.963	1.231	0.9999

REFERENCES

1. Fassel, V. A.; Kniseley, R. N. **Anal. Chem.** 1974, **46**, 1110A.

2. Fassel, V. A.; Kniseley, R. N. **Anal. Chem.** 1974, **46**, 1155A.

3. Barnes, R. M. **CRC Crit. Rev. Anal. Chem.** 1978, 203.

4. Layman, L. R.; Lichte, F. R. **Anal. Chem.** 1982, **54**, 638-642.

5. Hieftje, G. M.; Copeland, T. R. **Anal. Chem.** 1978, **50**, 300R.

6. Nisamaneepong, W.; Haas, D.; Caruso, J. A. **Spectrochim. Acta Part B** 1985, **40**, 3.

7. Browner, R. F.; Boorn, A. W. **Anal. Chem.** 1982, **54**, 1402.

8. Blades, W.; Caughlin, B. L. **Spectrochim. Acta Part B** 1985, **40**, 579.

9. Barrett, P.; Pruszkowska, E. **Anal. Chem.** 1984, **56**, 1927.

10. Spall, W. D.; Lunn, J. G.; Andersen, J. L.; Valdez J. G.; Gurley, L. R. **Anal. Chem.** 1986, **58**, 1340.

11. Krull, I. S.; Bushee, D. S.; Schleicher, R. G.; Smith, S. B., Jr. **Analyst** 1986, **111**, 345.

12. Irgolic, K. J.; Hobill, J. E., paper #52 presented at 1986 Winter Conference on Plasma Spectrometry, Kailua-Kona, Hawaii, January 2-8.

13. Biggs, W. R.; Brown, R. J.; Fetzer, J. C., paper #60 presented at 1986 Winter Conference on Plasma Spectrometry, Kailua-Kona, Hawaii, January 2-8, 1986.

14. Aulis, R.; Boulton, A.; Doherty, W.; Vander Voet, A.; Wong, P. **Spectrochim. Acta Part B** 1985, **40**, 377.

15. Hausler, D. W. **Spectrochim. Acta Part B** 1985, **40**, 389.

16. Ibrahim, M.; Nisamaneepong, W.; Haas, D. L.; Caruso, J. A. **Spectrochim. Acta Part B** 1985, **40**, 367.

17. Ibrahim, M.; Gilbert, T. W.; Caruso, J. A. **J. Chromat. Sci.** 1984, **22**, 111.

18. Boumans, P.W.J.M.; deBoer, F. J. **Spectrochim. Acta Part B** 1972, **27**, 1.

19. Greenfield, S.; Jones, I. L.; McGeachin, H.McD.; Smith, P. B. **Anal. Chim. Acta** 1975, **74**, 225.

20. Linn, H. **ICP Inf. Newsl.** 1976, **2**, 51.

21. Greenfield, S.; Jones, I. L.; McGeachin, H.McD.; Smith, P.B. **Anal. Chim. Acta** 1975, **74**, 225.

22. Hausler, D. W.; Taylor, L. T. **Anal. Chem.** 1981, **53**, 1223.

23. Olson, K. W.; Haas, Jr., W. J.; Fassel, V. A. **Anal. Chem.** 1977, **49**, 632.

24. Smith, D. D.; Browner, R. F. **Anal. Chem.** 1982, **54**, 533.

25. Ripson, P.A.M.; DeGalan, L. **Spectrochim. Acta Part B** 1981, **36**, 71.

26. Browner, R. F.; Smith, D. D. **Anal. Chem.** 1983, **55**, 373.

27. Browner, R. F. **ICP Information Newsletter** 1984, **9**, 778.

28. Gustavsson, A. **Spectrochim. Acta Part B** 1984, **39**, 743.

29. Nisamaneepong, W., Ph.D. Dissertation, University of Cincinnati, 1984, p. 38.

CHAPTER 3

EVALUATION OF THREE FIA INTERFACES USING ICP-OES

3.1 INTRODUCTION

Speciation is very important in the areas of toxicology, environmental modeling, clinical chemistry, food science, forensic science and industrial analyses. Often the toxicity and biological importance of metals and metalloids depend on this chemical form.[1,2] Since the metal containing organic species usually occur at very low concentrations (ca. ng/mL range) sensitive detectors are necessary. Detection methods range from inexpensive electrochemical techniques to very expensive mass spectrometric techniques. Unfortunately, it is not always possible to obtain unambiguous data from electrochemical methods. The expense of mass spectrometric methods may preclude its use from routine analyses.

Flame atomic absorption spectroscopy (AAS), furnace AAS, and flame atomic fluorescence spectroscopy (AFS) have been used as element selective detectors for liquid chromatogrpahic (LC) separations. FAAS has been used for arsenic speciation[3] and for the determination of tributyltin in coastal sea water.[4,5] Fish et al. used furnace AAS to investigate nanadyl and nickel compounds in heavy crude petroleum and asphaltenes.[6,7] Van Loon describes the multielement and increased sensitivity advantages of atomic fluorescence spectroscopy over AAS.[8] Mackey used AFS to study the interactions of simple cations with macroreticular resins.[9]

Inductively Coupled Plasma (ICP) Optical Emission Spectroscopy (OES) has become a very popular detection technique for liquid chroma-

tography. ICP-OES is sensitive for metal detection, and a large number of elements can be simultaneously excited under one set of conditions.[10,11,12] The selectivity of spectrometric techniques for metal species and the potential for obtaining speciation information make the ICP particularly attractive. Matrix effects and interferences, which can pose serious problems with AA and direct current emission, are reduced or eliminated. In addition, ICP offers linear dynamic ranges up to five orders of magnitude. **Table 3-1** lists some of the recent LC studies using ICP detection. Ebdon, Hill and Ward recently published a review on liquid chromatography using atomic spectrometric detection techniques.[26]

The objective of this study is to evaluate three low volume interfaces that could be used to couple LC with ICP-OES detection.

3.2 EXPERIMENTAL

The equipment used for the experimental setup is listed in **Table 3-2** and described earlier. The mass flow controller was used to monitor and control the solvent saturated argon for the positive suction injector. The solution uptake rate was approximately 1 mL/min. Plasma conditions are listed in **Table 3-3** and were approximately constant for all experimental interfaces. Detection limits were calculated as the concentration that would provide a signal equal to three standard deviations above the background. The standard deviation of the background was calculated based on 25 data points. Each element was optimized in terms of plasma viewing position and nebulizer flow rate by the following procedure:

1. The plasma was adjusted so that it was slightly above (1-2 mm) the inner torch and very symmetrical in nature. If plasma was not symmetrical, then either the torch was misaligned within the holder or the injector misaligned within the torch.

Table 3-1

ICP Detection for Liquid Chromatography

Column	Mobile Phase	Sample	Reference
250 x 4.6 mm Zorbax C-8 column	50-80% EtOH	Iron and molybdenum carbonyl complexes	13
Hypersil 100 x 4.6 mm	30% MeOH	DMA, MAA, p-APP, As^{V}, phenylarsonic acid	13
100-Å μStyragel Waters column	Pyridine	Ferrocene, copper & cobalt complexes in coal	14
250 x 1.6 mm anion exchange resin	Ammonium sulfate	NTA and EDTA chelates of Cu, Zn, Ca, Ng	15
600 x 7.5 mm TSIC 3000 SW Size exclusion	Water	Cu, Ca, Mg, Zn filtrates	16
Cation exchange Resin (UlPX-210SC)	Sodium phosphate	Amino Acids	17
Hamilton PRP-1 resin-based, reversed-phase column	Water	Arsenic, selenium and phosphorus compounds	18
Micro-HPLC (0.5x120 mm) Jasco SC-01 silica packing	MeOH/Water	Cu, Zn, Fe, Co organometallic compounds	19

Table 3-1 (continued)

ICP Detection for Liquid Chromatography

Column	Mobile Phase	Sample	Reference
600 x 2 mm, TSK GEL 3000 SW	0.9% NaCl Solution	Separation of Vitamin B_{12}, various proteins, etc.	20
Nagel-Nucleosil 10-SP cation exchange resin	Sodium phosphate	Arsenobetaine in shark muscle	21
Strong cation Exchange resin (1EX-2 10SC)	Ammonium lactate	Rare earth elements	22
Microbore l x 500 nm C_{18} coluumn	Tetrabutyl ammonium sulfate in MeOH and water	Inorganic and organometallic compounds	23
Microcolumn gel permeation chromatography	Water	Saccharides	24
Anion exchange resin 1EX-260-SA-SIL	Ammonium carbonate	Ribonucleotides	25

Table 3-2

Experimental Equipment

	Manufacturer
Plasma Spec 2.5 ICP Spectrometer	Leeman Labs Lowell, MA
Minipuls 4 Channel Peristaltic Pump	Rainin Woburn, MA
Mass Flow Controller, 0-5 L/min	Tylan California
Refrigerated Circulator Bath (RTE-8DD)	Neslab Portsmouth, NH
Spray Chambers and Fused Quartz Silica Injectors	Thomas Scientific Cincinnati, OH
Leeman ICP Fused Quartz Silica Torches	Precision Glass Parker, CO
Electronic Digital Pipette (EDP)	Rainin Woburn, MA

Table 3-3

Inductively Coupled Plasma Conditions

Plasma Power	1.5 Kilowatts
Ar Coolant Flow	25 L/min
Ar Auxiliary Flow	1.5 L/min (ACN only)
Ar Nebulizer Flow	Optimized for each element (0.5-0.6 L/min)

2. The top of the torch was positioned about 2 mm above the top of the load coil and the image of the torch, plasma and load coils was focused on the entrance slit to the spectrometer is shown in Figure 3-1. A 1 ppm solution of a particular element was nebulized into the plasma. The plasma was scanned, and the peak profile was examined to ensure that the peak was centered on its characteristic wavelength.
3. A Peak 3 routine was performed, which maximized signal intensity in the horizontal direction of the plasma. If the torch and injector are aligned properly, the plasma would invariably appear symmetrical about the cross marks on the entrance slit.
4. Initial nebulizer pressure settings were usually set at 20 psi for organic solvents and 40 psi for aqueous solvents. The analyte emission intensity and the background were determined, and a calculation of (signal-background)/background was calculated. Nebulizer pressure was then varied in increments of approximately 2.5 psi, a Peak 3 routine performed and then analyte and background emission was measured. This procedure was performed for many nebulizer flows until a maximum (signal-background)/background was obtained.
5. The vertical viewing position of the plasma was altered approximately 5 steps (approximately 3 steps = 1 mm) and analyte emission measured and (signal-background)/background was calculated. Nebulizer flow was then varied to obtain optimum response for this position by the previous procedure.
6. The position and nebulizer conditions that gave the highest (signal-background)/background was the point used for data collection.

Note that in most instances, the optimum viewing location was approxi-

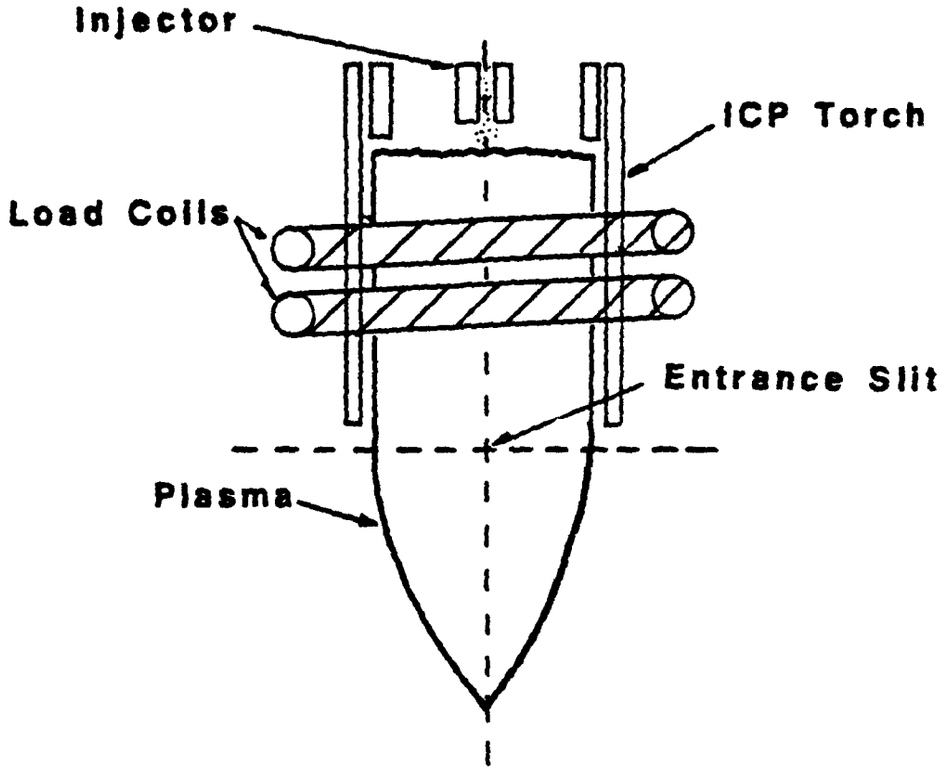

Figure 3-1. Leeman ICP Torch Image on Entrance Slit

mately 1-3 mm above the ICP torch. Figure 3-2 shows a typical ICP vertical position (in terms of steps above the load coil) versus the normalized emission intensity over background.

Figure 3-3 shows a typical nebulizer optimization plot for a variety of elements. Optimum nebulizer pressure ranged from 15 to 25 psi for organic solvents and approximately 30-50 psi for aqueous solutions. Optimization of plasma position and nebulizer gas flow for a particular element in the sequential single mode resulted in slightly better detection limits. For routine analysis, however, the simultaneous or sequential multielement modes would be preferred because analysis time is minimized.

This optimization procedure was used for all experiments in this chapter. This was done to maximize detection capability for transient signals.

3.3 INTERFACE REQUIREMENTS

Solution nebulization is usually the method of choice for sample introduction into the ICP. Typically the nebulizers used are either a cross flow or concentric. Ultrasonic nebulizers afford low detection limits, but are expensive and they require a desolvation system that sometimes cannot be used with high (<1%) dissolved solid solutions.[27]

All pneumatic nebulizers and ultrasonic nebulizers require use of a spray chamber. The function of a spray chamber is to facilitate the homogeneous transport of the aerosol stream to the ICP. The size and design of the spray chamber in part will determine the diameter of the largest droplet that can be transported to the plasma.

Typically a Scott double pass spray chamber is used for aqueous solution nebulization for ICP emission or mass spectrometry. When using

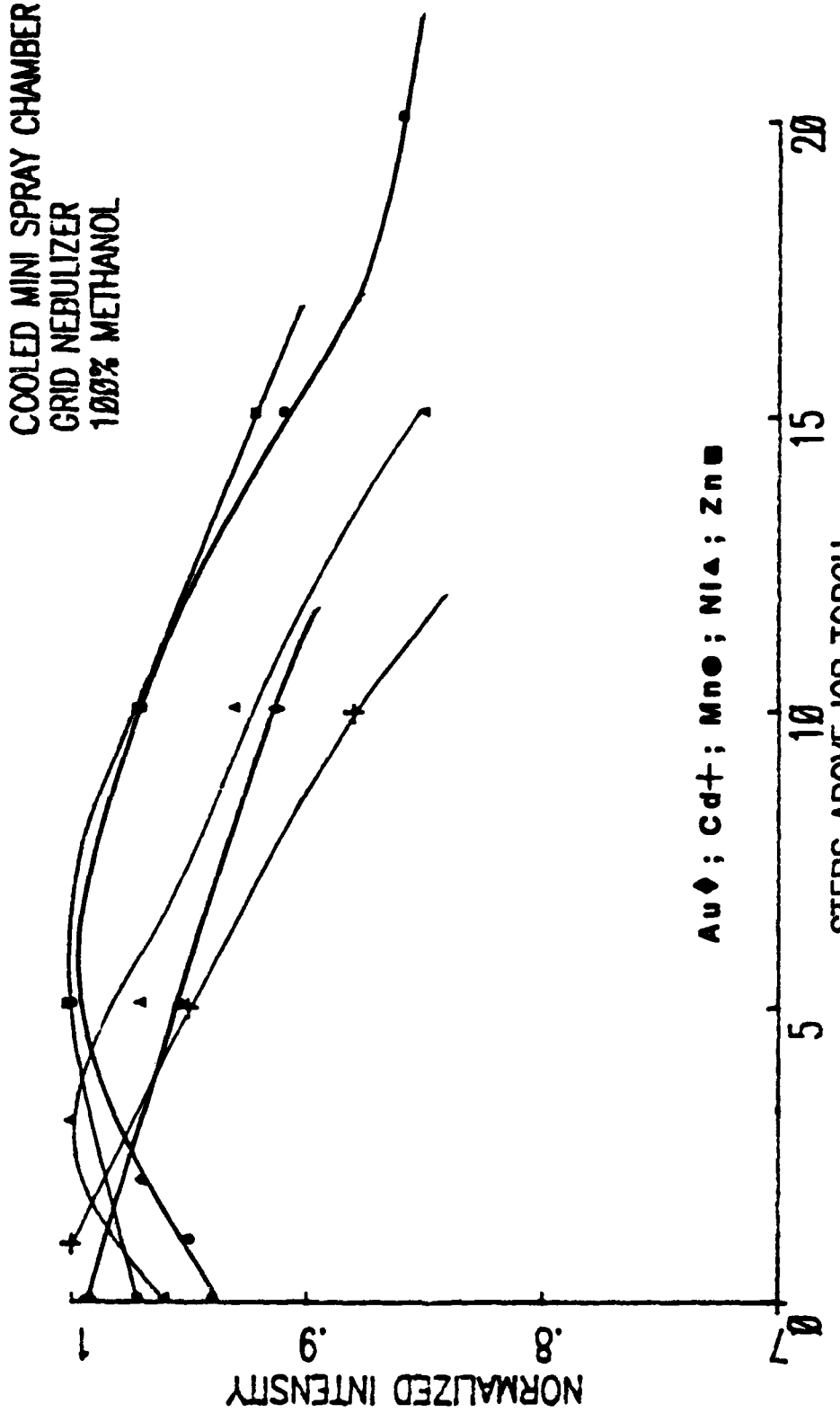

Figure 3-2. ICP Vertical Position vs. Normalized Emission Intensity

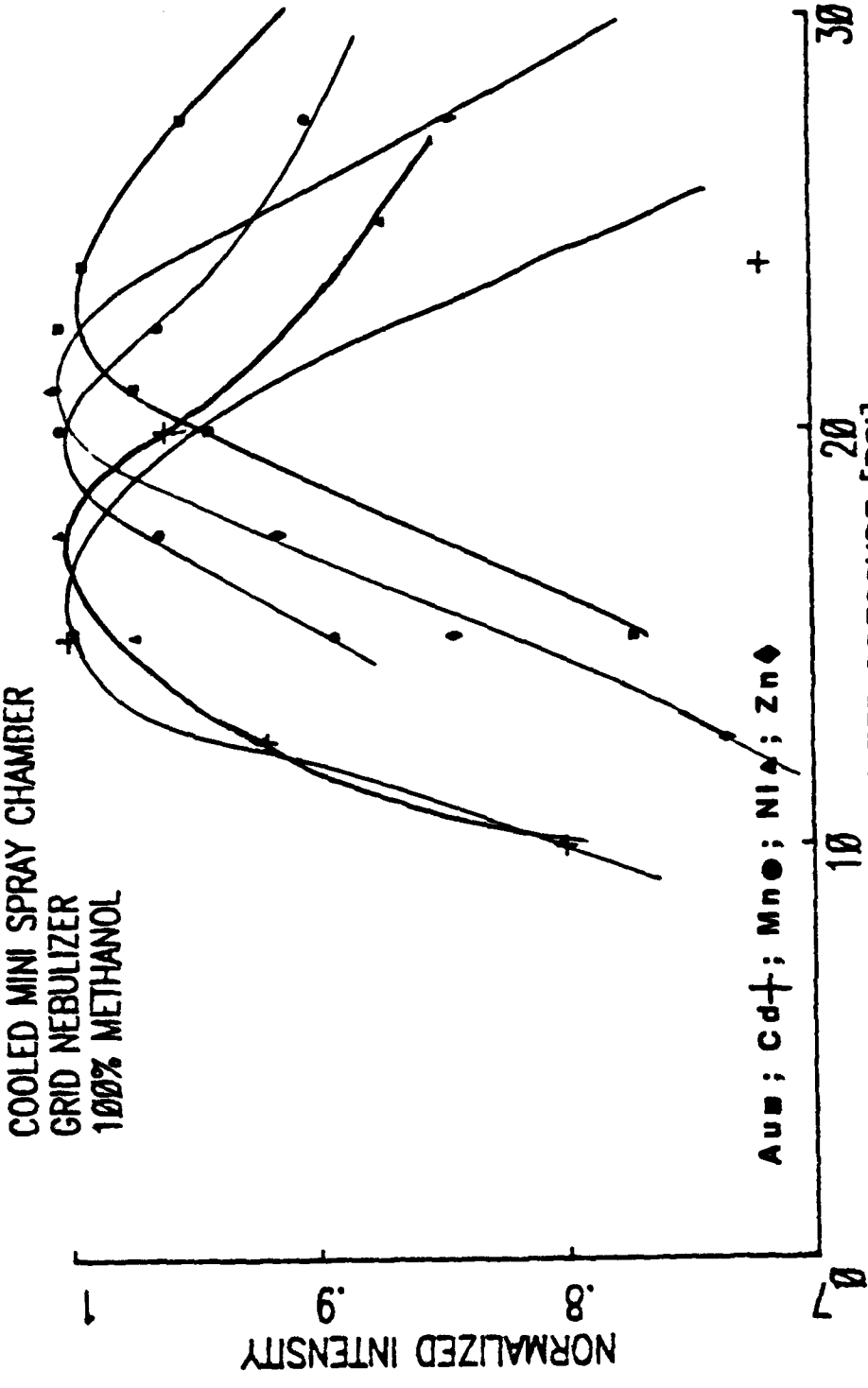

Figure 3-3. Nebulizer Pressure vs. Normalized Emission Intensity

a concentric or cross flow nebulizer with a Scott double pass spray chamber, the typical mass transport efficiency is about 1%. The Scott spray chamber also provides a very constant aerosol to the plasma.

Unfortunately, when using the ICP as a detector for Flow Injection Analysis (FIA) or HPLC, the spray chamber also increases band broadening. Since the volume of a Scott spray chamber is approximately 110 cm^3, peaks are broadened.

The requirements for an ICP interface for FIA or HPLC, is that band broadening be minimized, a constant homogeneous aerosol reaches the plasma and the spray chamber wash-out time is quick. For FIA or reversed phase HPLC involving volatile organic solvents, vapor must be minimized.

Given those interface requirements, three sample delivery systems have been designed for volatile organic solvents. The interfaces are referred to as a *Cooled Mini Spray Chamber (CMSC), a Heated/Cooled Interface* (HCI) and Positive Suction Injector (PSI). The CMSC and HCI removes solvent vapor by cooling the spray chamber whereas the PSI removes the vapor by taking into account differences in kinetic energy of the aerosol droplets relative to solvent vapor in the argon.

3.4 SOLUTION NEBULIZATION

The three interfaces were evaluated for solution nebulization and for flow injection analysis. The performance criteria for solution nebulization were percent relative standard deviation (precision) of emission signal, detection limits and linear dynamic range. All the interfaces allowed for aspiration rates of 1-2 mL/min.

3.4.1 Grid Nebulizer with a Cooled Mini Spray Chamber

The cooled mini-spray chamber described here is slightly different than that described in Chapter Two. **Figure 3-4** shows the cooled spray

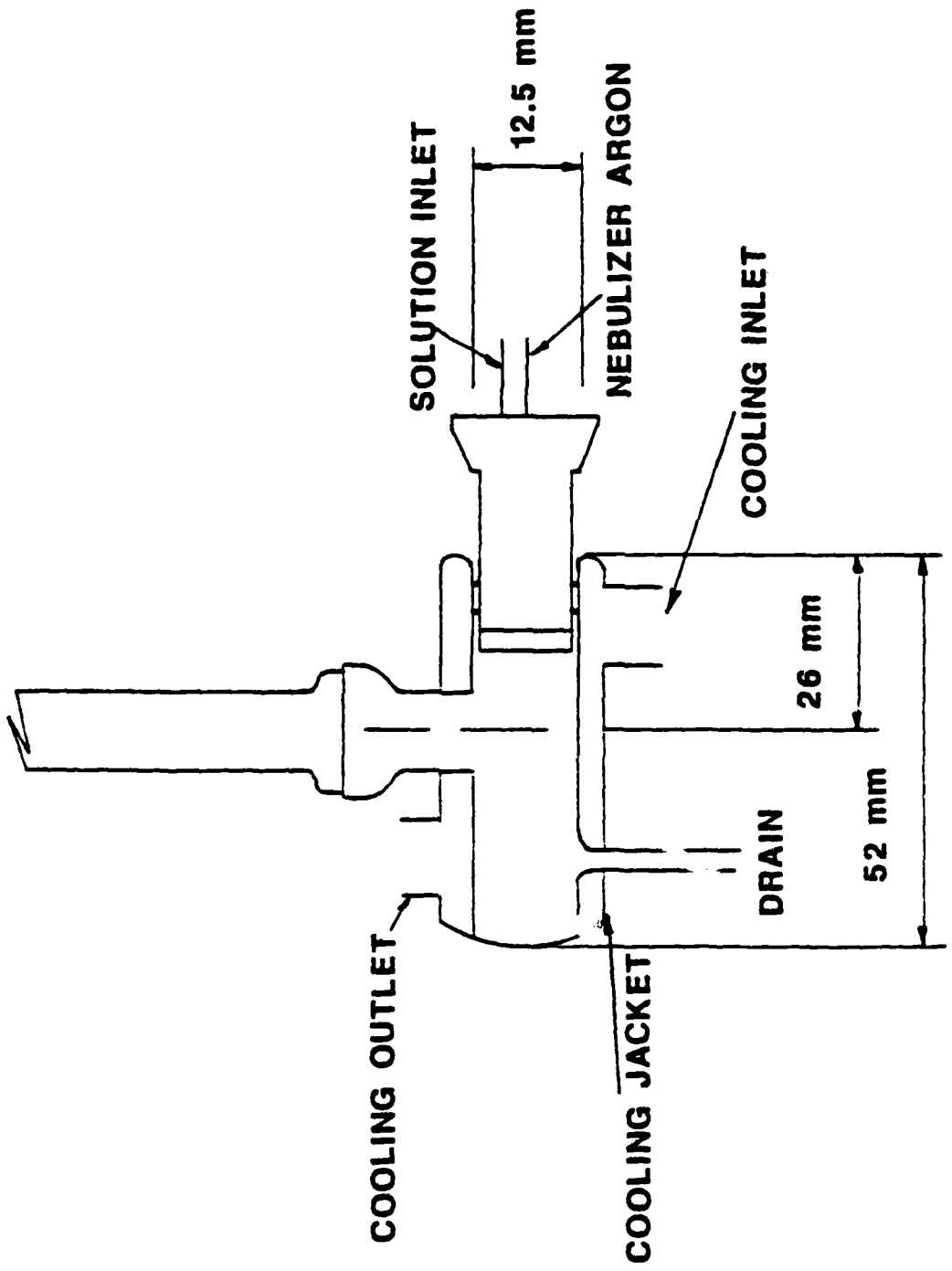

Figure 3-4. Cooled Mini-Spray Chamber Diagram

chamber. **Table 3-4** shows the volume of the cooled mini spray chamber along with other spray chambers used in this study.

The spray chamber is jacketed for cooling which allows use of volatile organic solvents. **Figure 3-5** shows the plot of temperature versus vapor pressure of methanol and acetonitrile commonly used for reversed phase HPLC. At a temperature of 40°C (which is typical in the ICP torchbox) results in a vapor pressure of 235 torr for methanol and 171 torr for acetonitrile. This can be compared with vapor pressure of 55 torr for an aqueous solution at the same temperature.

Assuming ideal gas behavior, approximately four times the amount of methanol vapor is transported to the plasma versus water vapor for a given nebulizer gas flow. The three basic steps required prior to exiting the analyte contained in an aerosol is desolvation, vaporization and atomization. Since there is 4 times the organic vapor (versus water vapor) to atomize, the plasma must use more energy to atomize the solvent vapor and, therefore, less energy is available for the excitation step.

Blades and Cauglin estimated that the introduction of organic solvent into the ICP lowers plasma power available for excitation by approximately 500 watts.[28] Since there are other processes going on within the plasma such as excitation of atomic species from solvent, detuning of the plasma resulting in less energy transfer to the plasma, and collisions between excited atoms, that also reduces the amount of energy available for ICP excitation.

Previous work has demonstrated that detection limits improve with a decrease in spray chamber temperatures. The spray chamber temperature used for the cooled mini spray chamber was -10°C for methanol and acetonitrile. If lower temperatures were used, and detection limits could be

Table 3-4

Spray Chamber Volume

Spray Chamber Type	Volume (cc)
Scott Spray Chamber	110
Conical Spray Chamber W/Impinger Ball	38
Cooled Conical Spray Chamber	17
Cooled Mini Spray Chamber	5
Heated/Cooled Interface (HCI)	15
Positive Suction Injector (PSI)	5
Baird Ultrasonic Nebulizer W/Aerosol Desolvation	467

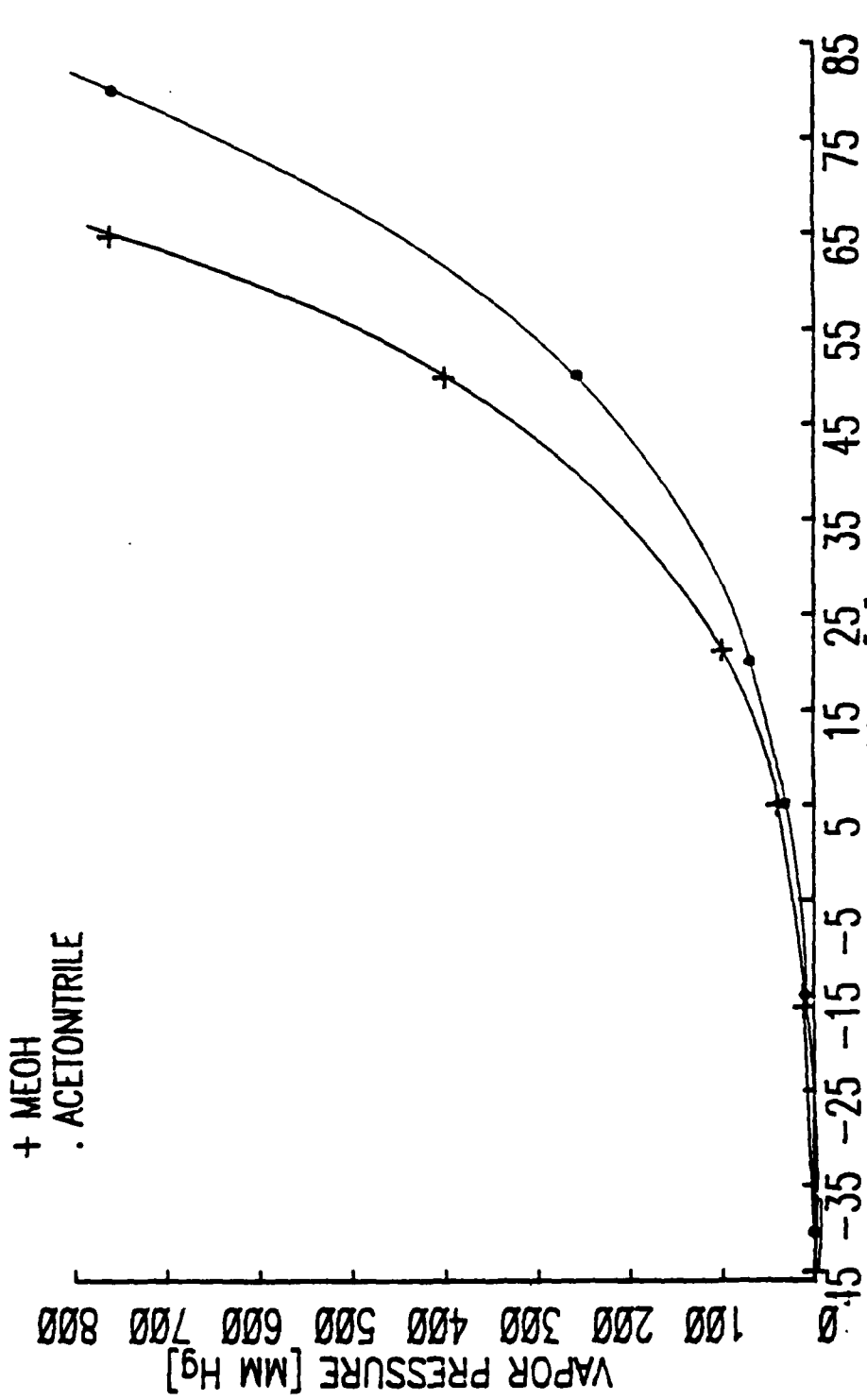

Figure 3-5. Temperature vs. Vapor Pressure of Methanol and Acetonitrile

improved, but our cooling system could not achieve steady temperatures much lower than -12 to -15°C.

3.4.1.1 Results

Table 3-5 shows the 3 sigma detection limits attained for Au, Cd, Cu, Fe, Mn, Ni, and Zn for 100% methanol and 100% acetonitrile. These detection limits are in the sub ng/mL to low ng/mL range. **Table 3-6** shows the average for seven elements, the % relative standard deviation (RSD) using the grid nebulizer, and the cooled mini spray chamber. Each % RSD was calculated on 20 data points. The average % RSD for all seven elements in methanol was approximately 0.5%, and it was 0.4% for acetonitrile.

The Linear Dynamic Range (LDR) was calculated for a variety of elements in methanol and acetonitrile using this interface. **Figures 3-6, 3-7, 3-8, 3-9** and **3-10** show that the LDR spans 3-4 orders of magnitude. The slope, intercept, and correlation coefficients are listed in **Table 3-7.**

In addition to providing a stable, reproducible sample transport system, the sample delivery system seems to deliver more analyte to the plasma. Emission intensity increased from approximately 90,000 counts (3 second integration time) to about 190,000 counts for 1 ppm manganese. Detection limits did not seem to improve much because the background and standard deviation of the background increased also.

3.4.2 Heat/Cooled Interface (HCI)

The preceding interface removes unwanted solvent vapor by maintaining a low temperature in the spray chamber and thus a low vapor pressure for the solvent. Evaporation of solvent from the droplet is minimal, and thus the organic solvent (from the aerosol droplet) is transported to the

Table 3-5

Detection Limits (ng/ml)

Solution Nebulization

Grid Nebulizer/Cooled Mini Spray Chamber

100% Methanol

Element	Detection Limit (ng/mL)	
	100% Methanol	100% Acetonitrile
Au	5.2	12.6
Cd	0.6	0.1
Cu	6.8	1.6
Fe	1.2	3.1
Mn	0.7	0.8
Ni	6.3	6.3
Zn	1.7	3.2

Table 3-6

% Relative Standard Deviation

Solution Nebulization

Grid Nebulizer/Cooled Mini Spray Chamber

Element	100% Methanol			100% Acetonitrile		
	Blank	1 µg/ml	10 µg/ml	Blank	1 µg/ml	10 µg/ml
Au	0.4	0.2	0.5	0.5	0.3	0.4
Cd	0.3	0.1	0.4	0.3	0.6	0.5
Cu	0.7	0.6	0.6	0.2	0.2	0.5
Fe	0.5	0.8	0.9	0.5	0.5	0.7
Mn	0.6	0.2	0.6	0.5	0.5	0.3
Ni	0.3	0.5	0.4	0.4	0.4	0.4
Zn	0.5	0.5	0.5	0.7	0.5	0.4
Avg	0.5	0.4	0.5	0.4	0.4	0.5

Table 3-7

Calibration Coefficients

Grid Nebulizer/Cooled Mini Spray Chamber

100% Methanol

Element	Slope	Intercept	Correlation Coefficient
Au	1.01	0.918	0.99996
Cd	0.98	1.555	0.99990
Cu	0.99	1.294	0.99975
Fe	1.00	1.282	0.99960
Mn	0.96	2.062	0.99981
Ni	0.99	0.809	0.99996
Zn	0.97	1.446	0.99981

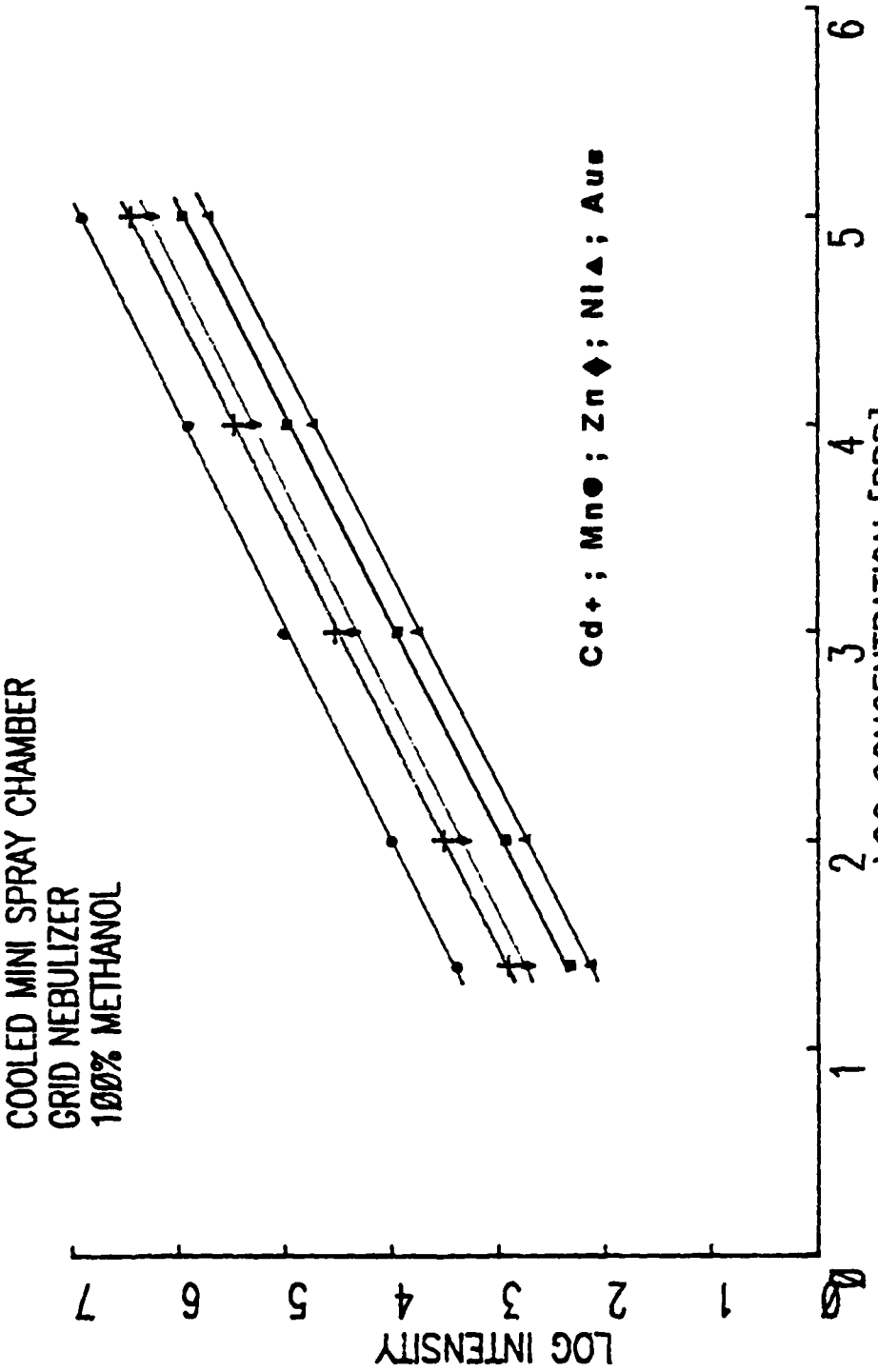

Figure 3-6. Log Concentration vs. Log Emission Intensity

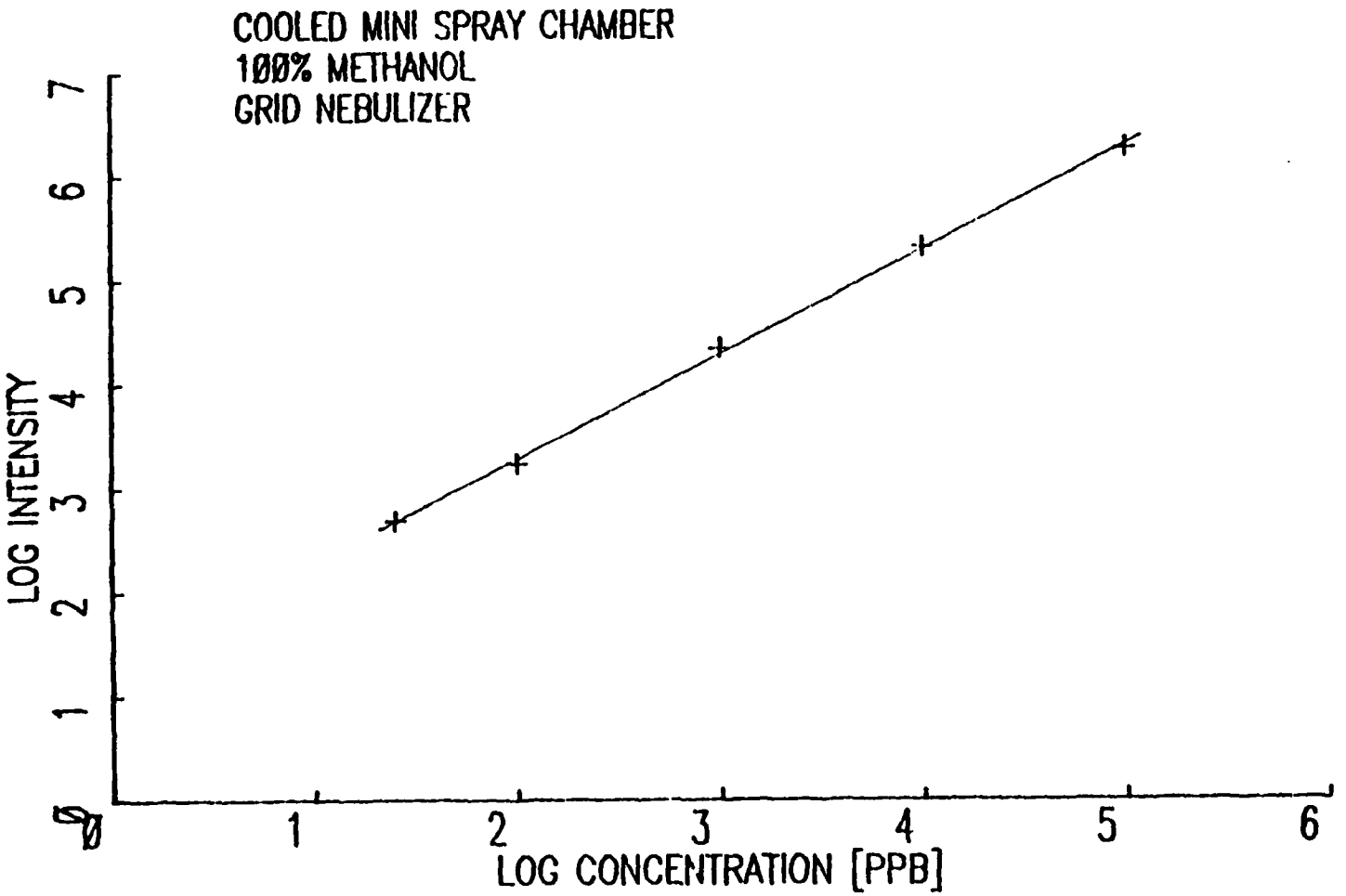

Figure 3-7. Log Concentration vs. Log Emission Intensity for Fe

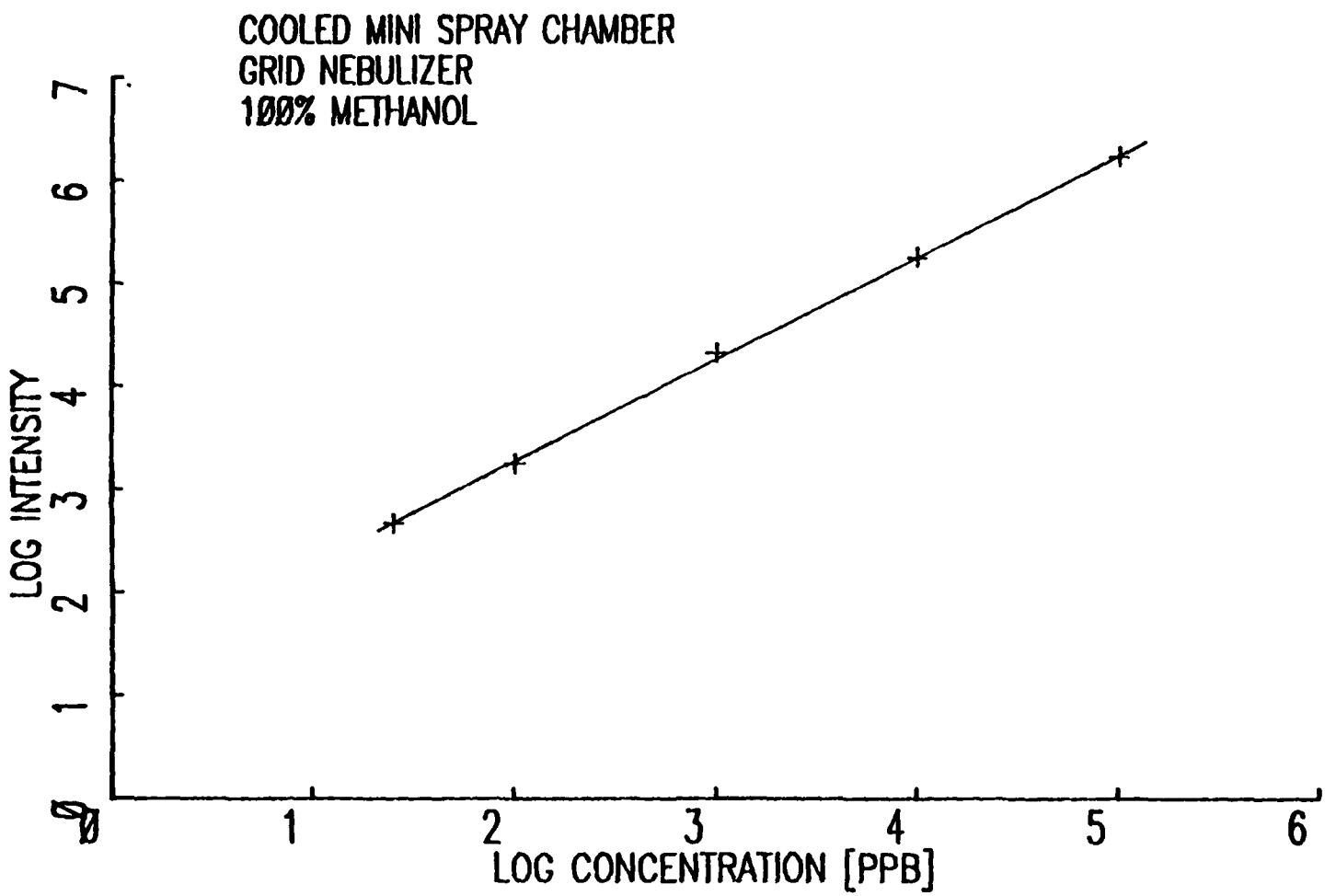

Figure 3-8. Log Concentration vs. Log Emission Intensity for Cu

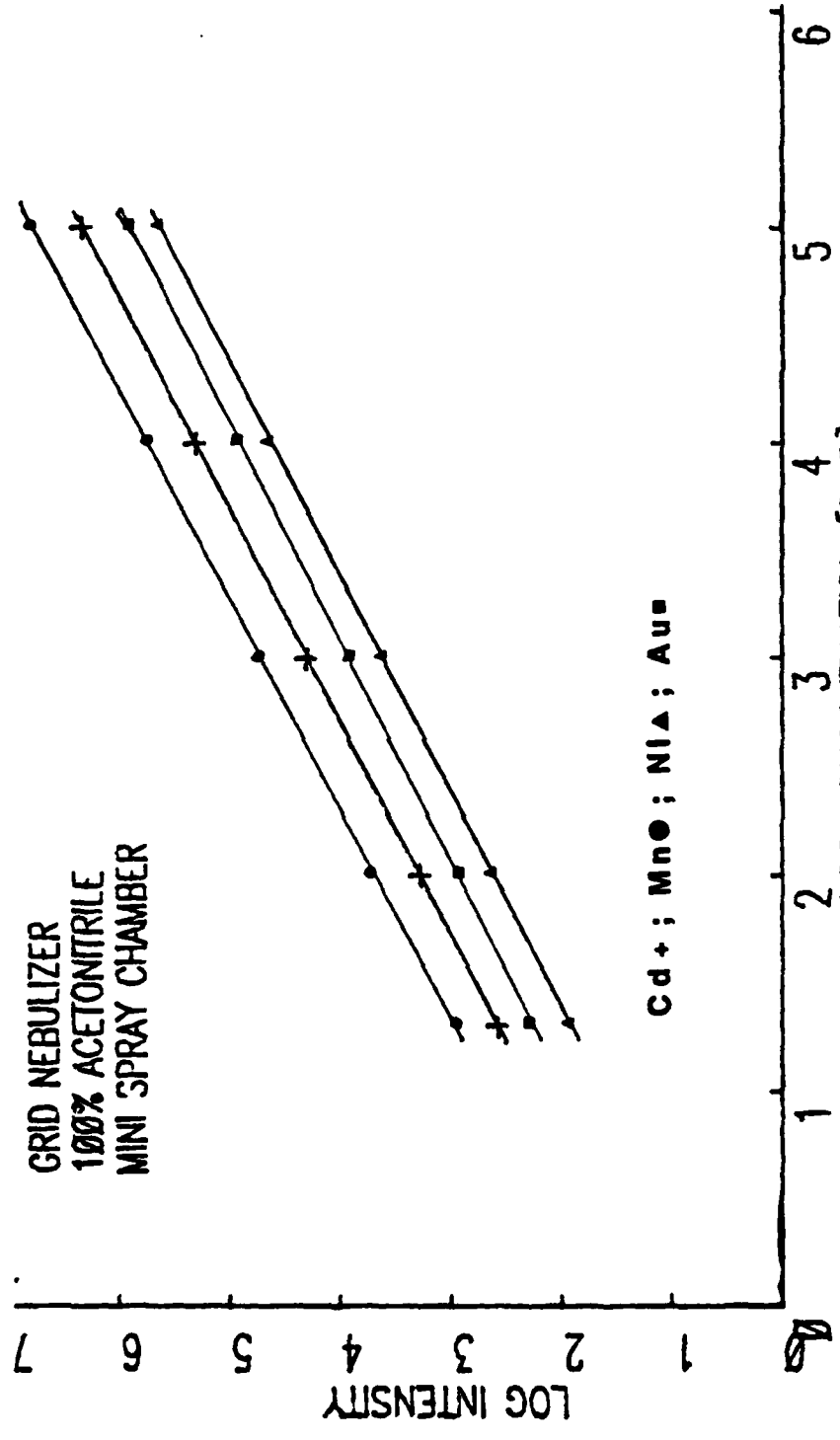

Figure 3-9. Log Concentration vs. Log Emission Intensity

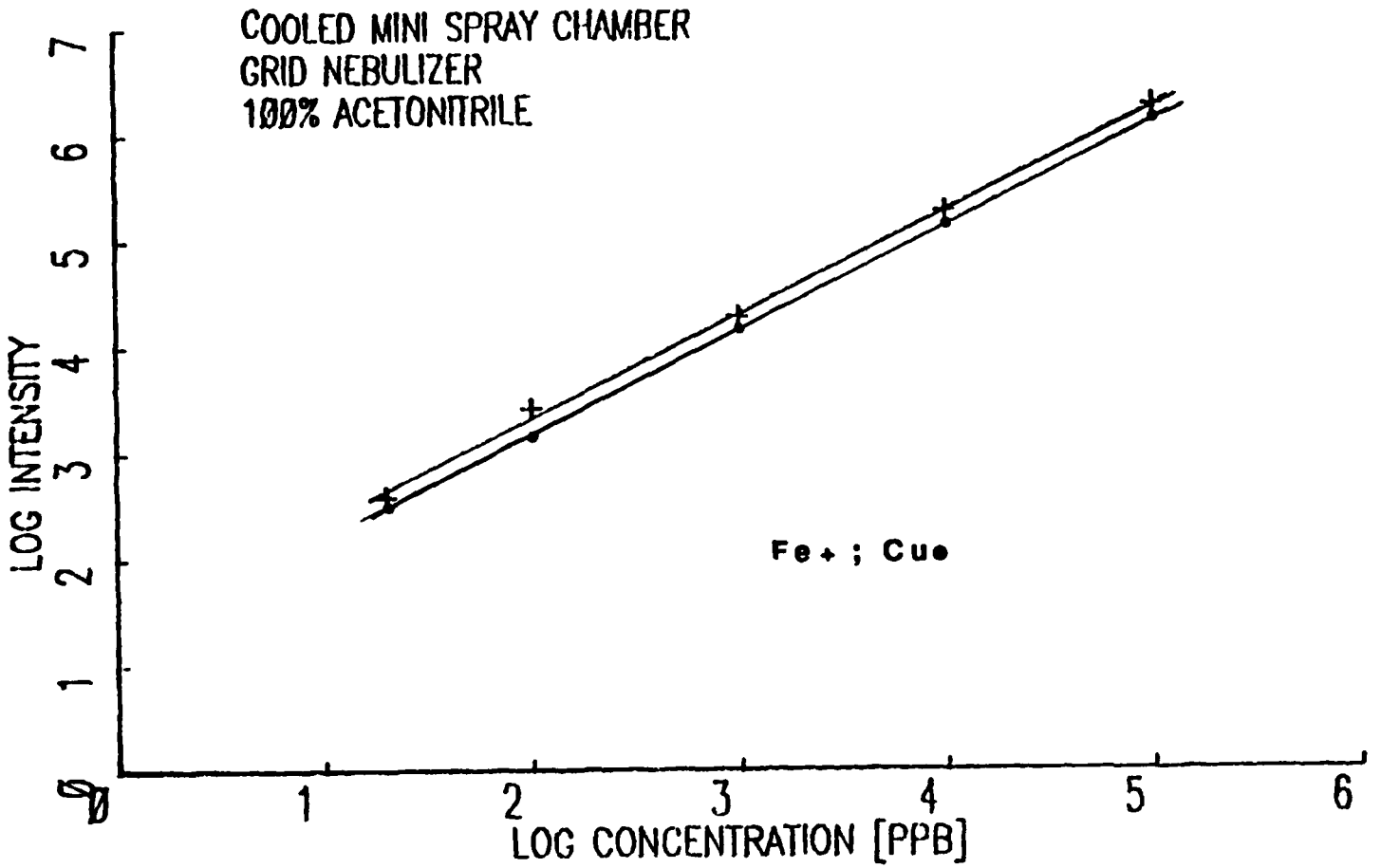

Figure 3-10. Log Concentration vs. Log Emission Intensity for Fe and Cu

plasma. The ideal ICP transport system would transport 100% analyte and no solvent or solvent vapor. The ultrasonic nebulizer approaches this by forming a very intense aerosol. Nebulization efficiencies with ultra sonic nebulizers can be as high as 30%, but typically are about 11%.[29] However, this results in excessive solvent and solvent vapor loading to the plasma. To prevent this, ultrasonic nebulizers (i.e. Baird) have a heated tube (ca. 1 ft.) which evaporates the solvent (in most cases, the solvent vapor is water) from the droplet. The aerosol and solvent vapor is then run through a condenser to condense the unwanted solvent vapor. The result is that a large number of very small droplets (containing analyte) are transported to the plasma. The disadvantages are that some analyte is lost in the condenser stage. Also, this system has reproducibility problems for high salt matrices. This would not be an extremely desirable interface for FIA or HPLC because of such a large dead volume estimated at 467 cc.

The heat/cooled interface uses the same principle as the ultrasonic desolvation system. However, the grid nebulizer is used instead of the ultrasonic nebulizer and the volume of the heated and cooled sections is much less than the ultrasonic desolvation system.

This system was evaluated initially by varying the heat applied to the heated section and by varying the temperature of the condenser. Data presented here show the effect of heating the first stage with a constant condenser temperature of -16^{o}C. **Figure 3-11** depicts the interface.

The temperature of the heating stage was varied to determine the effect on emission intensity. **Figure 3-12** shows the effect of heating on normalized emission intensity of Cd, Fe and Mn. It was anticipated that an increase in emission would be observed as the temperature of the

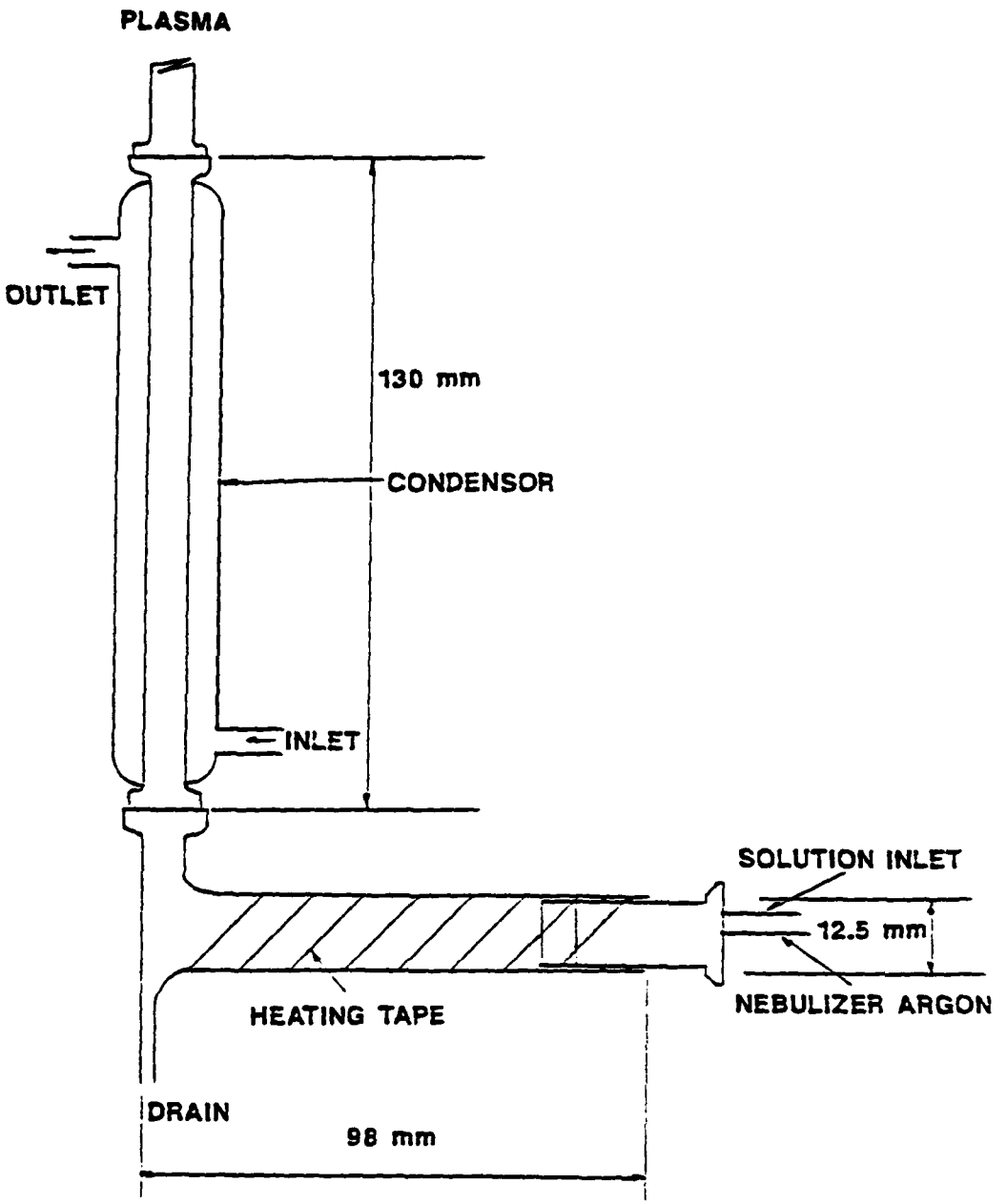

Figure 3-11. Diagram of Heated Cooled Interface

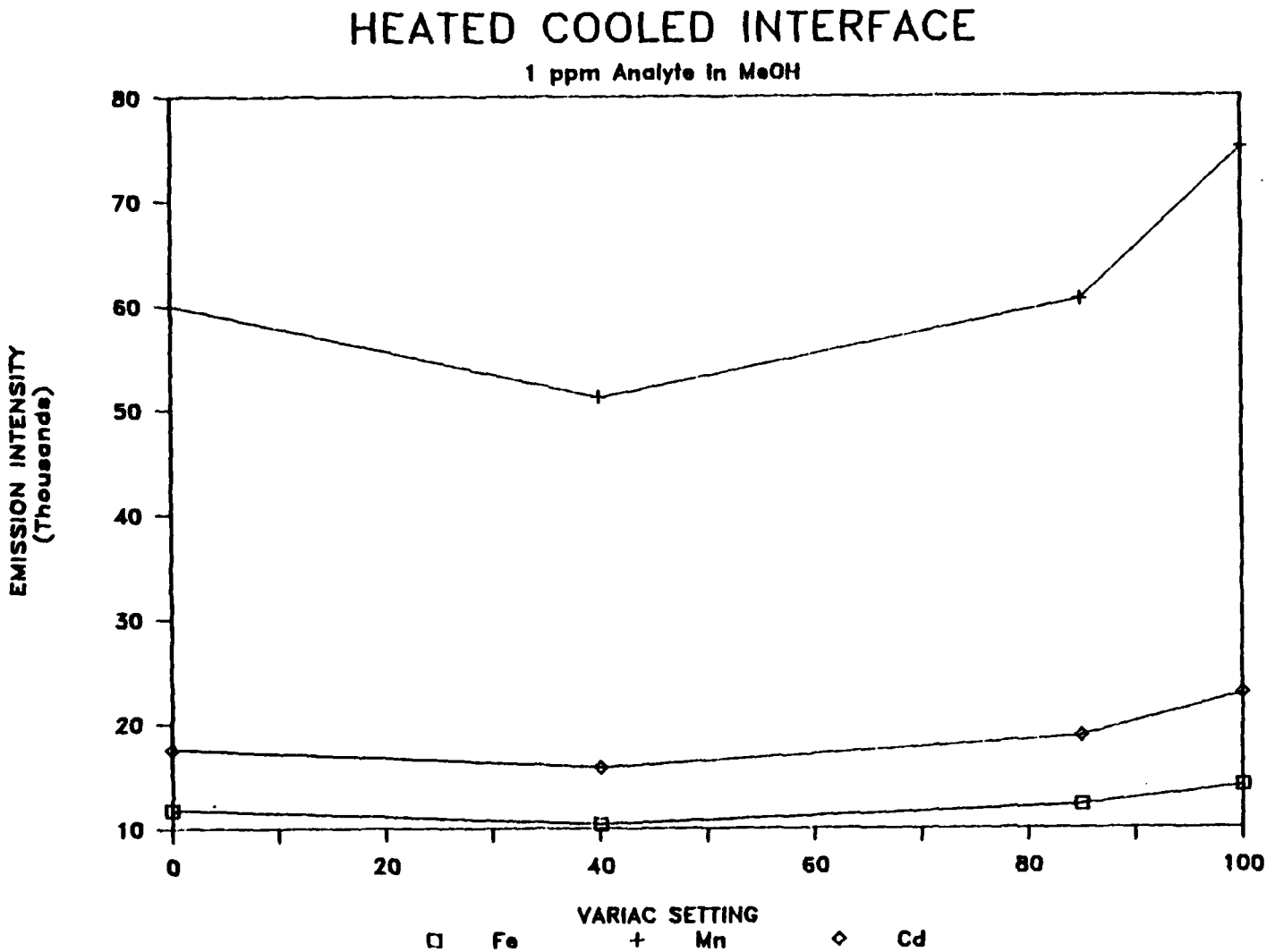

Figure 3-12. Variac Setting vs. Emission Intensity for Mn, Cd, Fe

heating stage increased, but it is unclear why for all elements at first emission decreased initially then increased. **Figure 3-13** shows the calibration of variac with respect to heating temperature.

One explanation may be that for the argon became saturated with methanol vapor at the low heat setting but no appreciable solvent was evaporated from the droplets. As the methanol saturated argon and the droplets were transferred to the condenser stage, the methanol condensed and in so doing "washed" some of the very large droplets down the drain. This resulted in less analyte transport to the plasma and thus lower emission intensity.

Though emission intensity over background for Mn, Cd, and Fe was maximum for a variac setting of 100, the conditions used to measure the DL and LDR was at a variac setting of 85. This was because the % RSD of the background was lower for the variac setting of 85.

3.4.2.1 Results

Table 3-8 shows the detection limits for the heated/cooled interface. These detection limits are very comparable to the cooled mini spray chamber. It was anticipated that this interface would enhance detection limits by driving off most of the solvent from the droplet. Unfortunately, the heating stage of the HCI may be too small to evaporate a large portion of solvent from the droplet. The HCI interface allows for high solution uptake rate of volatile organic solvent, but does not provide for much improvement in detection limits over the cooled mini spray chamber.

Table 3-9 shows the % RSD for a blank, 1 and 10 ppm solutions. The average % RSD for this interface is very similar to the cooled mini spray chamber. The average % RSD for the heat/cooled interface for seven

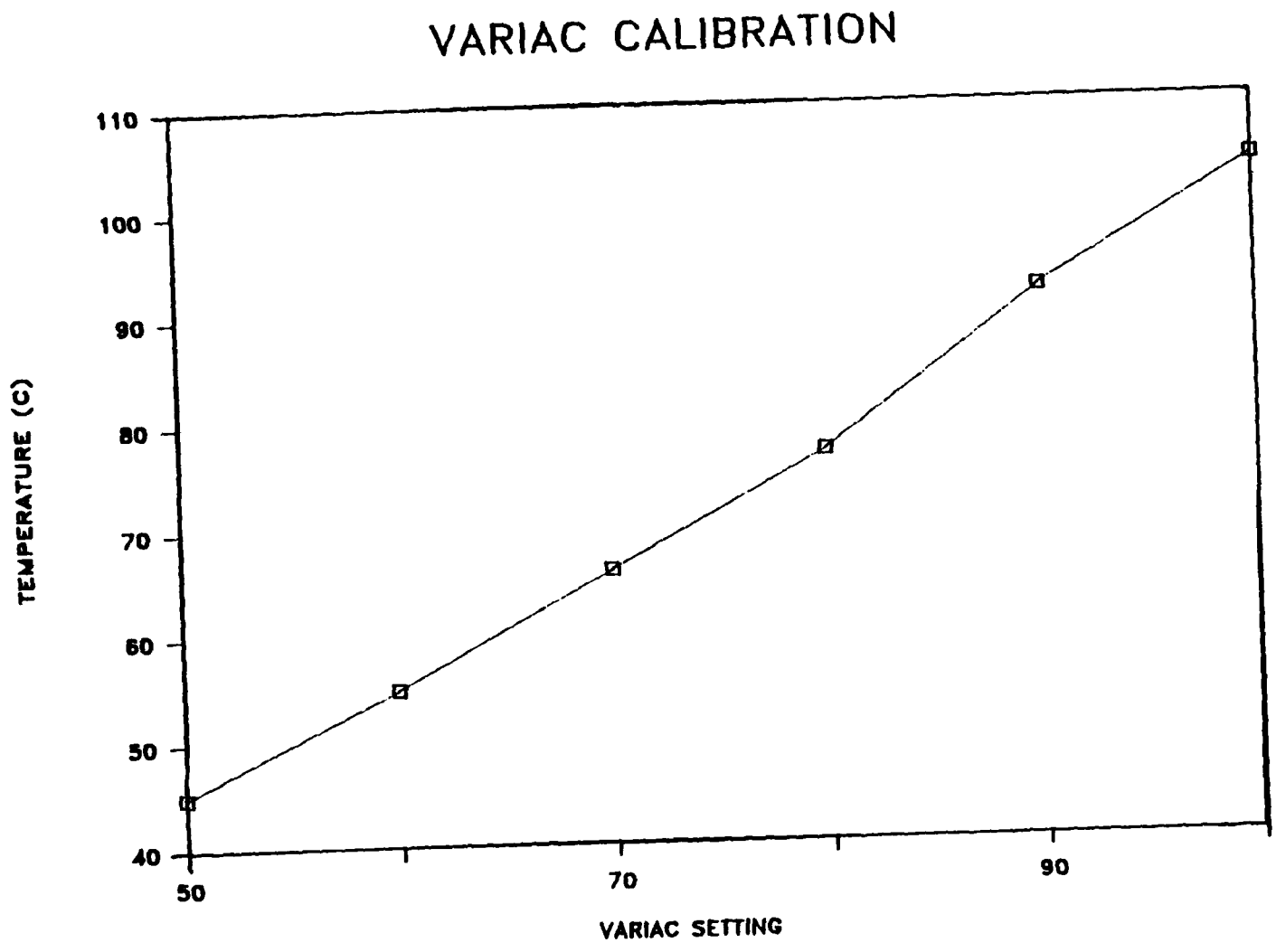

Figure 3-13. Variac Calibration - Setting vs. Temperature

Table 3-8

Detection Limits (ng/ml)

Solution Nebulization

Heat/Cool Interface (HCI)

Element	Detection Limit (ng/mL)	
	100% Methanol	100% Acetonitrile
Au	6.4	2.2
Cd	0.9	0.8
Cu	5.3	6.6
Fe	2.4	3.9
Mn	0.6	0.8
Ni	5.0	5.4
Zn	2.2	5.3

Table 3-9

% Relative Standard Deviation

Solution Nebulization

Grid Nebulizer Heated/Cooled Interface

Element	100% Methanol			100% Acetonitrile		
	Blank	1 µg/ml	10 µg/ml	Blank	1 µg/ml	10 µg/ml
Au	0.3	0.9	1.1	0.5	0.6	0.3
Cd	0.3	0.2	0.5	0.3	0.2	0.3
Cu	0.1	0.6	0.9	0.6	0.5	0.2
Fe	0.2	0.5	0.9	0.6	0.4	0.2
Mn	0.3	0.5	0.9	0.6	0.3	0.6
Ni	0.3	0.8	0.9	0.5	0.2	0.3
Zn	0.5	0.4	0.6	0.6	0.3	0.4
AVG	0.3	0.6	0.8	0.5	0.4	0.3

elements in methanol is 0.56% versus 0.47% for the cooled mini spray chamber. For the same elements in acetonitrile, the comparison is even closer -- 0.44% (HCI) versus 0.41% (CMSC).

Figures 3-14, 3-15, 3-16 shows the linear dynamic range for seven elements. The data show that this interface is very linear over 3-5 orders of magnitude. **Table 3-10** shows the calibration coefficients.

3.4.3 Positive Suction Injector

Both the cooled mini spray chamber and the heated cooled interface rely on condensing the unwanted solvent vapor. Another approach in removing unwanted vapor is to separate the droplets from the solvent vapor based on the different kinetic energies of the two. **Figure 3-17** depicts the positive suction injector. The aerosol is formed as in the case of the cooled mini spray chamber. However, the spray chamber need not be cooled (in our case we kept the spray chamber at a constant temperature so that evaporation within the spray chamber remains constant). The droplets are carried into the injector and travel at the rate approximately equivalent to the velocity of the argon. If one assumes that the aerosol droplets (methanol) range in diameter from 10-0.1 um, this equates to a mass range of .41 ng - 4.1×10^{-7} ng per droplet. Since they are traveling at more or less the same velocity, their kinetic energies would span six orders of magnitude and vary via the relationship $KE = 1/2\ MV^2$. Similarly, the kinetic energy of the methanol vapor and argon can be estimated via this same relationship. However, since the mass of an atom of argon and a molecule of methanol is approximately 6×10^{-17} ng, the kinetic energy is much less than any size aerosol droplet in our distribution.

The injector is equipped with two ports that are used to suction off

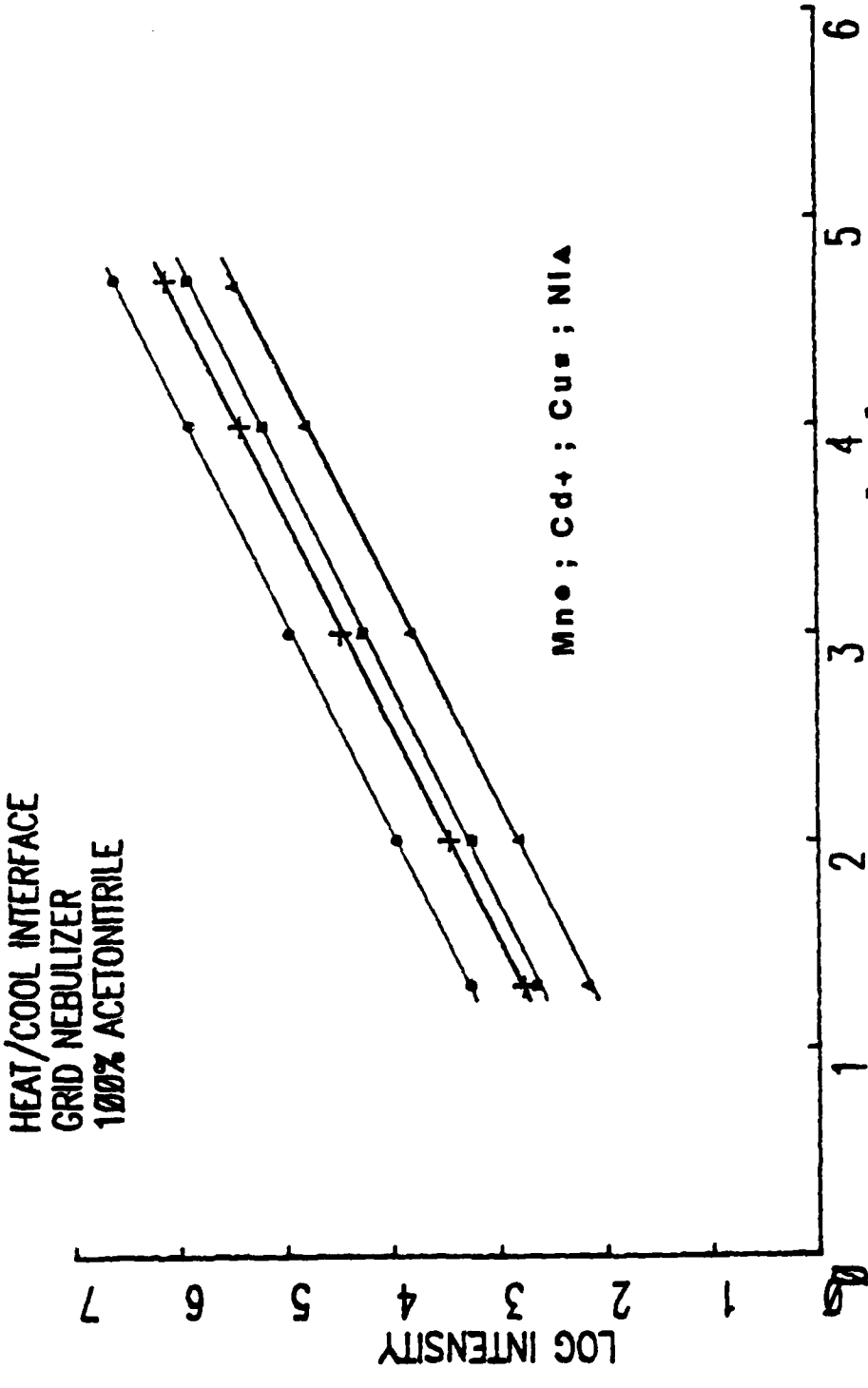

Figure 3-14. Log Concentration vs. Log Emission Intensity

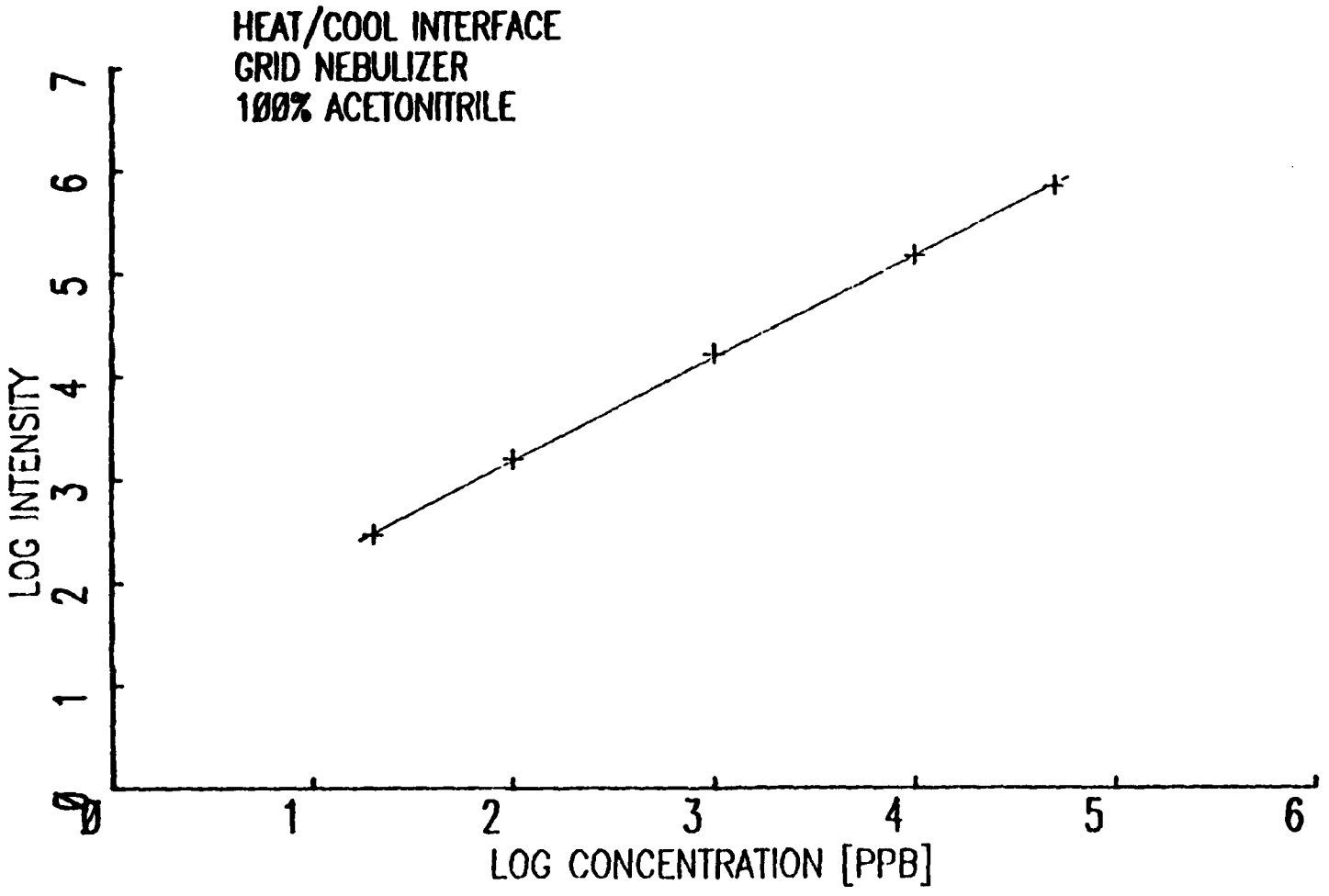

Figure 3-15. Log Concentration vs. Log Emission Intensity for Fe

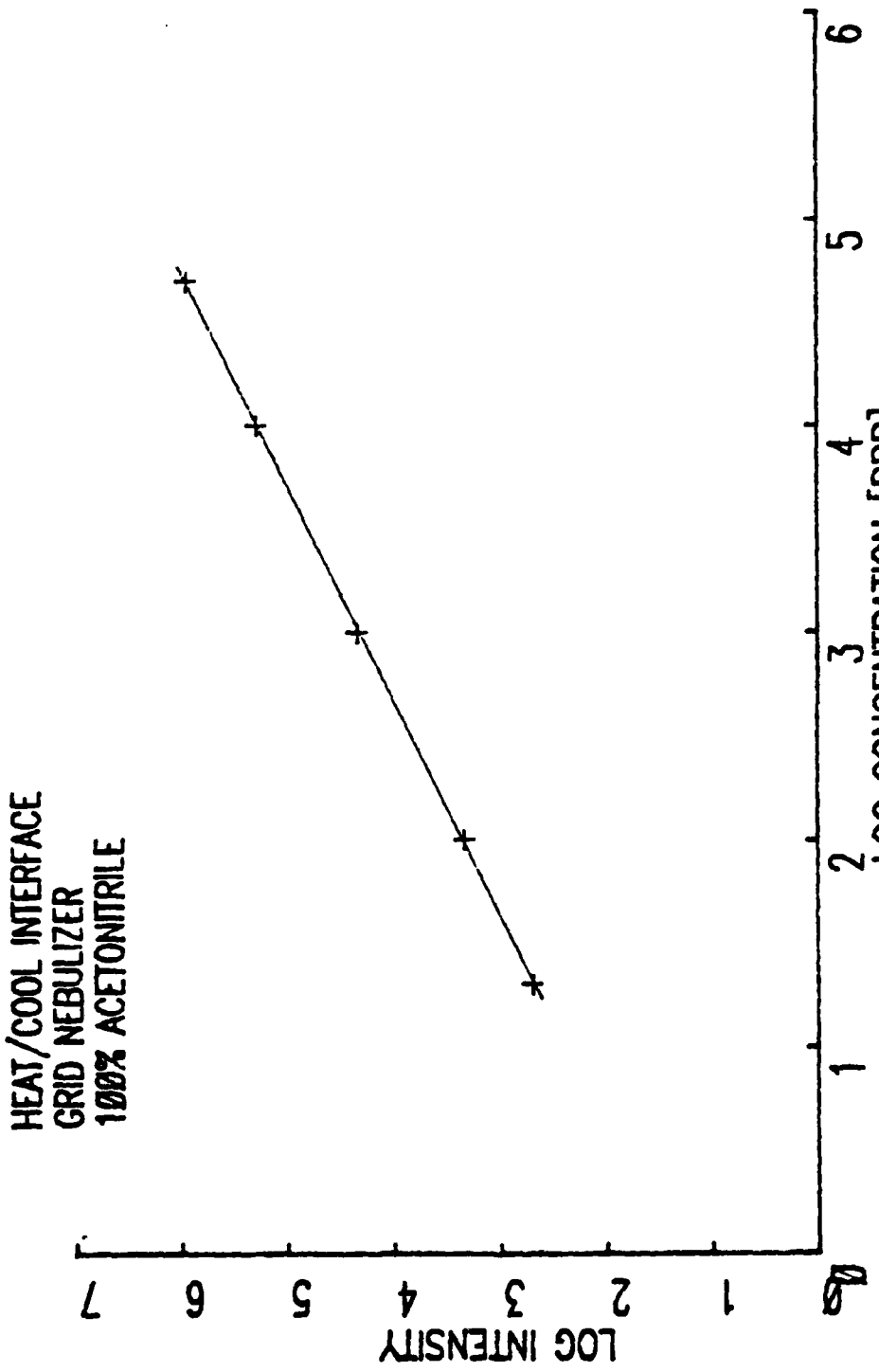

Figure 3-16. Log Concentration vs. Log Emission Intensity for Zn

Table 3-10

Calibration Coefficients

Grid Nebulizer Heated/Cooled Interface

100% Methanol

Element	Slope	Intercept	Correlation Coefficient
Cd	0.98	1.512	0.99991
Cu	0.96	1.339	0.99980
Fe	0.99	1.268	0.99985
Mn	0.97	2.010	0.99990
Ni	0.98	0.820	0.99980
Zn	0.96	1.447	0.99993

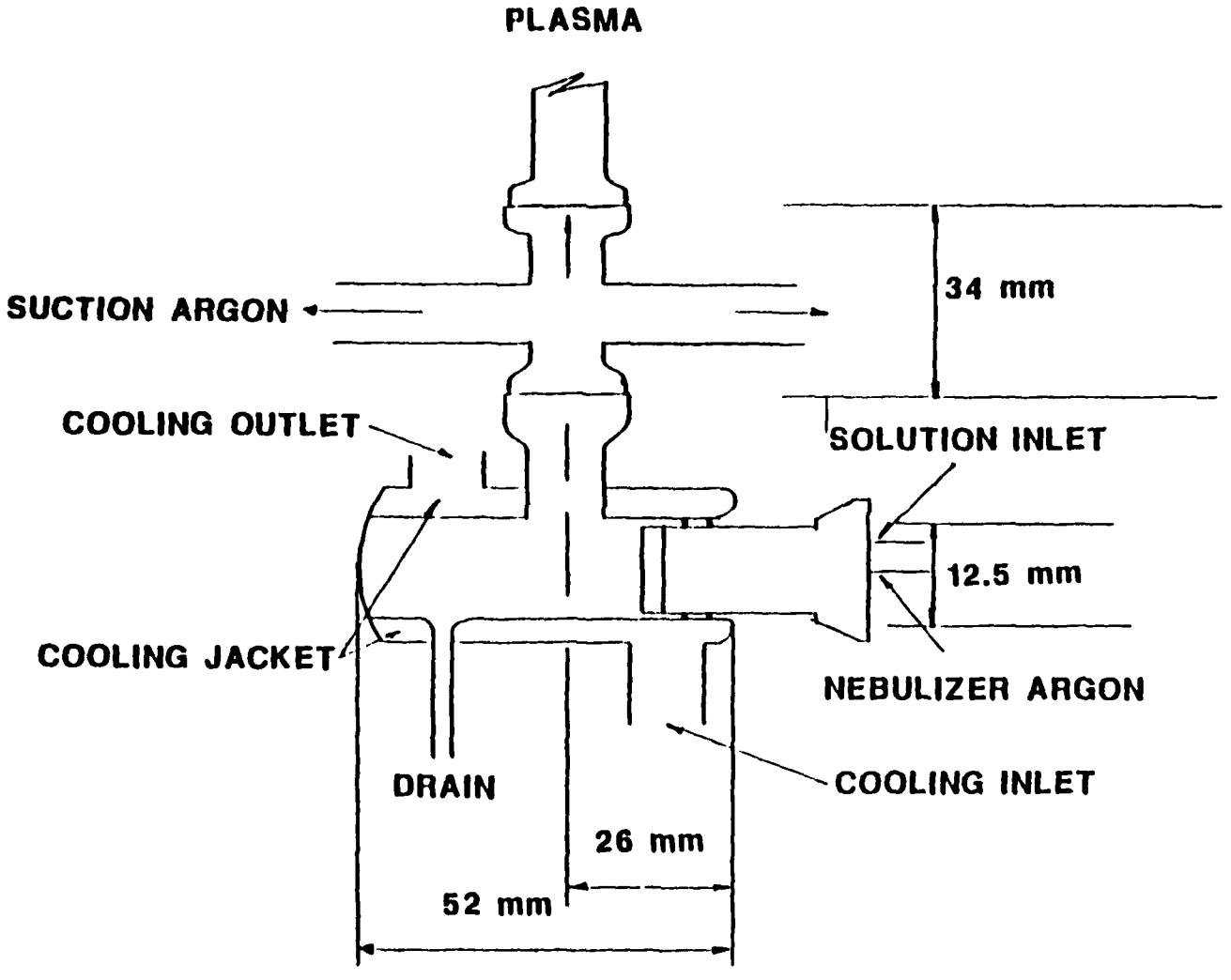

Figure 3-17. Diagram for Positive Suction Injector (PSI)

a certain amount of argon. Since methanol vapor is present in the argon, a portion of that vapor can be removed by suctioning out a certain percentage of argon. Since the droplets' kinetic energy is much greater than that of methanol vapor (mass of a molecule of methanol is 5.31 x 10^{-17} ng) or argon, the droplets would tend to preferentially travel up the injector with the argon that will travel to the plasma.

3.4.3.1 Experimental

The experimental setup for this is shown in **Figure 3-18.** For the purpose of clarification, the inlet argon to the nebulizer will be referenced to as nebulizer argon, the argon carrying the aerosol to the plasma will be referred to as plasma argon, and the argon that is suctioned off the sample delivery system will be called suctioned argon.

The design of the positive suction injector is very simple. Initially, an injector with two side ports was made and used on the ICP. Subsequently, an interface was made that would allow quick turnover from the normal ICP configuration to the positive suction injector (PSI) configuration.

The suctioned argon was controlled via a Tylan mass flow controller; the nebulizer argon was controlled with a rotometer. A liquid nitrogen trap was placed in line between the positive suction injector and the mass flow controller to keep solvent vapor out of the mass flow controller. A simple water aspirator system was used as the suction force for the mass flow controller.

The PSI was not used until after plasma ignition and a 15-30 minute warmup. The PSI valve was opened and this allowed the argon and aerosol to flow either up the injector or out the suction ports. The mass flow controller was typically set at about 100-150 mL/min for initial suction

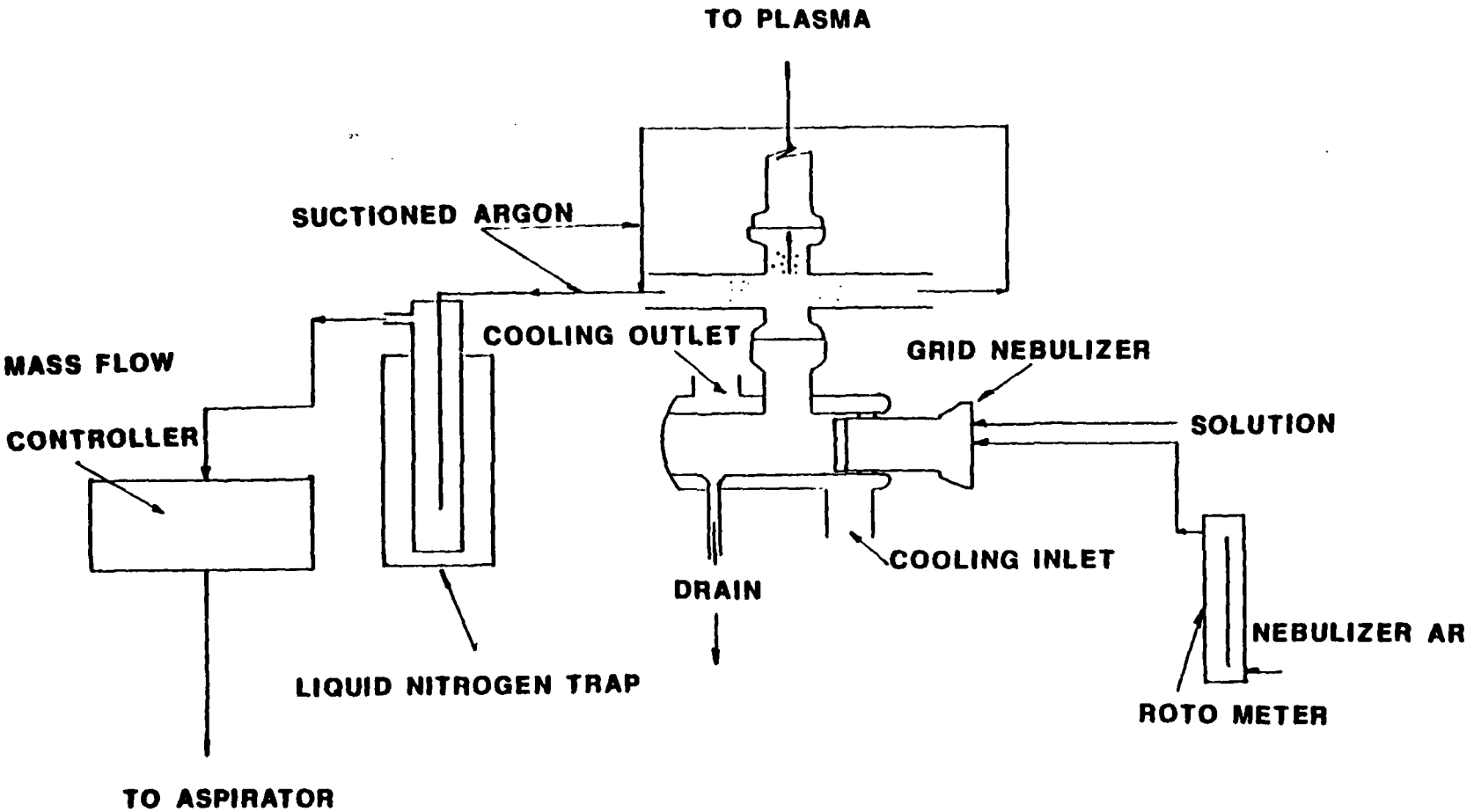

Figure 3-18. Schematic for Positive Suction Injector (PSI)

argon flow rate. The nebulizer argon flow rate was approximately 700 mL/min. Care was taken during the opening of the PSI valve to ensure that the plasma was not "suctioned" down to rest on the inner quartz tube.

Analyte was nebulized into the plasma and the optimization procedure previously outlined was performed. Data was collected for a particular nebulizer argon and suction argon flow rate. The suction argon was changed and the analyte optimization procedure was performed. After data were collected for various suction argon flow rates, nebulizer flow rate was changed and the whole procedure was repeated.

3.4.3.2 Results

The PSI allowed for a very high limiting aspiration rate for methanol and acetonitrile. The high LAR's could be achieved without use of a cooled spray chamber (unlike the previous interfaces). The spray chamber for the PSI was kept at a constant temperature to reduce random noise that may be due to temperature fluctuations. This interface could be used to accommodate a volatile organic solvent introduced at the rate of 1-2 mL/min. However, there are problems associated with this interface that need to be addressed.

The detection limits achieved with the PSI interface are listed in **Table 3-11.** As can be seen, these DL are 2-10 times more than either the CMSC or the HCI. **Table 3-12** shows the comparable detection limits for the three interfaces for solution nebulization. **Figures 3-19, 3-20** show the Linear Dynamic Ranges for various elements in 100% methanol. The LDR spans 3-4 orders of magnitude and exhibits good linearity as shown by the statistics for the plots listed in **Table 3-13.**

The detection limits are poor because the high noise associated

Table 3-11

Detection Limits (ng/ml)

Solution Nebulization

Grid Nebulizer/Positive Suction Injector (PSI)

Element	Detection Limit (ng/mL)		
	100% Methanol (Spray Chamber @ 0 C)	100% Methanol (Spray Chamber @ 25 C)	100% Acetonitrile (Spray Chamber @ 25 C)
Au	5.4	16.3	17.7
Cd	1.4	0.5	1.2
Cu	7.9	29.5	32.5
Fe	2.3	21.6	27.8
Mn	0.5	1.6	0.9
Ni	1.3	26.0	20.5
Zn	0.8	10.9	8.9

Table 3-12

Comparative Detection Limits (ng/mL)

100% Methanol

Element	Large Conical Spray Chamber	Cooled Mini Spray Chamber	Heated/ Cooled Interface (85°C/-15°C)	Positive Suction Injector 25°C	Positive Suction Injector 0°C
Au	--	5.2	6.4	16.3	5.4
Cd	15.7	0.6	0.9	0.5	1.4
Cu	194	6.8	5.3	29.5	7.9
Fe	--	1.2	2.4	21.6	2.3
Mn	13.1	0.7	0.6	1.6	0.5
Ni	71.5	6.3	5.0	26.8	1.3
Zn	23.1	1.7	2.2	10.9	0.8

Table 3-13

Calibration Coefficients

Grid Nebulizer/Positive Suction Injector (PSI)

100% Methanol

Element	Slope	Intercept	Correlation Coefficient
Cd	0.98	1.353	0.99997
Fe	1.04	0.896	0.99980
Mn	1.00	1.749	0.99983
Ni	0.99	0.594	0.99998
Zn	0.95	1.379	0.99942

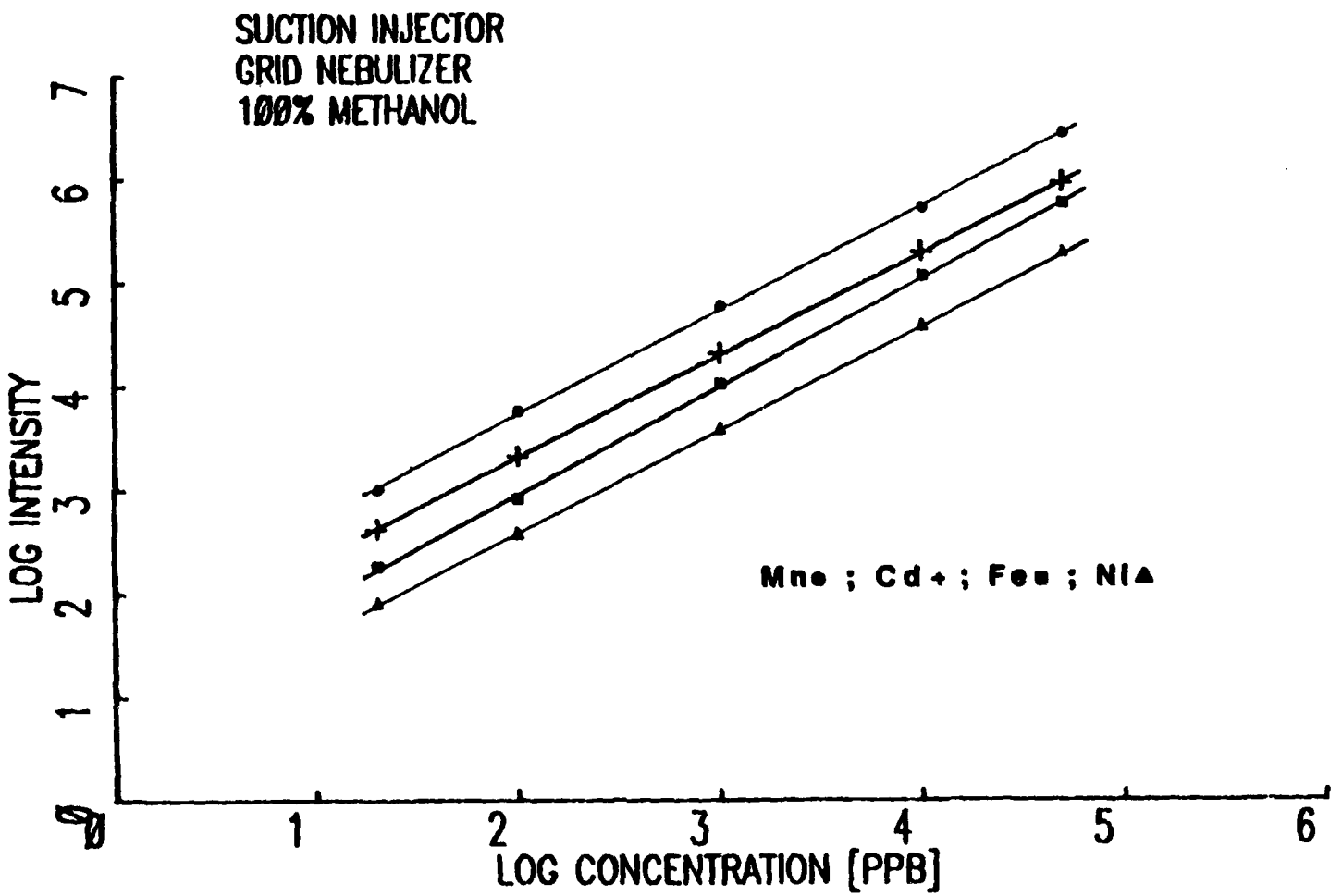

Figure 3-19. Log Concentration vs. Log Emission Intensity for Mn, Cd, Fe, Ni

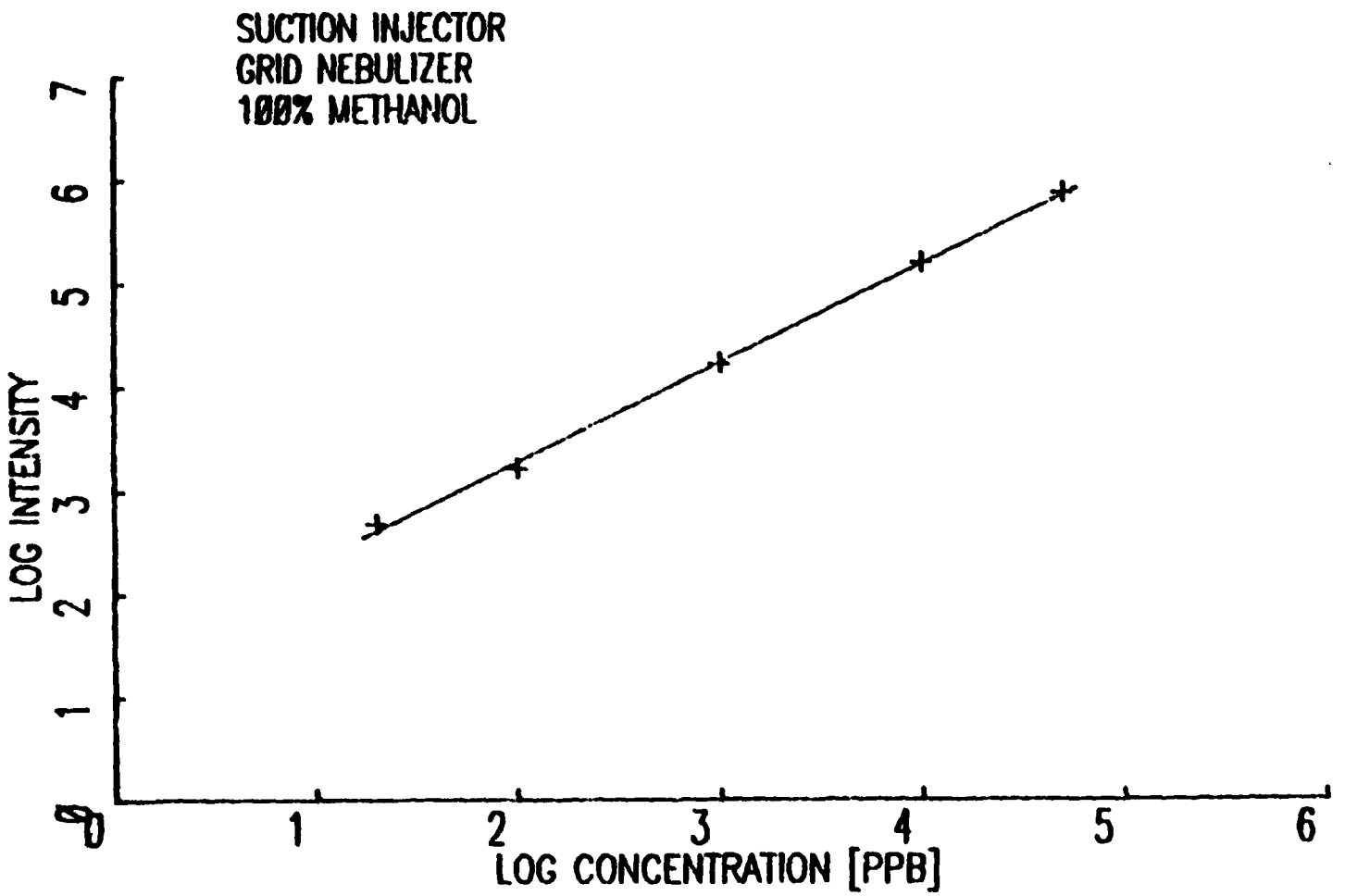

Figure 3-20. Log Concentration vs. Log Emission Intensity for Zn

with this interface. Table 3-14 shows the % RSD of blank, 1 ppm and 10 ppm solutions. The % RSD is 4-5 times that of both the CMSC or the HCI.

The primary reason for these high % RSDs is due to how the nebulizer argon and suction argon was controlled. The nebulizer argon was controlled via a single float rotometer and the suction argon was controlled with a Tylan mass flow controller, with a range of 0-5 L/min argon.

This experiment required that a vacuum be applied to the outlet side of the mass flow controller. Initially a rotary vacuum pump capable of 1 torr was used for the vacuum system. This induced an extremely large periodic fluctuations in the emission signal. The water aspirator was used because it did not exhibit the large periodic fluctuations in the emission signal. However, slight drift in aspirator vacuum pressure was observed (as could happen during high water usage periods).

The range of the mass flow controller was 0-5 L/min. The typical argon flow was 0.1-0.3 L/min, and because we were operating at such a low flow compared to the range of the controller, there was much fluctuation in the argon flow (and thus emission signal).

In spite of this, definite trends and conclusions can be made for this experiment concerning the effect that argon flow rate had on emission signal.

To determine the effect of argon flow rate on emission signal, a quantity called argon ratio was calculated. The argon ratio is defined as the (argon flow rate to the plasma)/(argon flow rate to the nebulizer) and was calculated as (argon flow rate to nebulizer - suction argon flow rate)/nebulizer argon flow rate.

Figures 3-21, 3-22, 3-23, 3-24 show normalized emission intensity as a function of argon ratio for various constant nebulizer flows. As can

Table 3-14

% Relative Standard Deviation

Solution Nebulization

Grid Nebulizer/Positive Suction Injector (PSI)

Element	100% Methanol			100% Acetonitrile		
	Blank	1 µg/ml	10 µg/ml	Blank	1 µg/ml	10 µg/ml
Au	--	--	--	0.6	1.5	1.9
Cd	0.5	0.8	0.5	0.4	1.1	2.1
Cu	2.3	1.7	4.0	2.7	2.9	3.2
Fe	2.2	5.5	1.5	2.3	3.5	5.3
Mn	0.9	0.6	0.6	0.3	0.3	0.6
Ni	1.6	1.5	1.2	1.2	2.9	3.1
Zn	2.5	0.9	1.2	2.6	5.1	4.9
AVG	1.7	1.8	1.5	1.4	2.5	3.0

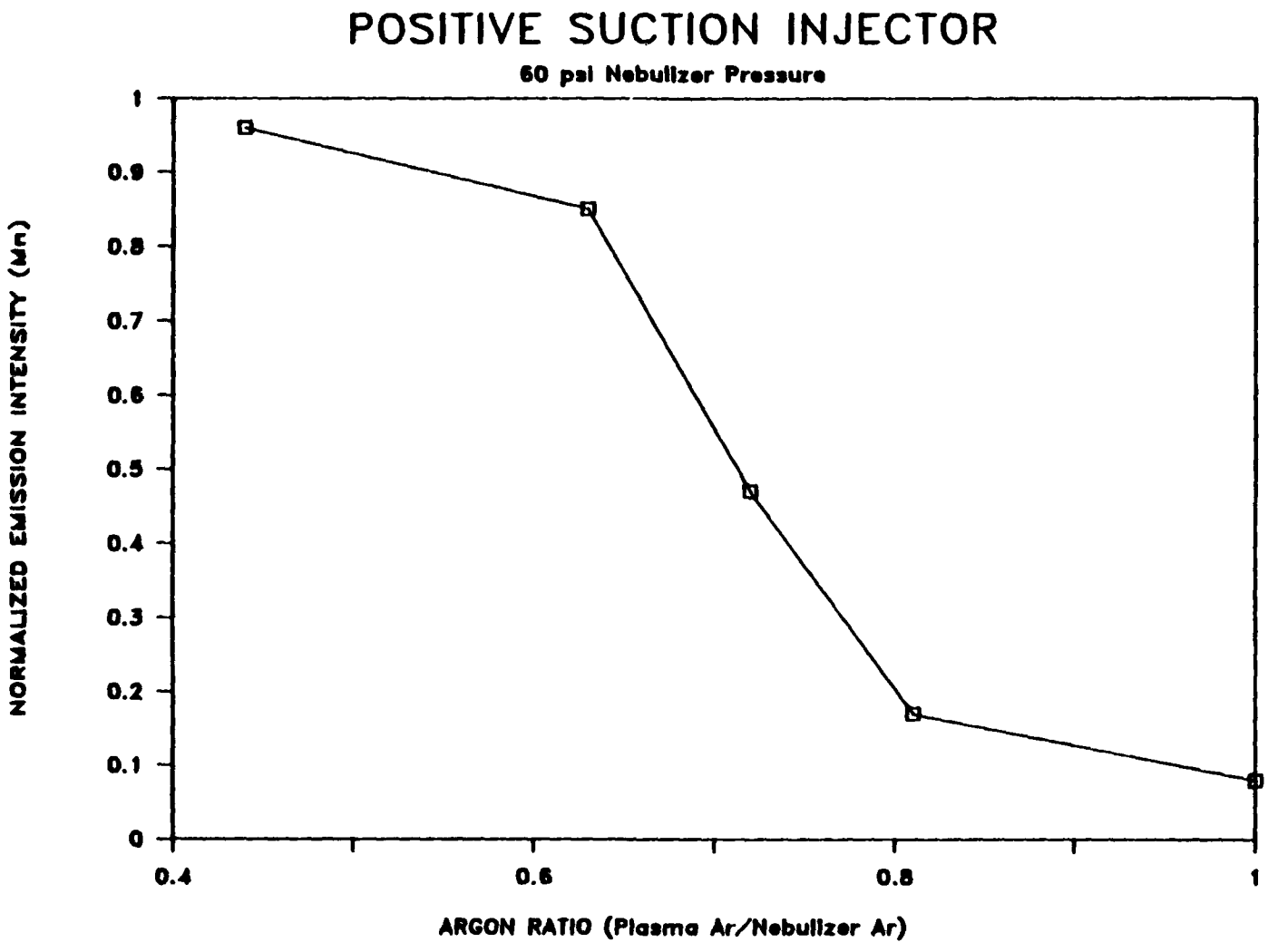

Figure 3-21. Argon Ratio vs. Normalized Emission Intensity

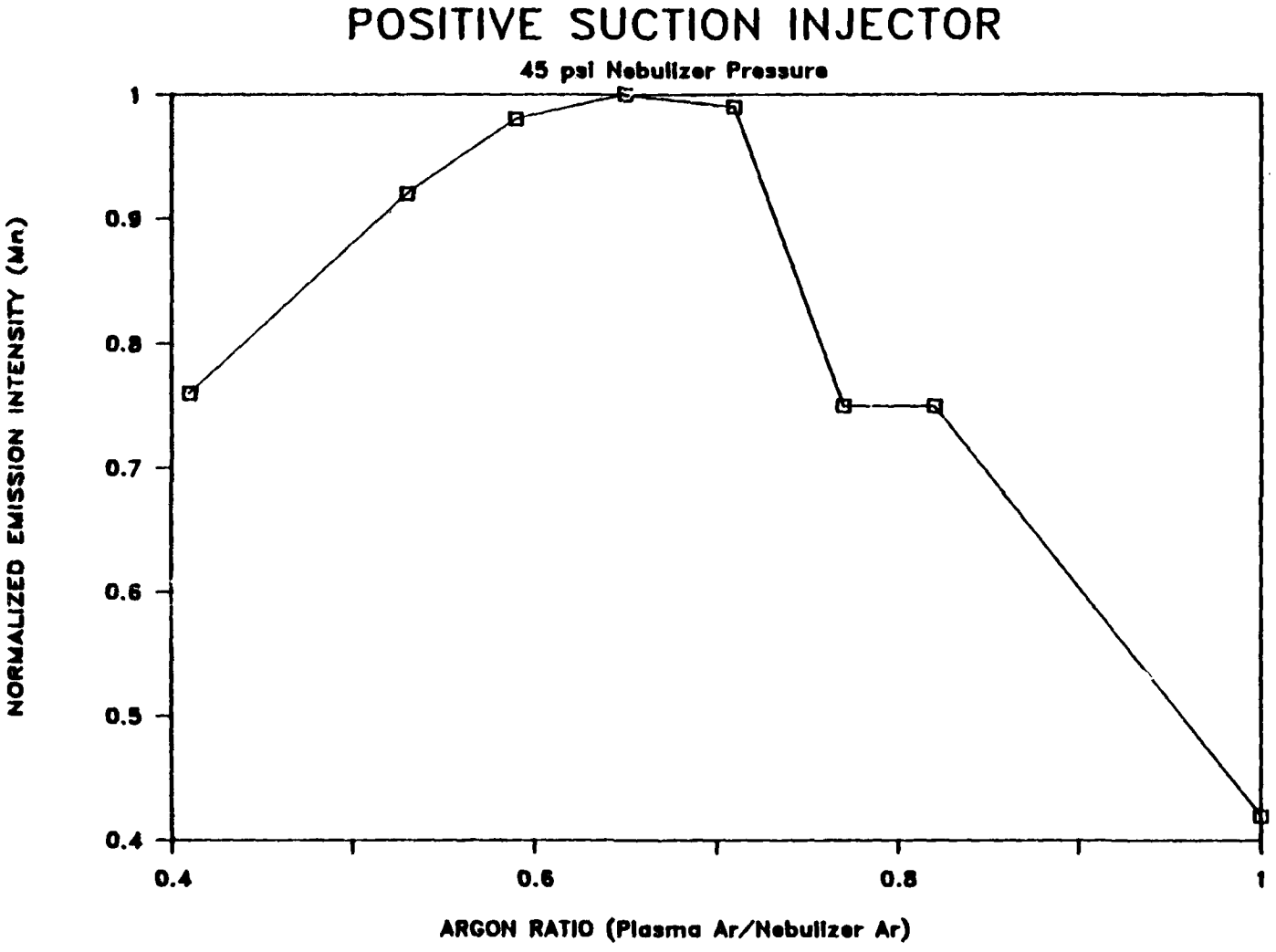

Figure 3-22. Argon Ratio vs. Normalized Emission Intensity

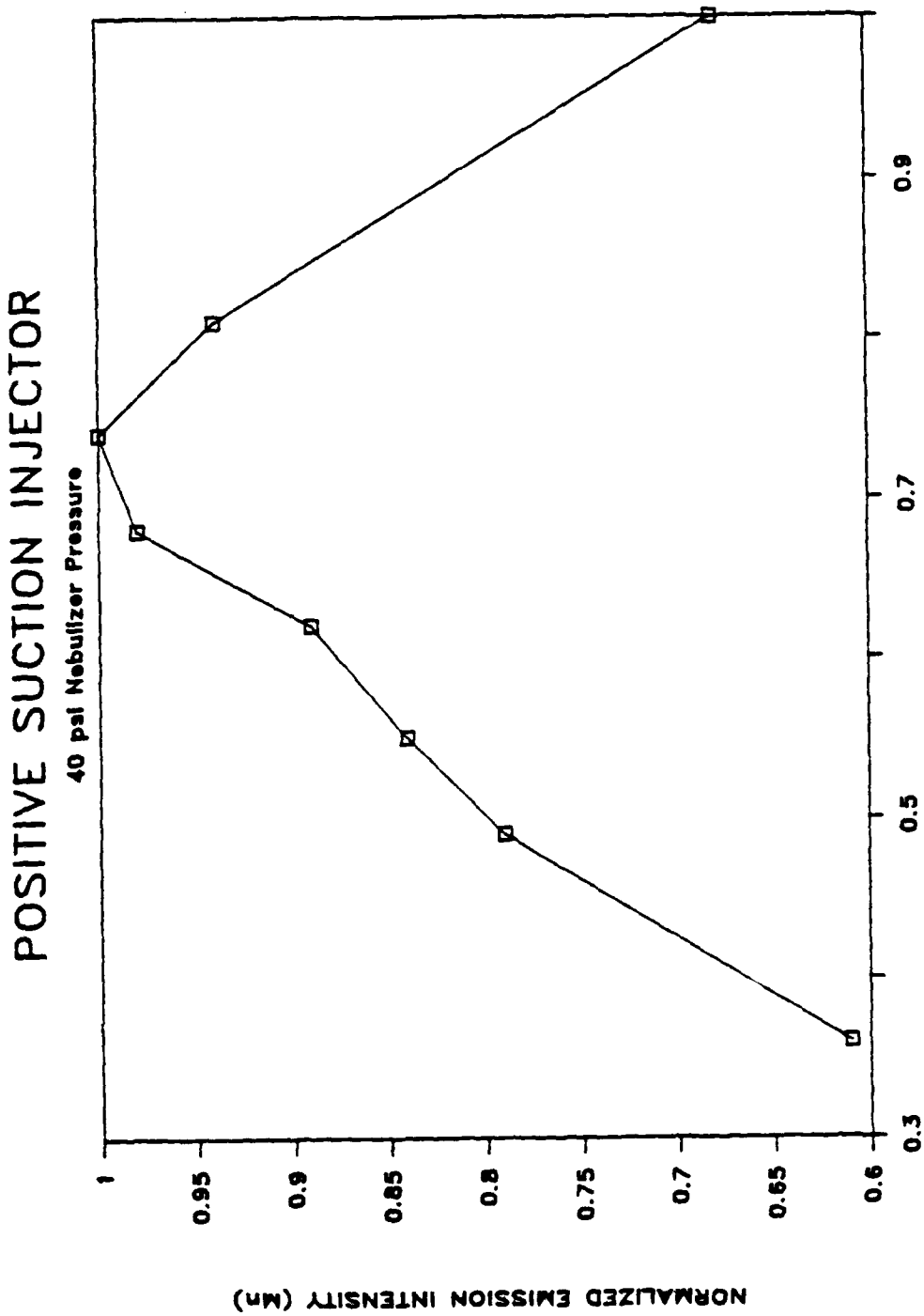

Figure 3-23. Argon Ratio vs. Normalized Emission Intensity

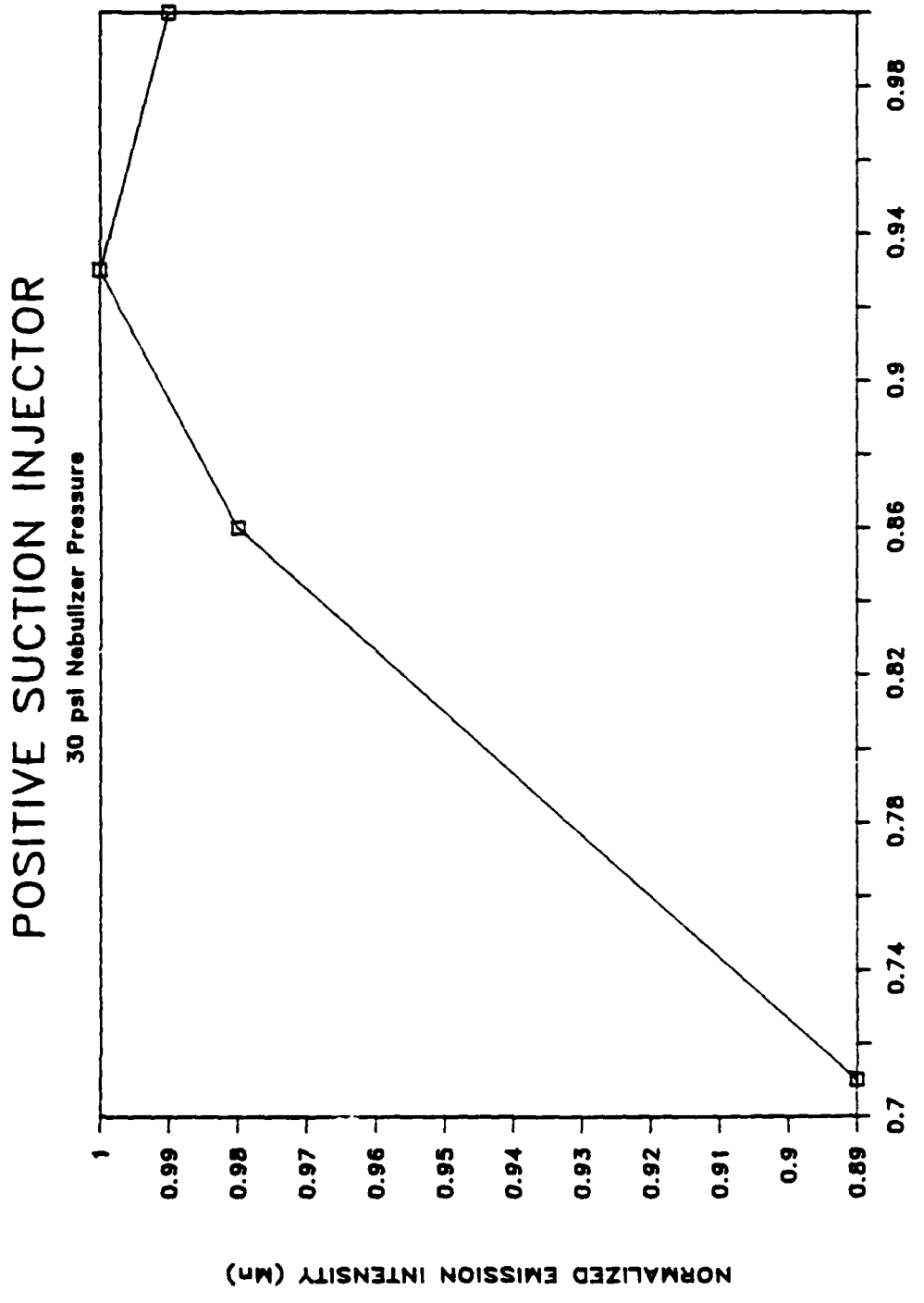

Figure 3-24. Argon Ratio vs. Normalized Emission Intensity

be seen, as total nebulizer argon flow rate is increased, maximum emission intensity is achieved for a smaller argon ratio for maximum signal intensity.

3.5 FLOW INJECTION ANALYSIS

Flow injection analysis was performed with a Rheodyne 6 port injection valve using all three interfaces. The experimental setup was essentially the same except transient data were collected via a Compupro computer instead of using the LEEMAN data collection system. All interfaces were evaluated in terms of % RSD, detection limits, peak width and linear dynamic range.

3.5.1 Sample Injection Size

Optimal sample size was the smallest injection that gave a peak height for a 1 ppm Mn solution approximately equal to steady state signal intensity for a 1 ppm Mn solution nebulized into the ICP. The optimal injection volume used for FIA was 50 μL. A constant flow rate of 1.0 mL/min was used for FIA. **Figure 3-25** shows various sample injections compared to solution nebulization.

3.5.2 Data Collection

PMT current was converted to a voltage (0-10 V) via a laboratory built auto ranging amplifier and digitized with an IO technology analog to digital converter. Signal averaged data (30 data points) were sampled at 4 Hz. Peak profiles were smoothed via a 9 point Savitsky Golay smoothing routine. **Figure 3-26** depicts this data collection scheme.

3.5.3 CMSC

As stated above, the requirements for HPLC or FIA are relatively straightforward - small volume, low % RSD of emission signal, and solvent vapor removal. Unfortunately, it is difficult to design a spray chamber

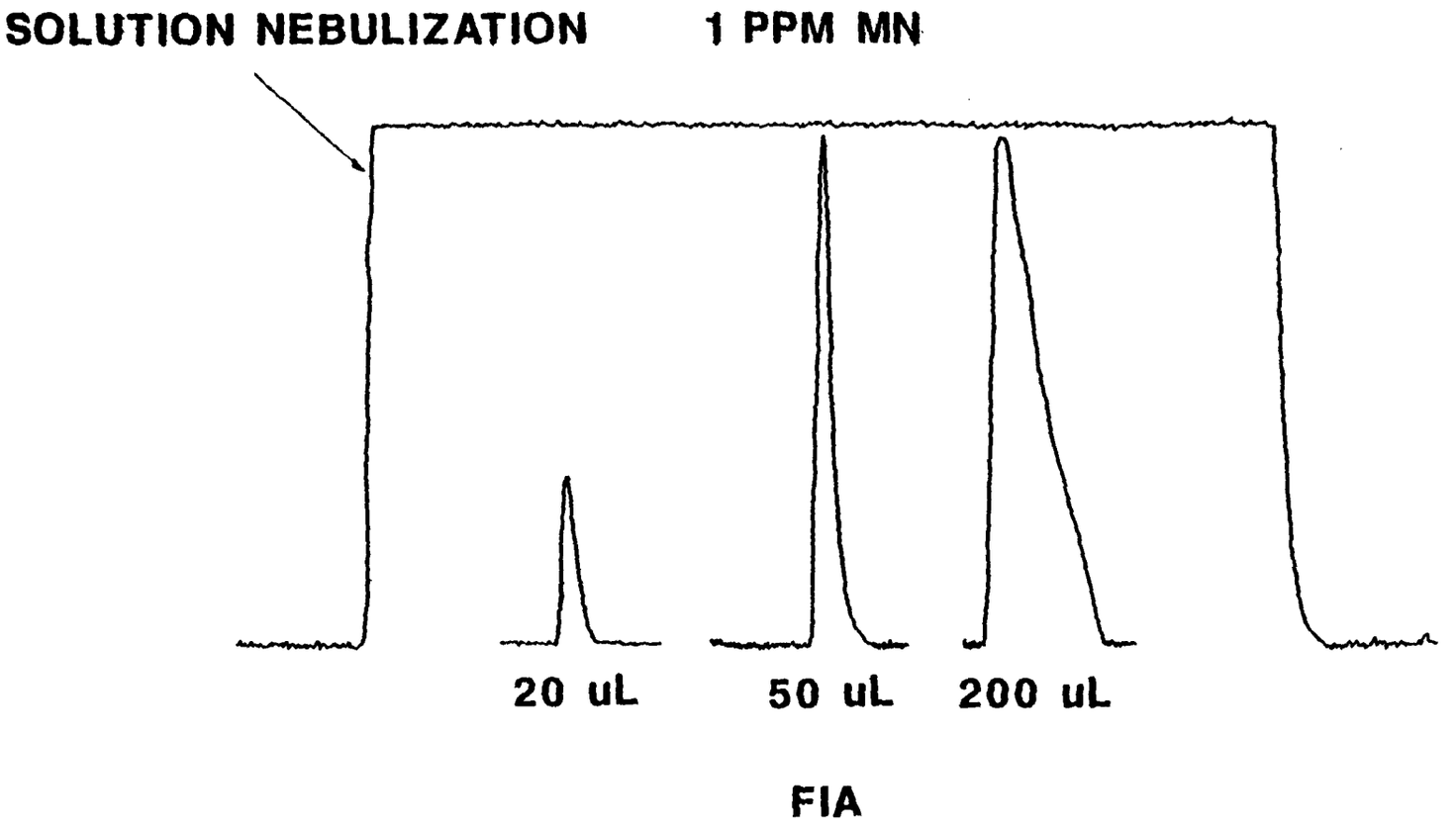

Figure 3-25. Sample Size Determination for Flow Injection Analysis (FIA)

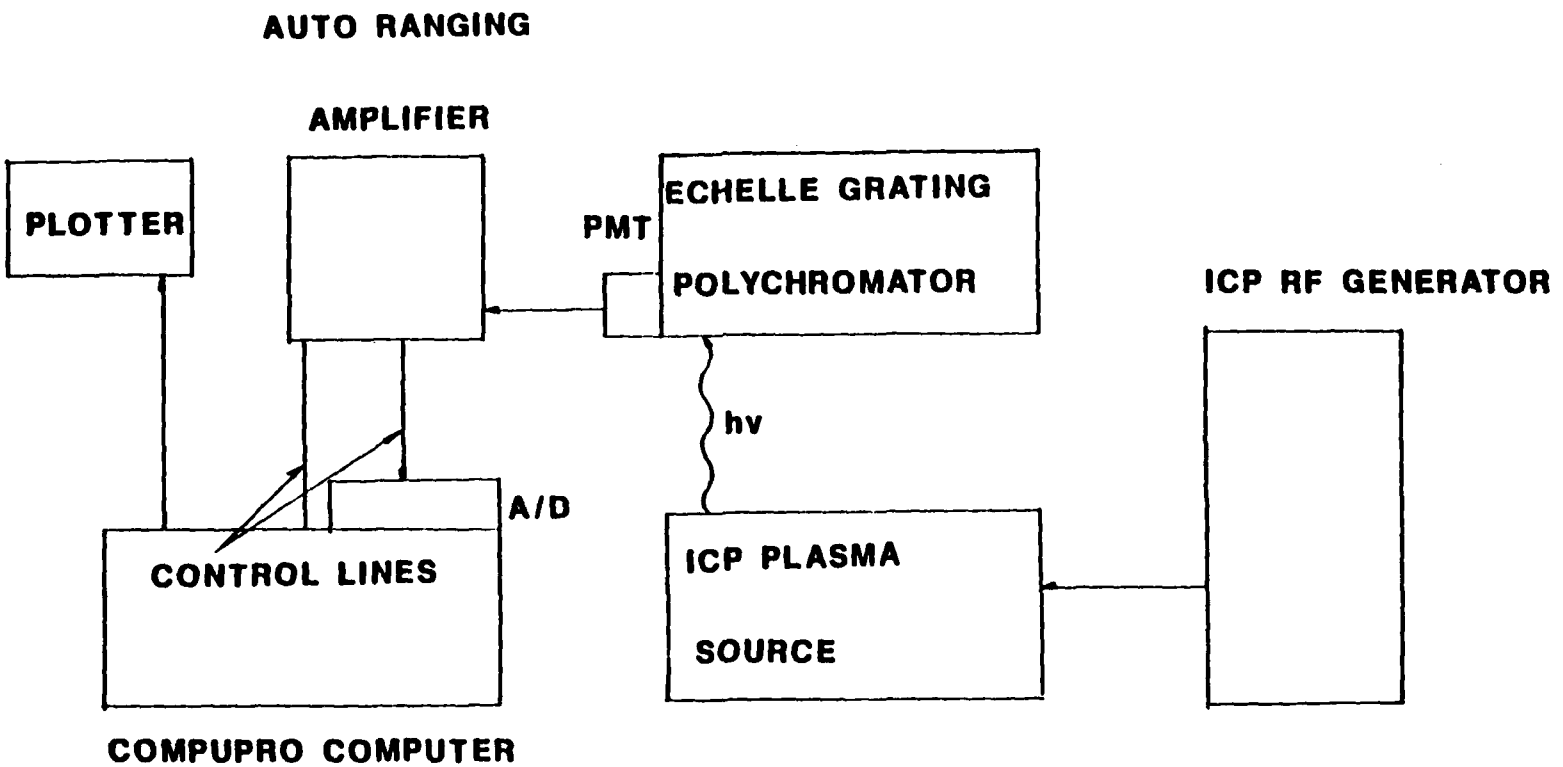

Figure 3-26. Data Collection Schematic for Flow Injection Analysis (FIA)

that can meet all the requirements simultaneously. Typically as spray chamber volume is decreased (as with a Scott double pass spray chamber to a conical spray chamber with impinger ball), the % RSD of emission signal increases due to fluctuations in aerosol flow. Similarly, as the volume of a cooled spray chamber is increased, more solvent vapor is condensed because there is more surface area, but transient signals are broadened significantly.

The cooled mini-spray chamber is designed so that the small volume minimizes band broadening due to sample transport. **Figure 3-26** depicts how the aerosol travels to the plasma. Large droplets are removed by impactions on the sides and rear of the spray chamber and are pumped down the drain.

As can be seen from **Table 3-15**, the average peak width is 13.3 seconds. Compared to solution nebulization, detection limits are degraded by one to one and a half orders of magnitude. The average % RSDs were degraded from 0.5% to 2.4%, and the linear dynamic range only spanned about 3 orders of magnitude **(Figures 3-27, 3-28)**.

3.5.4 HCI

The results of the HCI for FIA were very comparable to the CMSC. **Table 3-16** shows the average peak width is 14.3 seconds and % RSDs is about 2.6%. This approach may be improved if the aerosol and vapor could be efficiently heated without using a large volume heating stage (as is used in the ultrasonic nebulizer system). Currently our laboratory is investigating the use of heating one of the grids in the nebulizer. The linear dynamic range of the HCI are shown in **Figures 3-29, 3-30.**

3.5.5 PSI

The results of the positive suction injector are listed in **Table**

Table 3-15

Flow Injection Analysis

Cooled Mini Spray Chamber

50 uL Injection, Analyte Concentration 1 ug/mL

100% Methanol

Element	Average Peak Width (Seconds)	Peak Area	% RSD Background	Detection Limit (ng/mL)
Au	9.75	1037	2.0	137
Cd	18.5	5071	4.2	28.9
Cu	14.7	2288	1.6	123
Fe	15.3	3420	2.3	60.0
Mn	20.5	10107	2.3	14.6
Ni	11.5	952	8.7	121
Zn	13.1	3824	4.0	23.4
AVG	13.3		2.4	

100% Acetonitrile

Au	6.83	952	2.3	157
Cd	11.4	2392	3.2	51.9
Mn	21.3	8753	1.8	23.6
Ni	9.3	623	2.6	107
Zn	13.5	3155	2.3	31.2
AVG	12.5		2.4	

Table 3-16

Heated/Cooled Interface

50 µL Injection, Analyte Concentration 1 µg/mL

100% Methanol

Element	Average Peak Width (Seconds)	Peak Area	% RSD Background	Detection Limit (ng/mL)
Cd	14.3	3411	3.0	42

100% Acetonitrile

Cd	17.8	9215	2.4	20.7
Mn	13.3	2508	2.3	45.4

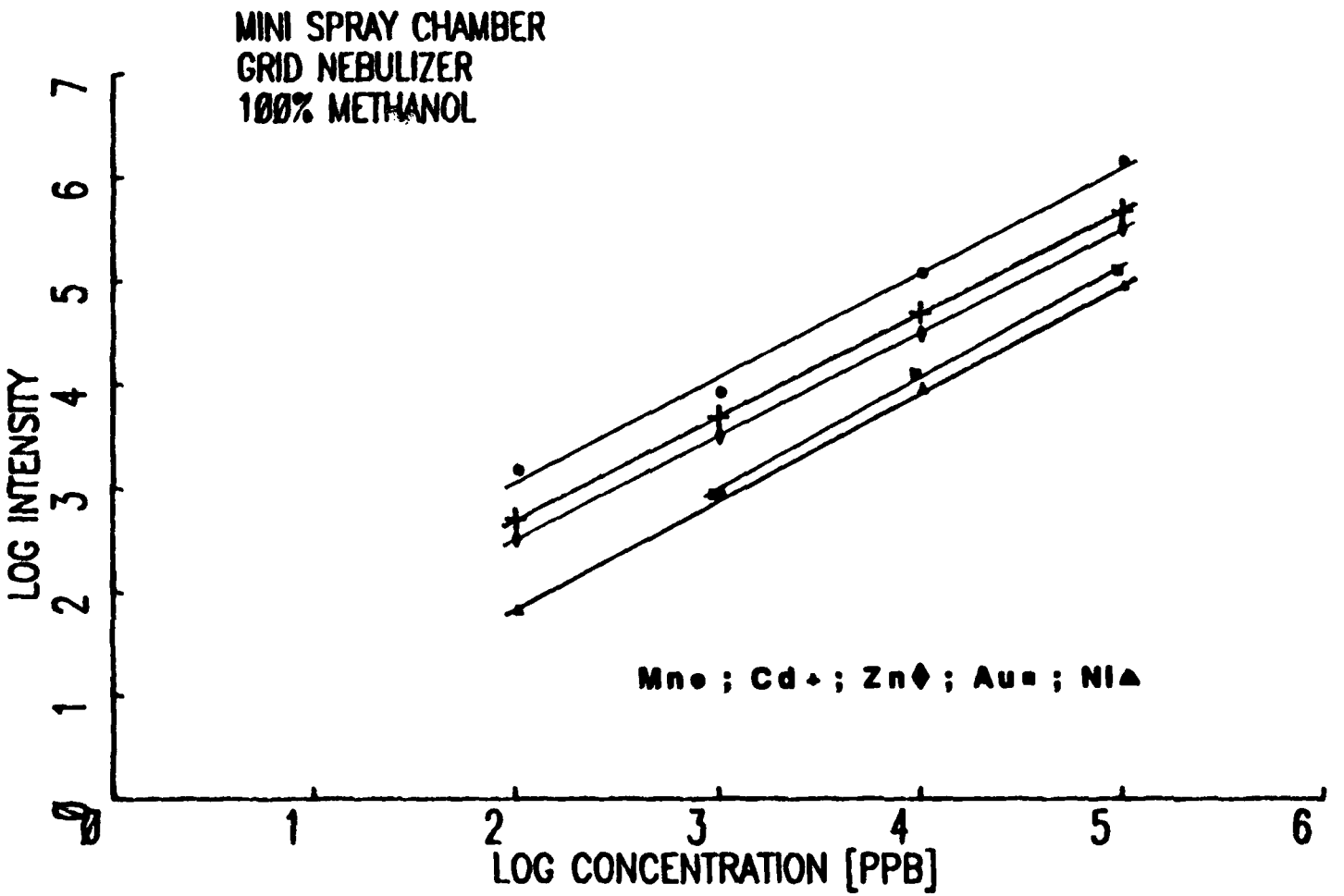

Figure 3-27. Log Concentration vs. Log Emission Peak Area Intensity

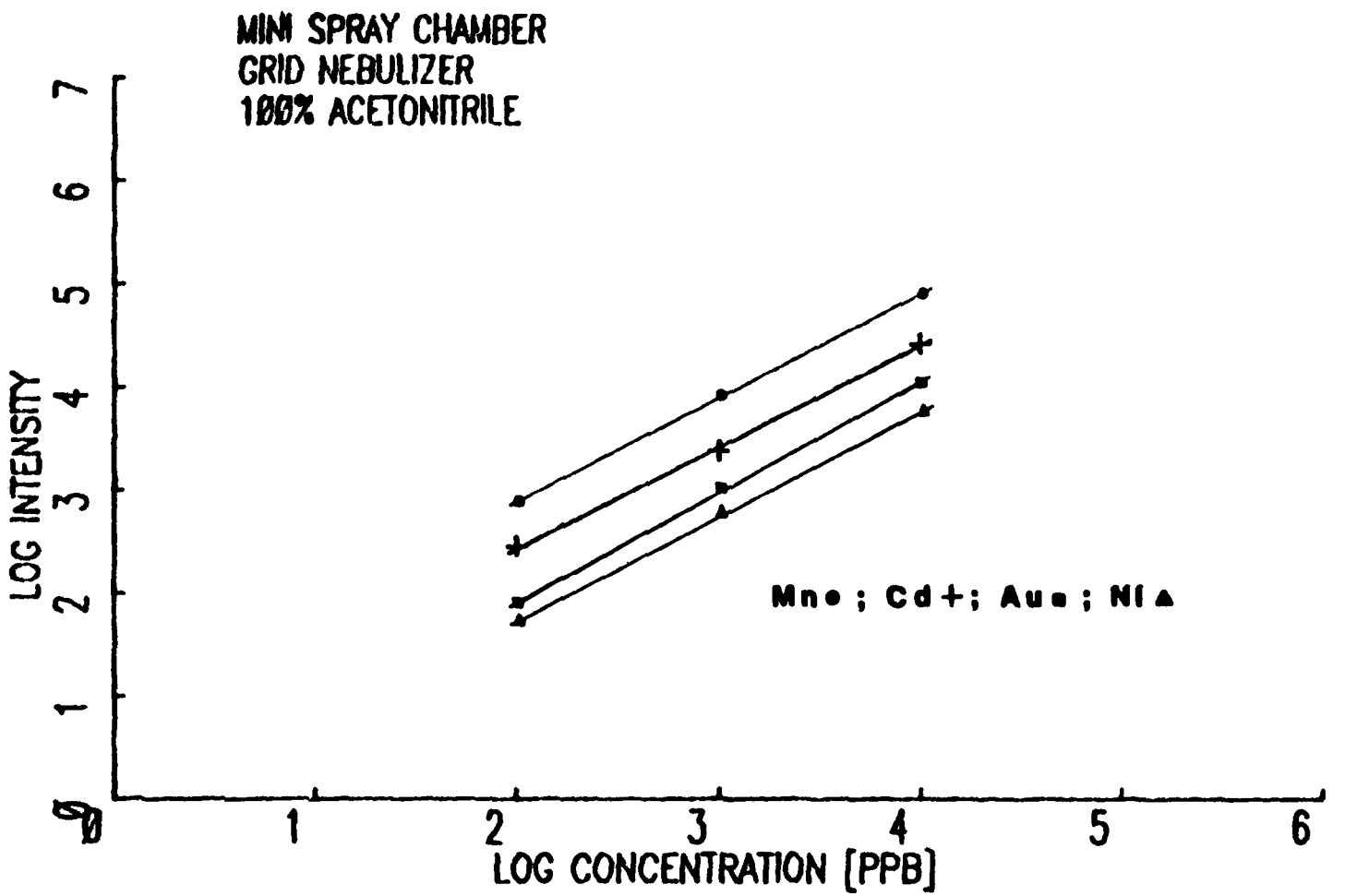

Figure 3-28. Log Concentration vs. Log Emission Peak Area

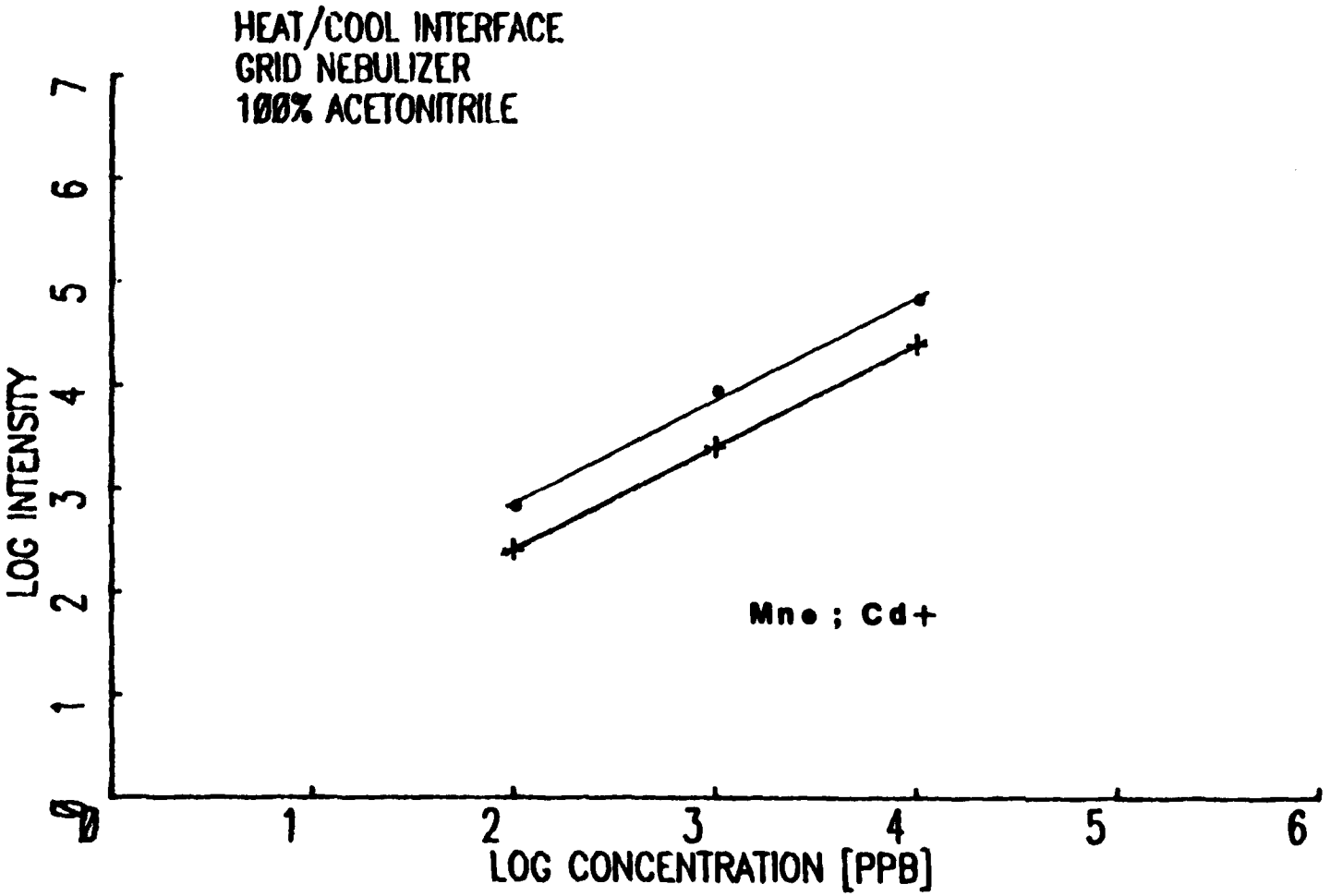

Figure 3-29. Log Concentration vs. Log Emission Peak Area

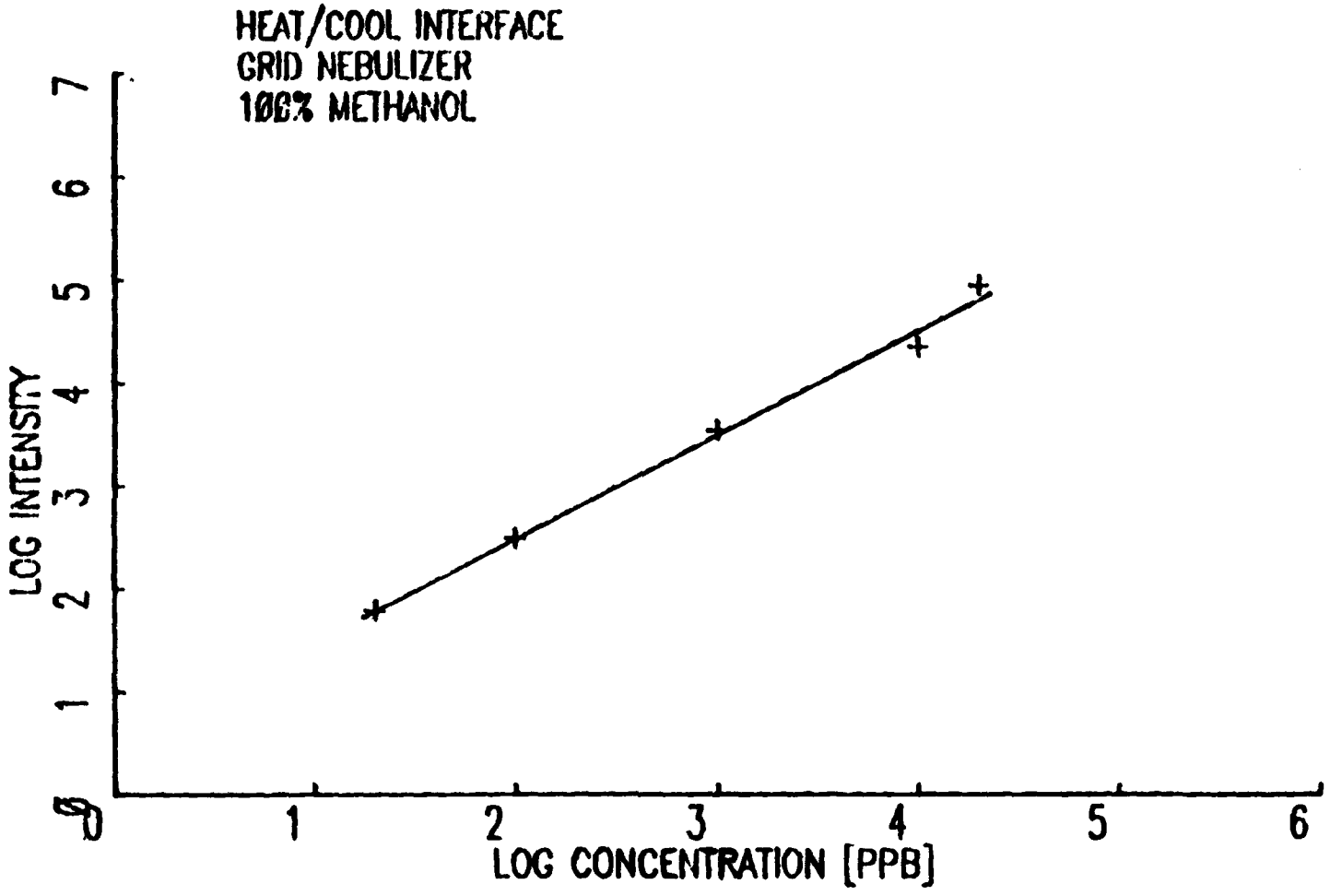

Figure 3-30. Log Concentration vs. Log Emission Peak Area for Mn

3-17. The % RSD (7.1%) is much higher for the PSI than either the CMSC on the HCI. Because of the high deviation, detection limits and LDRs are somewhat degraded. The average peak width is 8.7 seconds, but this is probably due to the fact that this interface is less sensitive and that it cannot distinguish between background and emission signal.

3.6 COMPARISON WITH DIN

The direct injection nebulizer (DIN) is a commercially available system that provides a low dead volume interface of an FIA/HPLC system to an ICP. Both organic and aqueous solutions can be used with the DIN, but the maximum flow rate possible is about 0.15 mL/min. Flow rates higher than 0.15 mL/min for organic solvents result in an unstable plasma. (Higher flow rates may be obtainable for aqueous solutions, but emission intensity decreases sharply due to the short residence times of analyte within the plasma.)

The CMSC and the HCI, however, can be used for flow rates as high as 1-2 mL/min. Though there is some band broadening due to the spray chamber and injector volume, it is less than the band broadening from a conical spray chamber and less than broadening from a commercial Scott spray chamber. Table 3-18 lists these band widths of flow injection peaks obtained with the DIN, CMSC, HCI and the grid nebulizer with a conical spray chamber. One reason peak width is greater for the DIN versus the CMSC and HCI is that the flow rate for the DIN is 0.12 mL/min versus 1.0 mL/min for the other two.

Comparing the DIN to the CMSC may not be appropriate since the DIN can be used only in limited applications where a flow rate of 0.15 mL/min or less is used. Detection limits of the DIN are superior to that of CMSC. However, the CMSC have two other advantages to the DIN. First, it

Table 3-17

Positive Suction Injector

50 µL Injection, Analyte Concentration 1 µg/mL

100% Methanol

Element	Average Peak Width (Seconds)	Peak Area	% RSD Background	Detection Limit (ng/mL)
Cd	10.3	1984	3.4	69.4
Cu	5.3	1342	11.4	361
Fe	5.6	1195	9.6	289
Mn	11.0	6316	5.8	68.3
Zn	12.3	2201	6.8	90.1
AVG	8.7		7.1	

Table 3-18

Band Broadening

100% MeOH

Interface	Flow Rate (mL/min)	Band Width (Seconds)
Cooled Mini Spray Chamber	1.0	14.7
Heated/Cooled Interface	1.0	14.3
Uncooled Conical Spray Chamber	1.0*	38.0
Direct Injection Nebulizer[23]	0.12	51

*35 mL/min argon coolant, 1.75 KW ICP

can be used at higher flows and still obtain adequate detection. Secondly, it costs only about $80 (assuming one would have a nebulizer and cooling system) versus about $800 for the DIN. In addition, the CMSC is very rugged and not as susceptible to damage as the DIN.

3.7 CONCLUSION

All three interfaces demonstrated different methodologies to achieve a stable plasma at organic solvent solution uptake rate of 1-2 mL/min. For nebulization, detection limits for the CMSC and HCI were very good. Detection limits for the PSI were somewhat degraded and were discussed previously.

For FIA, each interface minimized peak width primarily due to a small spray chamber volume. However, FIA detection limits for CMSC, HCI and PSI were degraded by factors of 2.15 to 50 times compared to solution nebulization. The primary reason for this is due to a noisy data collection system. The % RSD of the background should be the same for solution nebulization and flow injection. However, % RSD increased ca. four times for FIA versus solution nebulization. In addition, sensitivity may have been slightly degraded by smoothing the peaks.

Degraded FIA detection limits for the PSI can be attributed to both a noisy data collection system as well as the method used to control the nebulizer argon and suction argon.

The following are ways that could be used to improve results for these three interfaces.

a. Mass flow controller for nebulizer argon (range 0-2.0 L/min) and a mass flow controller for suction argon (0-.5 L/min).

b. Faster sampling rate

c. Auto ranging amplifier with wide LDR.

References

1. B. P. Hammond, R. P. Beliles, **Toxicology - The Basic Science of Poisons**, 2nd ed., J. Doull, C. D. Klassen, M. O. Amdur, Eds., p. 468; MacMillan: New York (1980).

2. H. Sigel, Ed., **Metal Ions in Biological Systems. Carcinogenicity and Metal Ions**, Vol. 10, Marcel Dekker: New York (1980).

3. S. J. Haswell, P. O'Neill, K.C.C. Bancroft, **Talanta, 32**, 69 (1985).

4. L. Ebdon, S. J. Hill, P. Jones, **Analyst, 110**, 515 (1985).

5. S. Hill, L. Ebdon, P. Jones, **Anal. Proc., 23**, 6 (1986).

6. R. H. Fish, J. J. Komlenic, **Anal. Chem., 56**, 510 (1984).

7. R. H. Fish, J. J. Komlenic, B. K. Wines, **Anal. Chem., 56**, 2452 (1984).

8. B. Radzuik, Y. Thomasson, J. C. Van Loon, Y. K. Chau, **Anal. Chim. Acta, 105**, 255 (1979).

9. D. J. Makey, **J. Chromatog., 236**, 81 (1982).

10. V. A. Fassel, R. N. Knisely, **Anal. Chem., 46**, 1110A (1974).

11 V. A. Fassel, R. N. Knisely, **Anal. Chem., 46**, 1155A (1974).

12. R. M. Barnes, **CRC Crit. Rev. Anal. Chem.**, 203 (1978).

13. C. H. Gast, J. C. Kraak, H. Poppe, F.J.M.J. Maessen, **J. Chromatog., 185**, 549 (1979).

14. D. W. Hausler, L. T. Taylor, **Anal. Chem., 53**, 1227 (1981).

15. D. M. Fraley, D. Yates, S. E. Manahan, D. Stalling, J. Petty, **Appl. Spectrosc., 35**, 525 (1981).

16. W. S. Gardner, P. F. Landrum, D. A. Yates, **Anal. Chem. 54**, 1198 (1982).

17. K. Yoshida, T. Hasegawa, H. Haraguchi, **Anal. Chem., 55**, 2106 (1983).

18. K. J. Irgolic, R. A. Stockron, D. Chakraborti, W. Beyer, **Spectrochim. Acta B, 38**, 437 (1983).

19. E. D. Katz, R. P. Scott, **Analyst, 110**, 253 (1985).

20. M. Morita, T. Vehiro, K. Fuwa, **Anal. Chem., 52**, 349 (1980).

21. D. W. Hausler, L. T. Taylor, **Anal. Chem. 53**, 1223 (1981).

22. K. Yoshida, H. Haraguchi, **Anal. Chem., 56**, 2580 (1984).

23. K. E. Lawrence, G. W. Rice, V. A. Fassel, **Anal. Chem.**, **54**, 292 (1984).

24. K. Jinno, S. Nakanishi, C. Fugimoto, **Anal. Chem.**, **56**, 1977 (1985).

25. K. Yoshida, H. Haraguchi, K. Fuwa, **Anal. Chem.**, **55**, 1009 (1983).

26. L. Ebdon, S. Hill, R. W. Ward, **Analyst**, **112**, 1 (1987).

27. P.W.J.M. Boumans, F. J. deBoer, **Spectrochim. Acta**, **31B**, 355 (1976).

28. W. Blades, B. L. Caughlin, **Spectrochim. Acta**, **40B**, 579 (1985).

29. K. W. Olson, W. J. Haas, Jr., V. A. Fassel, **Anal. Chem.**, **49**, 632 (1977).

CHAPTER 4

USE OF THE GRID NEBULIZER FOR HIGH DISSOLVED SALT/SOLID SOLUTIONS FOR ICP-OES

4.1 INTRODUCTION

One of the active areas of analytical research is the quantitative determination of metal species in a variety of sample matrices. The increased commercial availability of reasonably priced inductively-coupled plasma (ICP) spectrometers in the past several years has heightened interest in exploring their usefulness for difficult and complex sample analyses. The ICP is sensitive for metal detection, and a large number of elements can be simultaneously excited under one set of conditions.[1,2,3] The selectivity of spectrometric techniques for metal species and the potential for obtaining speciation information (the individual metal species present in the sample) make the ICP particularly attractive. Matrix effects and interferences, which can pose serious problems with DC plasma emission, are reduced or eliminated. In addition, the ICP offers linear dynamic ranges up to five orders of magnitude.

There are several methods of sample introduction into an ICP, the most common being pneumatic nebulization of liquid samples. These pneumatic nebulizers can be a limiting factor in utilizing ICP emission spectrometry, especially when the solution being nebulized contains a large amount of suspended particulates and dissolved solids. Both the cross flow and concentric nebulizers exhibit short-term noise, long-term

drift and are inefficient in sample transport.[4] The concentric nebulizer is particularly prone to clogging when aspirating a solution with high dissolved solids.[5]

The glass frit nebulizer operates by passing gas through a sintered frit. The sample liquid passes over the frit and the carrier gas shears the liquid into a fine aerosol. The glass frit nebulizer is highly efficient and has been used for organic solvent sample introduction.[6] The glass frit nebulizer, however, exhibits memory effects and can also become clogged when aspirating solutions with high dissolved solids.

There have been many nebulizers designed specifically for introducing high dissolved solids solutions into the ICP. Suddendorf and Boyer in 1978 reported using a "V" nebulizer for high dissolved solids yielding detection limits comparable to a conventional pneumatic nebulizer.[7] Garbarino and Taylor in 1980 reported on the use of a Babington nebulizer that was insensitive to suspended particulate matter and yielded detection limits equivalent to or better than pneumatic nebulizers.[8] Thelin reported on another variation of a "V" nebulizer that was used for high salt (10%) content steel samples.[9] Variations of the Babington nebulizer that could utilize solutions containing as high as 20% w/v of dissolved solids or slurries have been reported by Ebdon and Cave[10] and Wichman et al.[11] Baginski and Meinhard have reported use of a Meinhard Type C nebulizer with a recessed capillary tip nozzle that is used for high dissolved solids.[12] Walton and Goulter described a new slotted maximum dissolved solids nebulizer (MDSN) and compare against the Meinhard nebulizer in terms of sensitivity, precision, clean out and drift.[13]

Leeman Labs, Inc. (Lowell, MA) developed the Hildebrand grid nebu-

lizer for use with high dissolved solids solutions. The grid nebulizer design features a fine mesh grid of inert material positioned in front of a high velocity argon stream. Sample is introduced to the grid through a large cross section tube, and the liquid flows over the grid past the stream of high velocity gas. Nebulization takes place as a result of shearing from the wetted surface. Since the sample is introduced through a large cross section tube, dissolved or suspended solids are less prone to become clogged inside.

The objective of this study is to further evaluate the suitability of the grid nebulizer for use with high salt and dissolved solid matrices. Performance criteria that were used in the evaluation were:

1. Stability
2. Detection limit (multi-element mode)
3. Clogging
4. Memory effects
5. Use with difficult to nebulize samples
6. Linear dynamic ranges

The grid nebulizer was compared with a fixed cross flow nebulizer in terms of stability and detection limits.

4.2 EXPERIMENTAL

The experiments were carried out using a Leeman Labs Plasma Spec ICP 2.5 (Leeman Labs, Lowell, MA). The Plasma Spec incorporates an echelle grating spectrometer and uses a Huth-Kuhn free running tuned cavity oscillator as the rf power supply.

Some minor modifications were made to the Leeman labs instrument for this work. Solution uptake was with a Gilson Minipuls-2 peristaltic pump (Rainin Instruments Co., Woburn, MA) using PVC manifold pump tubing

for solution uptake. Tubing was calibrated prior to use.

The grid nebulizer used was developed and supplied by Leeman Labs. Figure 4-1 depicts this nebulizer as well as the fixed cross flow nebulizer used in this study. The second (downstream) grid is for purposes of pulse damping. A pyrex conical spray chamber was used. Reagents for synthetic ocean water and the 5% dissolved solids solutions were obtained from Fisher Scientific. Metal solutions were prepared and stored in glassware that had been rinsed in nitric acid prior to use. Standard solutions were prepared by serial dilutions of certified atomic absorption standards (Fisher Scientific).

4.2.1 Optimizing ICP Viewing Conditions

In performing sequential multielement detection, compromise viewing conditions must be used, since optimum viewing height is not the same for all elements. The Leeman Labs Spectrometer automatically maximizes the signal intensity of a selected element in both the horizontal and vertical directions by initializing the auto peaking function of the instrument. In this study Cu was the element that was so optimized when using the sequential multielement mode.

4.3 RESULTS AND DISCUSSION

4.3.1 Short Term Stability

Short term stability was determined by nebulizing solutions of 2% nitric acid, synthetic ocean water and a 5% dissolved solids solution for thirty minutes. The composition of synthetic ocean water and 5% dissolved solids solution is described in Table 4-1.

During a thirty minute nebulization span, 25 data points were taken and the percent relative standard deviation (% RSD) calculated. Stabilities of the grid nebulizer and the fixed cross flow nebulizer were

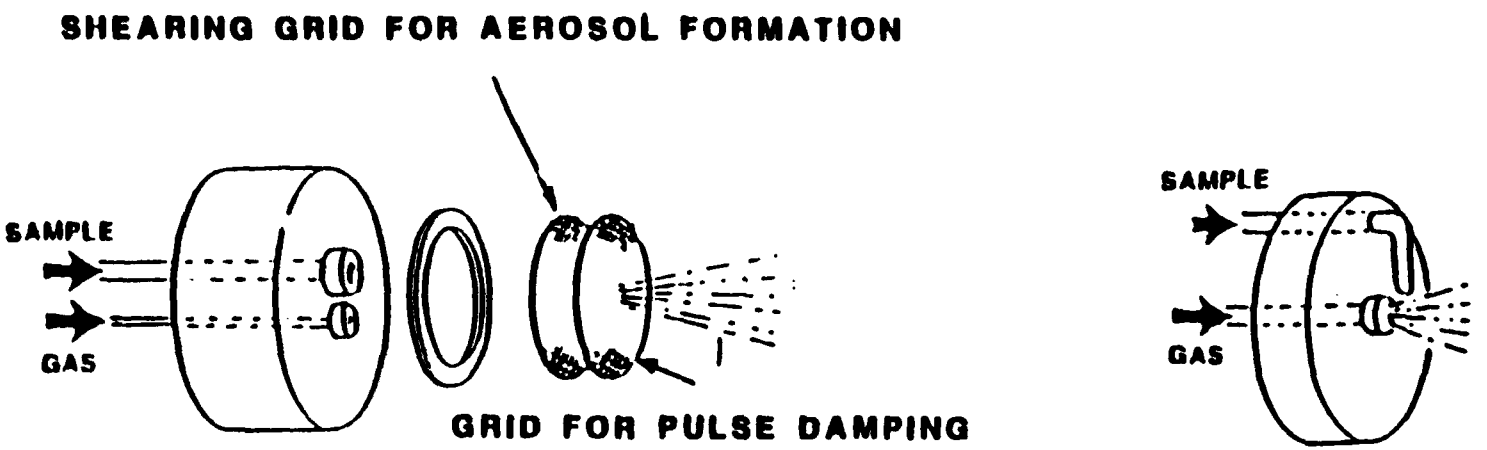

HILDEBRAND GRID

CROSS FLOW

Figure 4-1. Hildebrand Grid and Cross Flow Nebulizers

Table 4-1

Composition of Synthetic Ocean Water and 5% Dissolved Solids Solution

Salt	Synthetic Ocean Water(%)	5% Dissolved Solids(%)
NaCl (W/V)	2.11	3.0
$MgCl_2$ (W/V)	0.41	1.0
$CaCl_2$ (W/V)	0.12	0.5
KCl (W/V)	0.08	0.5
H_2SO_4 (V/V)	0.2	0.2
HCl (V/V)	0.4	0.4
Total Dissolved Solids:	2.7%	5.0%

determined for both 2% nitric acid and synthetic ocean water solutions and are listed in Tables 4-2 and 4-3. Emission lines of Pb, Ni, Cd, Mn, Zn, Cu and Fe were used. In addition, short term stabilities of the grid nebulizer using a 5% dissolved solids solution were determined. These are listed in Table 4-4.

The data in Table 4-2 indicate that the short term stability for the cross flow nebulizer used in the study and the grid nebulizer are comparable for 2% nitric acid solution. For the fixed cross flow nebulizer the average RSDs (of various metal species) are 0.78%, 1.87% and 2.21% for a blank, 1 ppm and 10 ppm solutions, respectively. For the grid nebulizer, the average RSDs for the blank, 1 ppm and 10 ppm solutions are 0.58%, 1.38% and 1.72%, respectively, somewhat of an improvement over the cross-flow.

The data in Table 4-3 indicate that the short term stability of the Hildebrand nebulizer for synthetic ocean water surpasses the short term stability of the fixed cross flow for the same solution. The average RSDs of the grid nebulizer for a blank, 1 ppm and 10 ppm SOW solution (Cu, Cd, Ni, Fe, Ni, Mn, Zn) are 0.91%, 1.26% and 2.37%, respectively. In comparison, the average RSDs of the cross flow nebulizer for the blank, 1 ppm and 10 ppm solution are 1.0%, 2.89% and 7.3%.

The grid nebulizer also demonstrated good short term stability for 5% dissolved solids. The average RSDs for a blank and 10 ppm solutions are 2.60% and 1.86% over a thirty minute span.

4.3.2 Detection Limit

The 3σ detection limits were calculated from a total of 25 data points. Since the data were acquired in the sequential multielement mode, compromise viewing conditions were used. Improved detection

Table 4-2

Short Term Stability for 2% Nitric Acid Solution
Short Term Stability (30 min)
2% Nitric Acid

		% RSD (25 Replicates)					
		Blank		1 ppm		10 ppm	
Element	λ(nm)	Grid	Cross-flow	Grid	Cross-flow	Grid	Cross-flow
Cu(I)	324.75	0.33	0.62	0.64	0.97	1.12	1.62
Mn(II)	257.75	0.41	0.66	1.75	1.60	1.92	2.10
Zn(I)	213.86	0.61	1.17	2.39	2.03	2.54	2.24
Cd(II)	214.44	1.08	0.94	1.28	2.37	1.58	2.82
Ni(II)	221.65	0.63	0.89	1.11	2.16	1.47	2.34
Fe(II)	238.20	0.42	0.42	1.11	2.08	1.71	2.15

Table 4-3

Short Term Stability (30 min) for Synthetic Ocean Water

		% RSD (25 Replicates)					
		Blank		1 ppm		10 ppm	
Element	λ (nm)	Grid	Cross-flow	Grid	Cross-flow	Grid	Cross-flow
Cu(I)	324.75	1.00	0.62	1.00	1.30	2.30	6.82
Mn(II)	256.61	0.64	0.34	1.04	2.98	1.68	4.00
Zn(I)	213.86	0.93	1.04	1.97	3.93	2.69	11.61
Cd(II)	214.44	0.87	1.09	1.22	4.92	4.21	7.72
Ni(II)	221.65	1.06	0.59	1.37	2.28	1.85	6.60
Fe(II)	238.20	0.96	2.42	0.96	1.92	1.48	7.56

Table 4-4

**Short Term Stability (30 minutes) for
5% Dissolved Solids Solution
Hildebrand Nebulizer (25 Replicates)**

Element		% Relative Standard Deviation	
	λ (nm)	Blank	10 ppm
Pb(II)	220.35	2.41	2.24
Ni(II)	221.65	2.74	1.99
Cd(II)	214.44	3.11	2.76
Mn(II)	257.61	2.77	1.12
Zn(I)	213.86	5.10	2.00
Cu(II)	324.75	2.45	1.04

limits could be obtained by optimizing for each element.

Detection limits determined for both the grid and the fixed cross flow nebulizers were comparable. Table 4-5 show the generally comparable detection limits obtained using the grid and the fixed cross flow nebulizers for 2% nitric acid and synthetic ocean water.

Table 4-6 shows the detection limits obtained using the grid nebulizer for a variety of elements in 5% dissolved solids solution. Detection limits of elements in a 5% dissolved solids solution are degraded by as much as an order of magnitude compared with a 2% nitric acid solution.

This degradation in detection limits can be attributed in part to the increased continuum and background noise of the 5% dissolved solids blank solution. Also the ion emission line intensity is suppressed when the solution contains a high amount of dissolved ionic species. Figure 4-2 shows the emission line suppression of 5 manganese emission lines when comparing a 10 ppm Mn solution in 2% nitric acid to a 10 ppm Mn in 5% dissolved solids solution. Emission line suppression may be more pronounced for ionic lines than for atomic lines.[14] Mn1, Mn2 and Mn3 are ion lines and emission line suppression is 75%, 74% and 45%, respectively. This can be compared with the atom emission line suppression of Mn4 (87%) and Mn5 (73%).

4.3.3 Clogging

When nebulizing high dissolved solids, an important consideration is the effect of clogging. Using a conventional Meinhard concentric nebulizer, a glass frit or a cross flow nebulizer, clogging can occur. The grid nebulizer never clogged with either synthetic ocean water or a 5% dissolved solids solution. These solutions were continually nebulized over an eight hour period and the nebulizer remained unclogged.

Table 4-5

Detection Limits (ng/mL) Obtained for the Grid and Cross Flow Nebulizer

	2% Nitric Acid		Synthetic Ocean Water	
Element	Grid	Cross-flow	Grid	Cross-flow
Cu	13.1	22.2	49.9	27.6
Mn	0.94	1.5	2.3	1.1
Zn	3.1	6.1	7.1	7.5
Cd	3.9	3.3	3.1	3.8
Ni	7.4	11.7	21.0	11.3
Fe	3.7	5.8	13.2	32.2

Table 4-6

Detection Limits (ng/mL)
5% Dissolved Solids Solution

Element	Detection Limit
Pb	24.7
Ni	46.4
Cd	10.2
Mn	7.4
Zn	33.8
Cu	72.6

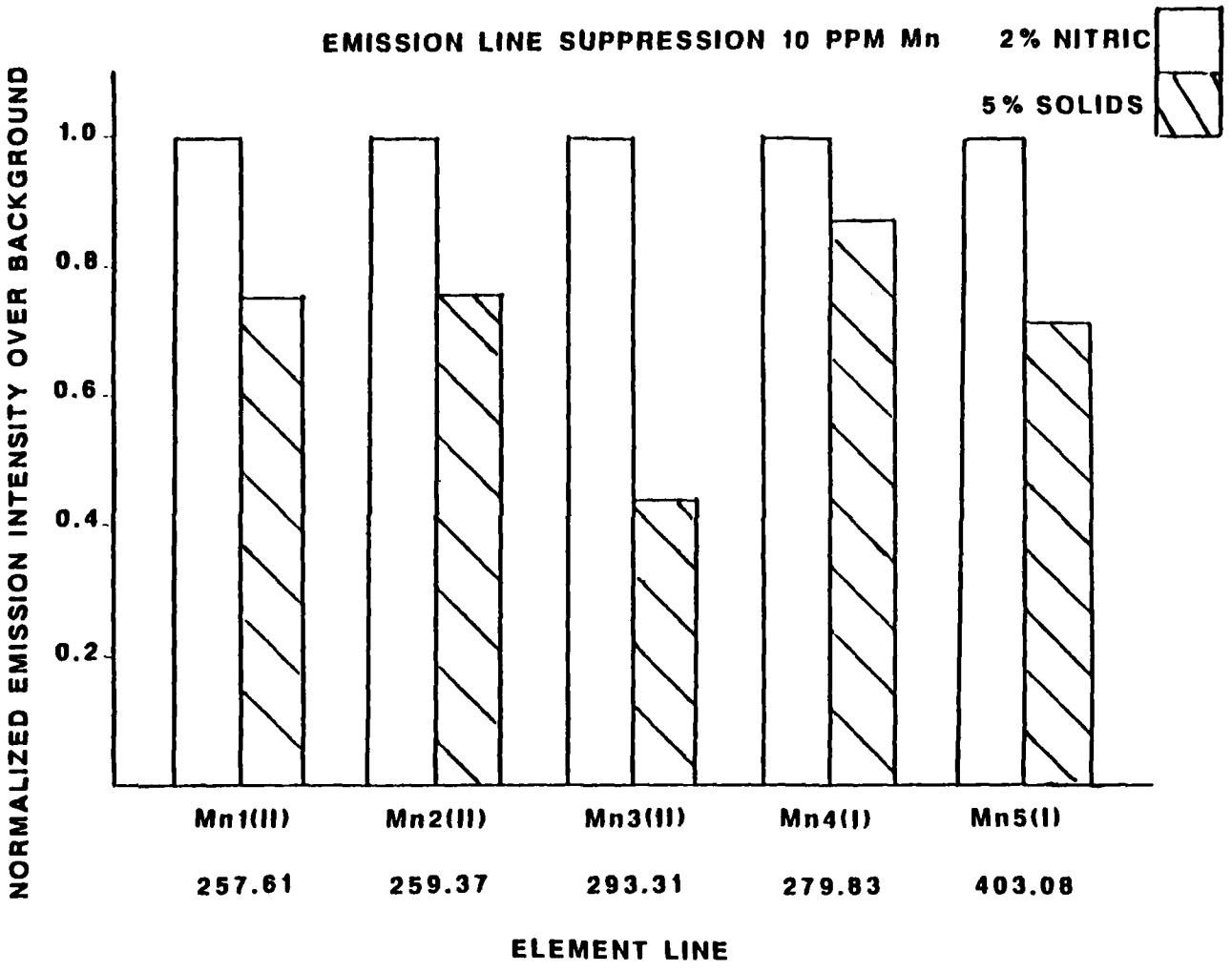

Figure 4-2. Mn Emission Line Suppression of 5% Solids Solution vs 2% Nitric

However, continual nebulization for 1½-2 hours of synthetic ocean water deposited salt crystals on the ICP torch injector tip which prevented sufficient amount of aerosol from reaching the plasma. Deposition was prevented by alternating nebulization with a 10 minute nitric acid wash cycle. Others have used humidified argon to prevent salt buildup on the injector tip.[13]

4.3.4 Memory Effects

Figure 4-3 depicts the procedure used to determine the memory effects of the grid nebulizer. A 2% nitric acid solution containing 1 ppm of Cu, Mn, Zn, Ni and Fe was nebulized into the ICP for twenty minutes. During this time data were collected. Afterwards a blank 2% nitric acid solution was nebulized for twenty minutes, data were collected, and a calibration curve was generated. Then a 2% nitric acid solution of 10 ppm Cu, Mn, Zn, Ni and Fe was nebulized into the ICP for 20 minutes. After that 20 minutes, a blank solution was nebulized for 90 seconds and data were collected and compared to the calibration curve. Values for Cu, Mn, Zn, Cd, Ni and Fe were within the % RSD of the initial blank values.

This same procedure was used for a synthetic ocean water solution. **Figure 4-4** shows that the values for Cu, Zn, Ni, Fe and Cd were no more than 5 standard deviations of the initial blank values. After 10 minutes the values were within the % RSD of the initial blank values.

The grid nebulizer exhibited virtually no memory effects for a 2% nitric acid solution but requires a slightly longer washout time (5-10 minutes) for solutions containing high dissolved solids. This test also demonstrated that the nebulizer provides good long-term stability. After one hour of continual nebulization, the blank solution is still

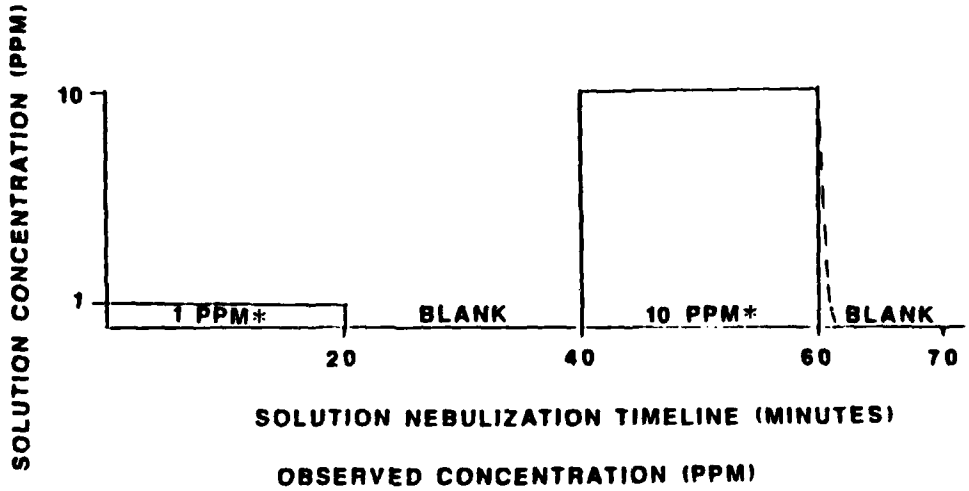

OBSERVED CONCENTRATION (PPM)
1 1/2 MINUTES AFTER SWITCHING TO BLANK

Mn	0.000
Cu	0.003
Zn	0.000
Fe	0.001
Ni	0.001
Cd	0.000

* 1 PPM AND 10 PPM SOLUTIONS CONTAIN Cu, Mn, Zn, Ni, Fe, Cd

Figure 4-3. Long Term Stability and Memory Effects of Various Elements in 2% Nitric Acid Solution

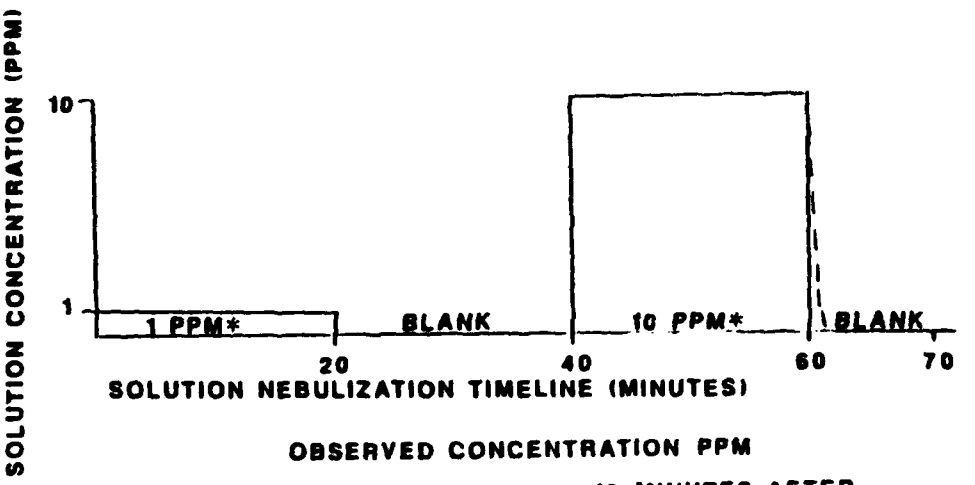

OBSERVED CONCENTRATION PPM

	1 1/2 MINUTES AFTER SWITCHING TO BLANK	10 MINUTES AFTER SWITCHING TO BLANK
Zn	0.018	0.009
Cu	0.060	0.005
Mn	0.002	0.000
Fe	0.022	0.013
Ni	0.027	0.003
Cd	0.016	0.005

Figure 4-4. Long Term Stability and Memory Effects of Various Elements in Synthetic Ocean Water

within the % RSD of the initial blank solution.

4.3.5 Use with Digested Samples

The Food and Drug Administration (FDA) of Cincinnati provided samples which are difficult to nebulize into the ICP. These were digested food samples of spinach, pork chops and rat femurs. These samples were analyzed using the grid nebulizer for comparison with FDA results. Table 4-7 shows the various matrices of the digested samples. Table 4-8 shows a comparison of our lab results with those of the FDA lab results (ICP emission) obtained in 1983. Results for the Femur 3974, 3979 and the California spinach agree very closely. The Fe and Zn content in the Texas spinach is slightly off. Magnesium was not analyzed and no iron was found in the pork chop sample.

Though there are small discrepancies in the comparison (which may be because the FDA samples were three years old), this study demonstrated that the Hildebrand grid nebulizer may be effectively used for real samples containing high dissolved solids.

4.3.6 Linear Dynamic Range

The Hildebrand nebulizer exhibited at least a 3-4 order of magnitude linear dynamic range (LDR) for elements in a solution of synthetic ocean water. Figure 4-5 shows the LDR for Cd, Fe, Mn and Zn. The slopes of the log-log curves are close to unity. Table 4-9 shows the correlation coefficients, slopes and intercepts of these curves.

4.4 CONCLUSION

The grid nebulizer is suitable for use with high dissolved solid solutions. Using a 2% nitric acid solution the short term stability for the grid and the fixed cross flow nebulizers are comparable, but the grid exhibited much better % RSD for synthetic ocean water which contains

Table 4-7

Matrix for FDA Samples (1983)

Sample	Matrix
Spinach	20% H_2SO_4
	1500 ppm Ca, Mg, Na
Pork Chops	4% Nitric
	600 ppm Na, Ca, Mg, K
Femurs	10% $HClO_4$
	2000 ppm Ca

Table 4-8

Comparison of Results (ppm)

Sample		Al	Cd	Cu	Fe	Mg	Ni	Mn	Sr	Ti	Zn
California Spinach	FDA	--	0.01	0.18	3.4	> 100	0.04	1.5	--	--	0.5
	Hildebrand	2.7	0.01	0.19	3.0	--	0.08	1.4	1.3	0.2	0.5
Texas Spinach	FDA	--	0.30	0.30	6.0	> 100	0.3	1.5	--	--	0.65
	Hildebrand	3	0.28	0.27	4.7	--	0.3	1.4	--	0.3	0.59
Pork Chops	FDA	--	--	--	0.8	2.0	--	--	--	--	2.4
	Hildebrand	--	--	--	--	--	--	--	--	--	2.3
Femur 3979	FDA	--	--	--	--	2.9	--	--	--	--	0.07
	Hildebrand	--	--	--	--	2.7	--	--	--	--	0.07
Femurs 3974	FDA	--	--	--	--	2.9	--	--	--	--	0.14
	Hildebrand	--	--	--	--	3.0	--	--	--	--	0.16

Table 4-9

Correlation Coefficients, Slopes and Intercepts for Log-Log Calibration Plots

Element	Slope	Intercept	Correlation Coefficient
Fe	0.95	1.442	0.9999
Zn	0.98	1.390	0.9999
Cd	1.02	1.300	0.9998
Mn	1.00	1.810	0.9999

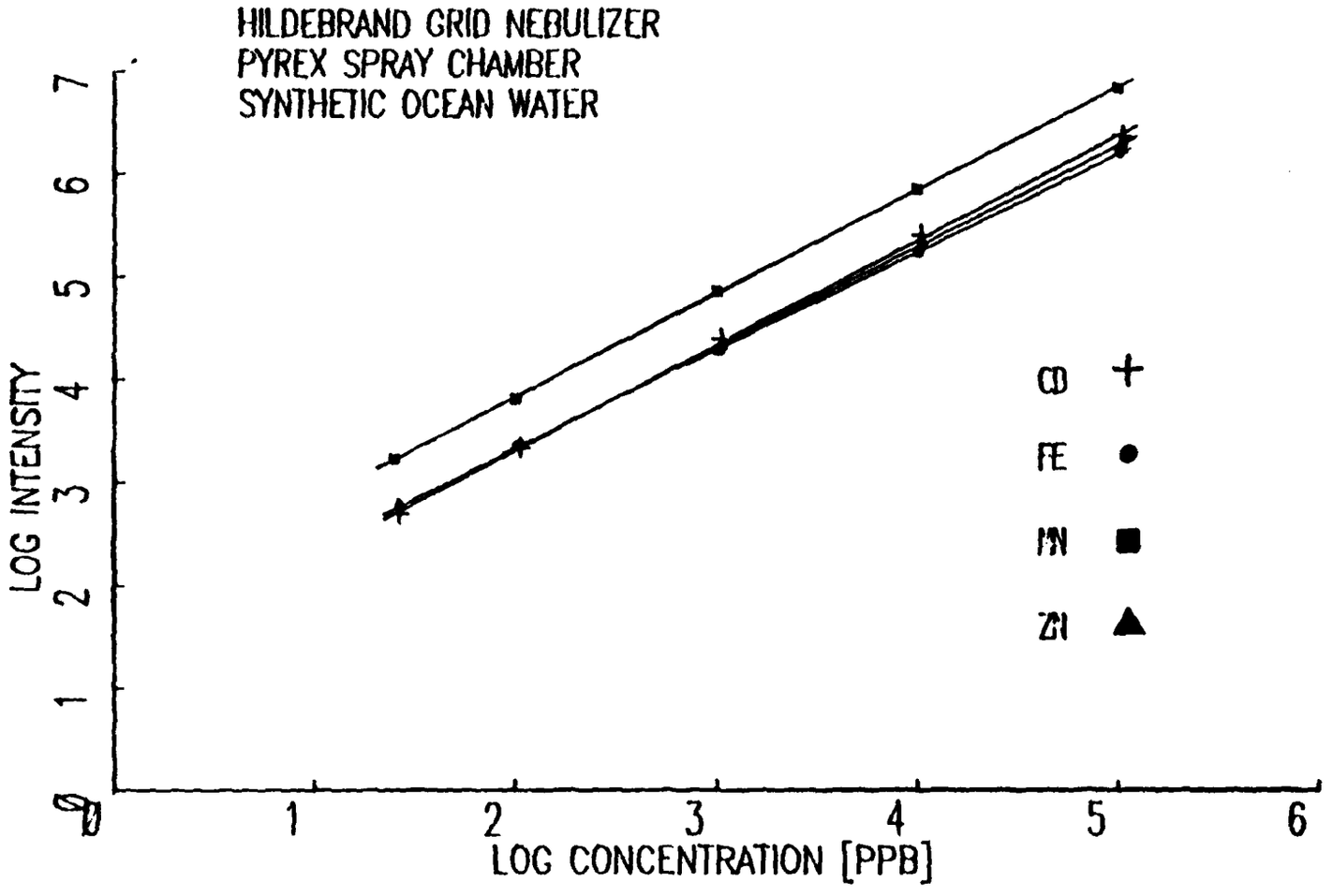

Figure 4-5. Log Concentration vs. Log Emission Intensity for Synthetic Ocean Water

approximately 2.7% dissolved solids. The grid nebulizer exhibited no clogging for SOW or a 5% dissolved solids solution. There were no memory effects for the 2% nitric acid solution and a slight memory effect for synthetic ocean water, which could be prevented by using a five to ten minute 2% nitric acid wash cycle. Long term stability was very good.

REFERENCES

1. Fassel, V. A.; Kniseley, R. N. Anal. Chem. 1974, 46, 1110A.
2. Fassel, V. A.; Kniseley, R. N. Anal. Chem. 1974, 46, 1155A.
3. Barnes, R. M. CRC Crit. Rev. Anal. Chem. 1978, 203.
4. Layman, L. R.; Lichte, F. R. Anal. Chem. 1982, 54, 638-692.
5. Hieftje, G. M.; Copeland, T. R. Anal. Chem. 1978, 50, 300R.
6. Nisamaneepong, W.; Haas, D.; Caruso, J. A. Spectrochim. Acta Part B 1985, 1/2, 3.
7. Suddendorf, R. F.; Boyer, K. W. Anal. Chem. 1978, 50, 1769.
8. Garbarino, J. R.; Taylor, H. E. Appl. Spec. 1980, 34, 584.
9. Thelin, B. Analyst 1981, 106, 54-59.
10. Ebdon, L.; Cave, M. R. Analyst 1982, 107, 172-178.
11. Wichman, M. D.; Fry, R. C.; Mohamed, N. Appl. Spec. 1983, 37, 254.
12. Baginski, B. R.; Meinhard, J. E. Appl. Spec. 1984, 38, 568.
13. Walton, S. J.; Goulter, J. E. Analyst 1985, 110, 531.
14. Haas, D. L.; Ph.D. Dissertation, University of Cincinnati, May 1984.

CHAPTER 5

USE OF GRID NEBULIZER FOR DIFFICULT TO NEBULIZE SOLUTIONS WITH ICP/MS DETECTION

5.1 INTRODUCTION

Inductively Coupled Plasma Mass Spectrometry (ICP/MS) is quickly growing to be the method of choice for ultratrace elemental analysis. ICP/MS is a very sensitive technique that is amenable to precise, rapid sample through-put. Though touted as being a very simple, highly automated technique, interpretation of ICP/MS data output requires a thorough understanding of the system and technique.

ICP/MS offers many advantages over ICP optical emission spectroscopy (OES). Detection limits of 0.01-0.1 ng/mL can be achieved across most of the entire periodic table, depending upon how one collects the data. This is an improvement of 1-2 orders of magnitude over ICP-OES. Major, minor and trace constituents of all elements in the periodic table can be identified in unknown samples in as little as one minute. ICP-MS provides a direct method for isotope ratio determination with precision of 1% or better. ICP/OES can produce line rich optical spectra which can pose significant interference problems. Since ICP/MS spectra consists only of peaks at integer mass/charge ratios from 1 to 240, these types of interferences are minimized.[1,2,3] This can reduce the linear dynamic ranges. There are some disadvantages of ICP/MS. There are inherent isobaric interferences associated with ICP/MS which result from the ionization of the plasma gas and solution concomitants and inhibits anal-

yses of elements such as Si, S, and Ca.[4,5,6] Also, since the instrument is very sensitive, saturation of the electron multiplier can occur for concentrations above 10 ng/mL, which limits the useful linear dynamic range.

The primary purposes of the ICP/MS experiments were (1) to determine the optimum experimental conditions in terms of nebulizer gas flow, ICP power and plasma sampling position for aqueous samples using the crossflow and Hildebrand grid nebulizers; (2) to determine detection capability of instrument on a routine basis; (3) to determine detection capability of instrument with complex matrices such as synthetic ocean water and urine; (4) to determine optimum operating parameters for organic solvents.

5.2 GENERAL EXPERIMENTAL

The VG Plasmaquad ICP/MS system was used. For detailed description of system, please refer to VG Isotopes Instruction Manuals.[6] **Figure 5-1** shows the ICP/MS system schematic. **Table 5-1** lists the major system components of the overall system.

Solution was introduced via a peristaltic pump at 1.2 mL/min into a nebulizer. **Figure 5-2** depicts the interface between the atmospheric argon ICP and the quadrupole mass filter. The expansion stage which operates at approximately 1 torr removes gaseous species and this results in a supersonically expanding jet of particles which are extracted or "skimmed off" through the skimmer. In this region, the neutrals are pumped away and the ions are focused by a number of axially symmetric electrostatic lens elements into the quadrupole mass filter where separation occurs.

Table 5-1

ICP/MS System Components

	Features
ICP Torch Box (Henry)	Power: 1.5-2.5 KW
	Frequency: 27.12 mHz
	Tuning: Automatic servo motor driven capacitance tuning
Argon Controls	Coolant: Rotometer (SS and glass floats) Auxiliary: Matheson rotometer (SS and glass floats)
	Nebulizer 1: AFM-360 mass flow controller Nebulizer 2: AFM-36 mass flow controller
Vacuum System	Edwards EIM-18 single stage rotary pump (20 L/Hr) - expansion stage
	Balzer oil diffusion pump - (2000 L/sec) - lens region
	Balzer oil diffusion pump - (150 L/sec) - quadrupole
	Edward (E2M-18) double stage rotary pump (20 L/Hr) - rough pump diffusion pumps
Quadrupole	VG 12-12S SIMS
Detector	Continuous dynode electron multiplier (ion counting mode)
Computer	IBM/XT, Princeton Color Monitor

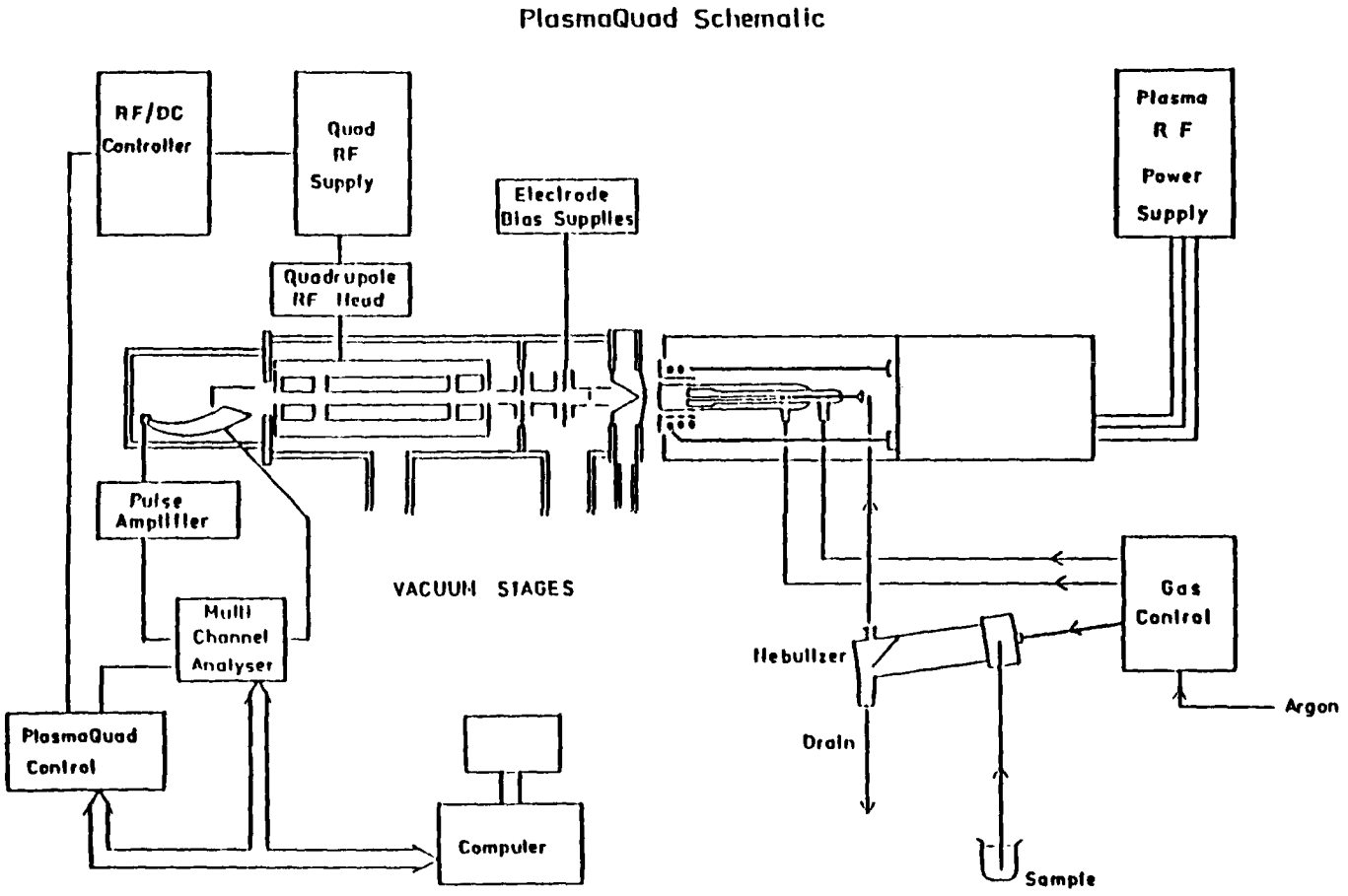

Figure 5-1. ICP/MS System Schematic

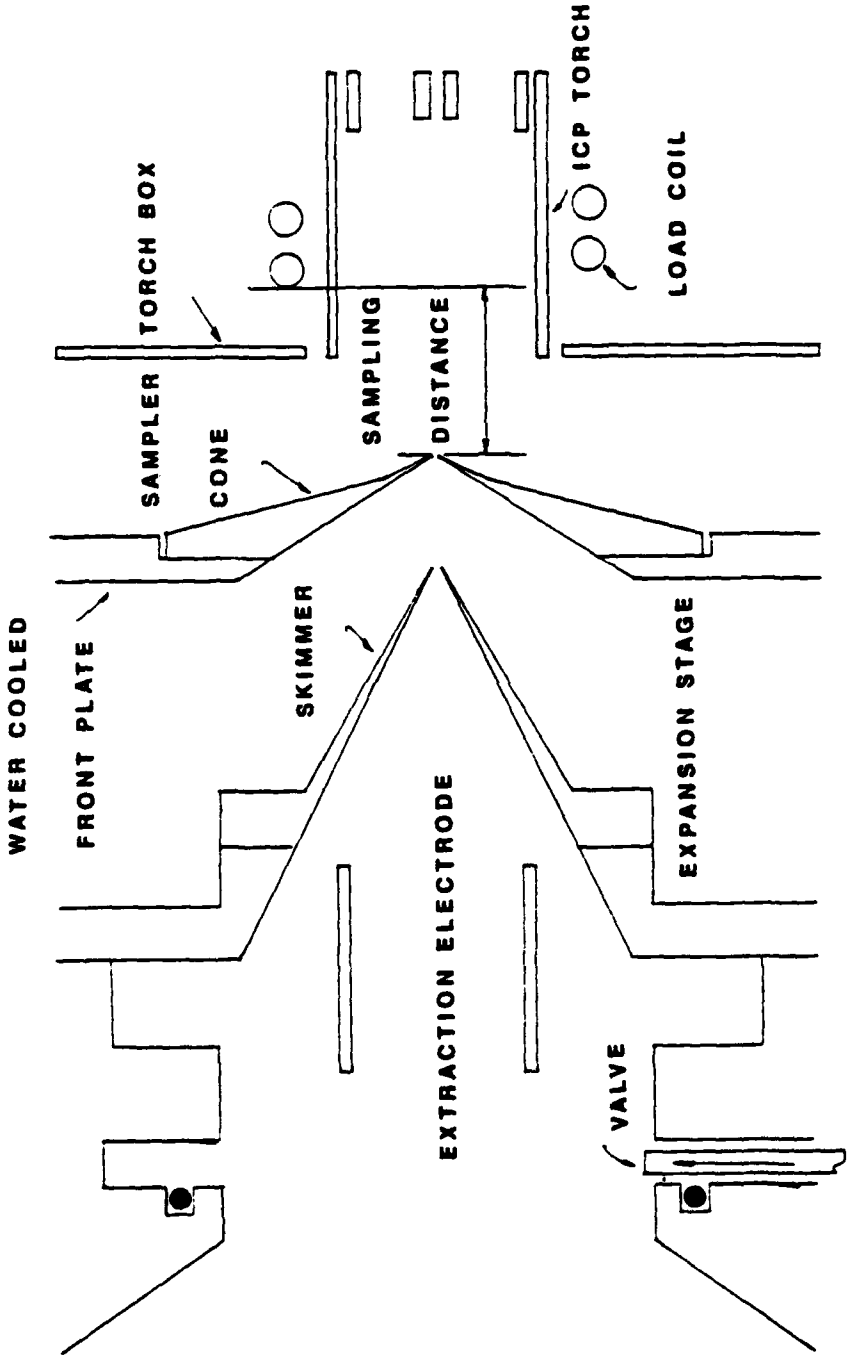

Figure 5-2. ICP/MS Interface

5.3 SYSTEM OPTIMIZATION STUDY

Optimal nebulizer flow, ICP power and sampling position were determined for the concentric, crossflow and Hildebrand grid nebulizers. The methodology of the study was as follows:

1. Fix sampling position (12 mm) and ICP power (1.20 KW).
2. Measure spectral response for various analytes @ 100 ppb in a 1% nitric acid solution as a function of nebulizer flow rate. For the crossflow nebulizer, flow rate was varied from 0.5 L/min to 0.8 L/min. For the grid nebulizer, flow was varied from 0.5 L/min to 0.72 L/min (maximum flow that could be achieved using the existing mass flow controller of the Plasmaquad). Spectral response data were collected by using the qualitative scan routine.
3. Increase ICP in increments of 0.05 KW (for range 1.2-1.5 KW) and repeat step number two for each power.
4. Change sampling position to 14 mm and repeat step 2 and 3 and then change sampling position to 17 mm and repeat steps 2 and 3.

Table 5-2 shows the typical ICP operating conditions. For the synthetic ocean water study and urine study nebulizer flow of 0.65 L/min and an ICP power of 1.35 KW were used. **Table 5-3** shows typical quadrupole mass filter voltage setting for aqueous and organic solvents. Settings varied slightly from day to day.

The initial ICP/MS optimization study was accomplished using the concentric nebulizer. Similar optimization and characterization studies using the concentric nebulizer have been published by Browner et al. and Horlick et al.[7-10] Study results in terms of optimal ICP power and nebulizer gas flow coincided with that of Zhu and Browner.[7]

However, our optimum sampling depth was determined to be 12 mm (as

Table 5-2

Typical ICP Operating Conditions

Plasmaquad

	Aqueous	Organic
Ar Coolant Flow (L/min)	17	22
Ar Auxiliary Flow (L/min)	0.5	1.5
Ar Nebulizer Flow (L/min)	0.65; Varied for nebulizer study	Varied for nebulizer study
ICP Power (KW)	1.20-1.50	1.5-2.0
Spray Chamber Temp ($0^{o}C$)	$5^{o}C$	$-10^{0}C$
Solution Uptake (mL/min)	1.2	1.2

Table 5-3

Typical Voltage Setting

VG Quadrupole Mass Filter

	Aqueous	Organic
Collector	3.49	3.2
Extractor	0.80	0.92
Lens 1	4.89	5.0
Lens 2	3.41	3.18
Lens 3	4.80	5.10
Lens 4	3.42	3.92
Differential Aperture	0.62	1.02
Front Plate	5.12	5.50
Pole Bias	4.7	4.6

measured from the sampler tip to the front of the ICP load coil) vis a vis an optimal sampling distance of 17 mm in Browner's study. (VG Isotopes state optimal sampling distance to be 10-12 mm.)

ICP/MS optimization studies using the Hildebrand grid and crossflow nebulizers were performed to determine if their behavior followed the concentric nebulizer. Moreover, since both the crossflow and grid nebulizers can nebulize solutions with high dissolved solids, these nebulizers could provide a means to introduce solutions such as ocean water, phosphate buffers (common with ion chromatography) and biological fluids.

5.3.1 Nebulizer Flow and Power

As in ICP-OES, nebulizer gas flow is a very critical parameter for ICP/MS. Too high a nebulizer flow decreases residence time within the plasma so that the aerosol may not have enough time for the desolvation, atomization and ionization processes to occur. Too low a gas flow may result in the aerosol not having enough kinetic energy to puncture the bottom plasma sheath, which results in gas flow around the outside of the plasma. **Figures 5-3-9** show the effect of nebulizer flow on signal (CPS) for various ICP powers. As can be seen, optimal signal falls in a very narrow and well defined range at 0.65 L/min for powers of 1.2-1.35 KW. For ICP powers between 1.4-1.5 KW, optimal signal occurs at a nebulizer flow rate at approximately 0.65-0.7 L/min. Similarly, **Figures 5-10-16** show the 3 dimensional plots of nebulizer flow, ICP power and signal intensity for 100 ppb Co, Ba, Sr, Y, Cd, In and Bi. These plots show how maximum signal intensity occurs at a nebulizer flow rate of 0.60-0.70 L/min as power is varied from 1.2 KW to 1.5 KW. Optimal signal for the elements plateaus at approximately 0.65 L/min nebulizer flow and 1.35 KW

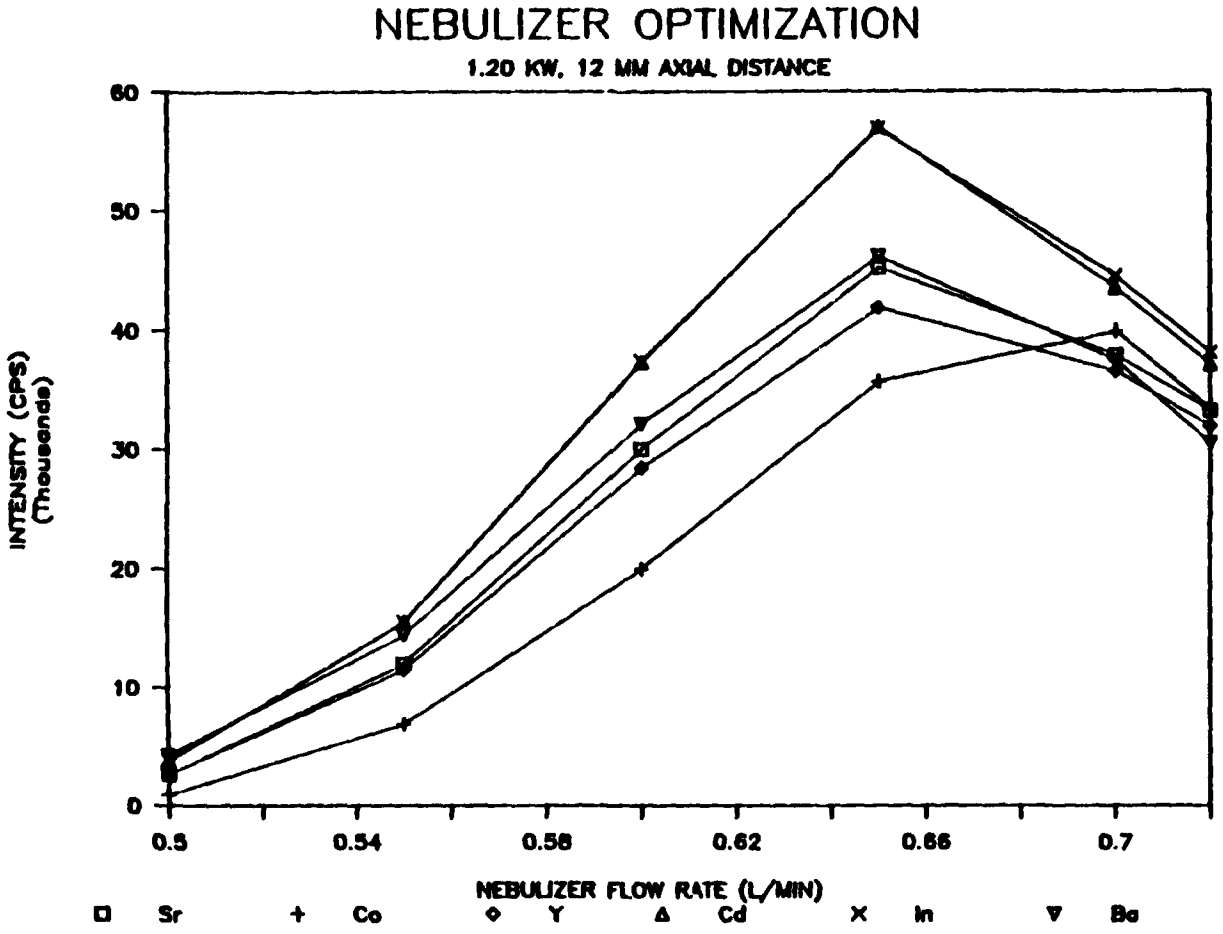

Figure 5-3. Nebulizer Flow vs. Signal Intensity @ 1.2 KW, 12 mm Sampling

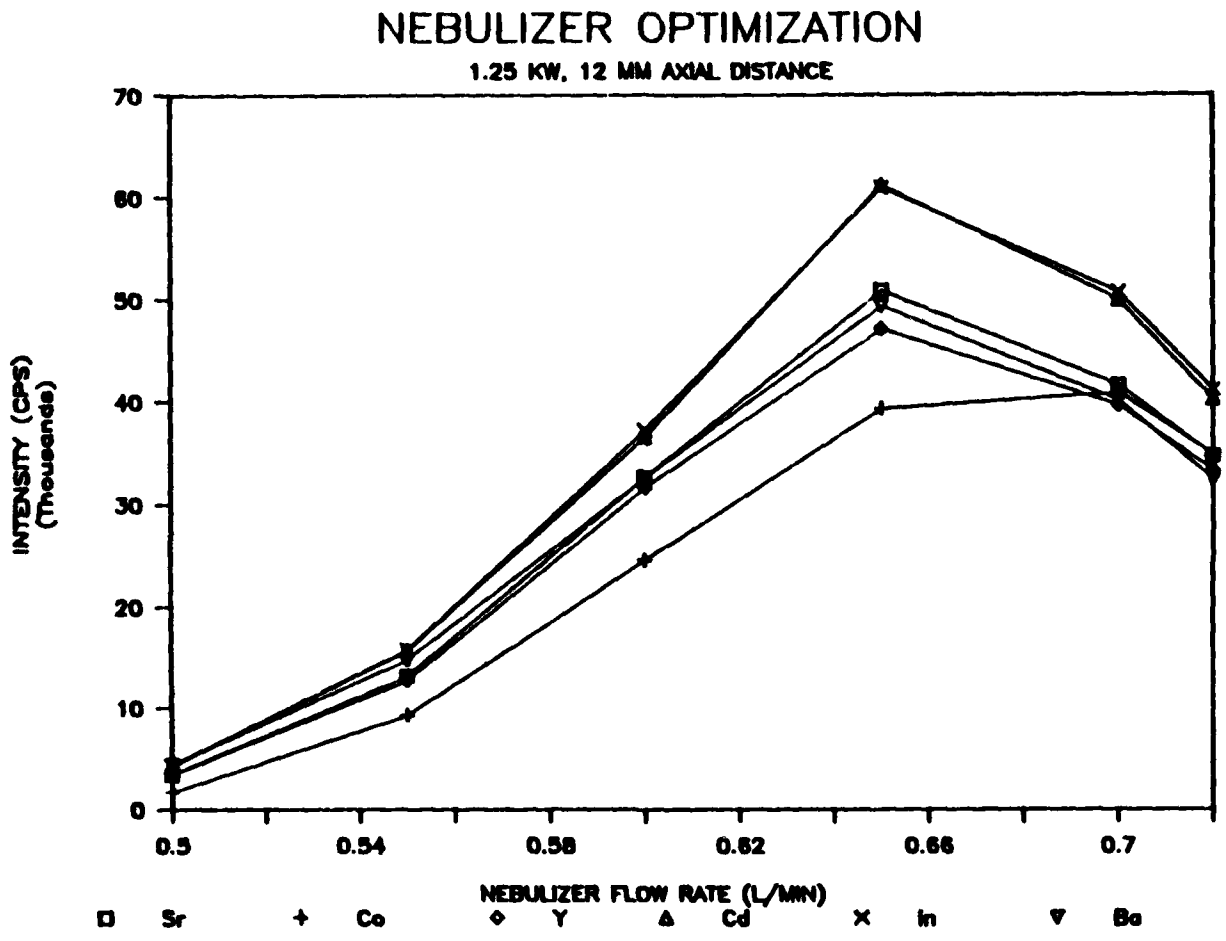

Figure 5-4. Nebulizer Flow vs. Signal Intensity @ 1.25 KW, 12 mm Sampling

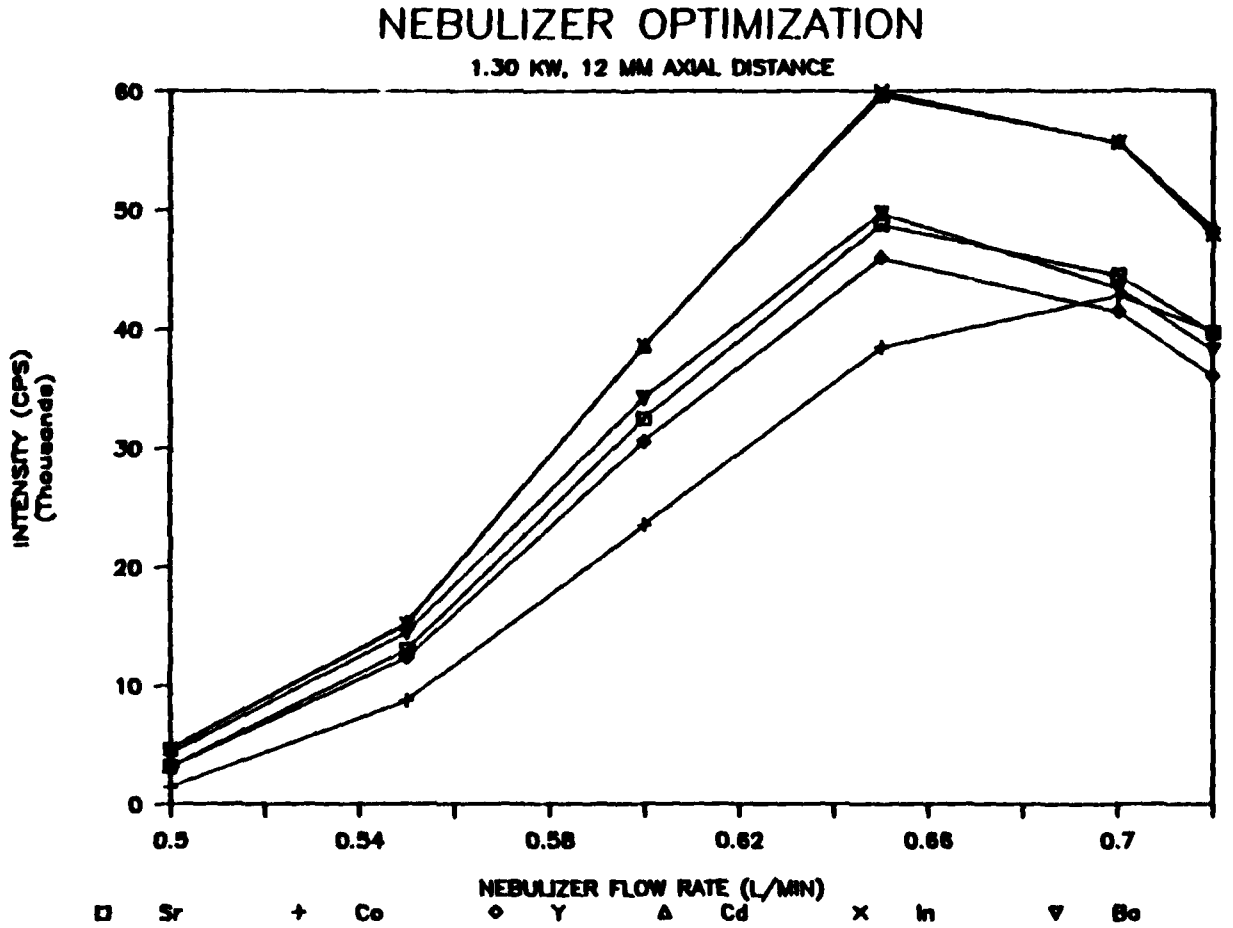

Figure 5-5. Nebulizer Flow vs. Signal Intensity @ 1.30 KW, 12 mm Sampling

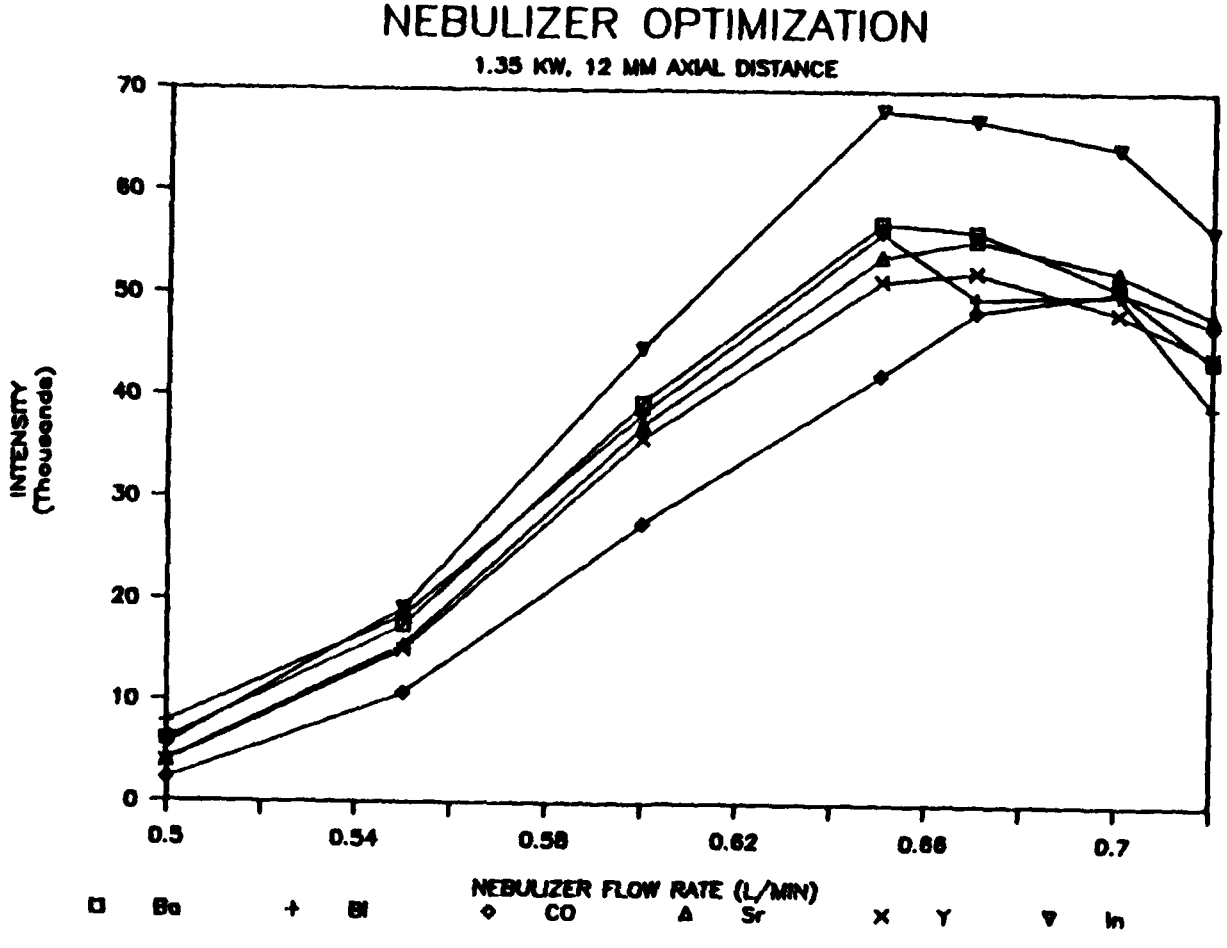

Figure 5-6. Nebulizer Flow vs. Signal Intensity @ 1.35 KW, 12 mm Sampling

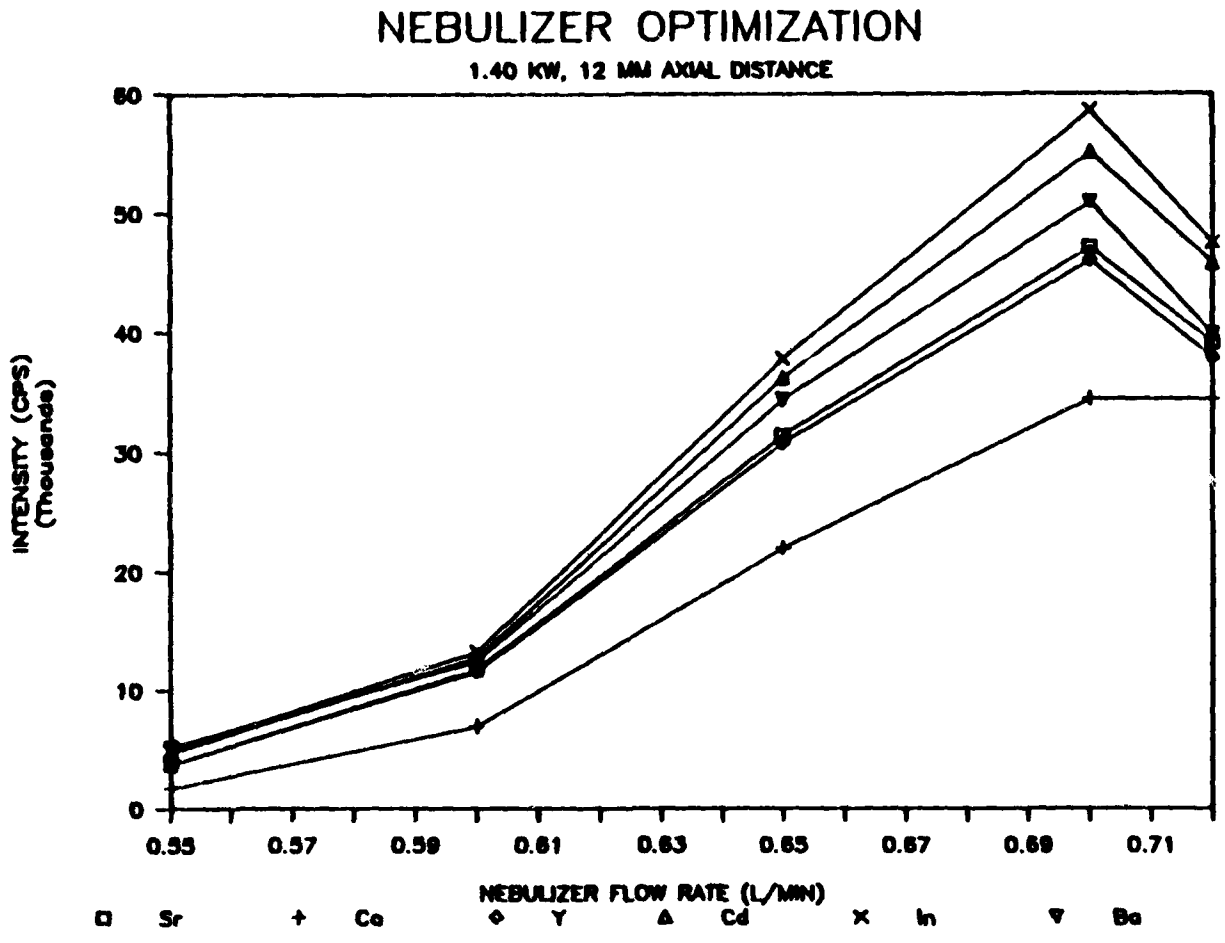

Figure 5-7. Nebulizer Flow vs. Signal Intensity @ 1.40 KW, 12 mm Sampling

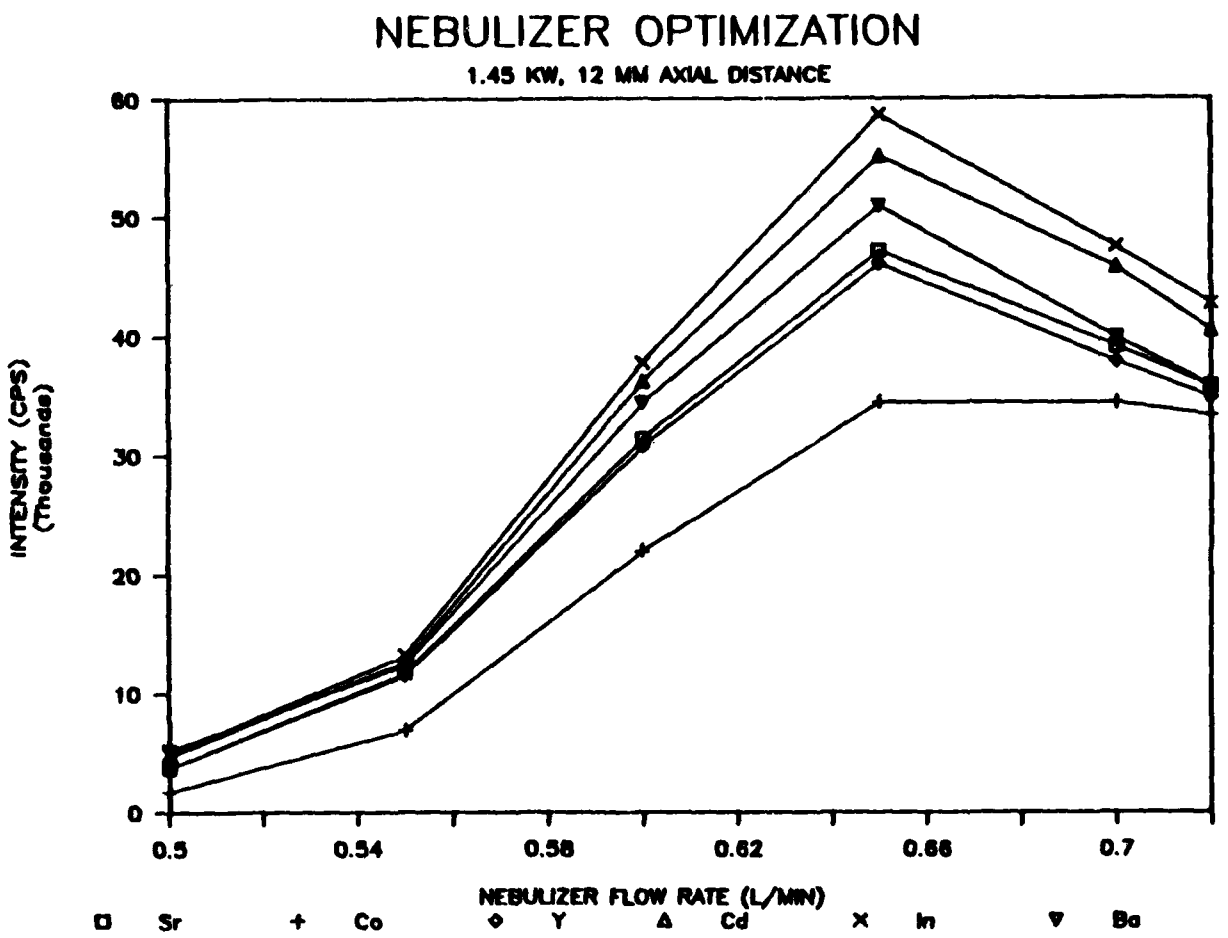

Figure 5-8. Nebulizer Flow vs. Signal Intensity @ 1.45 KW, 12 mm Sampling

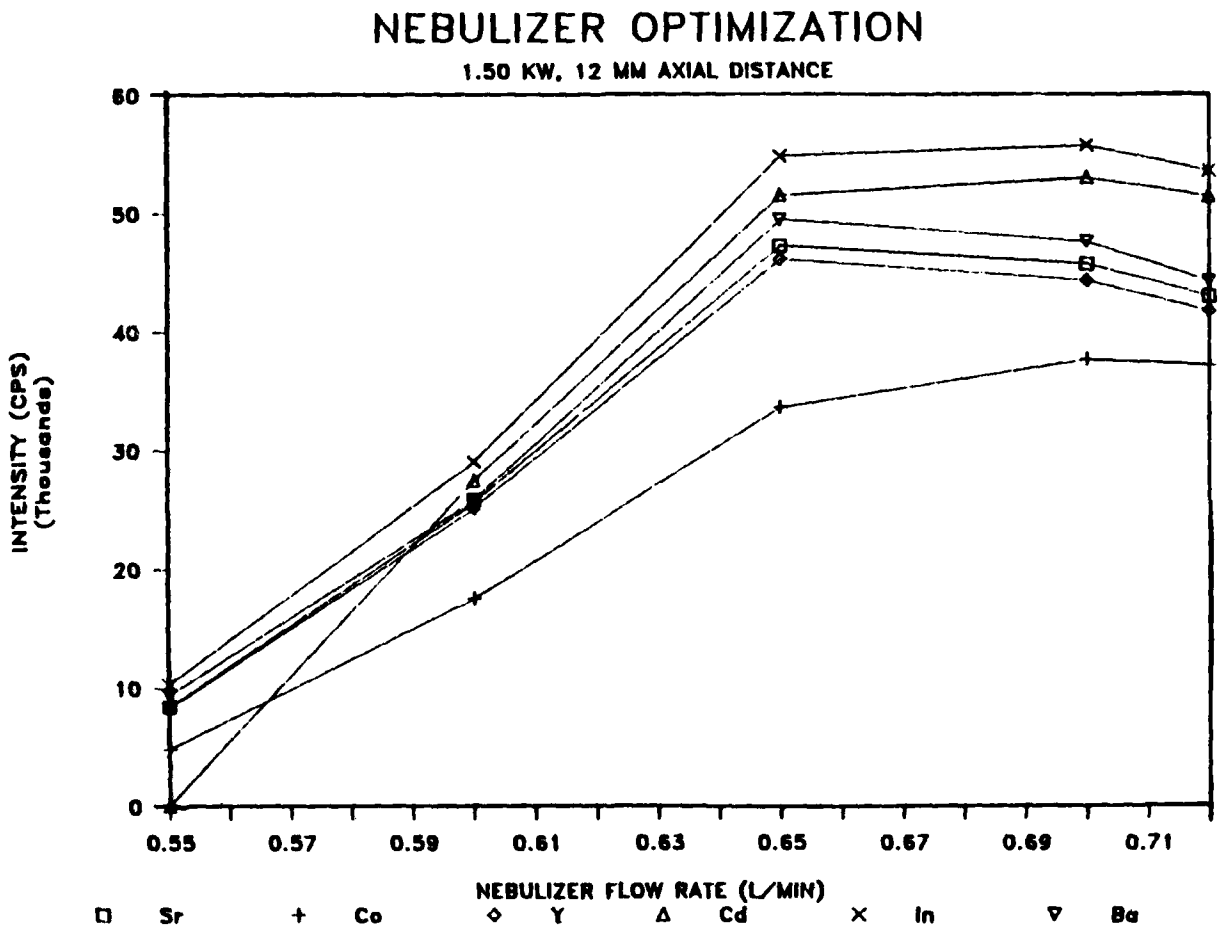

Figure 5-9. Nebulizer Flow vs. Signal Intensity @ 1.50 KW, 12 mm Sampling

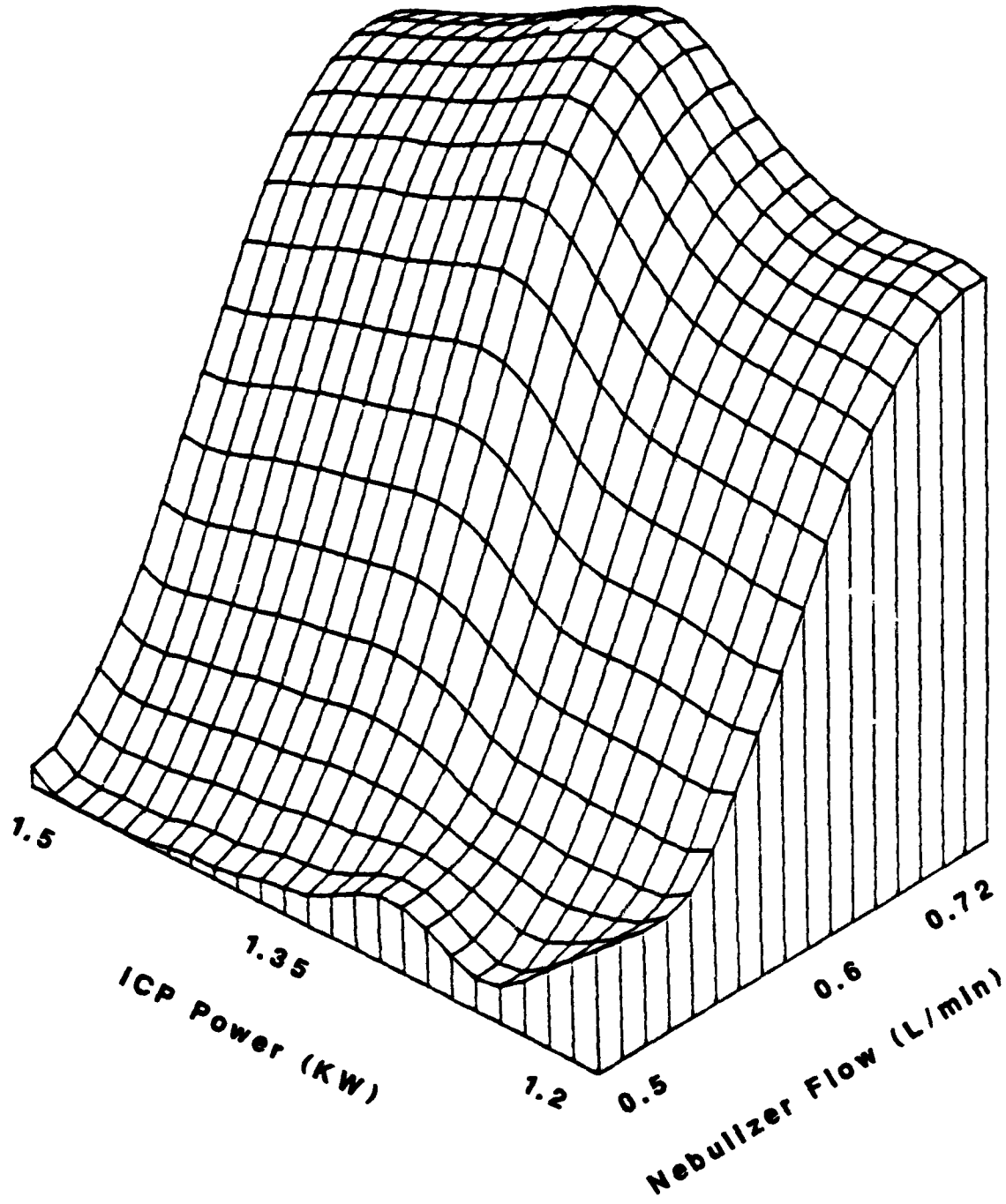

Figure 5-10. 3-D Plot; Nebulizer Flow, ICP Power, Signal Intensity; Co

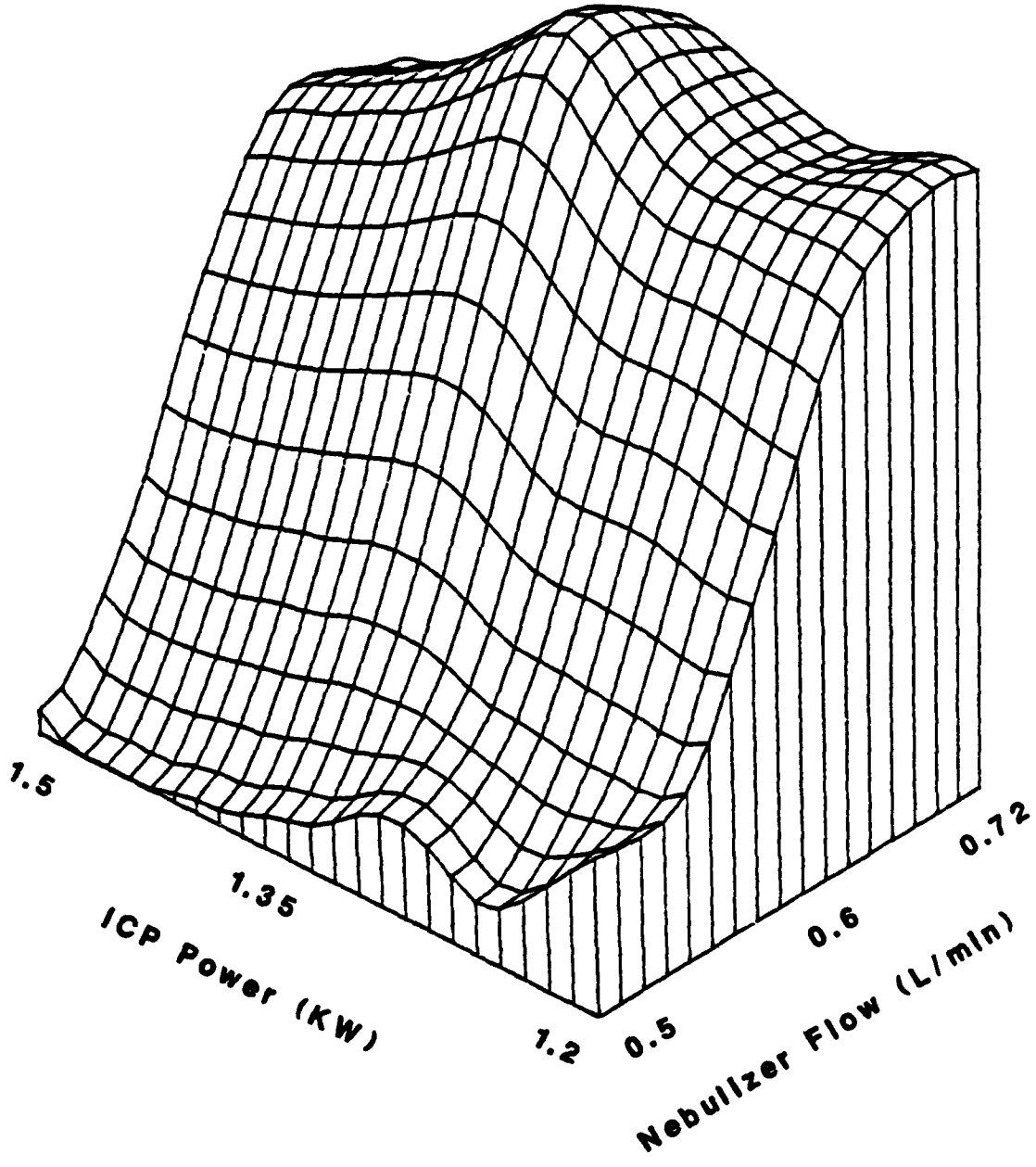

Figure 5-11. 3-D Plot; Nebulizer Flow, ICP Power, Signal Intensity; Ba

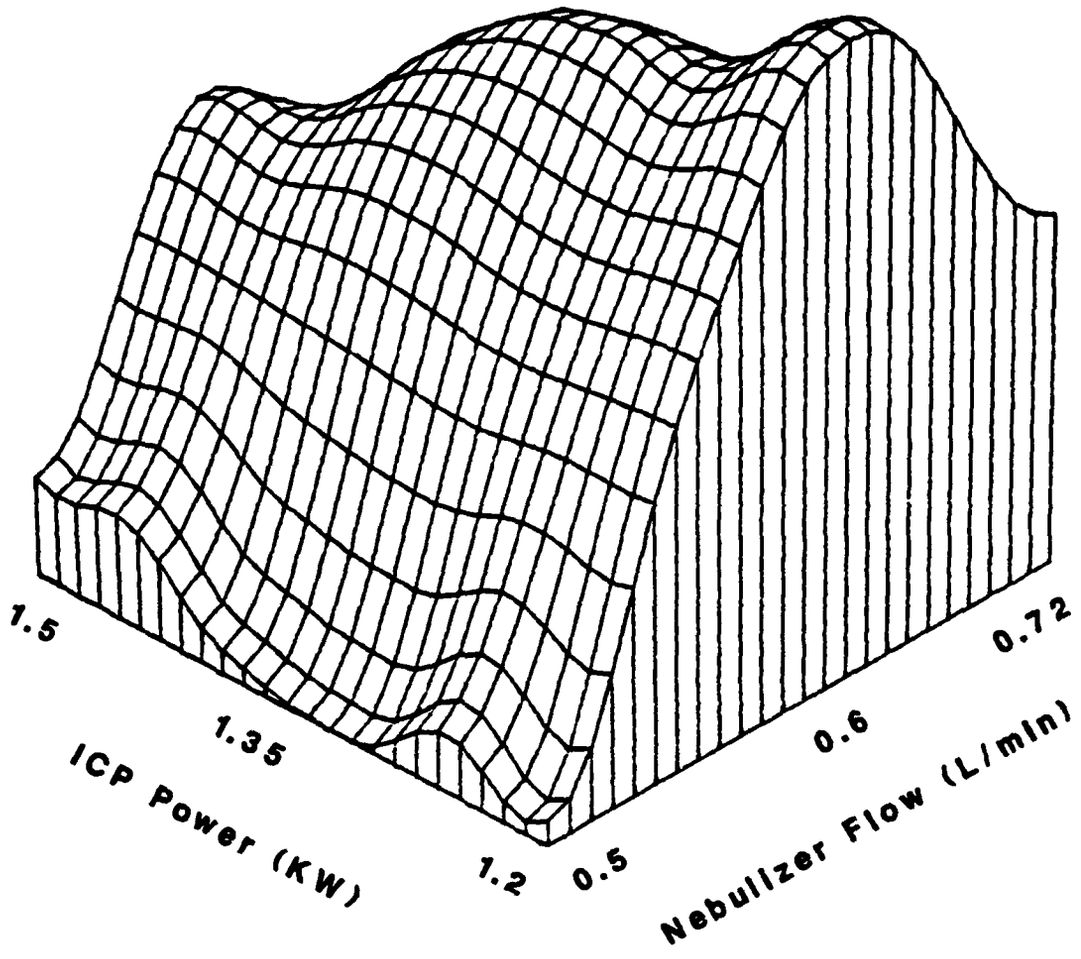

Figure 5-12. 3-D Plot; Nebulizer Flow, ICP Power, Signal Intensity; Sr

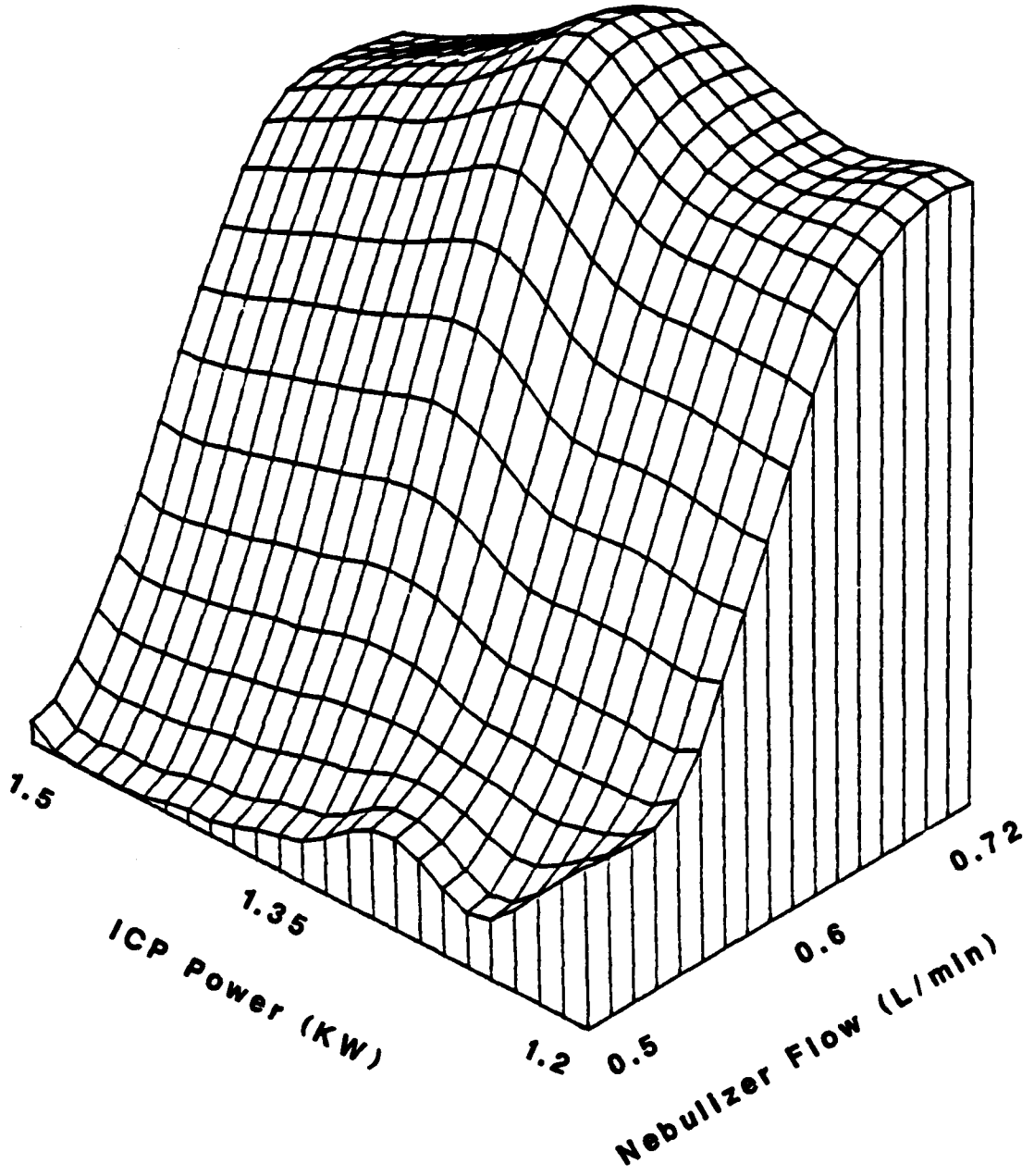

Figure 5-13. 3-D Plot; Nebulizer Flow, ICP Power, Signal Intensity; Y

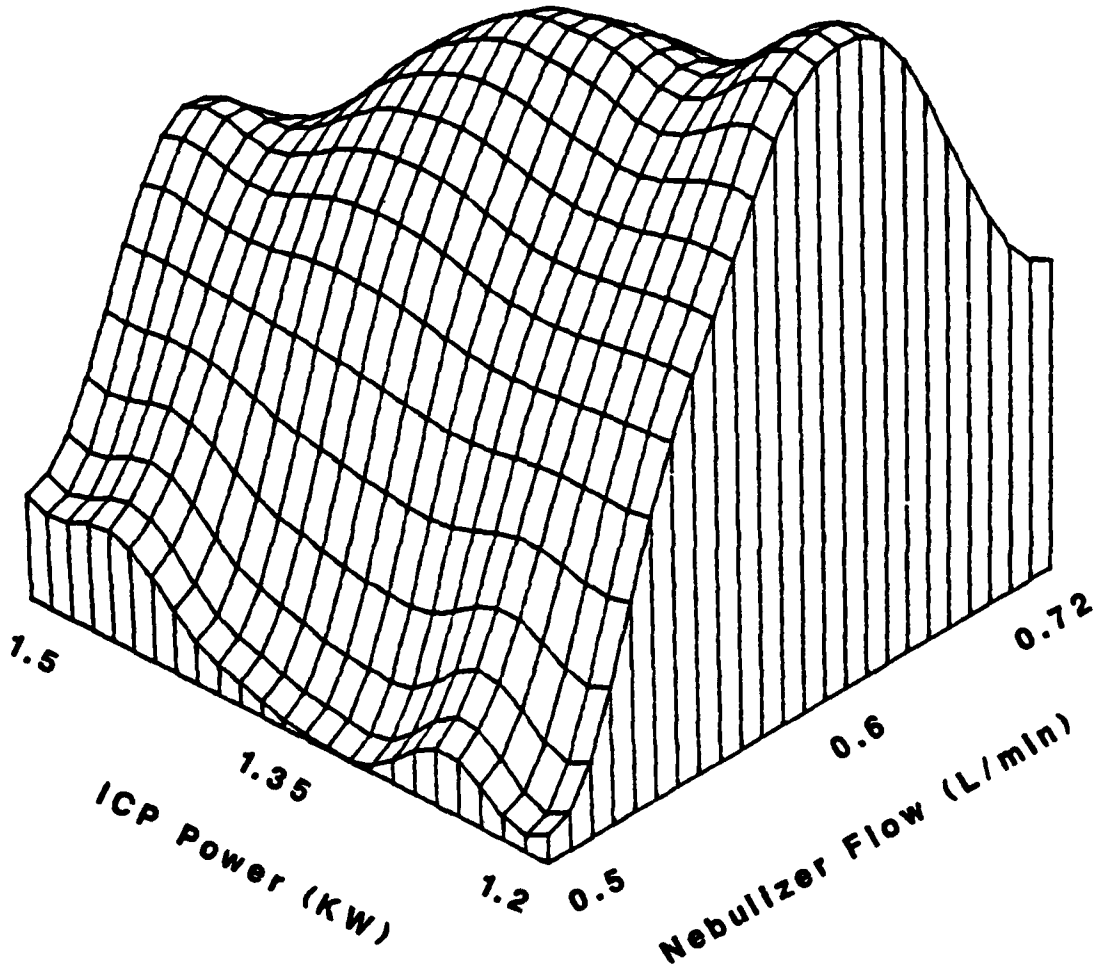

Figure 5-14. 3-D Plot; Nebulizer Flow, ICP Power, Signal Intensity; Cd

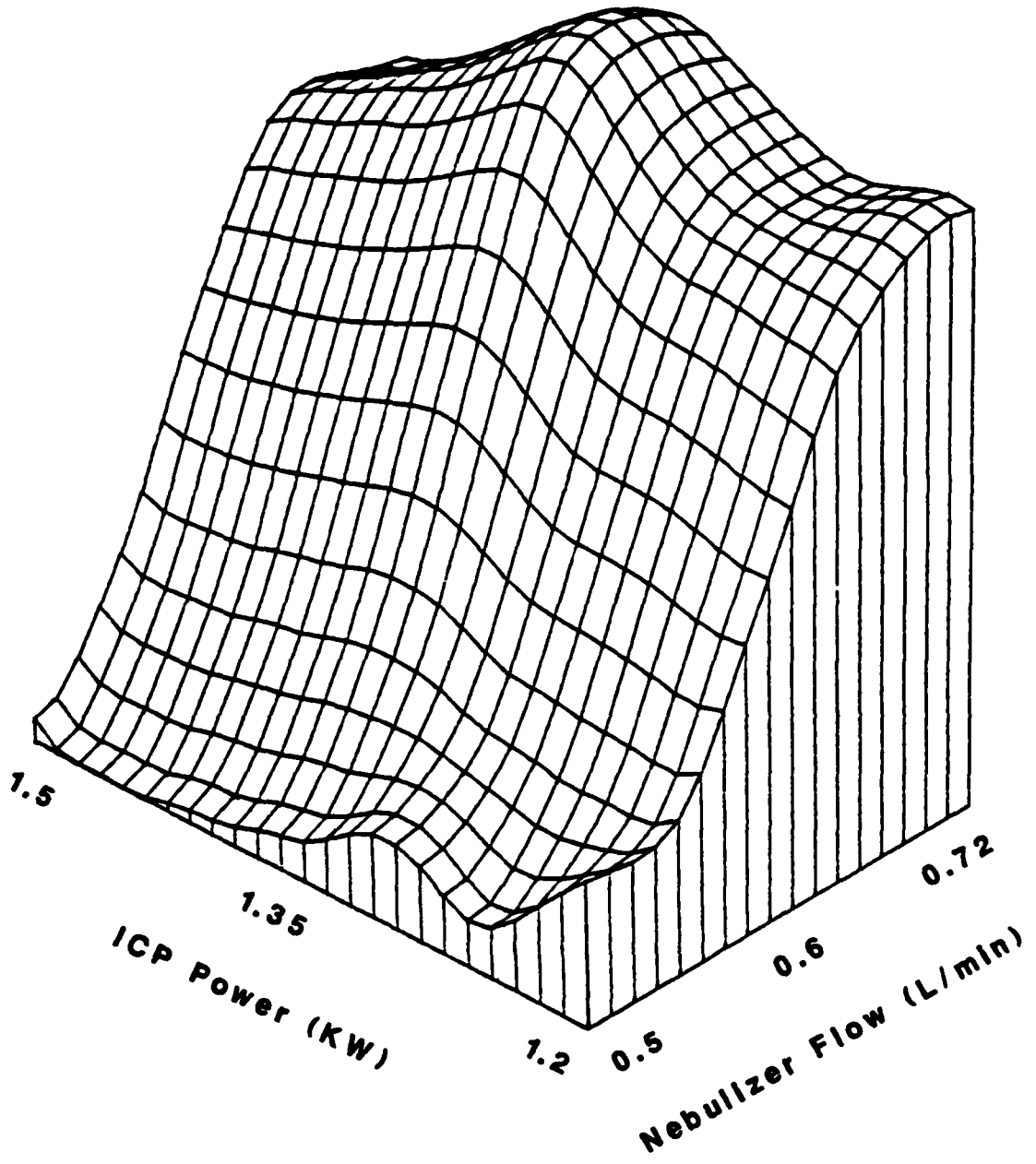

Figure 5-15. 3-D Plot; Nebulizer Flow, ICP Power, Signal Intensity; In

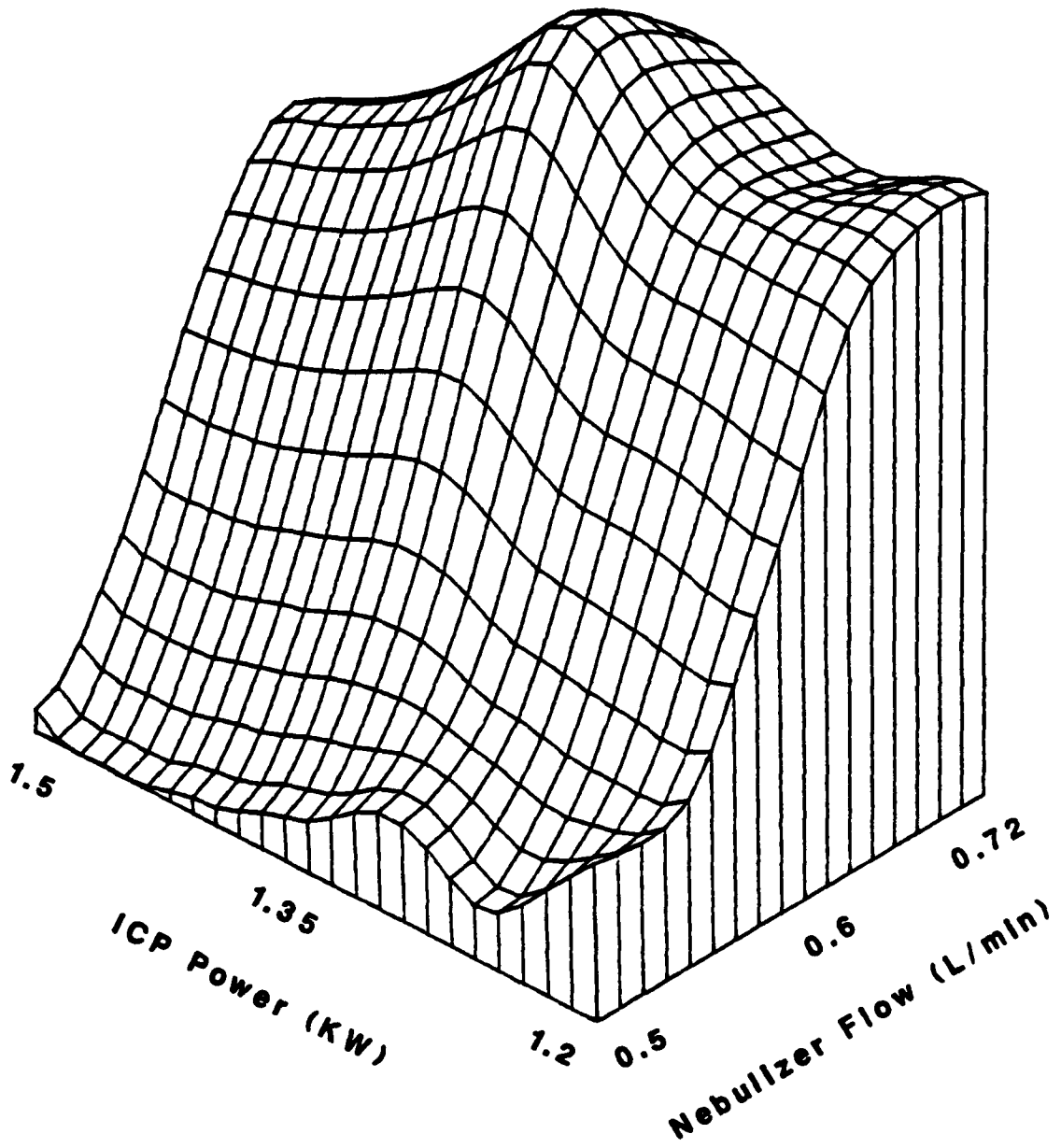

Figure 5-16. 3-D Plot; Nebulizer Flow, ICP Power, Signal Intensity; Bi

power.

5.3.2 Interferences

Table 5-4 lists the molecular species commonly found in ICP/MS spectra. Some particularly difficult elements to analyze via ICP/MS are Si, P, K, Ca, Fe and Se. Molecular ion species of nitrogen interfere with Si and P, whereas various argon ion and argon hydride ion species interfere with K and Ca. ArN^+ and ArO^+ make for a difficult analysis of Fe and the argon dimer interferes with Se.

Another potential for interferences within ICP/MS is the formation of doubly charged ions. **Figures 5-17,18,19** show the effect of nebulizer flow on the formation of Ba^{++}/Ba^+. As can be seen, this ratio is minimized (< 1%) at the optimal nebulizer flow rates (0.60-0.70 L/min).

5.3.3 Effect of Sampling Position

Sampling position is also very important for ICP/MS system optimization. Three different sampling positions were investigated. Ideally, more sampling positions should be investigated, but this was not practical since the ICP torch was difficult to move and the positioner was not very precise.

Figure 5-20 shows the effect of sampling position on signal intensity. Optimal sampling depth was determined to be 12 mm from the sampling tip to the load coil. This was as close in as the torch assembly could be positioned. The furthest back the torch box could be positioned was 17 mm. The data suggest that signal could be increased by moving the ICP torch closer to the sampler. In all cases for a given power and at the optimal nebulizer flow rate a decrease in signal intensity was found as plasma sampling depth increased.

Our results are similar to Browner et al.[7] All elements showed a

Table 5-4

Common Background Molecular Ions

Mol Ion	Mass	Interferes with
N_2^+	28	Si
N_2H^+	29	Si
NO^+	30	Si
NOH^+	31	P
O_2^+	32	S
O_2H^+	33	S
$^{38}ArH^+$	39	K
$^{40}Ar^+$	40	Ca
$^{40}ArH^+$	41	Ca
CO_2^+	44	Ca
ArO^+	56	Fe
$ArOH^+$	57	Fe
ArN^+	54	Cr/Fe
$ArNH^+$	55	Mn
$^{40}Ar^+$	80	Se
$^{40}Ar^{36}Ar^+$	76	Se
$^{40}Ar^{38}Ar^+$	78	Se

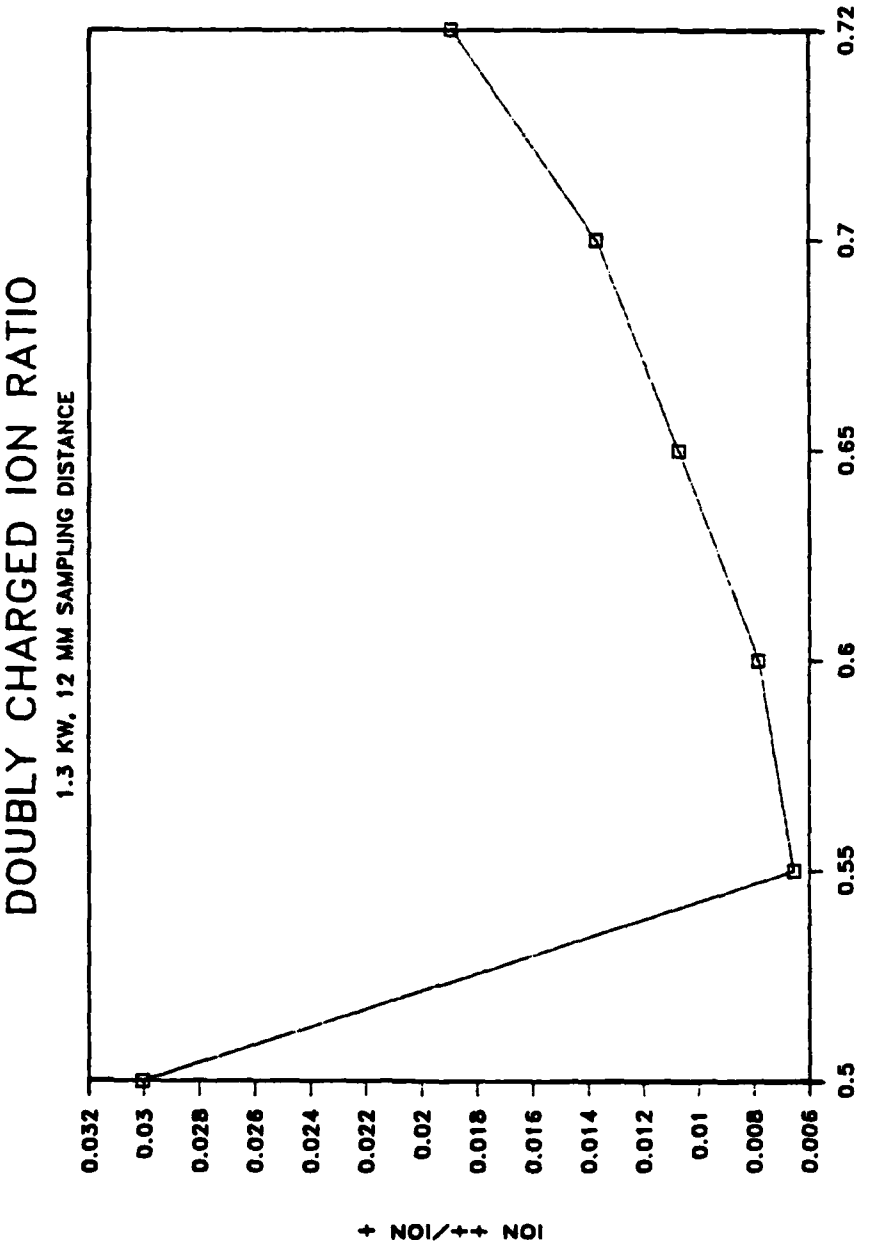

Figure 5-17. Nebullzer Flow vs. Ba Doubly Charged to Singly Charged Ion Ratio @ 1.30 KW, 12 mm Sampling

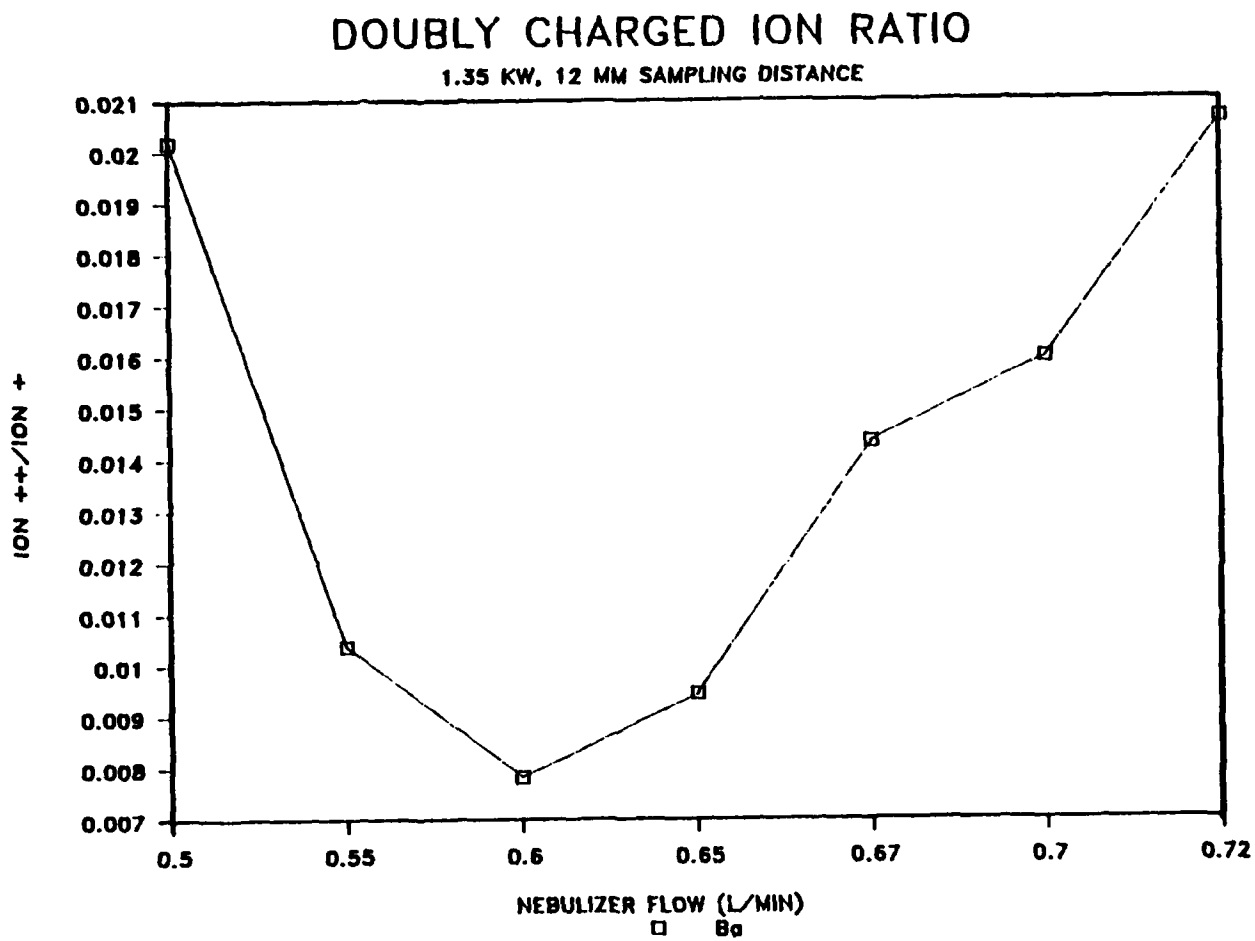

Figure 5-18. Nebulizer Flow vs. Ba Doubly Charged to Singly Charged Ion Ratio @ 1.35 KW, 12 mm Sampling

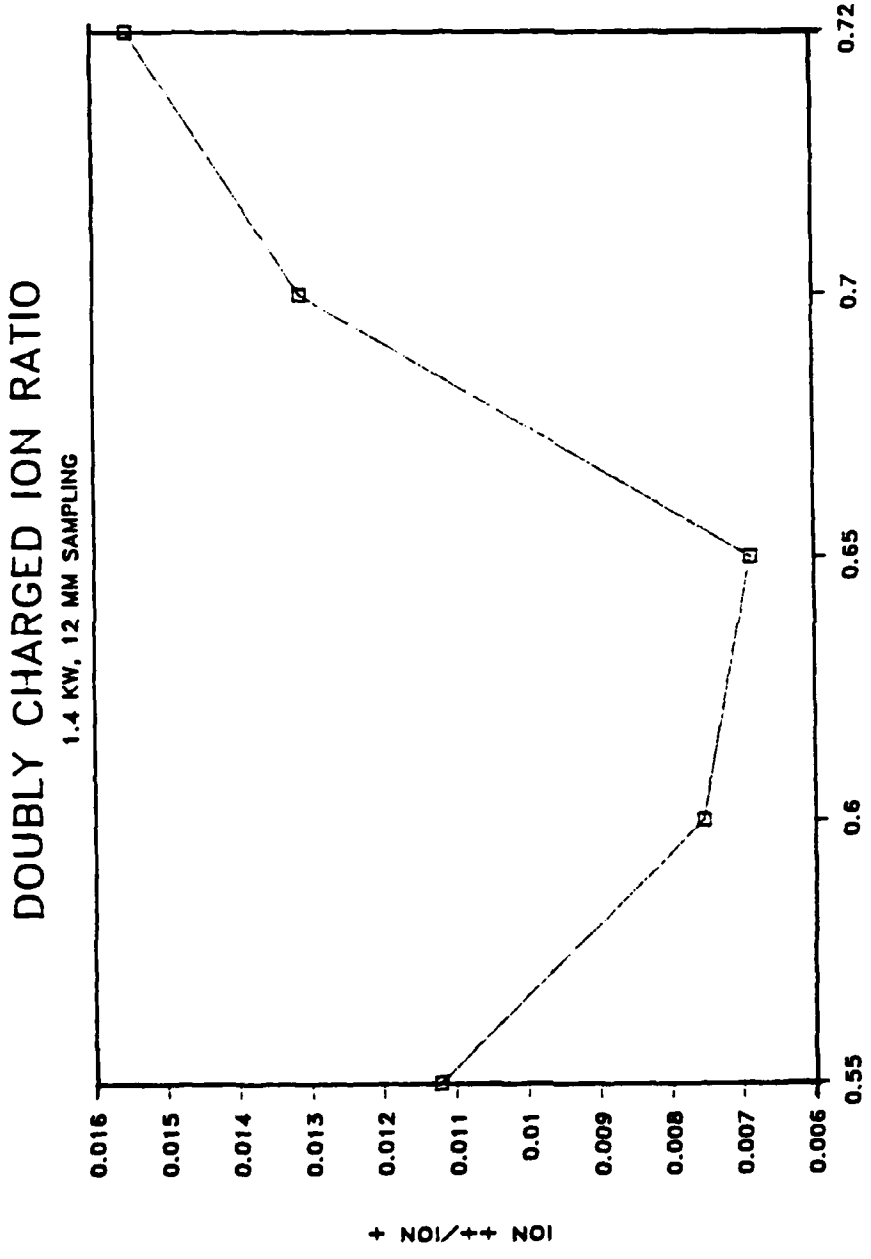

Figure 5-19. Nebullzer Flow vs. Ba Doubly Charged to Singly Charged Ion Ratio @ 1.40 KW, 12 mm Sampling

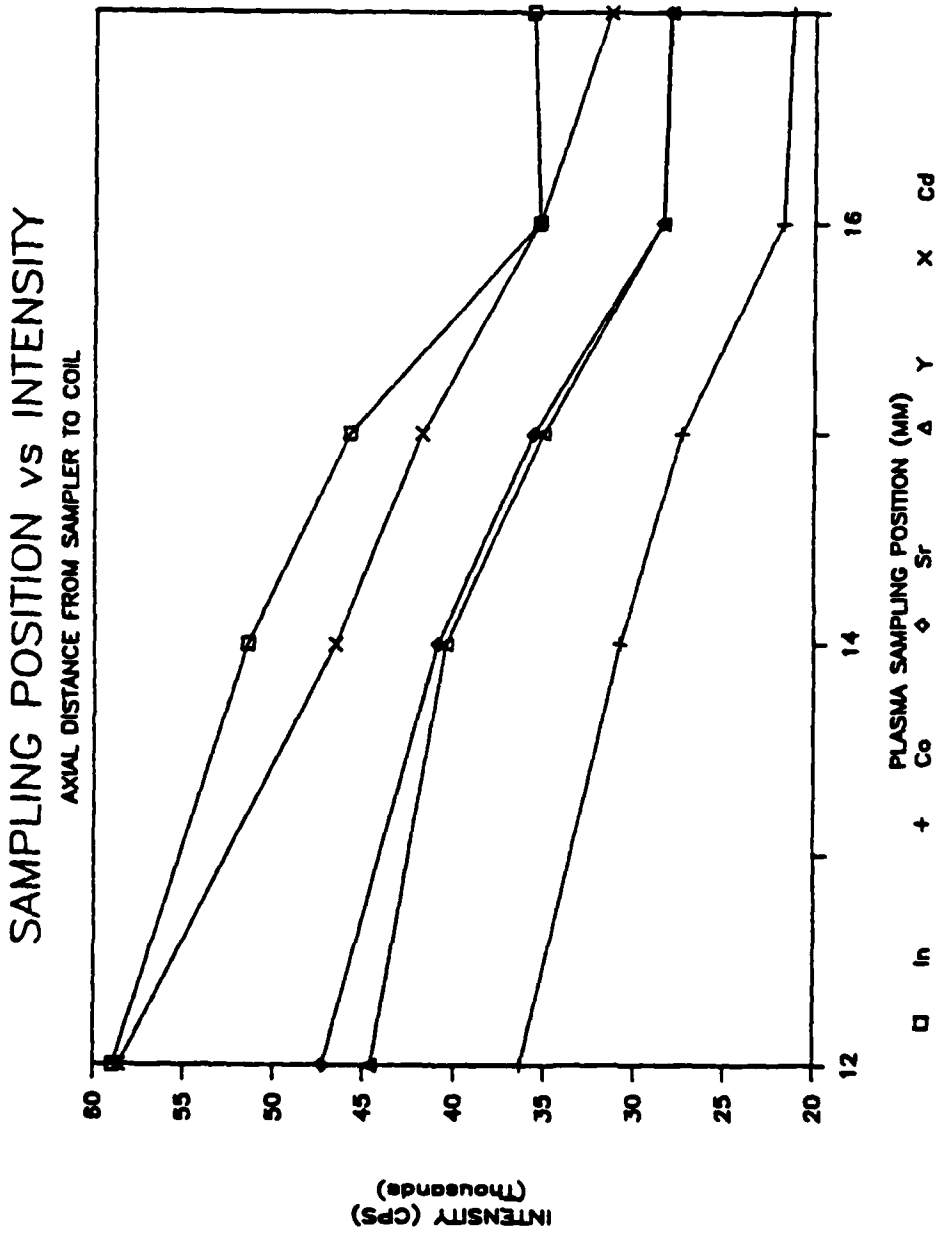

Figure 5-20. Plasma Sampling Position vs. Signal Intensity

maximum signal for one particular nebulizer flow at each sampling depth investigated. Signal intensity dropped off quickly as sampling depth was increased beyond the optimum sampling depth of 12 mm. Only slight shifts in positions of the maximum with changes in sampling depth were observed.

However, there were some observations different than those reported by Browner. Optimal sampling depth for our system was 12 mm (versus 17 mm). At sampling depths greater than 12 mm, the slight shifts in maximum signal observed were toward higher gas flows with increasing sampling depth (versus decreasing sampling depth in Browner's study).

The ICP/MS study results using the fixed crossflow nebulizer were very similar to that of the Hildebrand grid. No significant difference in sensitivities was determined. Optimal nebulizer flow, ICP power and sampling depth were essentially the same. **Figures 5-21,22,23** show nebulizer optimization plots at various powers. A three dimension pictorial of Co and Ba which shows how ICP power and nebulizer flow effect intensity is depicted in **Figures 5-24** and **5-25.**

5.3.4 Detection Limits

Detection limits (based on 3σ above background) were calculated using the qualitative scan mode of the instrument. Twenty background points used were in the region from 160-180 amu. This procedure was used for all detection limits in this chapter. Better detection limits could be obtained by using single ion monitoring. Detection limits listed are realistic estimates of ICP/MS detection capability on a routine basis. **Table** 5-5 shows some representative detection limits which range from 0.7-0.04 ng/mL.

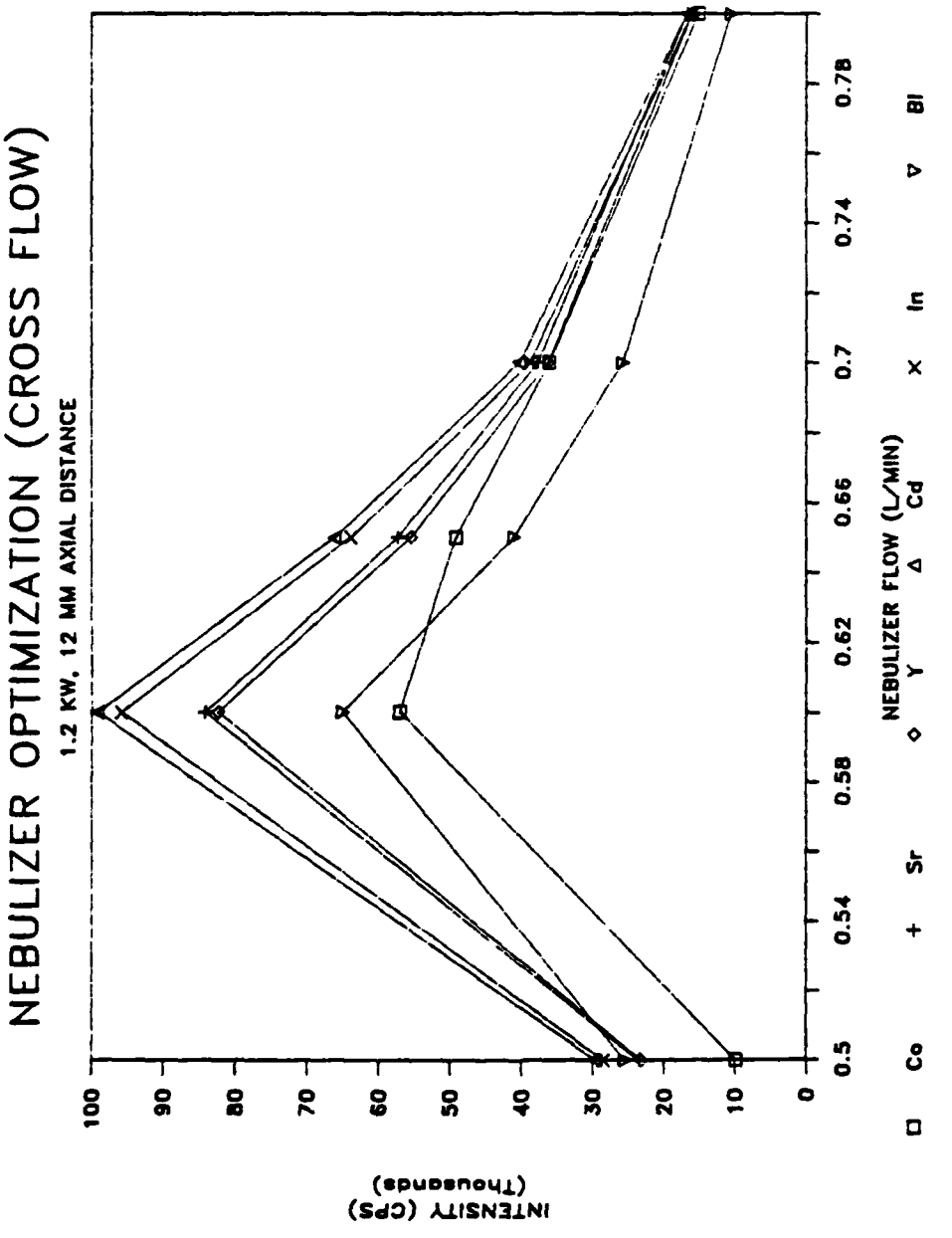

Figure 5-21. Nebulizer Flow vs. Signal Intensity @ 1.2 KW, 12 mm Sampling (cross flow)

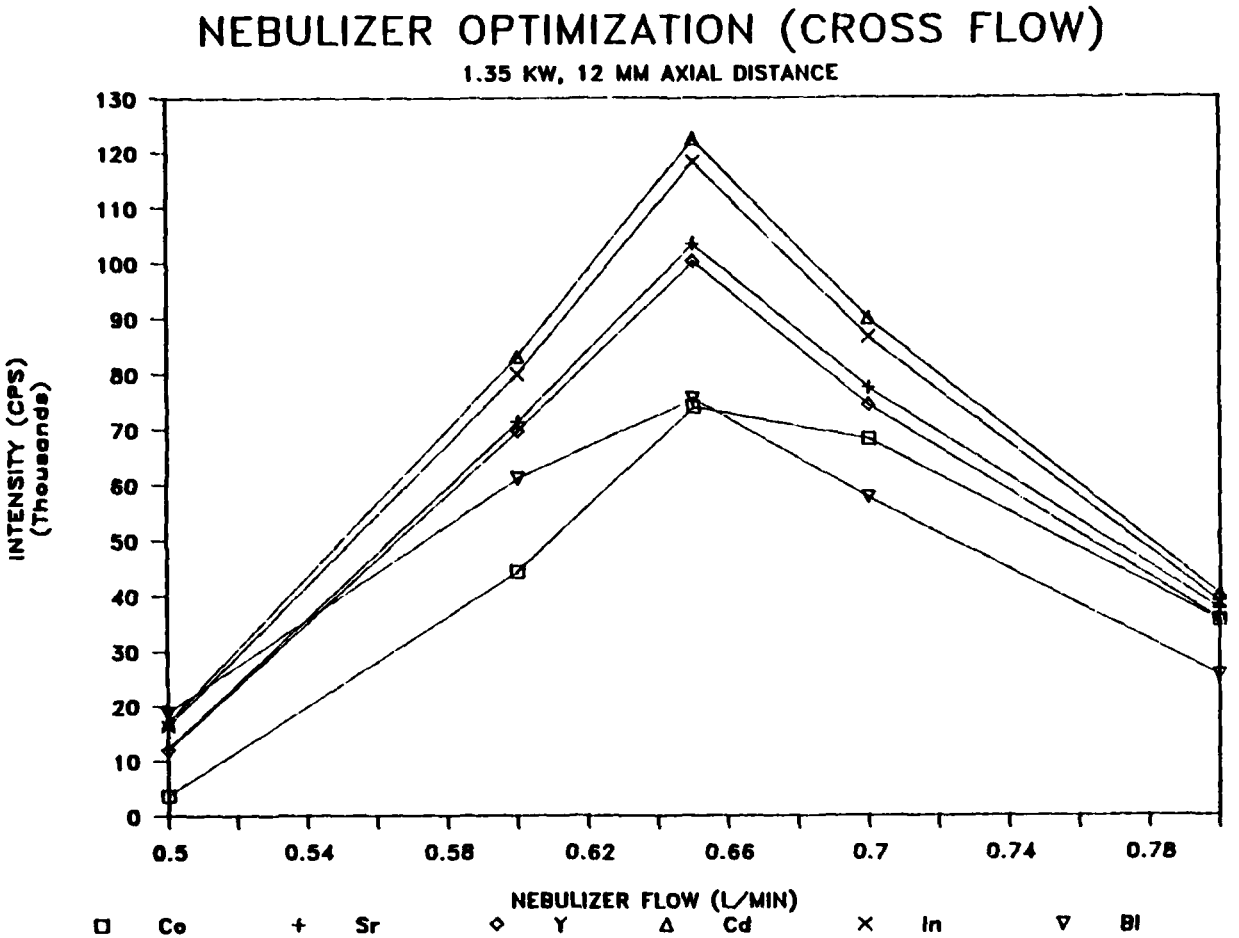

Figure 5-22. Nebulizer Flow vs. Signal Intensity @ 1.35 KW, 12 mm Sampling (cross flow)

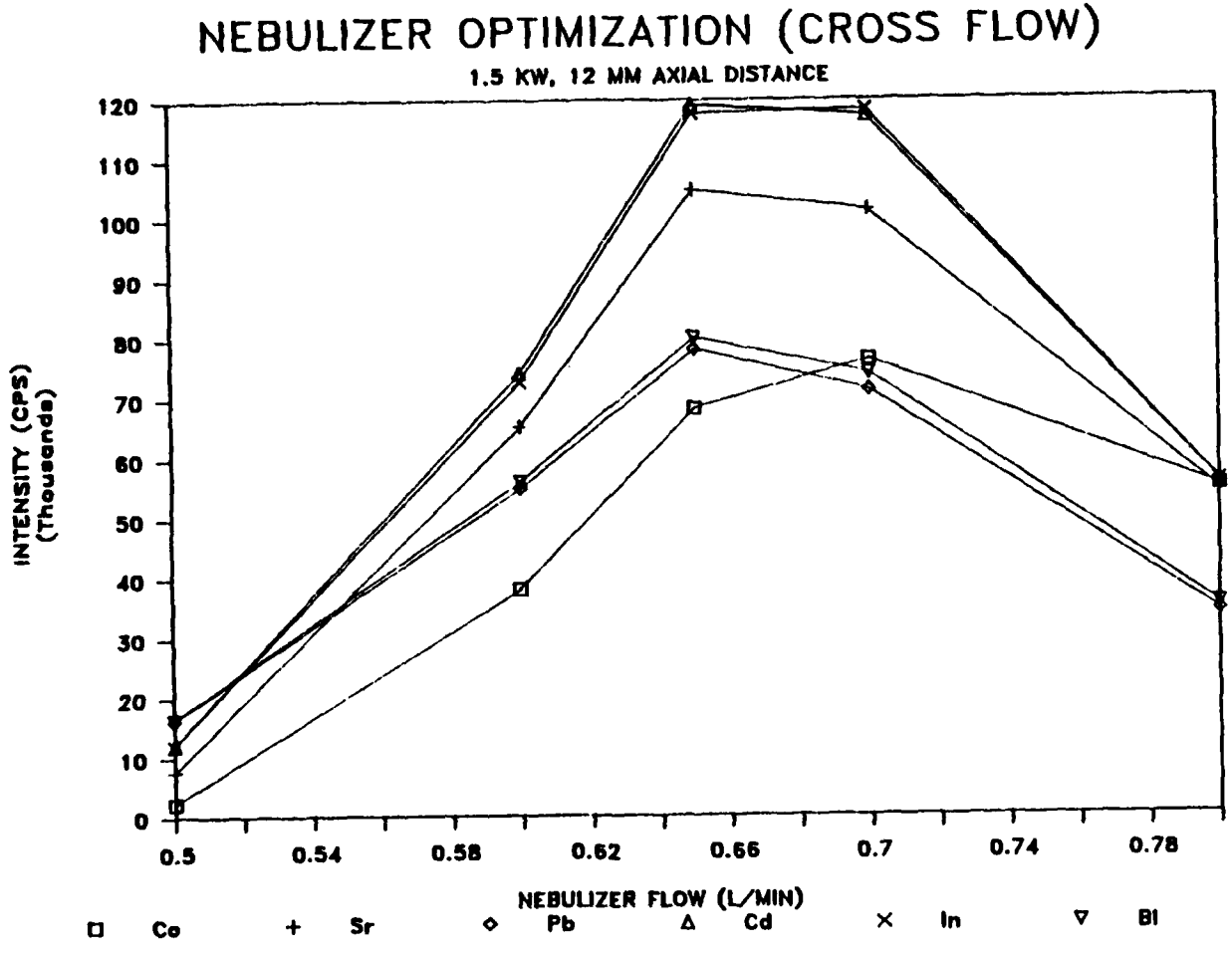

Figure 5-23. Nebulizer Flow vs. Signal Intensity @ 1.50 KW, 12 mm Sampling (cross flow)

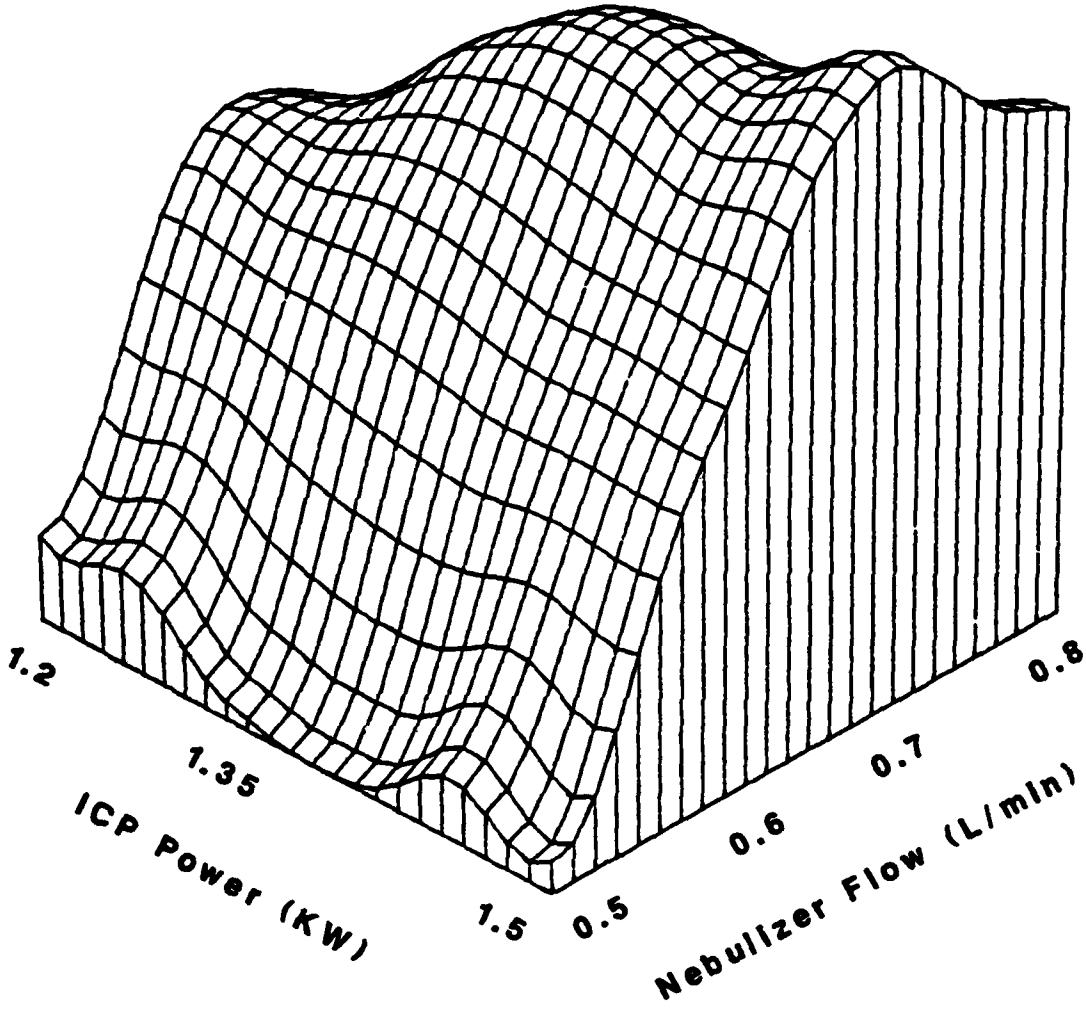

Figure 5-24. 3-D Plot, Nebulizer Flow, ICP Power, Signal Intensity; Co (Cross Flow)

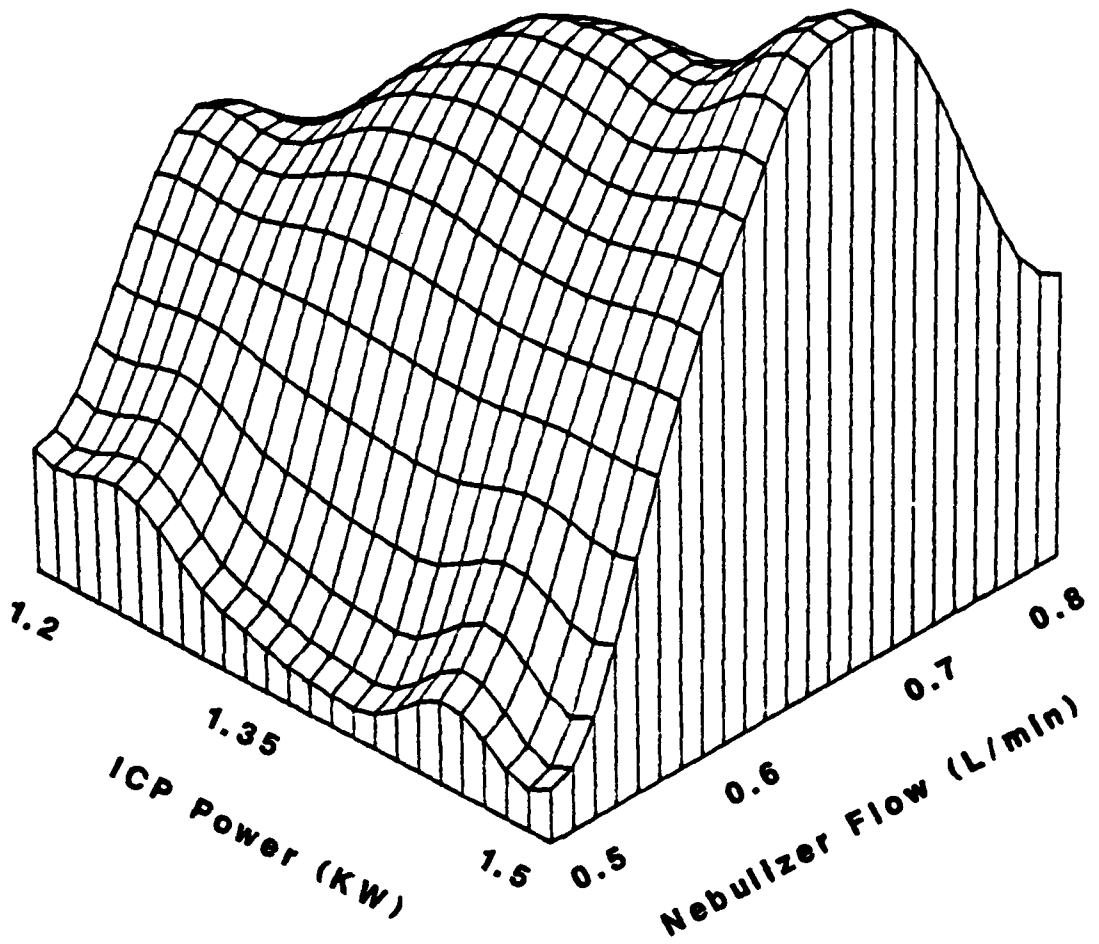

Figure 5-25. 3-D Plot, Nebulizer Flow, ICP Power, Signal Intensity; Ba (Cross Flow)

Table 5-5

Plasmaquad Detection Limits ng/mL

1% Nitric

Hildebrand Grid

Li	0.70
Mg	0.21
Co	0.06
As	0.53
Sr	0.05
Y	0.06
In	0.04
Ba	0.05
Bi	0.06

5.4 SYNTHETIC OCEAN WATER STUDY

ICP/MS can provide sub ng/mL detection capability for most elements of the periodic table. Early studies indicated that one disadvantage of ICP/MS is its inability to tolerate solutions with high dissolved salts/solids. In 1980 Houk et al. found that concentrations of .01% (w/v) Na suppressed cobalt and chromium signal by 10%.[11] As sampling interfaces evolved to the point of using 0.75-1.0 mm sampling orifices, the ability of the ICP/MS to tolerate solutions with high dissolved salt solutions improved. In 1983, Gray and Date reported that by using a 0.5 mm sampler, solution containing 0.1% Na suppressed cobalt and bismuth was about 10%.[4] In 1986, Houk et al. published an excellent paper that theoretically predicted the suppression of analyte signal by various concomitant salt solutions based on estimates of plasma electron number density, solution transport on efficiency and ionization temperature of the plasma.[12] His theoretical determinations were compared with experimental data obtained using an ICP/MS equipped with a 0.53 mm sampling orifice. A complete description of the system is described elsewhere.[13]

Houk predicted that Co^+ signal would be suppressed 10% for 0.1 M Na solution (assuming plasma ionization temperature of 7500 K). Experimentally it was found that a 0.01 M Na solution suppressed Co^+ signal by 10%.

There are primarily three reasons why ionization suppression is observed for ICP mass spectra of high dissolved salt solutions. Since the electrically neutral inductively coupled plasma has a large number of electrons (approximately 10^{15} electrons/cc), there must be an equivalent number of positively charged ionic species in the plasma. The primary ions found in the plasma consist of various atomic and molecular

species of Ar^+ (plasma gas), Sol^+ (solvent), M^+ (analyte) and A^+, B^+, C^+ (concomitant salt of formula $A_xB_yC_z$). If one assumes that the electron number density is constant, then introduction of easily ionizable elements such as Na^+ will suppress formation of other ions in order that the plasma remains electrically neutral. Often in salt solutions or biological fluids, Na (an easily ionizable element) concentration is 100-10,000 times higher than the analyte being assayed. This can result in severe analyte ion suppression and thus degradation in detection.

Another reason for suppression of analyte signal in high dissolved salt solution is that salt crystals condense and deposit on the sampling orifice. Any slight alteration to the sampler can result in less ion throughput. Another factor which contributes to ion suppression is that aerosol transport can be degraded by nebulizing salt solutions. Boumans and DeBoer reported that dissolved solids should be maintained below 0.1% to limit matrix effect to less than $\pm$10%.[14]

Beauchemin, McLaren and Berman, however, determined that some concomitant elements (Na, K, Cs, Mg, Ca) induce enhancement of the analyte signal while others (Li) has no significant effect and others (B, Al, U) cause a suppression. Their data suggest that a key factor linked to the effects may be the rate of atom-electron collisions; when it (rate) increases substantially (as with easily ionizable elements), the ionization of the analytes is favored more than their recombination with electrons, but if the concomitant elements form refractory oxides (B, Al, U), they can deposit on the interface, then the collisional rate is lower and recombination (with electrons) is favored.[15]

5.4.1 Experimental

Synthetic ocean water (SOW) preparation is described in Chapter 4.

SOW and various dilutions of SOW (10^{-1}M - 10^{-5}M) solution were spiked with Co, As, Y, In, Ba, Pb and Bi. Sample was introduced (@ 1.2 mL/min) with the grid nebulizer for one minute during which data were collected. The region from 1-55 amu was skipped to protect the electron multiplier. After each scan, a solution containing the same concentration of analyte elements in 1% nitric acid was introduced for 2 minutes. This was to help prevent clogging of the orifice and determine if overall system response was being degraded. There were three scans taken for each concentration of synthetic ocean water. Data were collected with the VG Plasmaquad in the qualitative scan mode. Standard ICP/MS conditions listed in previous section were used.

5.4.2 Results and Discussion

Figure 5-26 shows the effect of ionization suppression of various analyte lines for varying concentrations of synthetic ocean water. Generally, the 10% analyte suppression occurred for Co, In, Ba, Pb for 0.01-0.10 molar synthetic ocean water solutions. This corresponds to about a 0.15-1.5% (w/v) of various concomitant salts. This is similar to Houk's results.

Figure 5-26 also shows that Co Y and Ba signal increases slightly for the 0.001 M (SOW) solution. Though Houk's theoretical model would not predict this, these data corroborate Beuchemin, McLaren and Bermans[1] finding that Na, K, Cs, Mg and Ca can enhance analyte signal. Unfortunately, the effect of complex salt matrices on various analyte elements is very complex and not readily predicted by theory. An empirical method, therefore, is required to account for variances in ionization of analyte in a complex matrix.

Because of ionization suppression, it could be very difficult to

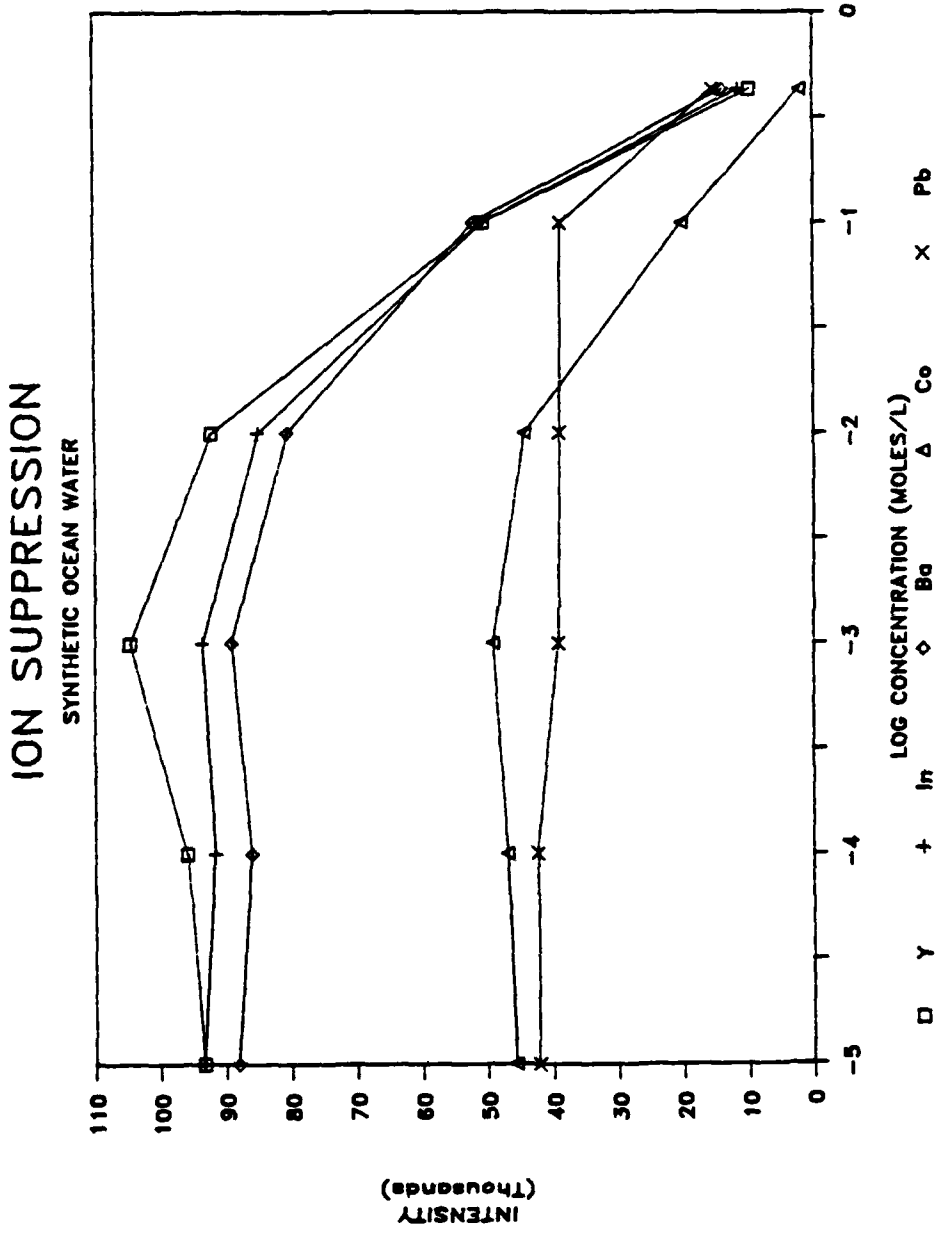

Figure 5-26. Concentration of Synthetic Ocean Water vs. Ionization Suppression of Analyte

quantitatively determine elemental concentrations in a salt matrix. In ICP-OES, one way to circumvent the problem of emission suppression due to matrix effects is to matrix match the standards to that of your unknown. This is not practical for ICP/MS since the system could not tolerate continual nebulization of high dissolved solids or biological fluids without clogging the sampling orifice.

The procedure, however, used on the VG Plasmaquad to compensate for emission suppression due to matrix effects is to spike the unknown with an internal standard of known concentration. By comparing the response of the known internal standard with that of a calibration curve stored on the computer, an estimate of ion suppression for all elements is determined. This is used to semi-quantitatively determine concentration of all elements in a sample in as little as one minute.

The semi-quantitative procedure is accomplished by generating a calibration curve (from a qualitative scan) that has elements at a certain concentration (e.g. 100 ng/mL) across the periodic table. The elements must be defined in an element menu called "Calelems". From this qualitative scan, a calibration curve of atomic mass unit vs. spectral response is generated. Next, an unknown solution which contains an internal standard is qualitatively scanned. All elements that are to be determined qualitatively should be listed in the "Allelems" element menu. The software of the Plasmaquad will then compare the unknown solution containing an internal standard (of known concentration) to the calibration scan. Based on the response of the internal standard, the calibration curve will be shifted and the concentration of all the elements (specified by Allelems) in the unknown solution will be calculated. **Figure 27** shows the procedure.

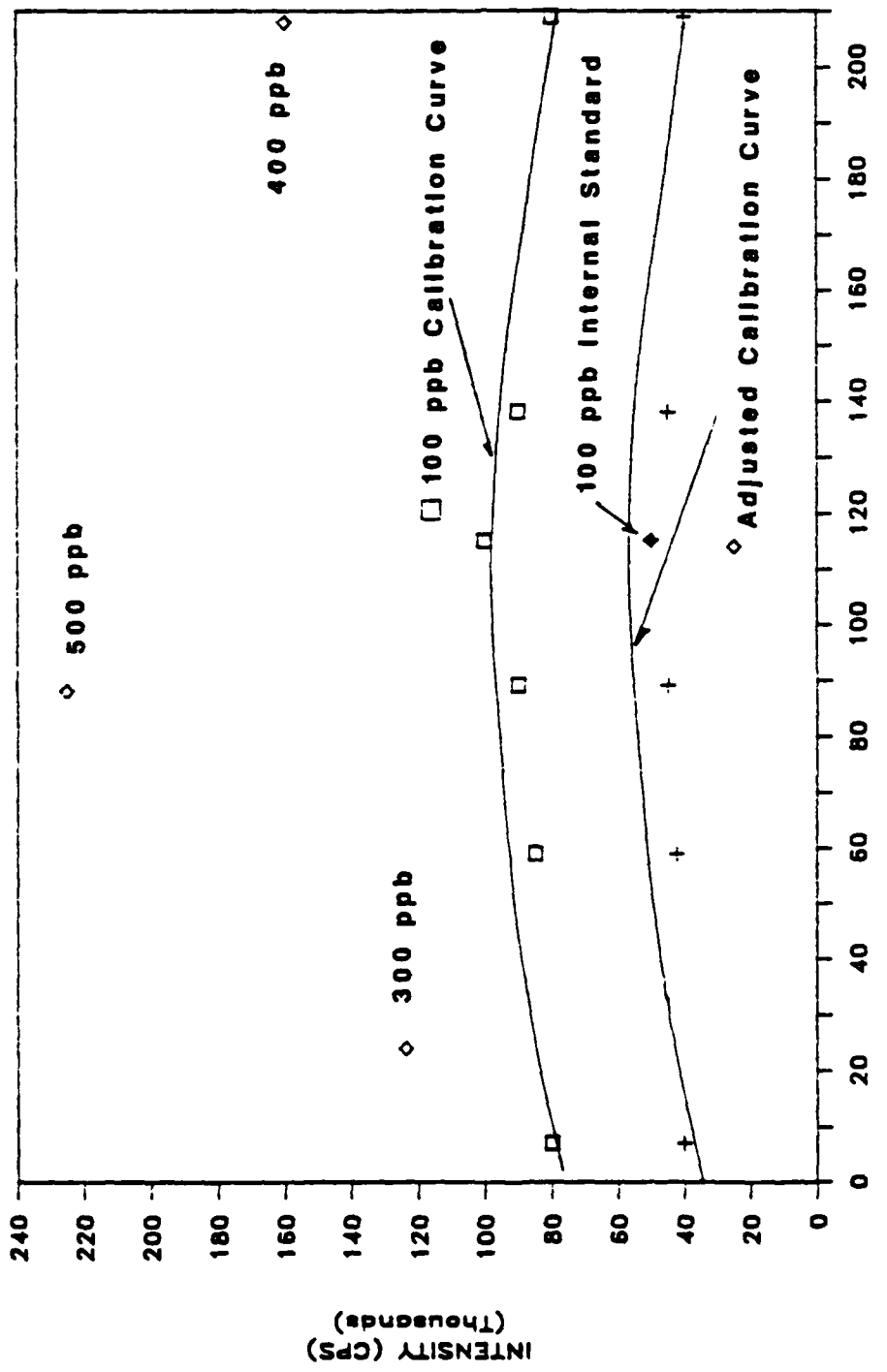

Figure 5-27. Semi-Quantitative Calibration Spectrum

This technique provides only an estimate (± 50%) of the concentration of the unknowns in solution. (It is important that one uses the VG SAHA corrected method which takes into account the ionization potential of each element analyzed.) In addition, the internal standard should be chosen so that it is close in mass and ionization potential to the particular element that is to be analyzed.

Table 5-6 shows the effect of estimating the concentration of unknowns in synthetic ocean water using an internal standard versus not using an internal standard. Values for the estimates based on using an internal standard are within ±75%-40%. This can be compared with the values obtained by not using internal standardization. In all cases, the values were approximately an order of magnitude lower than actual.

Table 5-7 shows the effect of using various internal standards for the same qualitative scan. Estimates vary a great deal depending upon which internal standard is used. Following are guidelines for choosing an internal standard.

1. If quantitation data is required for only one element, choose an internal standard that is close in mass and ionization potential to unknown.
2. If semi-quantification data are required for many elements, choose internal standard that is in the mid-mass range with a medium first ionization potential.
3. If semi-quantitative data are required for wide range of elements and ionization potentials spike sample with more than one internal standard, run calculations on same scan by specifying a different internal standards.

Table 5-8 shows the detection limits obtained using the qualitative

Table 5-6

VG Semi-Quantification Predicted Concentration (ng/mL)

100 ng/mL Analyte

Synthetic Ocean Water

	Internal Standard (Y)	No Internal Standard
Co	63	4
As	122	8
Y	100	9
In	90	12
Ba	131	15
Bi	175	23

Table 5-7

VG Semi-Quantification

Synthetic Ocean Water

SAHA Corrected

Spiked Element (100 PPB)	Predicted Concentration (ng/mL) Internal Standard Used					
	Co	As	Y	In	Ba	Bi
Co	100	51	63	164	48	36
As	195	100	122	191	93	70
Y	159	82	100	130	76	57
In	143	74	90	100	68	51
Ba	209	107	131	120	100	75
Bi	279	143	175	133	133	100

Table 5-8

Plasmaquad Detection Limits (ng/mL)

Hildebrand Grid

Element	1% Nitric	SOW
Co	0.04	0.67
As	0.19	1.45
Y	0.02	0.14
In	0.02	0.12
Br	0.02	0.10
Pb	0.05	0.10

scan mode of the instrument for synthetic ocean water solution (2.7% w/v dissolved solids) and a 1% nitric acid solution. With synthetic ocean water, detection limits are degraded from 50% to 1½ orders of magnitude.

5.5 URINE STUDY

An area that has been explored very little to date is the use of ICP/MS for assaying biological fluids. The ICP/MS advantages of speed, sensitivity and the ability to do isotope ratios, would lend itself well to clinical studies. Various urine concentrations were introduced into the ICP/MS to determine ionization suppression and detection capability.

5.5.1 Experimental

Various concentrations of fresh urine were spiked with Co, As, Cd, Ba, Bi and Pb. Solutions were fed to the grid nebulizer at a flow rate of 1.2 mL/min. Standard ICP/MS conditions were used. As in the SOW study, solution was fed to ICP/MS approximately 1 minute for data collection. After each run, 1% nitric acid standard containing the same analyte element was nebulized into the system. The standard solution was scanned to ensure that there was no instrument sensitivity degradation (i.e. due to orifice plugging). Three scans were made for each urine concentration. The region from 1-50 amu was skipped to prevent overload to the electron multiplier.

5.5.2 Results and Discussion

Urine contains a wide variety of elements that could pose severe matrix effects. **Table 5-9** lists the major components.[16] **Figure 5-28** shows the ionization analyte signal suppression for various elements as a function of % urine. The suppression for 100% urine matrix is approximately 40% for Co, As, Cd, Ba, Pd.

Figure 5-29 shows a typical mass spectra of urine with major peaks

Table 5-9

Typical Urine Composition

(over 24 hour period)

Element	Amount
Na	2-4 g
K	1.5-2.0 g
Mg	0.1-0.2 g
Ca	0.1-0.3 g
Fe	0.2 mg
NH_3	0.4-1 g N
Amino Acids	0.08-0.15 g N
Phosphate	0.7-1.6 g P
Organic Sulfate	0.06-0.2 g S
Urea	6-18 g N
Creatinine	0.3-0.8 g N
Peptides	0.3-0.7 g N
Uric Acid	0.08-2 g N
Inorganic Sulfate	0.6-1.8 g S

Total over 24 hr. period - 600-2500 mL/day.

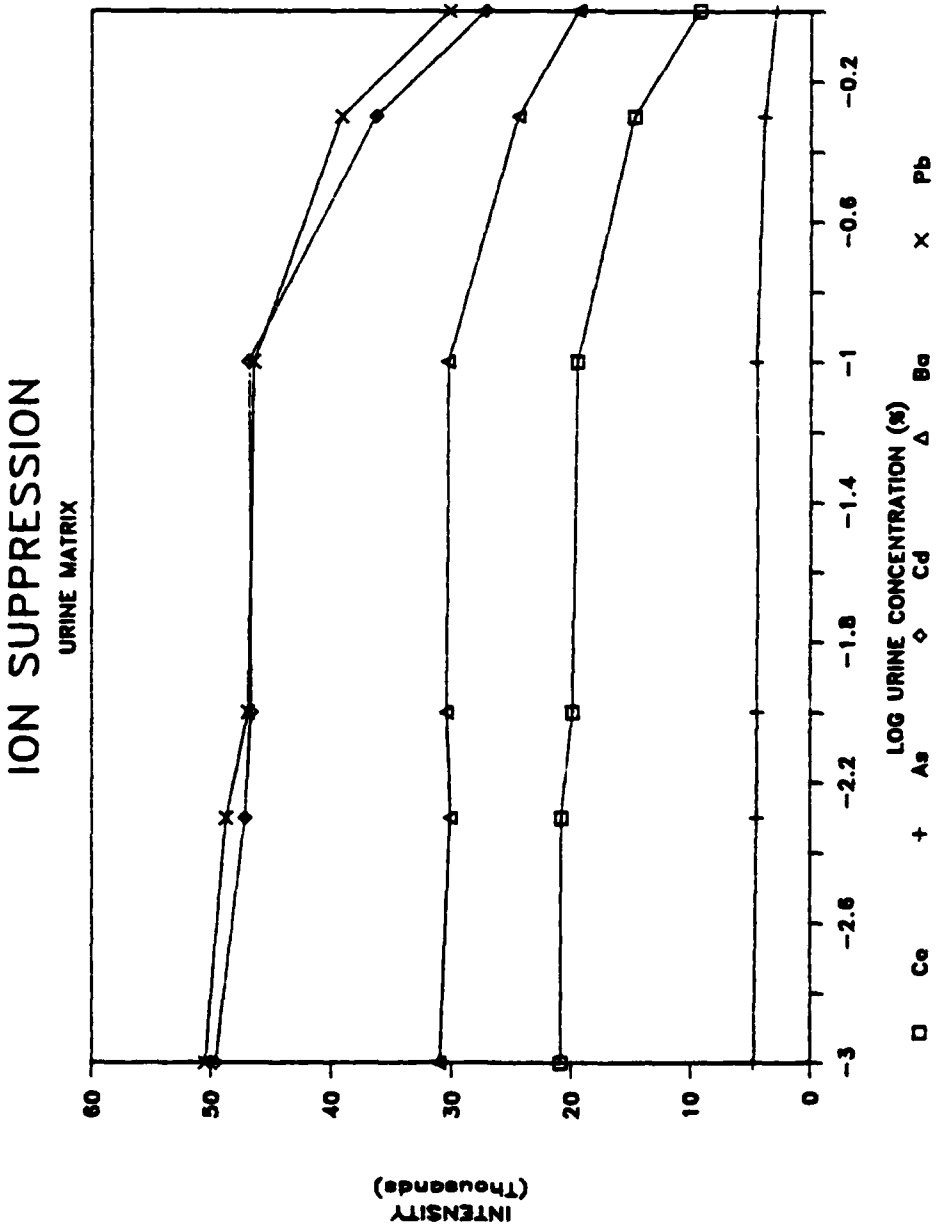

Figure 5-28. Urine Concentration vs. Ionization Suppression of Analyte

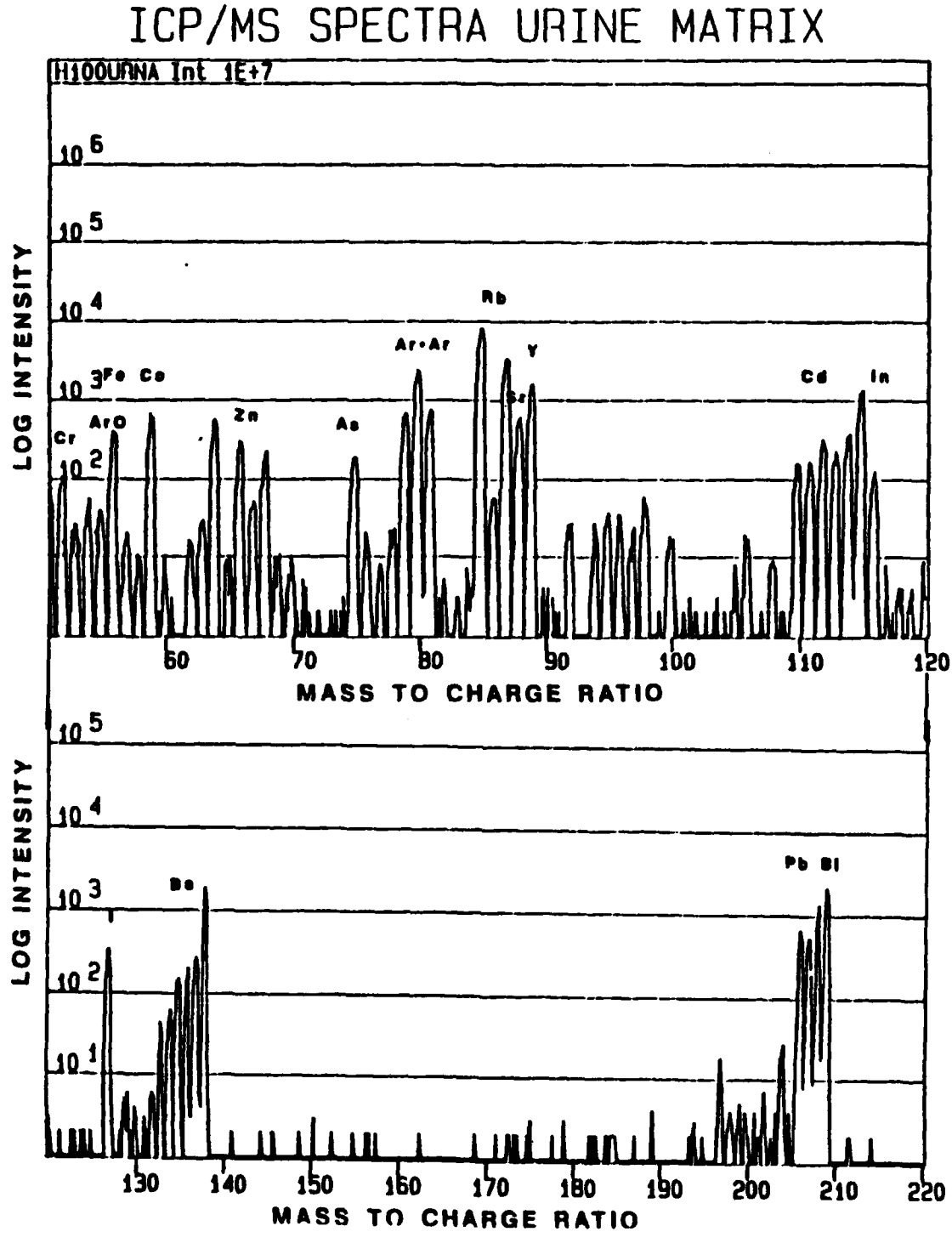

Figure 5-29. ICP/MS Mass Spectrum of Various Elements in Urine

identified. Data obtained from this spectrum was acquired in less than 60 seconds.

As in the case of synthetic ocean water, internal standards can alleviate problems associated with ionization suppression. **Table 5-10** shows the estimated concentration of elements spiked (@ 100 ng/mL) into a urine matrix for various internal standards. The guidelines outlined in the previous section for choosing internal standards also apply here.

Table 5-11 show the detection limits (DL) obtained for elements in urine matrix versus a 1% nitric solution. DLs for the 1% nitric solution ranged from 0.4 ng/mL-4.0 ng/mL. DLs were degraded from 15-40% for elements in urine matrix.

5.6 ORGANIC SOLVENTS

The toxicity and biological importance of many metals and metal loids depend upon their chemical form.[17,18] Unfortunately, most quantitative trace elemental techniques can only determine total element concentration. Use of ICP/MS as an element selective detection for HPLC could provide valuable speciation information not possible recently. Houk et al. have used ion pair reversed phase liquid chromatogrpahy with ICP/MS detection for speciation of As and Se compounds.[19]

The purpose of this study was to optimize and characterize the VG Plasmaquad for use with volatile organic solvents commonly used in reversed phase HPLC.

5.6.1 Experimental

Solutions of HPLC grade methanol were spiked with 100 ng/mL. Mg, As, Co, Y, In, Cd, Ba, Pb and Bi and system optimization studies using the Hildebrand grid and standard Scott spray chamber as described previously were performed. The powers used in these studies were 1.5, 1.75,

Table 5-10

VG Semi-Quantification

Urine Matrix

SAHA Corrected

Element (100 ppb)	Predicted Concentration (ng/mL) Internal Standard Used				
	Co	As	Cd	Ba	Bi
Co	100	54	107	72	92
As	117	100	325	254	327
Cd	94	51	100	68	125
Ba	139	75	148	100	128
Pb	139	75	148	100	128
Bi	108	59	116	79	100

Table 5-11

Detection Limits in Qualitative Scan

ng/mL

Element	1% Nitric Acid	Urine Matrix
Co	0.09	0.20
As	0.40	0.61
Y	0.04	0.07
Cd	0.20	0.31
Ba	0.04	0.06
Pb	0.06	0.09
Bi	0.04	0.06

2.0 KW. Similar nebulizer flow rates and sampling positions were used. The ICP operating conditions were substantially different than those used for aqueous samples. Table 5-2 describes ICP conditions used for the organic study. The differences in ICP operating conditions when using volatile organic solvent vapor can be summarized as follows.

1. Higher argon coolant flow was used to stabilize plasma.
2. O_2 was mixed with nebulizer flow to prevent the condensing of graphite carbon on the sampler.
3. Spray chamber was cooled to -10°C.

The quadrupole mass filter required retuning due to introduction of organic solvents. Lens settings for the quadrupole when using methanol and acetonitrile are listed in Table 5-3. These could be used as a starting point for quadrupole tuning when using organic solvents, but a fine adjustment should be made per the VG Plasmaquad manual. The cooled mini spray chamber with the Hildebrand grid was also used on the VG Plasmaquad.

5.6.2 Results and Discussion

The nebulizer optimization study with organic solvents provided valuable insight into using the ICP/MS. Careful control of the auxiliary O_2 gas is required. Too little O_2 gas will result in graphite carbon covering the outside and/or the inside of the sampler and also the skimmer. When that occurs, the system should be shut off and the sampler cleaned. At these high ICP powers, if too much O_2 is used, both the sampler and skimmer can be damaged due to oxidation of the orifice. Since the sampler and skimmer cost about $600 and $800 respectively, this can be a very costly mistake.

Hausler used a 2% O_2 mixed with nebulizer argon when analyzing

organically bound metals in a xylene solution. He obtained detection limits for most of the elements in the periodic table similar for aqueous solutions. Exceptions to those detection limits were those elements with isotopic masses less than 82, for which transitory species created in the plasma interfered with his data.[20]

The VG training manual recommends that no more than 10% O_2 (varied from 40 mL/min - 70 mL/min) be used as a mixed gas with argon. At this flow rate, however, over a two day period both the sampler and skimmer were oxidized significantly to the point of J.A.N.G. (just ain't no good).

Because of the gradual sampler and skimmer degradation optimization plots similar to ones shown in early sections (i.e. relating power, nebulizer flow, intensity) were not possible. However, trends in the data can be stated.

1. Signal decreased significantly at sampling depths greater than 12 mm.
2. Optimal nebulizer flow across entire mass range for a particular sampling distance and power was observed.
3. At a fixed position as plasma power was increased, optimal nebulizer flow increased.

Optimal nebulizer flow was approximately 0.60-0.70 L/min. Figures 5-30,31 show optimal nebulizer flow at powers of 1.75 and 2.0 KW. Figure 5-32 shows how the YO^+/Y^+ ratio varies with increasing power and flow rate. At the low power, oxide formation is high; as power increases yttrium oxide formation declines. Care, however, should be taken when operating the plasma at higher powers to prevent damage to the sampler and skimmer.

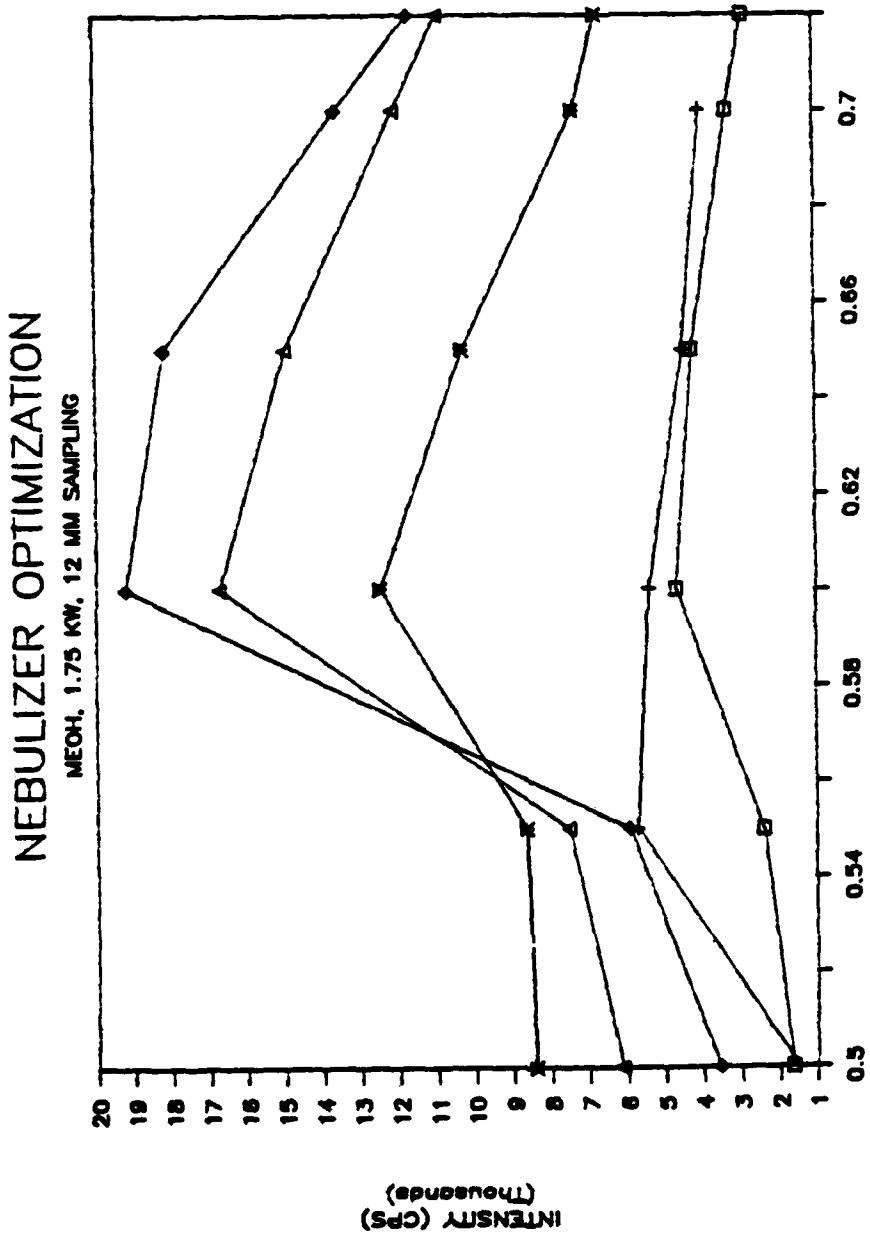

Figure 5-30. Nebullzer Flow vs. Signal Intensity @ 1.75 KW, 12 mm Sampling, MeOH

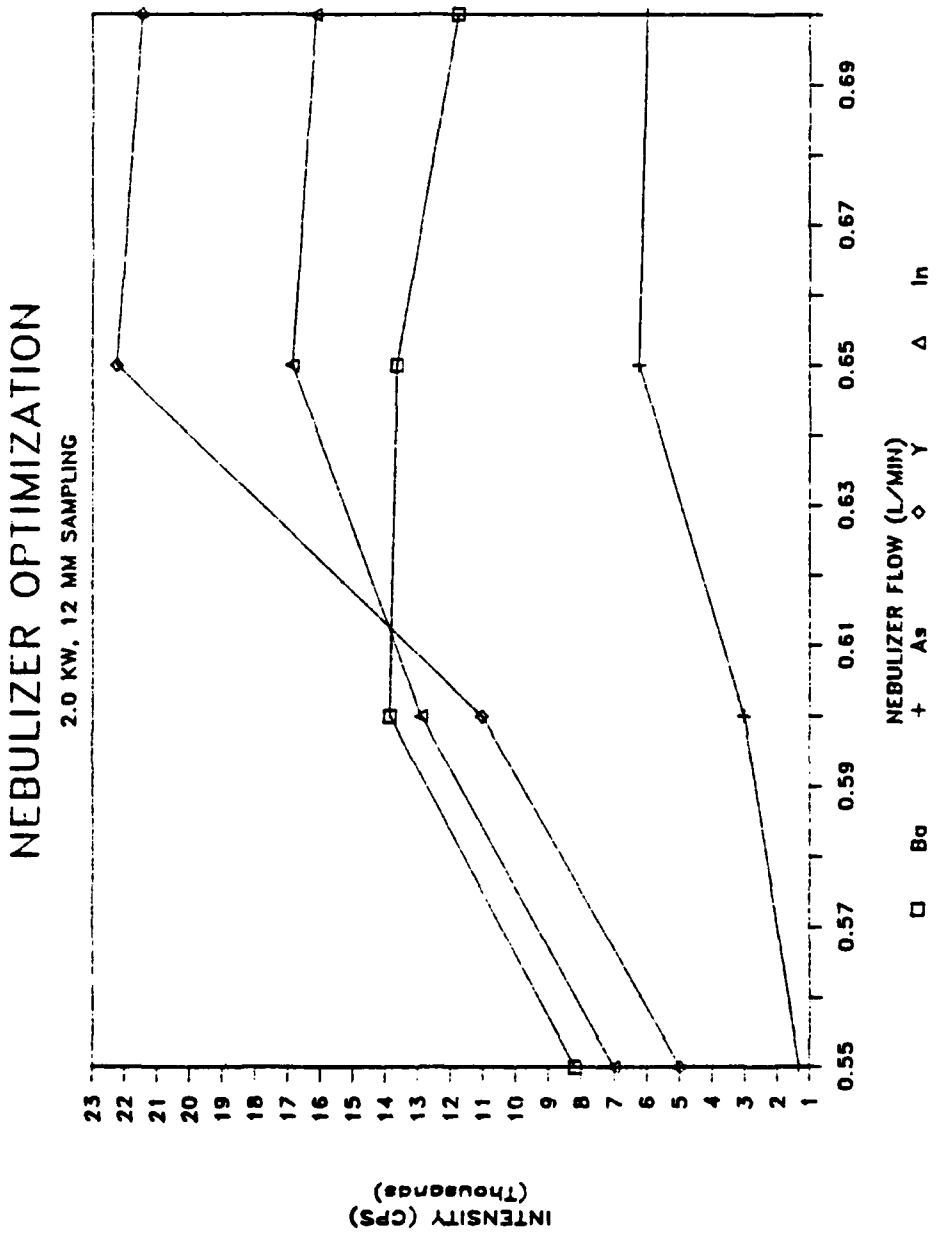

Figure 5-31. Nebulizer Flow vs. Signal Intensity @ 2.00 KW, 12 mm Sampling, MeOH

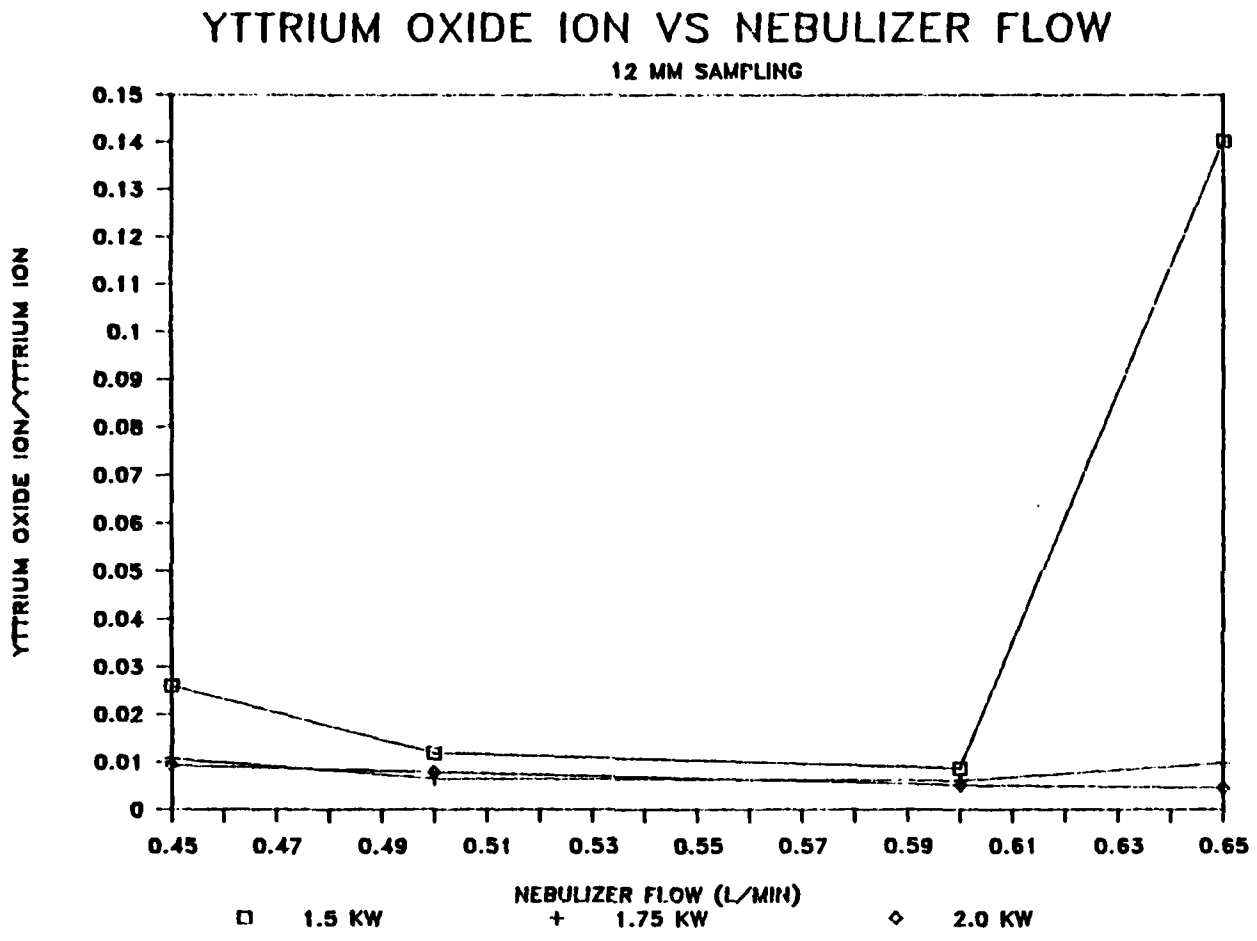

Figure 5-32. Nebulizer Flow vs. Yttrium Oxide Ion to Yttrium Ion Ratio @ 1.5, 1.75, 2.0 KW

Figure 5-33 shows typical spectra for various elements spiked in methanol analyte peaks and interferences are identified. **Table 5-12** shows some common molecular interferences resulting from introduction of organic solvents into the ICP/MS. **Table 5-13** shows the detection limits obtained for solutions in 100% methanol.

5.7 CONCLUSION

The ICP/MS provides a very sensitive method of detection for almost all elements in the periodic table. The Hildebrand grid, Meinhard concentric and the fixed crossflow nebulizers performed comparably in optimizing the ICP/MS for a 1% nitric acid solution. Data indicate that optimal system performance for all three nebulizers was obtained at a nebulizer flow of 0.65 L/min, 1.35 KW ICP power and a plasma sampling depth of 12 mm.

The Hildebrand grid nebulizer, which provides a good method of introducing high salt solutions into the ICP/MS, was used for the synthetic ocean water and urine study. Unfortunately, the limiting factor in introducing salt solution is not the grid nebulizer itself but the interface between the ICP and mass spectrometer. Introduction of high salt solution can clog the sampler and prevent efficient ion sampling of the bulk plasma. In addition, ionization of many elements can be suppressed by as much as an order of magnitude with just .01-.1% dissolved salt solutions. The grid also provides a means for introducing biological fluids such as urine into the ICP/MS. Ion suppression was about 40% for a urine matrix as compared with a 1% nitric acid solution.

Introduction of organic solvents require higher ICP powers, oxygen mixed with the nebulizer gas (to prevent carbon buildup on sampler) and a cooled spray chamber. Because of the higher ICP powers and input of

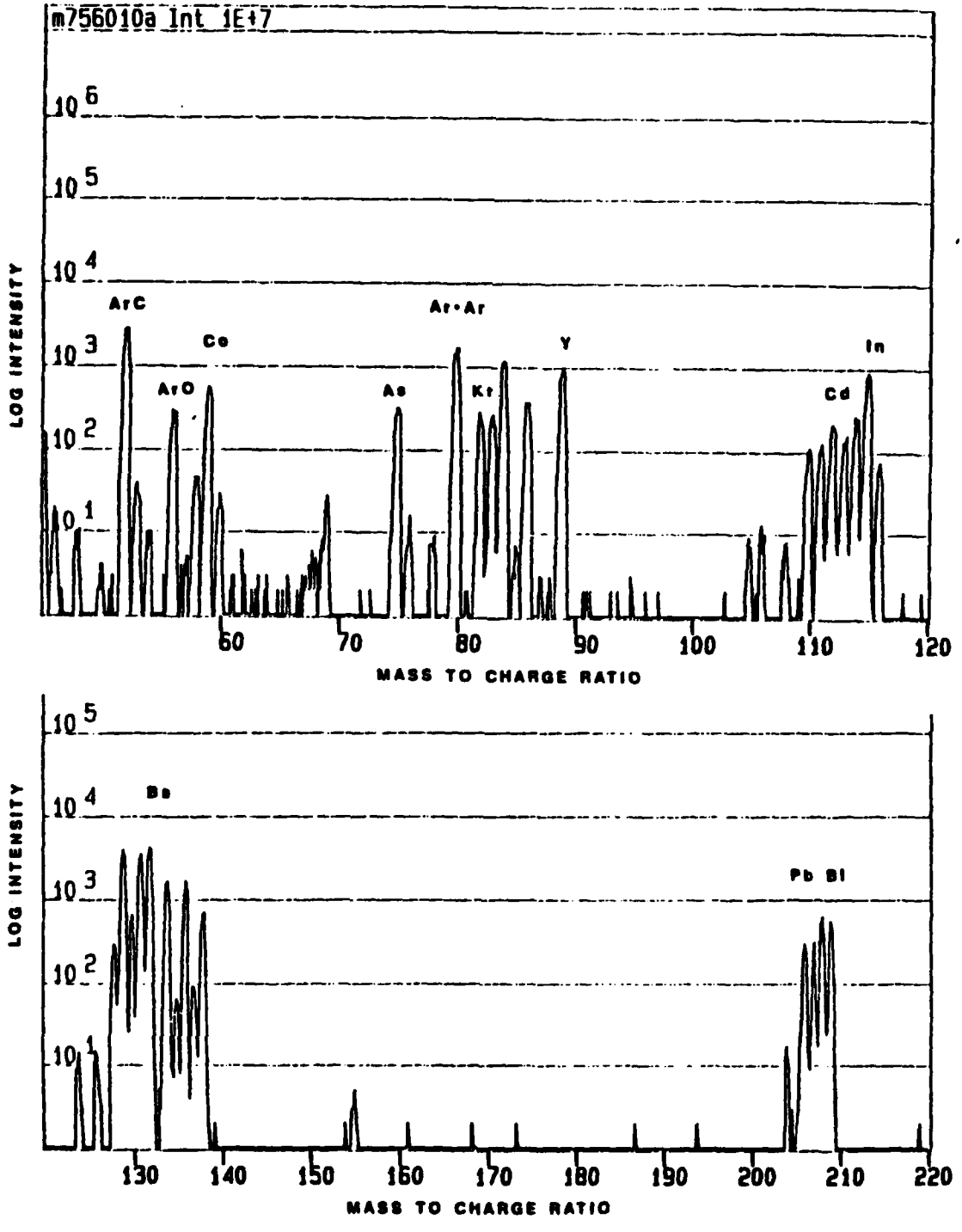

Figure 5-33. ICP/MS Mass Spectra of Various Elements in MeOH

Table 5-12

Common Molecular Ions From Organic Solvents

C_2^+	24	Mg
C_2H^+	25	Mg
$^{12}C^{13}C^+$		
CN^+	26	Mg
CO^+	28	Si
CO_2^+	44	Ca
$CO_2H/^{13}CO_2$	45	Sc
ArC^+	52	Cr

Table 5-13

ICP/MS Detection Limits (ng/mL)

Hildebrand Grid Nebulizer

100% Methanol

Element	
Co	0.04
As	0.28
Y	0.07
Cd	0.32
In	0.01
Ba	0.13
Pb	0.20

oxygen, care must be taken to avoid damage to sampler and skimmer. Detection limits of sub ng/mL for methanol solutions can be obtained routinely and thus this would be a very attractive element selective detector for HPLC.

References

1. A. R. Date, A. L. Gray, **Spectrochim. Acta, 40B**, 115 (1985).

2. D. J. Douglas, E.S.K. Quan, R. G. Smith, **Spectrochim. Acta, 38B**, 39 (1983).

3. A. R. Date, A. L. Gray, **Spectrochim. Acta, 38B**, 29 (1985).

4. A. L. Gray, A. R. Date, **Analyst, 108**, 1033 (1983).

5. A. L. Gray, **Spectrochim. Acta, 41B**, 151 (1985).

6. VG Isotopes Instruction Manual.

7. G. Zhu, R. F. Browner, **Appl. Spec., 41**, 349 (1987).

8. G. Horlick, S. H. Tan, M. A. Vaughan, C. A. Rose, **Spectrochim. Acta, 40B**, 1555 (1985).

9. S. H. Tan, G. Horlick, **Appl. Spec., 40**, 434 (1986).

10. S. H. Tan, G. Horlick, **Appl. Spec., 40B**, 445 (1986).

11. R. S. Houk, V. A. Fassel, G. P. Flesch, H. J. Svec, **Anal. Chem., 52**, 2283 (1980).

12. J. A. Olivares, R. S. Houk, **Anal. Chem., 58**, 20 (1986).

13. J. A. Olivares, R. S. Houk, **Anal. Chem., 57**, 2674 (1985).

14. P.M.J.M. Boumans, F. J. deBoer, **Spectrochim. Acta, 31B**, 355 (1976).

15. D. Beauchemin, J. W. McLaren, S. S. Berman, **Spectrochim. Acta, 42B**, 467 (1987).

16. A. White, P. Hamler, E. L. Smith, R. L. Hill, I. R. Lehman, **Principles of Biochemistry**, 1076, McGraw-Hill (1978).

17. B. P. Hammond, R. P. Beliles, **Toxicology - The Basic Science of Poisons**, 2nd ed., J. Doull, C. D. Klassen, M. O. Andres, Eds., p. 468; MacMillan: New York (1980).

18. H. Sigel, Ed., **Metal Ions in Biological Systems. Carcinogenicity and Metal Ions**, Vol. 10; Marcel Dekker: New York (1980).

19. J. J. Thompson, R. S. Houk, **Anal. Chem., 58**, 2541 (1986).

20. D. Hausler, **Spectrochim. Acta, 42B**, 63 (1987).

6.1 Conclusion

ICP-OES can provide sensitive (ng/mL), multielement detection for many elements (mostly metals) in the periodic table. ICP/MS offers 1-2 orders of magnitude improvement in detection limit over OES for most elements in the periodic table. One limitation and often referred to as the "Achilles Heel" of ICP spectrometry is sample introduction into the plasma.

The use of the Hildebrand grid nebulizer represents an improvement in sample introduction into the ICP. It provides a slightly more efficient method (over pneumatic nebulizers) of introducing sample into the plasma. The grid is capable of nebulizing organic, high salt (at least 5%) and biological solutions with little or no degradation of precision or stability. With specially modified spray chambers, the grid provides an attractive nebulization method for flow injection analysis using ICP-OES or ICP/MS detection. The Hildebrand grid is less expensive than the crossflow and specially designed high solids nebulizers (i.e. Babington). Though slightly more expensive than the concentric, the Hildebrand grid is rugged and durable.